



University of Strathclyde
Department of Pure and Applied Chemistry

Novel Enzymatic Methods of DNA Detection using
Enhanced Raman Scattering

By

Kristy Stephanie McKeating

A thesis presented to the Department of Pure and Applied Chemistry, University of Strathclyde, in fulfilment of the requirements for the degree of Doctor of Philosophy.

2013

This thesis is the result of the authors original research. It has been composed by the author and has not been previously submitted for examination which has led to the award of a degree.

The copyright of this thesis belongs to the author under the terms of the United Kingdom Copyrights Acts as qualified by University of Strathclyde Regulation 3.50. Due acknowledgement must always be made of the use of any material contained in, or derived from, this thesis.

Signed:

Date:

Acknowledgements

Firstly, I would like to thank my supervisors Dr Karen Faulds and Professor Duncan Graham for the opportunity to carry out this research and for their continued help and support throughout the course of my PhD.

A huge thank you to Dr Jen Dougan, who introduced me to the world of nanometrology and whose help and advice over the years has been invaluable. Thanks to Stacey Laing (not Lang) for all the discussions on TMB and for being an excellent desk buddy these past few years. I will miss our insightful discussions on tiredness and hunger. Thanks to Dr Sam ‘Mabs’ Mabbott for the SEM analysis (and the Tokyo Slings), to the cell crew: Dr Narayana Sirimuthu, Sarah Carthy and Derek Craig, and to Mhairi Harper and Kirsten Gracie for the help with PCR. Thanks to the final year undergraduate students Sian-Sloan Dennisoun and Anna Groom for their hard work and contribution. Also, thanks to everyone else within the Centre for Molecular Nanometrology who helped out with my research through numerous scientific chats, you know who you are and I am very grateful.

Thank you to all my friends and family who have had to put up with a crazy scientist over the years, especially to Gillian Horne who was always willing to help me forget the woes of the day with a ‘glass’ of wine. Most importantly thank you to my mum, Tricia McKeating, for always trying to help even when there wasn’t anything to be done.

Finally, thanks to all the Ramanators, past and present, for the outrageous behaviour, excellent banter, and excessive cake eating. You guys have been awesome.

Abstract

Over the years there have been a number of significant advances in DNA detection. In particular the advent of the Polymerase Chain Reaction (PCR) has enabled extremely low levels of DNA to be amplified and quantified, and along with fluorescence based detection measurements, has provided a reliable method of detecting genomic concentrations of DNA. However, throughout the years it has become apparent that although successful, these techniques have inherent complications that cannot be ignored in a research field as progressive as medical diagnostics. As a result, the future of biomolecule detection relies on the development of novel techniques that are able to eliminate the problems associated with conventional detection methods.

Detection methods amenable to this goal include oligonucleotide nanoparticle conjugates for colorimetric DNA detection, and surface enhanced resonance Raman scattering (SERRS), which provides improved sensitivity in comparison to fluorescence along with the potential for multiplexed analysis. Additionally, the use of enzymes in DNA detection to provide a method of target cycling and signal amplification provides a path toward amplification free analysis.

The overall aim of this research was to develop novel methods for the detection of DNA based on enzymatic activity. This primarily involved implementing the enzyme lambda exonuclease in a target cycling strategy, alongside DNA labelled with a donor and acceptor FRET pair for use in fluorescence detection. This enzyme was also utilised within a nanoparticle assembly system, whereby oligonucleotides were conjugated to gold and silver nanoparticles for use in SERRS analysis.

Finally, alternative enzymatic processes were investigated for the detection of DNA using resonance Raman and surface enhanced resonance Raman scattering. The catalytic activity of a DNAzyme on certain peroxidase substrates was investigated and used within a catalytic beacon assay protocol for the detection of DNA. Also, the enzymatic activity of gold and silver nanoparticles was investigated and their potential as enzyme mimetics for analyte detection was examined.

Abbreviations

A	Adenine
ABTS	2,2'-azino-bis(3-ethylbenzothiazoline-6-sulphonic acid)
C	Cytosine
CTC	Charge Transfer Complex
DLS	Dynamic Light Scattering
DNA	Deoxyribonucleic Acid
dsDNA	Double Stranded Deoxyribonucleic Acid
FAM	6-carboxyfluorescein
FRET	Förster Resonance Energy Transfer
G	Guanine
H33258	Hoechst 33258
HEG	Hexaethylene glycol
HHV-6	Human Herpes Virus 6
HIV	Human Immunodeficiency Virus
HRP	Horseradish Peroxidase
mRNA	Messenger Ribonucleic Acid
MRSA	Methicillin-resistant Staphylococcus aureus
MG-ITC	Malachite Green Isothiocyanate
NESA	Nicking Enzyme Signal Amplification
NEANA	Nicking Endonuclease Assisted Nanoparticle Amplification
OSN	Oligonucleotide Silver Nanoparticle
OGN	Oligonucleotide Gold Nanoparticle
P	Phosphate
PAH	Poly(allylamine) Hydrochloride
PCR	Polymerase Chain Reaction
PEG	Poly-ethylene glycol
PEI	Polyethylenimine
PSA	Prostate Specific Antigen
qPCR	Quantitative Polymerase Chain Reaction
RCA	Rolling Circle Amplification
RPM	Revolutions per Minute

RT-PCR	Real Time Polymerase Chain Reaction
RRS	Resonance Raman Scattering
SEM	Scanning Electron Microscopy
SERS	Surface Enhanced Raman Scattering
SERRS	Surface Enhanced Resonance Raman Scattering
SNA	Spherical Nucleic Acid
SNP	Single Nucleotide Polymorphism
SPB	Surface Plasmon Band
SPR	Surface Plasmon Resonance
ssDNA	Single Stranded Deoxyribonucleic Acid
T	Thymine
TBE	Tris-Borate-EDTA
TMB	3,3',5,5'-tetramethylbenzidine
TNF	Tumour Necrosis Factor
tRNA	Transfer RNA
UV-Vis	Ultraviolet-Visible Spectrometry

Contents

Acknowledgements	I
Abstract	II
Abbreviations	III
Contents	V
1. Introduction	1
1.1 An Introduction to Deoxyribonucleic Acid	1
1.1.1 Primary Structure	1
1.1.2 Secondary Structure	3
1.1.3 DNA Replication and Protein Synthesis	5
1.1.4 Alternative DNA Structures.....	6
1.1.5 The Chemical Synthesis of DNA.....	8
1.2 Current Methods of DNA Detection	8
1.2.1 Fluorescence	9
1.2.2 Förster Resonance Energy Transfer.....	10
1.2.3 Molecular Beacons.....	11
1.2.4 The Polymerase Chain Reaction.....	12
1.2.5 Alternative Detection Methods	16
1.3 An Introduction to Nanoparticles	17
1.3.1 Gold Nanoparticles	18
1.3.2 Gold Nanoparticles and DNA.....	20
1.3.3 Silver Nanoparticles and their Application to DNA Detection	22
1.4 Surface Enhanced Resonance Raman Scattering	23
1.4.1 Raman Scattering	23
1.4.2 Resonance Raman Scattering.....	25
1.4.3 Surface Enhanced (Resonance) Raman Scattering	26
1.5 Towards Amplification Free DNA Detection	31
1.5.1 Enzymatic Methods of Signal Amplification	31
1.5.2 Signal Amplification and SERS.....	34
1.6 Introductory Conclusions	37
1.7 Project Aims	37

2. Monitoring the Action of Lambda Exonuclease for the Detection of DNA using FRET	39
2.1 Introduction	39
2.1.1 DNA Binding Ligands	39
2.1.2 Hoechst 33258	40
2.2 Chapter Aims.....	41
2.2.1 The Detection of MRSA	41
2.2.2 Assay Design	42
2.3 Results and Discussion	43
2.3.1 Target DNA Detection using FRET	44
2.3.2 Fluorescent DNA Melting Profiles	45
2.3.4 Monitoring Lambda Exonuclease Digestion using FRET	47
2.3.5 Lambda Exonuclease as a Target Cycling Strategy for DNA Detection.....	49
2.4 Conclusions	52
3. Amplification Free Detection of DNA by Lambda Exonuclease and SERRS53	
3.1 Introduction	53
3.2 Chapter Aims.....	54
3.3 Results and Discussion	57
3.3.1 DNA-Nanoparticle Conjugates	57
3.3.2 Confirming DNA Conjugation	59
3.3.3 Confirming Hybridisation on a Nanoparticle	63
3.3.4 Investigating the Use of an Aggregator	66
3.3.5 Full Assay Trials using Plasmonic and SERRS Analysis.....	72
3.3.6 Magnetic Nanoparticle Based Lambda Exonuclease Assay	78
3.3.7 Confirming Lambda Exonuclease Digestion on a Nanoparticle.....	91
3.4 Conclusions	94
4. Monitoring the Catalytic Activity of DNazymes using Enhanced Raman Scattering	97
4.1 Introduction	97
4.1.1 Catalytic DNA	97
4.1.2 The Oxidation of ABTS.....	98
4.1.3 The Oxidation of TMB	100
4.1.4 Applications of HRP-Mimicking DNazymes	101
4.2 Chapter Aims.....	103
4.2.1 Assay Design	103
4.2.2 Beacon Design	104

4.3	Results and Discussion	105
4.3.1	Optimising DNAzyme Parameters	106
4.3.2	Resonance Raman Scattering of DNAzyme Activity	109
4.3.3	Catalytic Beacons for DNA Detection.....	116
4.3.4	A Split Probe DNAzyme Assay for the Detection of DNA.....	123
4.3.5	SERRS Analysis of DNAzyme Activity.....	128
4.4	Conclusions	135
5.	Nanoparticles as Enzyme Mimetics.....	137
5.1	Introduction	137
5.2	Chapter Aims.....	139
5.3	Results and Discussion	140
5.3.1	Nanoparticle Characterisation.....	140
5.3.2	Citrate-Capped Gold Nanoparticles.....	141
5.3.3	Citrate-Capped Silver Nanoparticles	147
5.3.4	Positive Particles.....	151
5.3.5	Comparing TMB Formulations.....	152
5.3.6	Silver Nanoparticle as Enzyme Mimetics for H ₂ O ₂ Detection.....	155
5.3.7	Nanoparticle Enzyme Mimetics for use in Cellular Tracking	166
5.4	Conclusions	168
6.	Conclusions	171
7.	Experimental	174
7.1	Monitoring the Action of Lambda Exonuclease for the Detection of DNA using FRET.....	174
7.1.1	Materials	174
7.1.2	Instrumentation	174
7.1.3	Preliminary Fluorescence Measurements	175
7.1.4	Fluorescent DNA Melts	175
7.1.5	Monitoring Lambda Exonuclease Digestion using FRET	175
7.1.6	Lambda Exonuclease for DNA Detection	176
7.2	Amplification Free Detection of DNA by Lambda Exonuclease and SERRS	176
7.2.1	Materials	176
7.2.2	Instrumentation	178
7.2.3	Preparation of Gold and Silver Nanoparticles	178
7.2.4	Preparation of DNA Nanoparticle Conjugates	179
7.2.5	Gel Electrophoresis of DNA Nanoparticles Conjugates.....	179

7.2.6	DNA Melting Experiments	179
7.2.7	UV-Vis Detection of Lambda Exonuclease Digestion	180
7.2.8	SERRS of DNA Nanoparticle Conjugates.....	180
7.2.9	Synthesis of Gold and Silver Shelled Magnetic Nanoparticles	181
7.2.10	DNA Magnetic Nanoparticle Conjugates	182
7.2.11	SERRS of DNA Magnetic Nanoparticle Conjugates.....	182
7.2.12	Confirming Digestion on a Nanoparticle.....	182
7.3	Resonance Raman and Surface Enhanced Resonance Raman Scattering of	
	DNAzyme Activity for Oligonucleotide Detection	183
7.3.1	Materials	183
7.3.2	Instrumentation	184
7.3.3	Formation of DNAzymes.....	184
7.3.4	Resonance Raman Scattering of DNAzymes	185
7.3.5	DNAzyme Concentration Study	186
7.3.6	Catalytic Beacon Assay Protocol.....	186
7.3.7	Catalytic Beacons for the Detection of PCR Product	187
7.3.8	Split Probe DNAzyme Assay Protocol.....	187
7.3.9	SERRS of DNAzyme Activity.....	188
7.4	Nanoparticles as Enzyme Mimetics	190
7.4.1	Materials	190
7.4.2	Instrumentation	190
7.4.3	Nanoparticle Synthesis.....	190
7.4.4	Nanoparticle Characterisation.....	191
7.4.5	Initial Experimentation	191
7.4.6	Preparation of TMB and H ₂ O ₂ Stock Solutions.....	192
7.4.7	Silver Control Experiments.....	192
7.4.8	Size and Zetasize Experiments	192
7.4.9	SEM Analysis	193
7.4.10	SERRS Time Study.....	193
7.4.11	H ₂ O ₂ Concentration Study	193
7.4.12	Comparing Positive and Silver Nanoparticles	193
7.4.13	Nanoparticle Tracking in Cells	194
8.	References	195
	Appendix : Publications.....	206

1. Introduction

The ability to detect disease biomarkers in a sensitive and specific manner is of vital importance to the field of molecular diagnostics as it advances towards point-of-care-diagnosis and patient-specific treatment. Proteins and DNA are the primary biomolecules of interest and a vast amount of research has focussed on novel techniques for their detection and the subsequent detection of a variety of different disease strains.

Interest in the detection of DNA for diagnostics has grown exponentially since the completion of the human genome project and a variety of assay formats and analytical techniques have been combined with molecular recognition processes to push for lower detection limits, with the ultimate aim always to improve upon disease diagnosis and treatment in a field where efficiency is the key to success.

1.1 An Introduction to Deoxyribonucleic Acid

1.1.1 *Primary Structure*

There are two types of naturally occurring nucleic acid; Deoxyribonucleic acid (DNA) and Ribonucleic acid (RNA). DNA contains the genetic instructions used in the development and functioning of all known living organisms, and enables such organisms to reproduce their complex components from one generation to the next.^{1,}

²

DNA is a template for its own synthesis, as well as that of RNA, and subsequently controls the synthesis of proteins. It is found in the nucleus of all eukaryotic cells, where, along with chromatin proteins, it is compacted and organised into structures called chromosomes. These chromosomes contain the genes, which are the unit of inheritance, and enable characteristic traits to be passed down through generations.

A nucleic acid strand consists of a series of repeating units known as nucleotides that are composed of three main parts; a pentose sugar, a heterocyclic nitrogenous base,

and a phosphate group. In DNA the pentose sugar is 2-deoxy- β -D-ribose and the base is attached to the 1' position via an *N*-glycosidic bond, while the phosphate group is attached to the 5' position, as is shown in Figure 1.1.

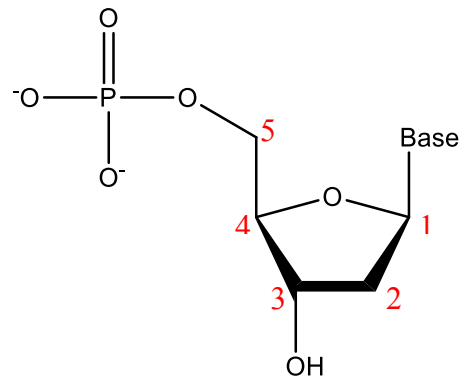


Figure 1.1 The structure of a DNA nucleotide.

There are four possible nitrogenous bases in a strand of DNA. These bases can be divided into two main categories; the pyrimidines and the purines. The pyrimidines are six-membered rings, while the purines consist of a six-membered ring fused with a five-membered ring. Adenine and Guanine are the bases belonging to the purine family, and Thymine and Cytosine are the pyrimidines (Figure 1.2).

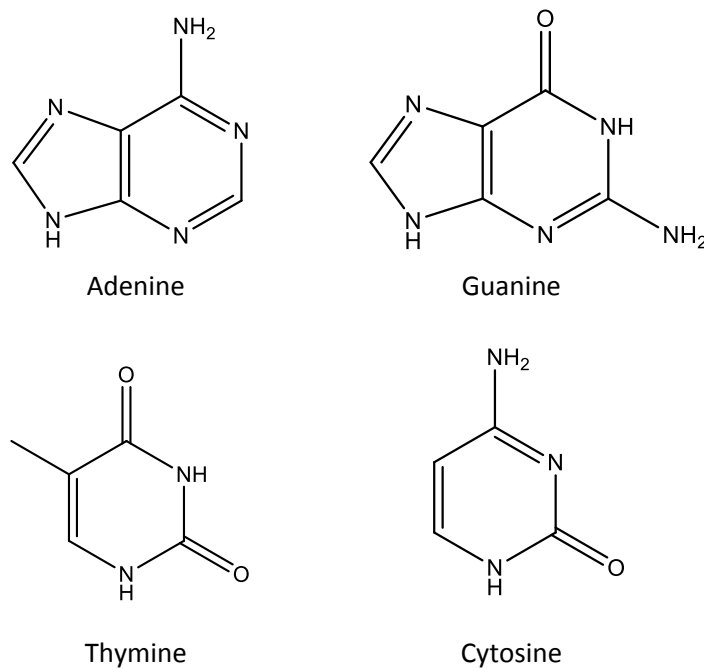


Figure 1.2 The structures of the four DNA bases.

Nucleotides are bonded through a phosphodiester link formed between the 3' hydroxyl group of one nucleotide, and the 5' position of the next.^{1, 2} Due to the presence of the phosphate group in the DNA strand it exists as a negatively charged molecule at physiological pH (Figure 1.3).

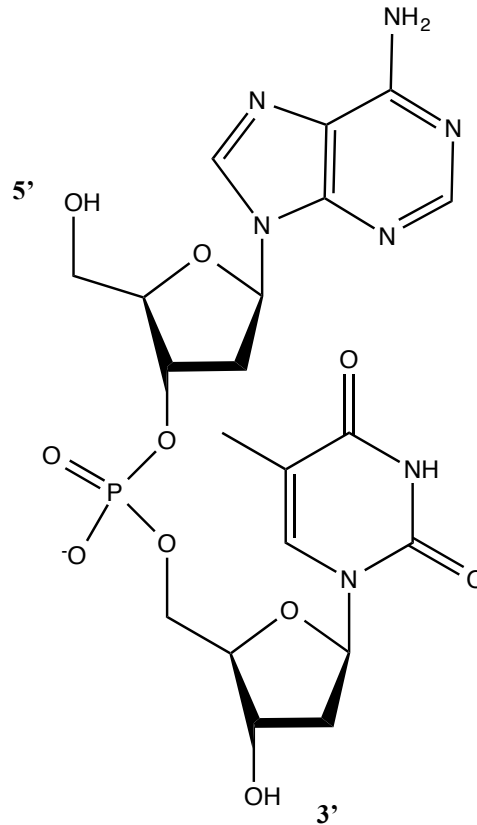


Figure 1.3 Two nucleotide units, one with an adenine base and one with a thymine base, joined via a phosphodiester link between the 3' hydroxyl position of the upper nucleotide, and the 5' position of the lower nucleotide.

The sequence of bases along a DNA strand is unique to a particular gene, which in turn codes for a specific amino acid sequence. These amino acids are the building blocks of proteins, and their sequence specifies a protein's functionality. Since genes can be thousands of nucleotides long, the number of possible base sequences is effectively limitless, giving rise to the significant genetic variation among species.

1.1.2 Secondary Structure

During the 1930's and early 1940's, a lot of research focussed on the transformation of hereditary characteristics³ and there was much speculation over the unit of

inheritance. Many at the time believed proteins to be the hereditary material, however in 1944, Avery, McClelland and McCarty published a paper supporting the belief that DNA was the fundamental unit involved in the transformation of certain strains of bacteria.⁴ They concluded that these findings could also be applied to genes, and this theory became widely accepted. However, while it had been determined how genetic information was stored within an organism, the question still remained of how it was passed down through generations.

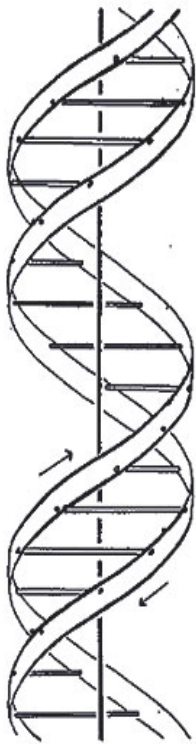


Figure 1.4 Diagrammatic representation of the DNA double helix as proposed by Watson and Crick.¹

In 1953, James Watson and Francis Crick published a paper detailing the three dimensional structure for deoxyribonucleic acid.¹ This paper was published not long after Pauling incorrectly suggested a model consisting of three intertwined chains as the structure of nucleic acids.⁵ In their 1953 paper, Watson and Crick discussed the stereochemical problems associated with Pauling's structure, and went on to suggest a possible alternative, a representation of which is shown in Figure 1.4. They proposed a double helix coiled around a centre axis, with the sugar phosphate backbone on the outside, and the bases perpendicular to the axis, on the inside of the coil. This structure was deduced based on X-ray diffraction data collected at King's College in London by Rosalind Franklin,^{6, 7} and on discussions of this data with Maurice Wilkins,⁸ who in 1962 was jointly awarded the Nobel Prize in Physiology or Medicine with Watson and Crick for the discovery of the molecular structure of DNA.

In their 1953 paper, Watson and Crick proposed that the double stranded structure of DNA suggested a possible copying mechanism. Later that year, they published another paper in the journal *Nature*,² discussing the features of the double helix in more detail, in particular base pairing between the two strands, and suggested a possible mechanism of self replication.

The double helix is held together by hydrogen bonds between the nitrogenous bases on the nucleotide chains, shown in Figure 1.5. Due to steric constraints deduced from the X-ray crystallography data, one member of a base pair must be a purine, and the other must be a pyrimidine. More specifically, adenine must always pair with thymine, and guanine with cytosine, if all the bases remain in the same tautomeric forms. The double helix therefore supported earlier findings by Chargaff,⁹ who in 1952 reported that for all samples of DNA analysed the ratio of thymine to adenine, and the ratio of guanine to cytosine, was close to unity.

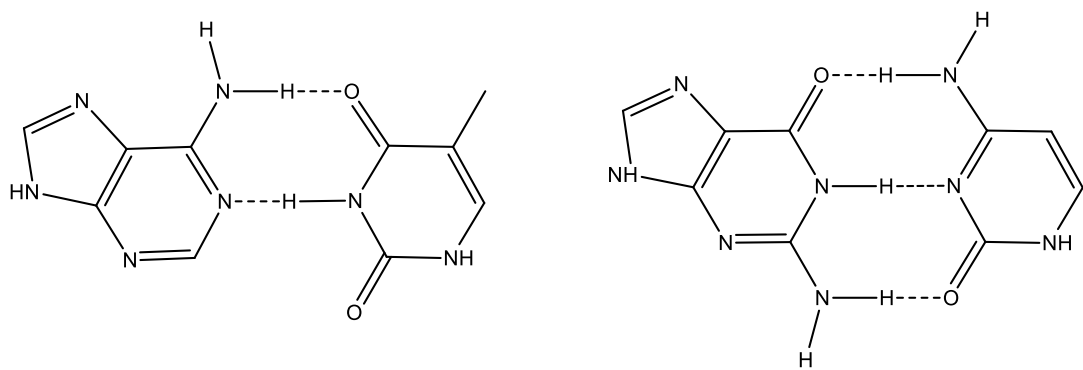


Figure 1.5 Base pairing between adenine and thymine (left) and guanine and cytosine (right).

It was therefore noted by Watson and Crick that, due to the specific base pairing, if the bases on one strand of DNA is known, it would be possible to predict the sequence on the opposite strand, thus meaning the DNA double helix is effectively a pair of complementary templates, ideal for use in replication.

1.1.3 DNA Replication and Protein Synthesis

This method of replication proposed by Watson and Crick remained untested until 1958, when Meselson and Stahl experimentally confirmed DNA replication to be in a semiconservative manner.¹⁰ Each DNA strand acts as a template that will determine the order of nucleotides along a new complementary strand, which will then be joined together by the sugar phosphate backbone, to yield two daughter molecules, each consisting of one original strand and one newly synthesised and complementary strand.

Closely following these publications Francis Crick proposed the “Central Dogma” of Molecular Biology, which was later published in *Nature* in 1970.¹¹ In his original presentation in 1958, Crick described the relationship between DNA, RNA and proteins, and concluded that “once information has got into a protein, it can’t get out again”, and that the transfer of information most commonly flows from DNA to RNA to proteins. This sequence of events is essential, since proteins are synthesised in the cytoplasm of the cell, and DNA is contained in the nucleus of eukaryotic cells. In order for the genetic information contained in the DNA sequence to begin synthesis of a specific protein, it must first be transcribed into messenger RNA (mRNA), in a process similar to that of DNA replication. The information is then moved to the cytoplasm of the cell, by the mRNA, and translated into a sequence of amino acids by base pairing of messenger RNA with transfer RNA (tRNA). The sequence of the amino acids specifies a proteins structure and hence it’s functionality.¹² These groundbreaking discoveries involving nucleic acids paved the way for modern molecular biology.

1.1.4 *Alternative DNA Structures*

Aside from the classical secondary structure of DNA first described by Watson and Crick, guanine-rich sequences of DNA can also exist in an alternative form known as a G-quadruplex. Indeed, the discovery of this arrangement precedes the double helix by over 40 years,¹³ although it took until 1962 for the structure to be confirmed.¹⁴ Using X-ray diffraction data, a core structure of 4 guanine bases, known as a G-quartet or G-tetrad, was discovered (Figure 1.6). The bases are held together in a square planar arrangement by Hoogsteen hydrogen bonds,¹⁵ and as a result of π - π interactions, stack one on top of another to form the G-quadruplex.¹⁵⁻¹⁷ These structures can vary in molecularity and

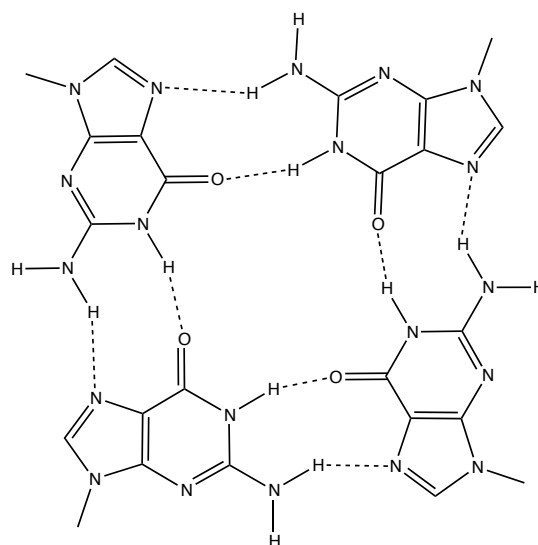


Figure 1.6 The chemical structure of a G-quartet.

structure depending on the DNA sequence and how the guanine bases are orientated. They can be formed from one, two or four separate strands of DNA resulting in either unimolecular, bimolecular, or tetramolecular G-quadruplexes which can further be characterised by their strand polarities and folding patterns (Figure 1.7). A G-quadruplex is stabilised by monovalent cations, notably Na^+ and K^+ , which interact with the oxygen atoms on the guanine bases. Depending on the cation used they are found either in the same plane as an individual G-tetrad or in the interstices of the structure between two successive G-tetrads.^{16, 18}

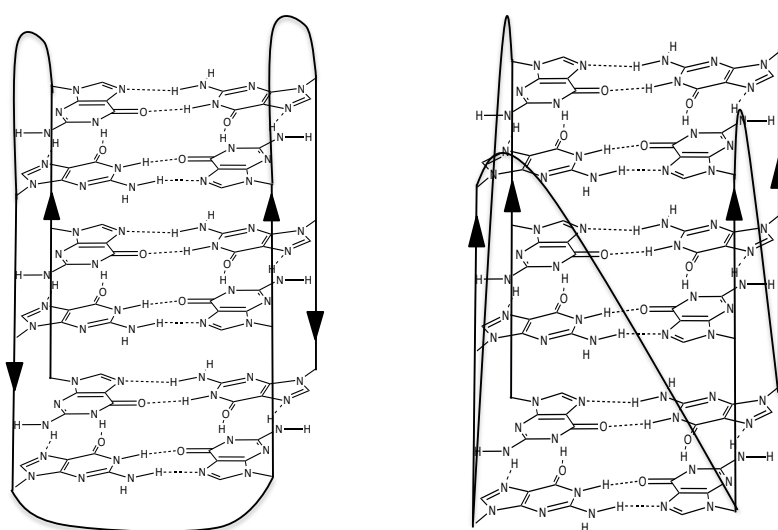


Figure 1.7 Unimolecular G-quadruplex structures with antiparallel (left) and parallel (right) strands.

This alternative DNA form is most commonly found in human telomeric DNA.¹⁹⁻²² Telomeres are noncoding guanine-rich tandem repeats of single stranded DNA and are found at the ends of eukaryotic chromosomes. They are fundamental in preventing cell degradation and death through elongation by telomerase, which will only act on single stranded DNA. As such the ability of a G-quadruplex to inhibit telomerase and hence promote cell degradation is an increasing topic of interest for cancer therapeutics.^{23, 24} Recent work on quadruplex DNA has successfully moved from *in vitro* to *in vivo* experimentation²⁵ culminating in the quantitative visualisation of G-quadruplex structures in human cells.²⁶

1.1.5 The Chemical Synthesis of DNA

Since the publication of the double helix, DNA research has advanced exponentially, culminating in a substantial body of knowledge about its structure and function. A significant advancement is the ability to synthesise specific sequences of oligonucleotides which have been used to advance genome research, allowing for such breakthroughs as the invention of the Polymerase Chain Reaction (PCR), and the discovery of novel detection methods, based on specific hybridisation probes, such as molecular beacons.²⁷

Early methods of DNA synthesis involved complicated solution phase chemistry that was extremely time consuming, and required specialised expertise.²⁸ The process advanced through the combined efforts of a number of research groups²⁸⁻³⁰ until eventually in the early 1980's there existed a fully automated method of oligonucleotide synthesis based on the use of phosphoramidites and solid phase synthesis, which was introduced by Letsinger *et al.*^{31, 32} and further developed by Caruthers and co-workers.^{33, 34}

Chemical synthesis of DNA means that oligonucleotides can be modified at the 3' end, the 5' end, or internally, with different chemical modifications depending upon the application of the sequence.³⁵ Common methods of modification include the incorporation of a fluorescent dye into a DNA sequence for use in various detection strategies.^{27, 36, 37} Also, the addition of a thiol or disulfide moiety at one terminus will enable conjugation to metal nanoparticles, for use in sensitive detection methods.³⁸⁻⁴⁰

1.2 Current Methods of DNA Detection

The ability to synthesise specific sequences of DNA with predetermined modifications has greatly aided research in the area of DNA detection. In recent years, a number of assays have been developed that are able to detect very low levels of DNA through the use of target amplification. These developments, in particular the advent of PCR, have revolutionised modern molecular diagnostics.

1.2.1 Fluorescence

One of the most specific molecular recognition events is the hybridisation of a nucleic acid strand to its complement. However, changes in the physical properties of DNA upon hybridisation are not easily measured. Thus, many methods of DNA detection involve the use of fluorescent probes. Fluorescence is a phenomenon that involves the emission of light from a substance resulting from a change in electronic state of a molecule. This process can best be described through the use of a Jablonski diagram (Figure 1.8).

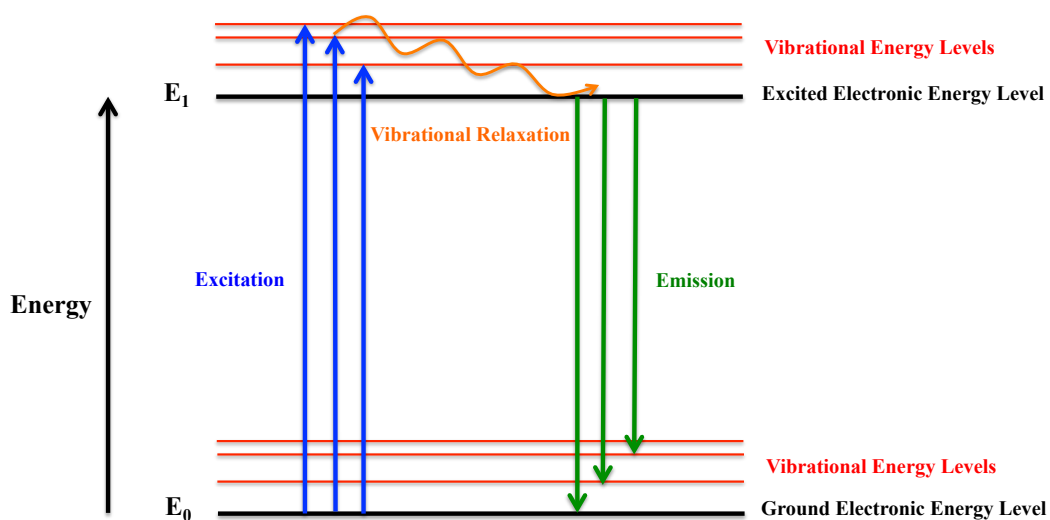


Figure 1.8 A Jablonski diagram showing the principles of absorption and emission.

Following the absorption of a photon of light, a species is promoted from the ground electronic state, to a higher vibrational level within one of the excited electronic states. Vibrational relaxation to the ground state of the excited electronic level occurs rapidly after absorption. Relaxation back to the ground electronic state then occurs, and when it is accompanied by the emission of a photon of light the process is known as fluorescence. This emission will have a longer wavelength than the absorbed light, and this difference is known as the Stokes shift.

Since fluorescence intensity is generally proportional to the concentration of the fluorophore present, the emission spectrum can be used for quantitative purposes if the emission wavelength of a particular molecule is known. However, problems arise

with its qualitative capabilities, since the spectrum produced is not specific to the molecule being analysed and no structural information can be obtained. Another problem with fluorescence are the broad emission peaks produced, making multiple sample analysis extremely problematic due to large spectral overlap between different fluorophores.

These problems aside, fluorescence spectroscopy can be extremely useful in the area of DNA detection. A fluorescent label can be incorporated into a probe sequence of DNA, whereby the fluorophore will be indicative of the presence of a specific sequence of DNA. By attaching a fluorophore either through chemical modification, or through the use of small molecule binding methods, such as intercalation, detection can be obtained down to the single molecule level.^{41, 42} Many of the assay formats that prove successful in the detection of DNA go beyond simple absorption and emission and involve a process known as Förster Resonance Energy Transfer (FRET).

1.2.2 Förster Resonance Energy Transfer

FRET is a phenomenon that was discovered by the German scientist Theodor Förster, and reported in 1948.⁴³ Again, this process can best be described through the use of a Jablonski diagram (Figure 1.9).

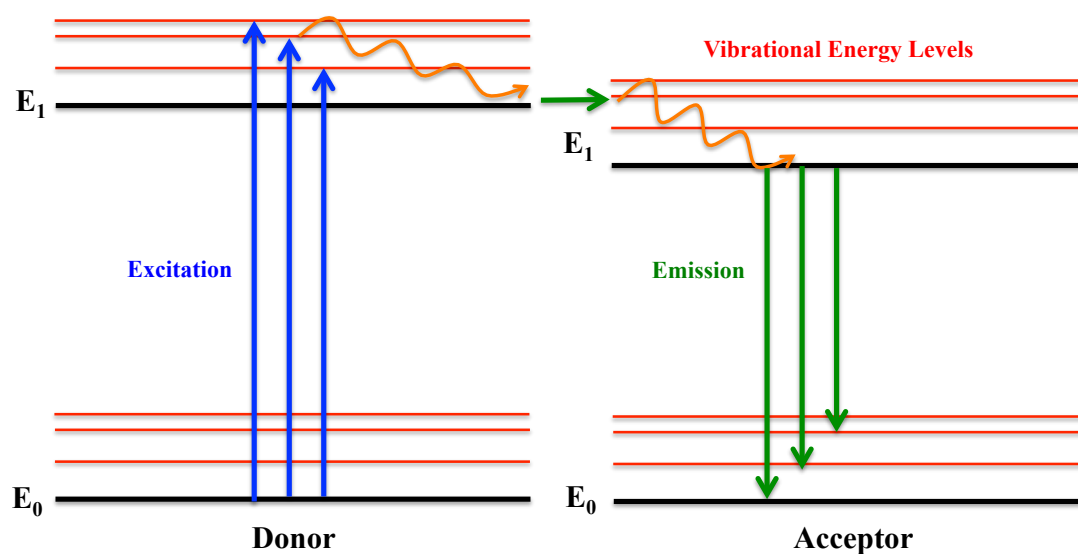


Figure 1.9 Jablonski diagram showing the process of FRET.

The basis of FRET involves a non-radiative transfer of energy between an acceptor and a donor pair of fluorophores. The essential FRET requirement is that the emission spectrum of the donor must overlap the absorption spectrum of the acceptor.³⁷ Another requirement is that the donor and acceptor molecules are within 1-10 nm of each other^{37, 44} Thus if a probe sequence and target sequence of DNA are labelled with a donor and acceptor pair, the detection of fluorescence at the acceptor emission wavelength will prove that the two are physically within a few nanometers of each other. If the pair move out with the Förster radii, the acceptor molecule will not be excited and no fluorescence observed, indicating a disruption of the FRET system. Alternatively, a dark quencher is an acceptor molecule that dissipates the absorbed energy as heat as opposed to light, thus when the FRET pair are within close contact there will be no fluorescence, and this time when the pair move out with the Förster radii, signal will resume. It is upon this theory that DNA detection strategies such as molecular beacons are based.

1.2.3 Molecular Beacons

Although the theory of FRET was first published in the 1940's,⁴³ its use as an important method of DNA detection was not realised until the late 90's, when Tyagi and Kramer first published their paper detailing molecular beacons, the concept of which is represented in Figure 1.10.²⁷

Molecular beacons are essentially single stranded nucleic acid molecules that possess a stem and loop structure, where the loop sequence is complementary to that of a specific target, and the stem consists of two self complementary sequences unrelated to the target. A fluorophore is attached to one end of the stem, and a quencher is attached to the other. In the closed beacon conformation no fluorescence is observed. However, when a target molecule is introduced, the loop and target sequences are able to hybridise forming an energetically more favourable duplex. Thus, the probe undergoes a conformational change, whereby the fluorophore and quencher are separated beyond the Förster radii, and the donor fluorophore is no longer quenched. Put simply, in the presence of a target sequence this system will 'light up'.

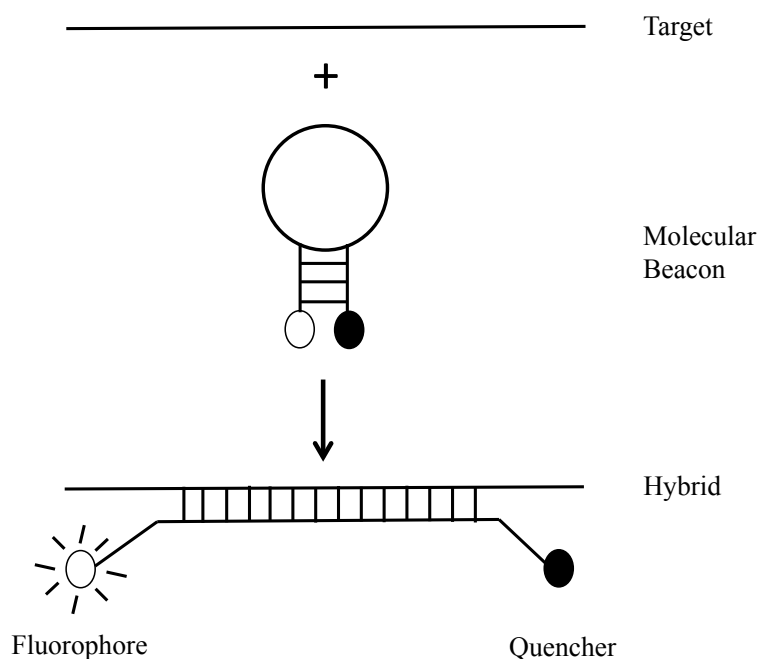


Figure 1.10 Principle of operation of molecular beacons as first proposed by Tyagi and Kramer.²⁷

When the concentration of molecular beacon and target molecule is high enough, this process can be detected by conventional fluorescence spectrometers. However, since human samples will yield DNA in extremely low concentrations, it is essential for the target to be amplified before introducing the molecular beacon. Thus PCR is commonly used in conjunction with molecular beacons for the detection of target DNA.

1.2.4 The Polymerase Chain Reaction

In 1983, Kary Mullis developed a method of amplifying extremely low levels of DNA through a process of thermal cycling, which would later win him the Nobel Prize in Chemistry.⁴⁵ The Polymerase Chain Reaction, or PCR, takes a small amount of DNA, and through a series of chemical and biological processes, is able to amplify a specific target by approximately 2^n , where n is the number of cycles in the reaction.^{46, 47} The inherent sensitivity of this technique lends its use to a variety of applications, including forensic analysis and genetic fingerprinting, as well as molecular diagnostics, where only a small amount of genomic DNA is available for analysis. Its diagnostic capabilities extend to the early detection of malignant

diseases such as leukaemia, and allows for the detection of viral DNA before the onset of disease, making PCR an extremely useful tool in rapid patient diagnosis and treatment.

A number of components are required for a PCR reaction, most importantly the DNA sequence requiring amplification. Short primers, complementary to the target sequence, and free nucleotides are essential components. DNA polymerase, an enzyme able to create a strand of DNA from these individual nucleotides, is also required. The process of PCR is outlined in Figure 1.11.

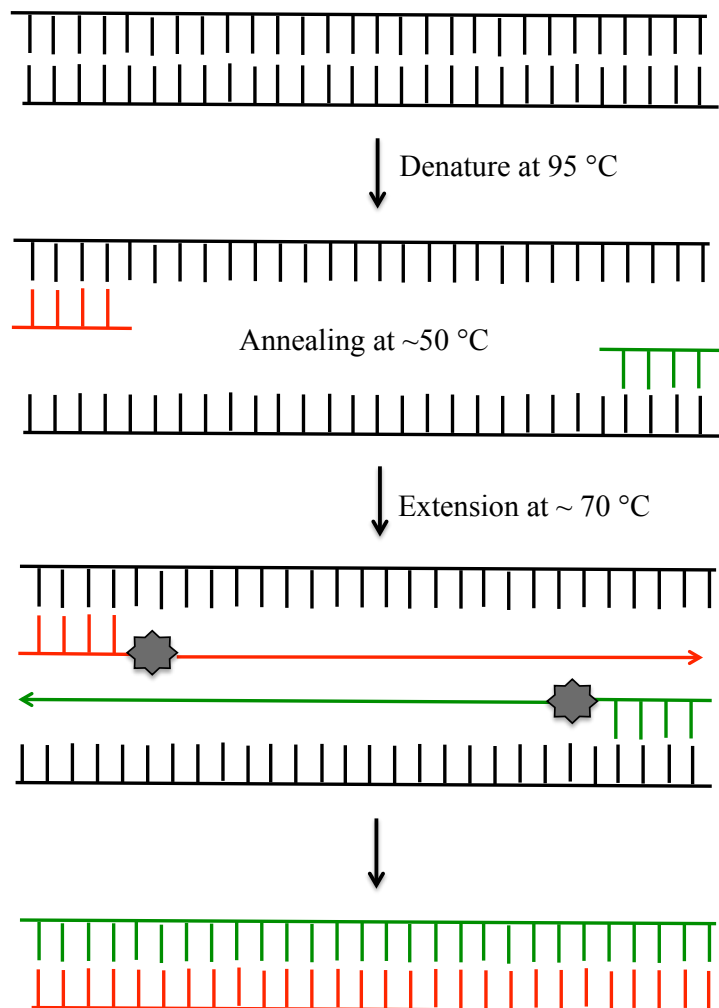


Figure 1.11 Basic mechanism of action of a PCR cycle.

The reaction starts with a denaturing step, where the target duplex is separated by heating the sample to 95 °C for a short period of time. The reaction is then cooled to

50-65 °C, allowing the primers to anneal to their complement, flanking the target sequence which is to be amplified. The next stage involves the elongation of the primer sequences using the enzyme DNA polymerase, thereby synthesising a new DNA strand in the 3' to 5' direction, from the unbound deoxynucleoside triphosphates in the reaction mixture. Initially *E. coli* DNA polymerase was used for this purpose,⁴⁶ however it could not withstand the high temperatures needed during the denaturing process and new aliquots of enzyme needed to be added after each cycle. The use of *Thermus aquaticus* (*Taq*) DNA polymerase, which is relatively heat-resistant, solved this problem, allowing for a simplified procedure which was amenable to automation.^{47, 48} The cycle is then repeated a number of times, with each strand produced serving as a template for the synthesis of further DNA strands in the next cycles. Thus, the amount of target DNA increases exponentially.

1.2.4.1 Quantitative PCR

Quantitative or Real-Time PCR (qPCR or RT-PCR) allows for the simultaneous amplification and quantification of a target that can be performed in a closed tube system, requiring no post-PCR manipulation of the sample. Older methods of quantification included separation and ethidium bromide staining of the PCR products on an agarose or acrylamide gel, which was extremely time consuming, and prone to inaccurate measurements.

Therefore, methods of quantification were developed involving the use of fluorescently labelled DNA strands that could be measured *in-situ*.⁴⁸⁻⁵¹ These particular detection methods utilise the 5' nuclease activity of the *Taq* polymerase, along with a fluorophore and quencher labelled oligonucleotide probe, to give an increase in fluorescence proportional to amplification of the target. The probes used in this method of detection have been termed TaqMan probes. The probe is modified at the 5' end with a fluorophore and at the 3' end with a fluorescent quencher (Figure 1.12). The probe sequence is complementary to that of the target, and thus is able to hybridise during the annealing stage of the PCR cycle. At this point, since the fluorophore and quencher pair are in close contact with one another, no fluorescence is observed. However, once the *Taq* polymerase begins to synthesise the new DNA strand, the probe is not resistant to the nuclease activity of the enzyme and is

consequently digested. The fluorophore is no longer in close contact with the quencher, and fluorescence is observed. This fluorescent signal will increase exponentially in proportion to the amplification of the target, providing a simple and effective way of quantifying PCR product in a closed tube system.

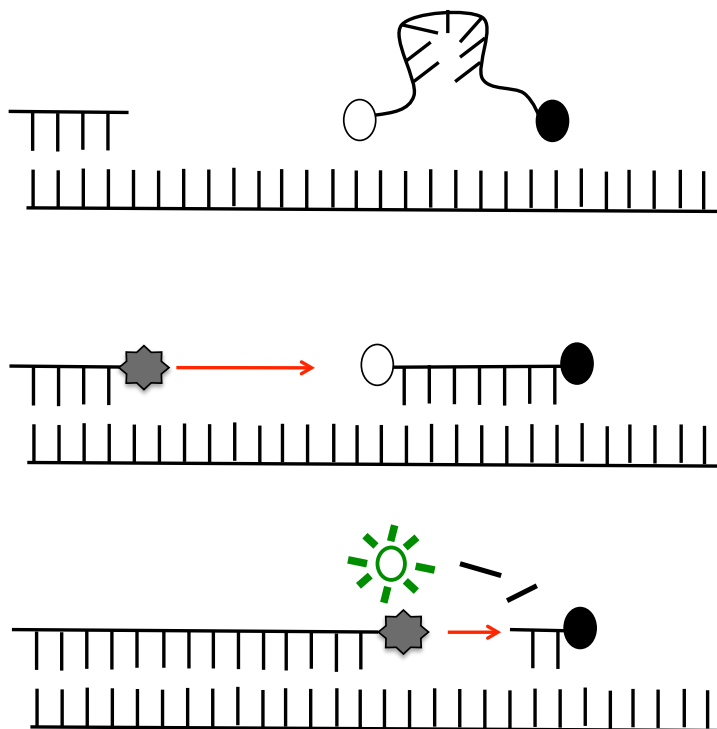


Figure 1.12 A representation of the action of a TaqMan probe in quantitative PCR

With the success of TaqMan probes, it is easy to see why FRET systems such as molecular beacons could also be utilised in PCR quantification, with the hairpin loop being complementary to part of the amplified product. This is most commonly seen in Scorpion probes,⁵² which are held in a hairpin loop configuration by complementary stem sequences on the 5' and 3' ends of the probe, that are modified with a fluorophore and quencher, respectively. Unlike molecular beacons this probe is linked to the 5' end of a primer via a PCR blocker, such as a monomer of hexaethylene glycol (HEG), which will prevent the replication of the stem-loop sequence. The primer is elongated during PCR amplification, creating a sequence complementary to the loop. During the next denaturing and annealing cycle these complements are able to hybridise. Since the new configuration requires less energy it is thermodynamically favoured over the beacon format and upon separation of the

FRET pair, a signal will be emitted that is representative of an amplified target strand. Unlike molecular beacons and TaqMan probes, the scorpion probe is directly incorporated into the PCR cycle, thus increasing specificity

1.2.4.2 Intercalators

The desire to develop a closed tube PCR system to avoid contamination, resulted in an alternative method of quantification to be developed that did not require hybridisation of a probe to an amplified target. These methods use fluorescent dyes that are able to intercalate between the base pairs of a DNA strand, and have a marked preference for double stranded DNA. Ethidium bromide was used as one of the first intercalators for this purpose,⁵³ showing an increase in fluorescence as the free ethidium bromide becomes bound to the double stranded DNA produced from the PCR cycles. Due to the toxicity of ethidium bromide, SYBR Green I is now the most commonly used intercalator for PCR quantification, showing an 11-fold increase in fluorescence when bound to double stranded as opposed to single stranded DNA.^{54, 55} Initially, no fluorescence is seen during the denaturing step of PCR, since the SYBR Green I remains free in solution. Once the primers have annealed to the target strand, a low level of fluorescence starts to appear, which continues to increase as the *Taq* polymerase synthesises a new DNA duplex. While this method can be carried out in a completely closed tube manner and is easily automated, the technique does not have the same sensitivity and, perhaps more importantly, specificity as the probes previously mentioned. These intercalators will bind to any double stranded DNA in the reaction, whether it is the sequence requiring amplification, or an unknown sample of DNA resulting from contamination within the amplification process.

1.2.5 Alternative Detection Methods

The polymerase chain reaction has proven to be an extremely effective method of amplifying and quantifying genomic levels of DNA through a fairly simple automated process. It is effective in a number of diagnostic applications, such as the prenatal detection of sickle cell anemia,⁴⁶ the detection of certain Cystic Fibrosis

amplicons⁴⁹, and the detection of the human herpes virus 6 (HHV-6).⁵⁶ It is also able to detect mutations and single nucleotide polymorphisms (SNP).^{27, 57}

PCR is not, however, without disadvantages, the most significant of which is the possibility of contamination. Any unwanted DNA in the initial reaction mixture can also be amplified as PCR proceeds, which effectively lowers the sensitivity of the technique. Also, in an age requiring quicker and more effective methods of early disease detection and treatment, PCR can be seen as a time consuming and expensive process, especially since it can only be carried out by trained personnel. Additionally, when combined with fluorescence, qPCR also has the added disadvantage of broad emission spectra, which limits the possibility of detecting multiple disease biomarkers simultaneously. These drawbacks inhibit the potential of PCR in the future of disease diagnosis and as such a significant amount of research is involved in the development of assay formats and spectroscopic techniques that are able to detect down to the genomic level, rivalling PCR and providing a more efficient method of early disease diagnosis. One of the techniques amenable to this goal is the conjugation of biomolecules to metallic nanoparticles for use in surface enhanced Raman scattering.

1.3 An Introduction to Nanoparticles

In 1959, a mere 6 years after the discovery of the double helix, Nobel Prize winning physicist Richard P. Feynman gave a lecture in which he first described the then unnamed field of nanotechnology as he proclaimed “There is plenty of room at the bottom”.⁵⁸ He envisioned a future whereby bottom up as opposed to top down strategies would allow for key biological problems to be solved on the atomic scale, and that improving the electron microscope sufficiently would allow for the manipulation of such nanoscale materials. His vision is being realised today, with the field of nanotechnology rapidly expanding into a variety of different scientific disciplines, from electronics to biotechnology. Indeed, the combination of nanoscale materials with biology has created an altogether new field of research, and in recent years bio-nanotechnology has seen an exponential growth in interest as it strives to solve the limitations inherent in conventional molecular biology.

1.3.1 Gold Nanoparticles

Nanoparticles can be defined as particles in which one dimension is in the order of 100 nm or less, and a number of metallic elements can exist in this form, including copper, silver and gold.⁵⁹ The first colloidal suspensions of gold nanoparticles date back to roughly around the 5th century B.C. when they were used to colour glass and ceramics.⁶⁰ The science behind colloidal suspensions, however, was not investigated until 1857 when Michael Faraday introduced the first method of synthesising gold colloid and observed that the properties of such solutions differed from that of the bulk material.⁶¹ This discovery effectively initiated metallic nanoparticle research, and a vast amount of information has been accumulated since this time.

A number of methods of synthesising gold colloid have been trialled since the first approach devised by Faraday, which involved the solution phase reduction of chloroauric acid.⁶⁰ The most popular to date is a citrate reduction method that was first devised by Turkevich in 1951⁶² and improved by Frens in 1973.⁶³ This method is still in use today for the synthesis of citrate-capped spherical nanoparticles with diameters ranging from 5 to 250 nm.^{60, 64}

The specific optical properties of gold nanoparticles can be attributed to the collective oscillation of electrons at the surface of a spherical nanoparticle that are coupled with the electromagnetic field of incoming light (Figure 1.13).^{60, 65} For gold nanoparticles with diameters in the region of 13 nm, this oscillation is induced by the interaction of light at a wavelength of 520 nm. This results in a strong absorption band observed in the extinction spectrum of gold nanoparticles known as the surface plasmon band (SPB). Mie first described this phenomenon in 1908 in his classical paper on light scattering by dielectric spherical nanoparticles.⁶⁶ He attributed the plasmon band to dipole oscillations of the free electrons in the conduction band occupying energy states immediately above the Fermi energy level.

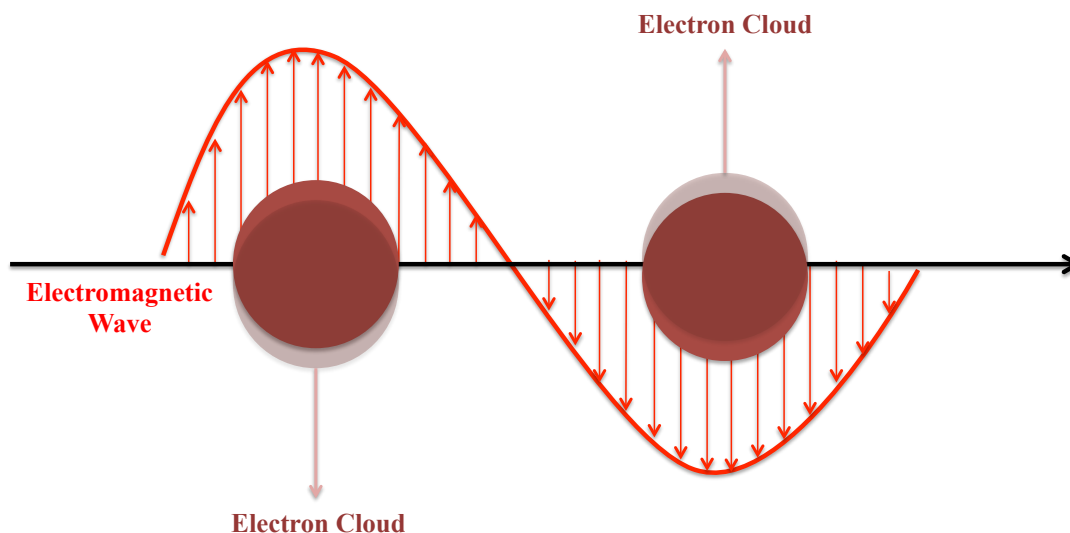


Figure 1.13 Schematic of the oscillation of electrons of spherical nanoparticles in an electromagnetic field.

The SPB will shift depending on a range of factors, including the size, shape and inter-particle distance of the nanoparticles.⁶⁵ For example, an increase in nanoparticle size will cause a bathochromic shift and broadening of the SPB due to a larger surface plasmon on each nanoparticle, and for gold, depending upon the extent of this shift, a colour change may be seen from red to purple. Additionally, as the distance between the nanoparticles decreases, the surface plasmons will combine and the exciting light will no longer be able to oscillate the electrons homogeneously, also resulting in a red shift in the extinction spectrum.⁶⁰

Nanoparticles require a stabilising ligand on their surface in order for them to remain dispersed in solution. The popular citrate reduction method of gold nanoparticle synthesis results in a layer of negatively charged citrate ligands on the surface of each nanoparticle and thus they are electrostatically prevented from aggregating. Other stabilisers can include small molecules, such as phosphine and amine ligands,⁶⁷ which cause electrostatic stabilisation due to surface charge, and polymers that physically prevent nanoparticles from coming into close contact with one another, for example poly-ethylene glycol (PEG).⁶⁸ In 1993 Mulvaney *et al.* devised a method of alkanethiol stabilisation,⁶⁹ which helped towards the development of DNA-nanoparticle conjugates, where DNA itself acts as an effective stabiliser as it is

a negatively charged polymer, hence providing stability through both steric and electrostatic interactions, even at high salt concentrations.

The ability to manipulate the surface plasmon band of gold nanoparticles by altering the inter-particle distance has recently become a significant tool in biodiagnostics.

1.3.2 Gold Nanoparticles and DNA

The strong recognition event between two complementary stands of DNA can be combined with the unusual optical properties of gold nanoparticles, to create simple and effective colorimetric methods of monitoring nanoparticle assembly. Two different research groups reported this design simultaneously in 1996,^{70, 71} and initiated a substantial amount of research into nanoparticle conjugations for biomolecule detection.^{59, 64, 72, 73}

In 1996, Alivisatos and his research group published a method of organizing nanocrystals through a specific DNA hybridisation event between particles in the region of 2 nm⁷¹ It was the aim to improve upon traditional ‘top down’ techniques for patterning matter, such as lithography, which can only reach the upper end of the nanometer region. Attaching single-stranded DNA of defined length and sequence to individual particles created dimer and trimer assemblies through the hybridisation of complementary oligonucleotides attached to a gold nanoparticle.⁷⁴ This method of nanoparticle assembly was subsequently used with both gold and silver nanoparticles to create a molecular ruler that could measure the distance between single pairs of particles up to 70 nm.⁷⁵

In the same issue of *Nature* Mirkin and co-workers described their design for nanoparticle assembly.⁷⁰ They utilised two batches of thiolated DNA attached to 13 nm gold nanoparticles, each batch with a different oligonucleotide sequence, the ends of which were complementary to a target sequence of DNA (Figure 1.14).

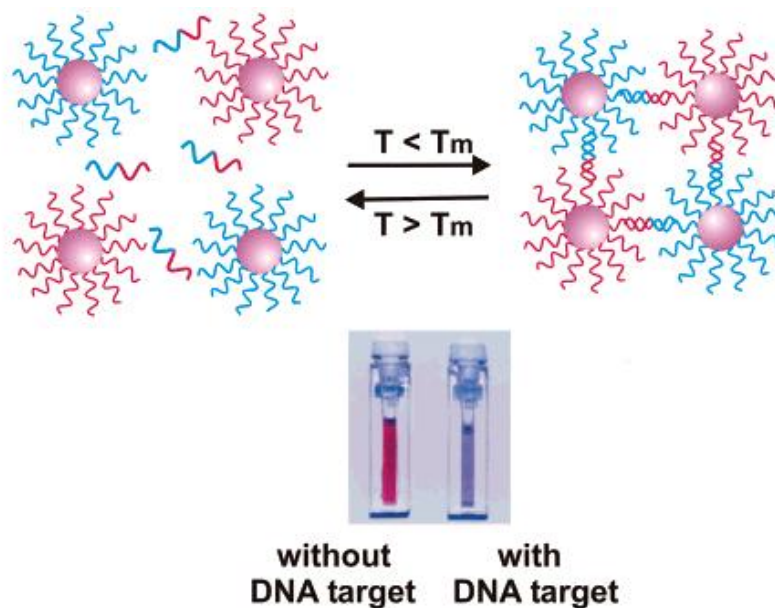


Figure 1.14: Crosslinking DNA gold nanoparticle assay as first developed by Mirkin and co-workers in 1996.⁷⁰

Upon hybridisation to a target sequence, the nanoparticles self assemble into aggregates, hence reducing the inter-particle distance. Such aggregation causes the surface plasmons to combine, resulting in a red shift in the SPB. A red to purple colour change can be observed during the aggregation process either by eye or using UV-Vis spectroscopy.

Since this initial publication, Mirkin and his research team have further explored the potential of these DNA-nanoparticle conjugate assays.^{59, 64, 76} The group at Northwestern University developed a method of differentiating single base-pair mismatches from target DNA by monitoring the transition temperatures of such hybridisations mixtures,⁷⁷ and transferring these to a reverse-phase silica plate to create the “Northwestern Blot” a method of visually detecting 10 femtomoles of target oligonucleotide.⁷⁸ Additionally, they employed DNA-nanoparticle conjugates within a scanometric DNA array to provide a sensitive and selective method of target DNA detection that rivals PCR.^{79, 80} Recently, nucleic acid-nanoparticle conjugates, or spherical nucleic acids (SNAs), as they have since been termed, have spanned the fields of chemistry, molecular diagnostics, medicine and materials science. A review of such has been published by Mirkin *et al*,⁷³ which includes their own work on

SNAs, notably their ability to detect mRNA in live cells⁸¹ and using antibody-linked SNAs for cellular targeting.⁸²

1.3.3 Silver Nanoparticles and their Application to DNA Detection

Silver nanoparticles, compared to gold, are less widely used in diagnostic research. Lee and Miesel first reported their synthesis in 1982, using the citrate reduction of silver nitrate.⁸³ However, this synthesis, unlike gold, is not as reproducible and the colloid produced can become unstable over time. It is likely due to this instability that researchers over the years have favoured gold, which has a well studied and documented surface chemistry, for DNA-nanoparticle conjugations.

Although gold is favoured, oligonucleotide-silver nanoparticle (OSN) conjugates are still an on going area of study and in 2008 Thompson *et al.* reported on the first use of these for target DNA detection.^{84, 85}

Similar to Mirkin's original design a sandwich assay was used to detect a target oligonucleotide through colorimetric analysis (Figure 1.15) and the authors were able to differentiate a single-base mismatch using DNA melting profiles.

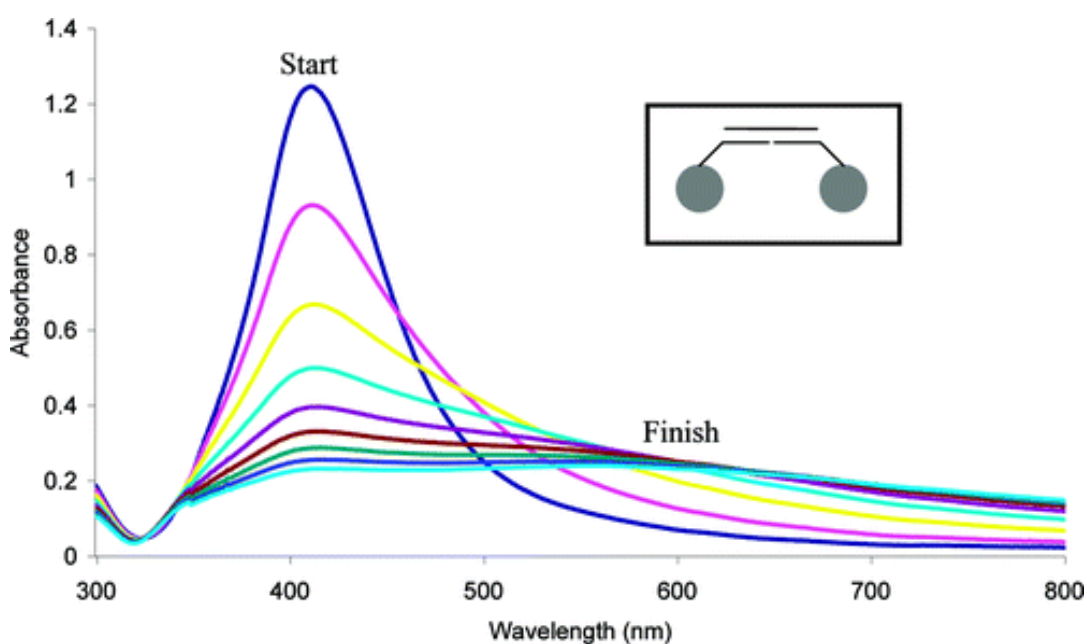


Figure 1.15 UV-Vis spectra of OSN conjugates in the presence of a fully complementary target sequence taken over a period of 80 min, showing the shift in SPB due to aggregation of the nanoparticles.⁸³

Although providing a successful method of detection, OSN conjugates have yet to be used in an assay format that provides levels of sensitivity rivalling that of PCR. However, the benefit of using silver nanoparticles is their high molar extinction coefficient, which in theory should increase sensitivity when using absorption spectroscopy. Thus, due to their optical brightness, the success of OSN conjugates lies in their ability to lend themselves to surface enhanced resonance Raman scattering.

1.4 Surface Enhanced Resonance Raman Scattering

Since the surface plasmon of metallic nanoparticles was first exploited for the detection of DNA, their use in diagnostic research has increased exponentially, and as such extremely sensitive and selective assays have been developed over the years. However, PCR and fluorescence still remain the dominant techniques in clinical analysis. While plasmonic detection mechanisms aim to improve upon the simplicity of analysis in an effort to move away from PCR and towards point-of-care diagnosis, an alternative spectroscopic technique to fluorescence is being considered in surface enhanced resonance Raman scattering.

1.4.1 Raman Scattering

In 1923 Smekal first postulated a theory on the inelastic scattering of light,⁸⁶ which remained untested until 1928 when Krishnan and Raman experimentally confirmed the hypothesis.⁸⁷ In this original experiment, sunlight was focussed onto a sample and the scattered light was collected using a second lens. Through a system of optical filters it was shown that the scattered radiation had an altered frequency to that of the incident light, thus defining the modern theory of Raman spectroscopy.

When light interacts with matter, it can be absorbed or scattered. The process of absorption is the result of a photon coinciding with the band gap energy of an electronic transition in a molecule, and thus excitement of an electron from the ground state to an excited electronic state. Scattering, however, does not require such a match in energy, and is the result of incident radiation polarizing the electrons surrounding the nuclei in a molecule. This creates a 'virtual state' the energy of

which is determined by the excitation source used. It is an unstable state due to its limited lifetime, and thus the photon is rapidly de-radiated, commonly through elastic, or Rayleigh scattering, whereby there is almost no change in the frequency of the photon (Figure 1.16).

If, upon interaction with light, there is nuclear motion within the molecule, the process is inelastic and the energy of the scattered photon will differ from that of the incident photon by one vibrational unit. This is known as Raman scattering. Since most molecules at room temperature will exist in the lowest vibrational energy state, Stokes scattering is the more dominant process, where upon the molecule is promoted to an excited vibrational state. However, sometimes molecules will already exist in this excited state and upon scattering will transfer energy to the photon resulting in movement to the ground vibrational state.

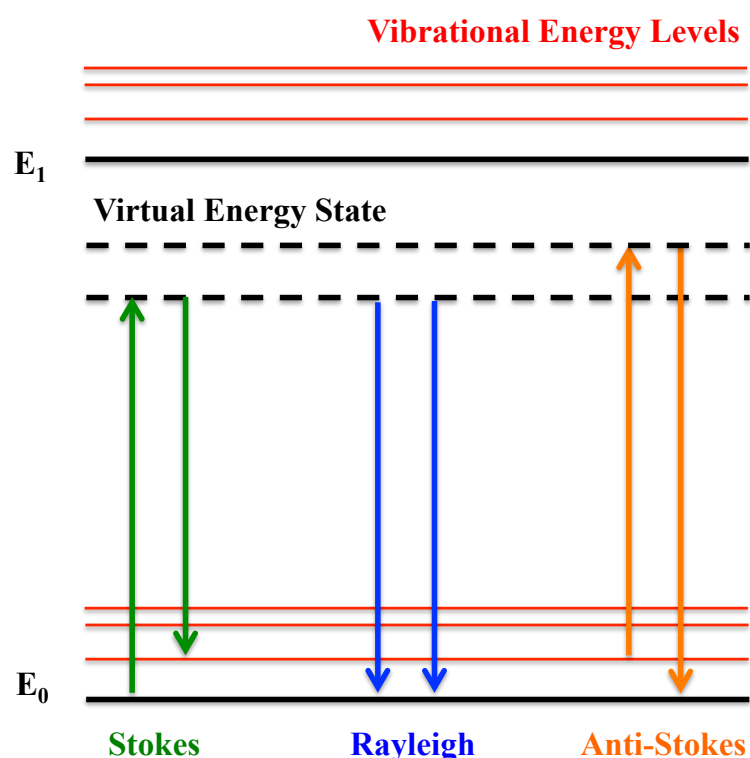


Figure 1.16 Jablonski diagram showing the processes of Rayleigh and Raman scattering.

Since the number of molecules expected to be in an excited vibrational state at room temperature will be small, anti-Stokes scattering is a much weaker process than

Stokes scattering, and thus the latter is the more commonly obtained spectra in Raman spectroscopy.

In comparison to Rayleigh scattering, Raman scattering is a much rarer process with only 1 in every 10^6 - 10^8 photons being Raman scattered.⁸⁸ Thus resonance Raman scattering and surface enhanced Raman scattering are common techniques used to improve upon the signal obtained in Raman spectroscopy.

1.4.2 Resonance Raman Scattering

When the frequency of the laser beam is coincident with the frequency of an electronic transition in a molecule, Raman scattering becomes a much more sensitive technique, and resonance Raman scattering can be used to obtain both electronic and vibrational information from a molecule, with signal enhancements in the region of 10^4 compared to conventional Raman.⁸⁸

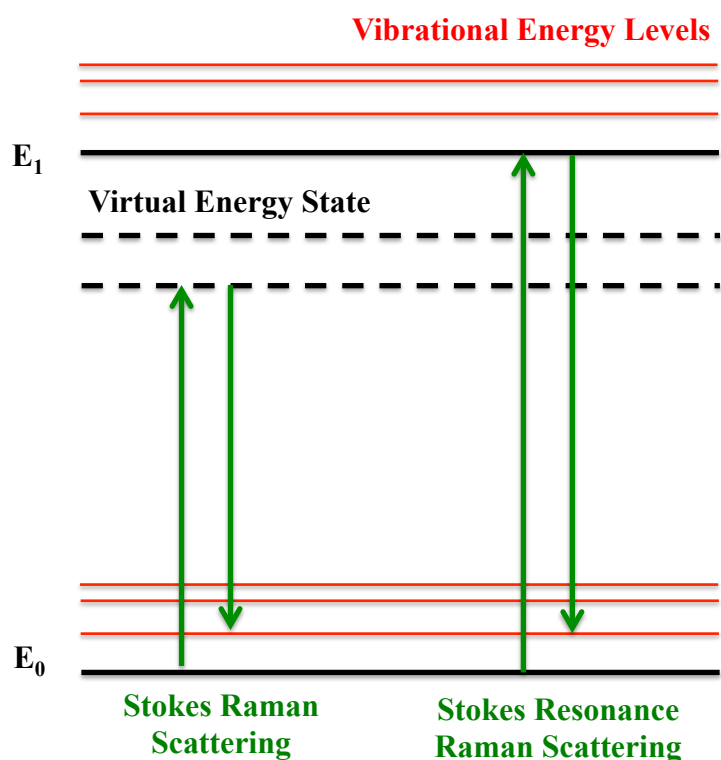


Figure 1.17 Jablonski diagram comparing the processes of Raman and resonance Raman scattering.

The main difference between Raman and resonance Raman scattering is depicted in Figure 1.1.7. In resonance Raman scattering absorption results in the excitation of a

molecule to an excited vibronic state, whereby in Raman scattering excitement is to a virtual energy level. As a result, more intense spectra can be obtained from this process, allowing resonance Raman scattering to be used to positively identify a molecule within a complex matrix, which is extremely useful in the analysis of biological systems. Limitations, however, lie in the unavoidable absorption process that can occur alongside resonance Raman scattering which may result in sample decomposition and an unwanted fluorescent background.

1.4.3 Surface Enhanced (Resonance) Raman Scattering

These limitations can be minimised through the use of surface enhanced Raman scattering (SERS) and surface enhanced resonance Raman scattering (SERRS). The SERS phenomenon was first reported in 1974 when Fleischman *et al.* observed an enhanced Raman scattering signal of pyridine at roughened silver electrodes.⁸⁹ At the time this enhancement was attributed to an increase in the electrode surface area allowing more pyridine molecules to be absorbed onto the surface. However, this theory was soon disputed by Jeanmarie and Van Duyne⁹⁰ and Albrecht and Creighton⁹¹ who noted that the intense enhancement seen, which was in the order of 10^6 compared to conventional Raman scattering, could not be explained solely by an increase in surface area.

Since the discovery, many theories have been proposed on the mechanism of SERS, and two distinct theories are still in use today. Electromagnetic enhancement theory deals with the interaction between the adsorbed analyte and the oscillating surface plasmons of the metal, while chemical transfer theory describes the analyte as being chemically bonded to the surface of the metal, and excitation occurs through transfer of electrons from the metal to the molecule, and back to the metal again. There is evidence for both these theories and it is usually agreed that both play a part in SERS, however, electromagnetic enhancement is generally thought to be the more dominant process. Additionally, since the first experimentation on a silver surface, many metals have been used for SERS enhancement, most notably other coinage metals including copper and gold in their colloidal form.⁸⁸ Other SERS substrates now exist in the form of structured metal arrays^{92, 93} and specially designed solid

surfaces such as Klarite⁹⁴, however this is outwith the scope of this thesis where the main focus will be silver and gold spherical nanoparticles.

Surface enhanced resonance Raman scattering is a combination of resonance Raman scattering and SERS, and was first reported in 1983 by Stacy and Van Duyne⁹⁵. The analyte that is absorbed onto the metal surface has a chromophore close in energy to the exciting radiation, and thus enhancement is due to surface plasmon resonance (SPR) and molecular resonance. This allows for greater enhancement factors to be observed gaining sensitivity surpassing that of fluorescence spectroscopy, and enabling single molecule detection.^{96, 97} One of the greatest advantages of SERRS lies in the ability of the metal surface to quench any fluorescence background obtained from a molecule, allowing for an improved spectra and a wider range of resonant molecules to be used for biomolecule detection.

1.4.3.1 Applications of SERS and SERRS

There have been a number of recent developments in SERS for bioanalysis, with a focus on the detection of biomolecules such as DNA and proteins.⁹⁸ Conventional labelling techniques involving molecular fluorophores give rise to spectra with broad emission bands, which provide limited structural information and large spectral overlap. The advantage of SERS in biomolecule detection lies in the sharp fingerprint spectra obtained, which allows for multiplexed analysis, meaning different disease biomarkers could potentially be detected simultaneously. Additionally, SERRS has proven to be 3 orders of magnitude lower in sensitivity than fluorescence for the detection of labelled oligonucleotides,⁹⁹ and as such a variety of assays have been developed for the detection of DNA using this technique.

Unlabelled sequences of DNA can be detected using SERS due to their orientation on the surface of the metal, as sequences perpendicular to the surface will have an increased signal compared to those that lie flat, and this was incorporated into a molecular beacon style assay for the detection of target DNA.¹⁰⁰ However, the majority of detection mechanisms involve the use of labelled DNA for SERS analysis, whereby the presence of a fluorophore is indicative of a particular DNA sequence. Many different commercially available fluorophores have been covalently

attached to DNA and used to obtain a quantitative SERRS response.^{99, 101} Additionally, Faulds *et al.* were able to simultaneously detect 5 labelled oligonucleotides within one sample and 6 labelled oligonucleotides when employing chemometric analysis, demonstrating the ability of SERRS to provide multiplexed analysis.¹⁰² Thus, labelled oligonucleotides have been incorporated into a number of DNA detection assays, and the initial coupling of SERS analysis and PCR allowed for the successful detection of the human immunodeficiency virus (HIV) *gag* gene.¹⁰³ Since this time, SERS analysis has been combined with PCR to detect a number of clinically relevant gene sequences.^{104, 105} Monaghan *et al.* utilised a lab-on-a-chip format for the detection of post-PCR *Chlamydia trachomatis*,¹⁰⁶ while Harper *et al.* used a modified version of the TaqMan assay for the detection of methicillin-resistant *Staphylococcus aureus* (MRSA).¹⁰⁷ Molecular beacon designs have also proven useful in combination with SERRS for the detection of specific gene sequences. Vo-Dinh *et al.* reported on the use of molecular sentinals,¹⁰⁸ which comprises a sequence of DNA, attached via a thiol group to a silver nanoparticle at one end and covalently labelled with a SERRS active dye at the other. With the beacon held in its closed loop format a high intensity signal was obtained from the dye. However, upon addition of DNA, the beacon opens, separating the dye from the metal surface and hence reducing the signal obtained. This technique was used for the multiplexed detection of two genes associated with *erbB-2* and *ki-67* breast cancer markers by implementing two different dye labels onto the molecular sentinals.¹⁰⁹

Another method of SERS for DNA detection, exploits the varying affinities that a sequence of DNA has for the surface of a metallic nanoparticle. MacAskill *et al.* developed a homogenous assay for the simultaneous detection of three DNA sequences coding for genes relating to hospital-acquired infections.¹¹⁰ The design is based on the theory that single-stranded DNA has a much greater affinity for the surface of silver nanoparticles than double stranded DNA. As such, in the absence of target, the labelled oligonucleotide is free to adsorb onto the surface of the nanoparticle, providing a strong SERRS signal. Upon introduction of a target, however, the signal intensity will be reduced since the duplex formed between labelled probe and complementary target will not have as great an affinity for the

surface. The main disadvantage of this design is that it is a negative assay, therefore van Lierop *et al.* improved upon this by utilising a dye-labelled SERS primer providing a positive assay that is fully compatible with PCR.¹¹¹ Figure 1.18 outlines this design, which was used for the successful detection of a genomic sequence of DNA from *Staphylococcus epidermidis*.

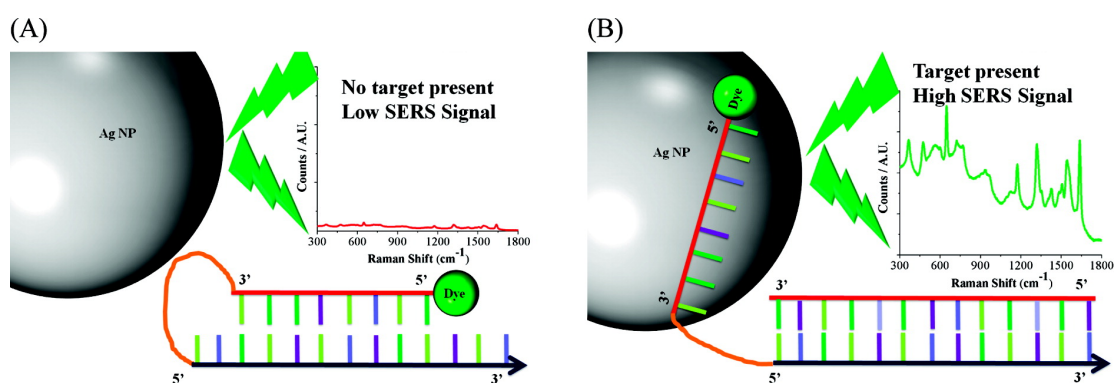


Figure 1.18 Schematic of specialised SERS primer for genomic DNA detection. In the presence of target, the primer opens and the single stranded region is free to adsorb onto the surface of the silver nanoparticle, increasing the SERS response.¹¹¹

In order to achieve optimum SERRS enhancement, a dye labelled oligonucleotide with an appropriate excitation energy must be chosen along with a suitable surface. Also, it is imperative to promote aggregation of the colloid in order to achieve ‘hot spots’ between the nanoparticles, where the SERRS response is greatest.¹¹²⁻¹¹⁴ The most common method of promoting aggregation for DNA detection is to use an external charge modifying agent, most commonly spermine. This serves the dual purpose of aggregating the colloidal particles via a positive spermine bridge while simultaneously promoting adsorption of the DNA onto the nanoparticle surface. However, since Mirkin and Alivisatos demonstrated the ability to detect DNA using surface plasmon resonance, research has focussed on the ability of biomolecules to promote aggregation, and thus enhancing the SERRS output.¹¹⁵

Cao *et al.* exploited this process to achieve the multiplexed detection of six different DNA targets with varying Raman reporter molecules using a split probe assay design and micro-array format.¹¹⁶ Although gold nanoparticles were used to create the conjugates used in this assay, they were subsequently coated with silver to enhance

the signal obtained. A more simplistic design is to use the oligonucleotide-silver nanoparticle conjugates, which were discussed in section 1.3.3. Thompson *et al.*⁸⁴ first reported on the use of these conjugates for the detection of DNA and Graham *et al.*⁸⁵ then demonstrated how these could be used to turn on SERRS as a result of a specific biological interaction (Figure 1.19). Silver nanoparticles were coated with a Raman active dye as well as oligonucleotide probes complementary to a region of the target DNA. Upon hybridisation the two batches of OSN's are aggregated into large assemblies and an enhanced SERRS signal is observed.

Subsequently, Qian *et al.* reported on a similar concept and utilised SERS beacons alongside long range plasmonic coupling.¹¹⁷ Oligonucleotide-gold nanoparticle (OGN) conjugates were used in this assay, which cannot compete with silver in terms of SERRS enhancement and thus sensitivity. However, as discussed previously, these OSN conjugates, though successful in providing SERRS enhancement, have not yet been trialled on clinically relevant samples due to the problems associated with silver colloid synthesis and conjugate preparation.

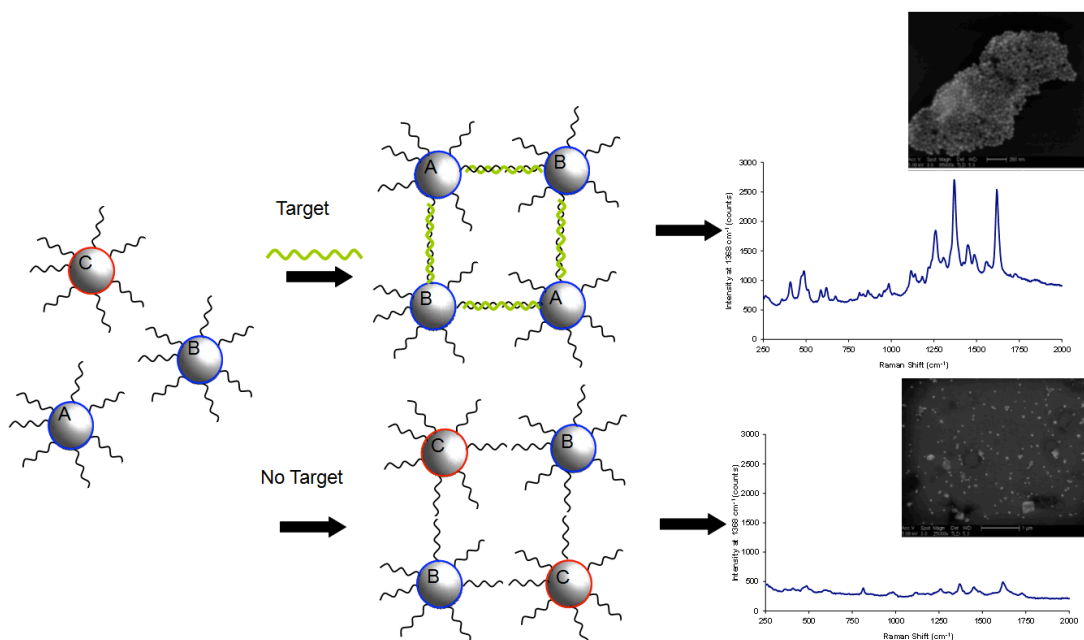


Figure 1.19 Schematic of the process of nanoparticle aggregation via a specific hybridisation event. Labelling of the silver nanoparticles allows a SERRS response to be obtained, which is increased in the presence of target and is shown via the spectra. Inset images are the SEM results obtained before and after the addition of target confirming aggregation due to hybridisation.¹¹³

Due to the problems associated with DNA-silver conjugates, oligonucleotide anchors have been tested in order to improve upon the stability^{38, 118} and mixed metal systems have been utilised that combine the stable surface chemistry of gold with the surface enhancement of silver.¹¹⁹

While SERRS of OSN conjugates has not yet provided a method of detecting genomic material, research into inducing aggregation through a specific biomolecular recognition events is one avenue of research that continues to strive towards amplification-free analysis.

1.5 Towards Amplification Free DNA Detection

Oligonucleotide nanoparticle conjugates aim to develop simple colorimetric methods of DNA detection with PCR-like sensitivity. Meanwhile, SE(R)RS is being used as an alternative spectroscopic method of detection to combat the limitations inherent in fluorescence spectroscopy, and the two have been combined in recent years for the sensitive detection of target DNA. Recently a novel method of detection has emerged that is amenable to both oligonucleotide nanoparticles conjugates and SER(R)S analysis. Signal amplification as opposed to target amplification is of great interest to the development of PCR-less methods of DNA detection, and has already been combined with a range of existing spectroscopies, from fluorescence to SERS.

1.5.1 Enzymatic Methods of Signal Amplification

As research surrounding the structure and function of DNA has progressed, a number of enzymes have been elucidated that aid in the significant biological processes that are essential to cellular life. These enzymes have been isolated and can now be implemented in bioassays for a number of different functions. In particular DNA nucleases have been used to great effect in the development of PCR-less bioanalysis within assays that promote signal amplification as opposed to the conventional target amplification method of DNA detection. DNA nucleases can be divided into two categories; endonucleases and exonucleases, and can sometimes be termed restriction enzymes.¹²⁰ These are bacterial enzymes that provide defence against foreign DNA,

including viruses, by selectively cutting up the DNA inside an invading host. Endonucleases are able to cleave the phosphodiester bonds between nucleotides on a strand of DNA when they reach a particular recognition site. Exonucleases, on the other hand, progressively digest DNA, either from the 3' terminus releasing 5' mononucleotides or from the 5' terminus releasing 3' mononucleotides.^{120, 121} The action of these enzymes has been exploited recently to promote target recycling, whereby a target strand of DNA can hybridise to a number of different probe sequences throughout the course of an assay, thus enhancing the chosen output signal. This improves upon current methods of DNA detection that require a 1:1 ratio of probe and target, such as molecular beacons.

Li *et al.* reported on the use of enzymatic signal amplification of molecular beacons for DNA detection.¹²² The group designed a method of nicking enzyme signal amplification (NESA), to improve upon the sensitivity of molecular beacons. Upon target hybridisation, and beacon opening, a nicking endonuclease enzyme will cleave one strand of the duplex, via a specific recognition site, leaving the target free to re-hybridise to another beacon, hence amplifying the fluorescent signal obtained. This design increased the detection sensitivity by nearly three orders of magnitude compared to conventional molecular beacons. Since these nicking enzymes are sequence specific, the group also reported on a method of NESA combined with rolling circle amplification (RCA), boosting the sensitivity by a further two orders of magnitude, and allowing for universal target detection.

Another method of implementing signal amplification for universal target detection is to employ an enzyme that is not sequence specific, such as an exonuclease, the attributes of which are discussed further in section 1.5.2. Exo-III in particular has been implemented in a number of different assays that utilise signal amplification.¹²³⁻¹²⁷ Zuo and co-workers used molecular beacons in a similar manner to the NESA approach first proposed by Li *et al.* (Figure 1.20).

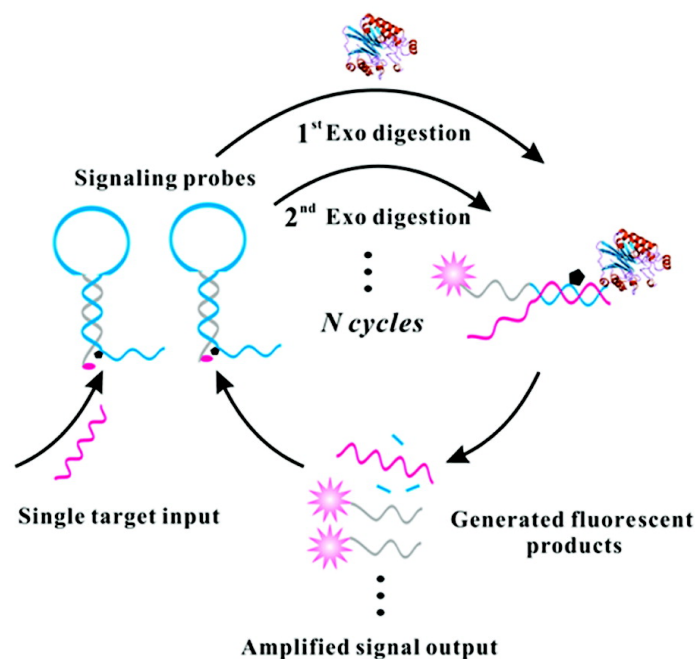


Figure 1.20 Schematic of Exo-III aided target cycling strategy, whereby the signal output from a molecular beacon approach to DNA detection is enhanced through the action of a non-specific exonuclease enzyme.¹²³

However, by employing Exo-III as opposed to a nicking endonuclease, they developed a detection mechanism that was amenable to a variety of different target sequences. This simple and effective method of detection boasted a detection limit of 10 femtomolar, with a 10-fold increase in sensitivity over conventional molecular beacons.

In addition to fluorescence detection, nanoparticles have been employed amongst signal amplification strategies for colorimetric detection methods. Xu *et al.* reported on nicking endonuclease assisted nanoparticle amplification (NEANA), whereby a 3-component sandwich assay was used to detect target oligonucleotides with single-base mismatch selectivity.¹²⁸ While Cui *et al.* used Exo-III, again to employ a universal platform for DNA detection.¹²⁵ In this method, target DNA forms a duplex with a linker strand, which is digested by Exo-III, leaving the target free to recycle. Gold nanoparticles modified with sequences of DNA complementary to the linker strand are then added to the system, which will remain dispersed in solution and red in colour if digestion has occurred. In the absence of target, however, the Exo-III

will not digest the linker, leaving it free to hybridise to the complementary DNA conjugates, aggregating the colloid and providing a red to blue colour change. Using this method a colorimetric detection limit of 15 pM was obtained, with single-base mismatch discrimination.

1.5.2 Signal Amplification and SERS

Signal amplification has recently been combined with SERS to develop a novel DNA detection mechanism involving the enzyme lambda exonuclease.¹²⁹ The unique catalytic attributes of this enzyme along with its distinct and specific binding properties has made it ideal for use in the study of DNA structure and function.^{121, 130} It was first described in 1967, when J. W. Little and co-workers reported that they had isolated the deoxyribonucleic acid exonuclease induced by the bacteriophage λ in a crystalline and physically homogenous form.¹³⁰ The group were then able to characterise the specific nature of the enzymatic reaction, giving proof that it was in fact an exonuclease, and that it digested DNA from the 5' terminus, releasing 5' mononucleotides, which is unique to this particular enzyme. Additionally, they noted that this enzyme showed a marked preference for 5' phosphorylated DNA, and required the presence of the cofactor Mg^{2+} , for optimum digestion.¹²¹ Other notable experiments, published not long after these initial results, showed that λ -exonuclease cannot degrade DNA from nicks or gaps in a DNA sequence,¹³¹ though it can digest single stranded DNA from the 5' terminus, albeit with much less efficiency.^{131, 132} It was also shown to be a highly processive digestion in that the enzyme remains bound to the DNA strand while it sequentially cleaves roughly 3000 nucleotides at a rate of around 12 nucleotides per second.^{131, 133, 134} The structure of λ -exonuclease was elucidated in 1997.¹³³ It was shown to consist of three protein subunits forming a toroid, with the central channel tapered from an inner diameter of roughly 30 Å to 15 Å. The channel is large enough to accommodate double stranded DNA at the wide end but only single stranded DNA at the narrower end (Figure 1.21). The enzyme fully encloses the substrate, and it is this specific binding mode that accounts for the high processivity seen, as once cleavage is underway the enzyme remains bound until the end of the strand is reached.¹³⁵

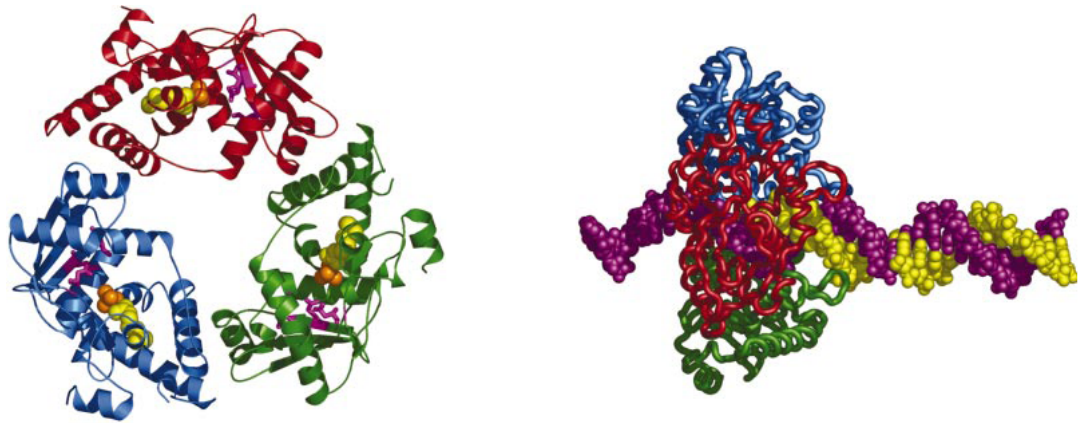


Figure 1.21: Ribbon diagram of the λ -exonuclease structure (left) and a proposed model of λ -exonuclease interaction with DNA (right).¹³⁵

The mechanism of action was not fully understood until Zhang *et al.* recently elucidated the crystal structure of λ -exonuclease in a complex with DNA.¹³⁶ A representation of the proposed digestion mechanism is depicted in Figure 1.22. The structure revealed that the enzyme unwinds the DNA prior to cleavage and two nucleotides at the 5' end of the strand insert into the active site of one subunit, leaving the 3' strand free to exit through the central channel. Additionally, it was noted that the 5' phosphate of the DNA binds to a positively charged pocket at the end of the active site, driving forward the movement of the enzyme and confirming a possible mechanism for processivity at the monomer level.

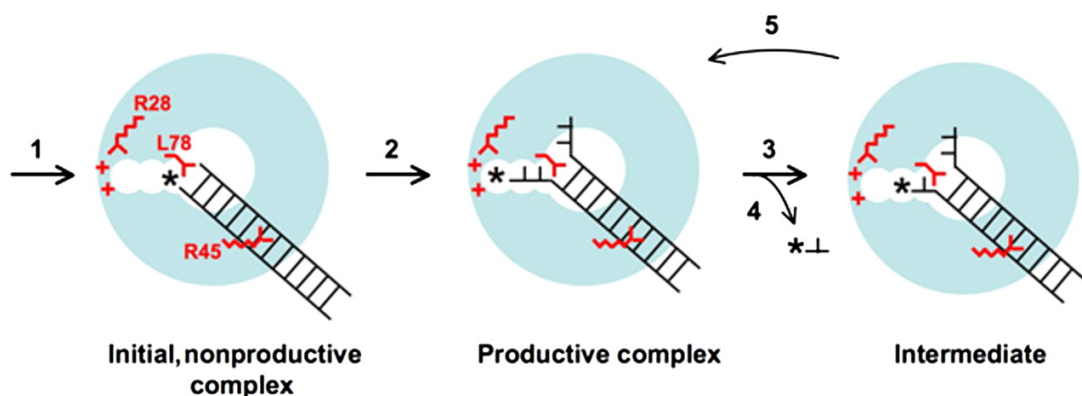


Figure 1.22 A representation of the digestion process as suggested by Zhang *et al.* whereby the 5' strand of DNA enters the active site of one subunit of the toroid.¹³⁶

Unlike Exo-III, λ -exonuclease has not been as heavily reported in relation to signal amplification strategies. However, recently Dougan *et al* successfully utilised this enzyme alongside SERS for the successful detection of a clinically relevant sequence of target DNA.¹²⁹ Figure 1.23 (a) outlines the mechanism for DNA detection through lambda exonuclease aided target cycling.

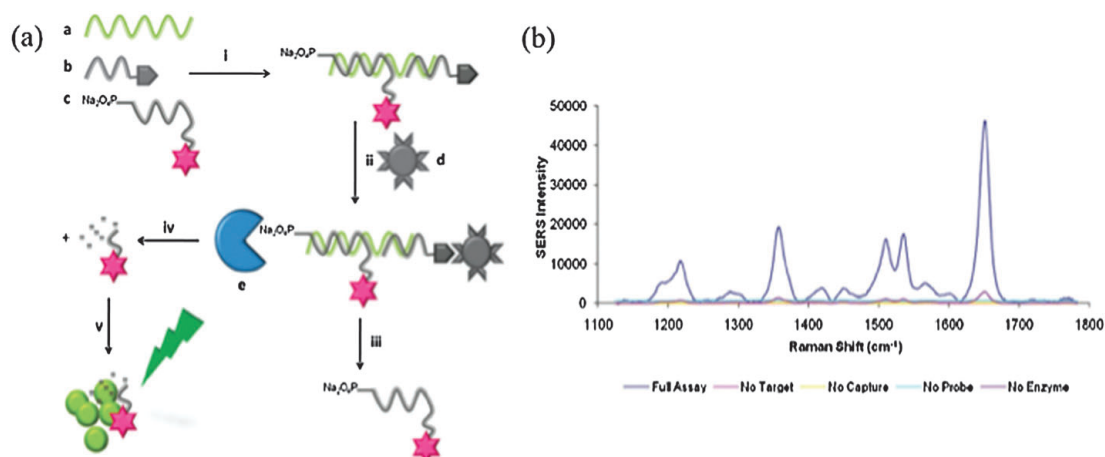


Figure 1.23 (a) Schematic of Exo assay and (b) SERS enhancement when all assay components are present^{98, 129}

In the first step a target sequence of DNA hybridises to a biotinylated 'capture' probe and 5' phosphorylated dye-labelled 'reporter' probe. The duplex is then captured on streptavidin coated magnetic beads via a biotin-streptavidin interaction, and stringent washing steps remove any excess probe. λ -exonuclease is then added to the system, which will digest the reporter probe, only in the presence of target, yielding mononucleotides that were removed from the system and added to silver nanoparticles and spermine for SERS analysis. Figure 1.23 (b) shows that in the presence of all assay components the SERS signal is greatly enhanced. Additionally, due to the specificity of λ -exonuclease for 5' phosphorylated DNA, only the reporter probe will be digested, leaving the target free to repeat the cycle. This assay allowed for the detection of duplex DNA relating to *Chlamydia trachomatis* derived from PCR product, proving the success of λ -exonuclease and SERS in a strategy for signal amplification, and paving the way towards amplification-free DNA detection using enhanced Raman spectroscopy.

1.6 Introductory Conclusions

Molecular biology, and in particular the field of molecular diagnostics, has developed rapidly since the discovery of the double helix in 1953. Notable advances, including the ability to synthesise oligonucleotides and the advent of PCR paved the way for a vast amount of research into the nature of genomic diseases.

Successful assays involving fluorescence detection were developed and then improved by combining these methods with the PCR process to yield quantitative PCR assays with extremely low detection limits and as such, these techniques have dominated the field of DNA detection. They are not, however, free of limitations and both fluorescence spectroscopy and PCR have inherent drawbacks that limit their use in point-of-care diagnosis and in the detection of multiple biomarkers for rapid disease state confirmation.

As a result, alternative detection methods have been investigated in recent years, the most notable of which is the conjugation of oligonucleotides to metallic nanoparticles for simple colorimetric methods of detection that provide PCR-like sensitivity and single-base mismatch discrimination. Additionally, the use of enhanced Raman spectroscopy as an alternative to fluorescence has provided more sensitive levels of detection by a technique amenable to multiplexed analysis.

Thus, the future of amplification-free analysis lies within a combination of these methods, alongside enzymatic target recycling, to provide, simple, sensitive and selective methods of DNA detection for clinical diagnostics.

1.7 Project Aims

The ultimate aim of this project was to develop a novel assay for the detection of target DNA in genomic samples via amplification free analysis and specific enzymatic activity.

Two methods were initially investigated, both involving the digestive enzyme λ -exonuclease. The first of these methods is outlined in Chapter 2 and involves the labelling of synthetic DNA with a donor and acceptor FRET pair for use in fluorescence detection. Chapter 3 involves the conjugation of synthetic oligonucleotides to gold and silver nanoparticles for use in both plasmonic detection and SERRS analysis. Both of these designs utilise the enzyme to provide a method of target cycling in an attempt to detect DNA with PCR-like sensitivity.

The enzymatic action of catalytic DNA is investigated in Chapter 4, as an alternative to conventional protein enzymes. The oxidation of certain peroxidase substrates is monitored using resonance and surface enhanced resonance Raman scattering, and this DNAzyme is incorporated into a catalytic beacon assay design for the detection of target DNA.

Finally, in Chapter 5, metallic nanoparticles are examined as enzyme mimetics and their potential use in analyte detection is investigated.

2. Monitoring the Action of Lambda Exonuclease for the Detection of DNA using FRET

2.1 Introduction

Many popular DNA detection strategies, such as molecular beacons²⁷ and TaqMan probes⁴⁸ utilise the phenomenon of Förster resonance energy transfer or FRET. The main disadvantage of many detection mechanisms that utilise this concept lies within the assay design, which often requires one target DNA molecule per fluorescent probe to exhibit a response, thus limiting the sensitivity. Another disadvantage exists in the need for expensive oligonucleotides labelled with fluorescent donor and acceptor pairs.

2.1.1 DNA Binding Ligands

As an alternative to difficult and expensive labelling methods, DNA intercalators can be utilised as a cheaper and more readily available method of fluorescence detection.³⁶ For example, the intercalator PicoGreen has a high fluorescent output when bound to double stranded DNA in comparison to single stranded DNA,¹³⁷ and has been used for the quantification of pre- and post-PCR samples,¹³⁸ as well as monitoring the activity of certain nucleases.^{36, 139} One of the enzymes investigated using PicoGreen was lambda exonuclease, which will preferentially digest one strand of a DNA duplex, provided there is a 5' terminal phosphate group. The assay employed to characterise this enzyme utilised the double stranded fluorescent activity of PicoGreen, which was able to intercalate into the DNA duplex. Upon action of the enzyme, and digestion of one strand of the DNA duplex, the fluorescent output decreased as the amount of double stranded DNA present was reduced. In addition to being used to monitor the activity of the enzyme, it was suggested that this assay involving PicoGreen could be used for quantitative DNA detection.

Intercalation is not the only way in which small molecules can bind to DNA. They can interact in three principle ways. Firstly, intercalation involves a planar aromatic

ring system inserting between two base pairs, perpendicular to the helical axis. Alternatively, outside-edge binding involves interactions, namely electrostatic, between the ligand and the sugar-phosphate backbone, and finally groove binding is when a ligand makes direct molecular contact with the functional groups on the edges of the bases that protrude into the major or minor grooves, hence the terms major groove binding and minor groove binding.¹²⁰

2.1.2 Hoechst 33258

Amongst the ligands that preferentially bind to the minor groove of DNA are the bis-benzimidazole dyes, specifically Hoechst 33258 (Figure 2.1). This is a synthetic compound containing two consecutive benzimidazole rings with a phenolic and *N*-methyl-piperazine group at either end of the molecule.¹⁴⁰

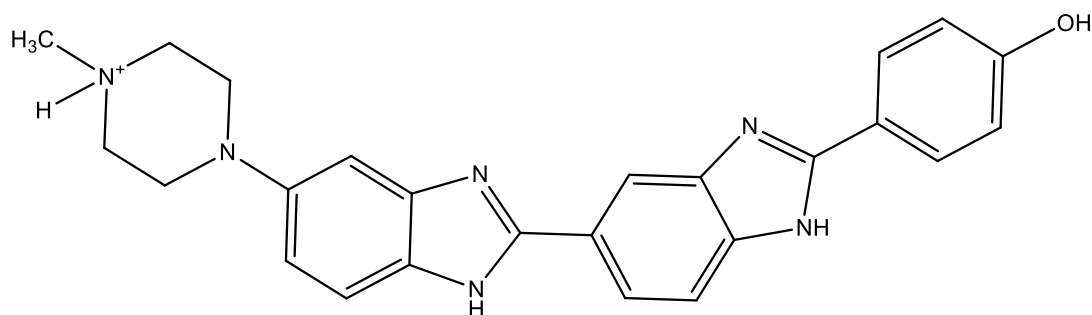


Figure 2.1 The structure of Hoechst 33258.

Due to structural limitations, this dye is unable to intercalate between the base pairs of a helical polynucleotide¹⁴¹, and instead binds to the minor groove of DNA via a combination of hydrogen bonds, van der Waals interactions, and electrostatic interactions.¹⁴⁰ More specifically, Hoechst 33258 (H33258) is reported to bind preferentially at AT-rich regions of DNA, as is the case with most minor groove binding ligands, and has optimum binding over four consecutive A-T base pairs.¹⁴⁰⁻¹⁴² The specificity of this molecule for double stranded DNA means there is a marked increase in fluorescence when bound to a double helix,¹⁴³ thus making H33258 another attractive alternative to labelled oligonucleotides for a fluorescence based detection assay. As such this minor groove binder has been used in a variety of

applications from the detection of single nucleotide polymorphisms,^{144, 145} to the detection of parasites and other microorganisms.¹⁴⁶

2.2 Chapter Aims

The use of H33258 within a FRET system for the detection of target DNA was investigated. Additionally, lambda exonuclease was implemented in this assay design in an attempt to improve upon the sensitivity by introducing a method of target cycling.

2.2.1 The Detection of MRSA

The probe used in the assay design was complementary to a sequence of DNA correlating to the *MecA* gene that codes for the methicillin antibiotic resistance in *staphylococcus aureus*, a bacterium commonly found in the human respiratory tract and on the skin. The emergence of antibiotic resistant forms of *staphylococcus aureus* (MRSA) has led to infections that are inherently more difficult to treat, resulting in a dangerous and potentially life-threatening disease. MRSA is most commonly found in hospitals, where patients with open wounds and lowered immune systems are at a greater risk of infection. As a result, it is of the utmost importance to detect MRSA in a timely manner in order to implement contamination controls, as well as to effectively treat patients diagnosed with MRSA. Currently, the most common methods of detection are via real-time or quantitative PCR, techniques that, although successful, are prone to contamination and false positive results. Additionally, in order for a patient sample to be analysed in this manner, the bacterium must first be cultured in sufficient quantities from biological fluids. This is a time consuming protocol that can only be carried out by highly trained personnel. As such there is a need for novel methods of MRSA detection to be developed, that are simple, rapid and potentially amenable to point-of-care diagnosis.

In order to achieve this goal, research must initially focus on developing extremely sensitive methods of PCR-less DNA detection, and enzymatic methods of target

cycling and signal amplification are novel techniques that have the potential to allow for this sensitivity.

2.2.2 Assay Design

A schematic of the assay developed is depicted in Figure 2.2. H33258 has an excitation and emission wavelength of 350 nm and 460 nm, respectively. This was combined with 6-carboxyfluorescein or FAM, which absorbs at 460 nm and emits in the region of 520 nm. Thus the two are an ideal FRET pair, since excitation at 350 nm will result in an H33258 emission at 460 nm, the absorbance maximum of FAM.

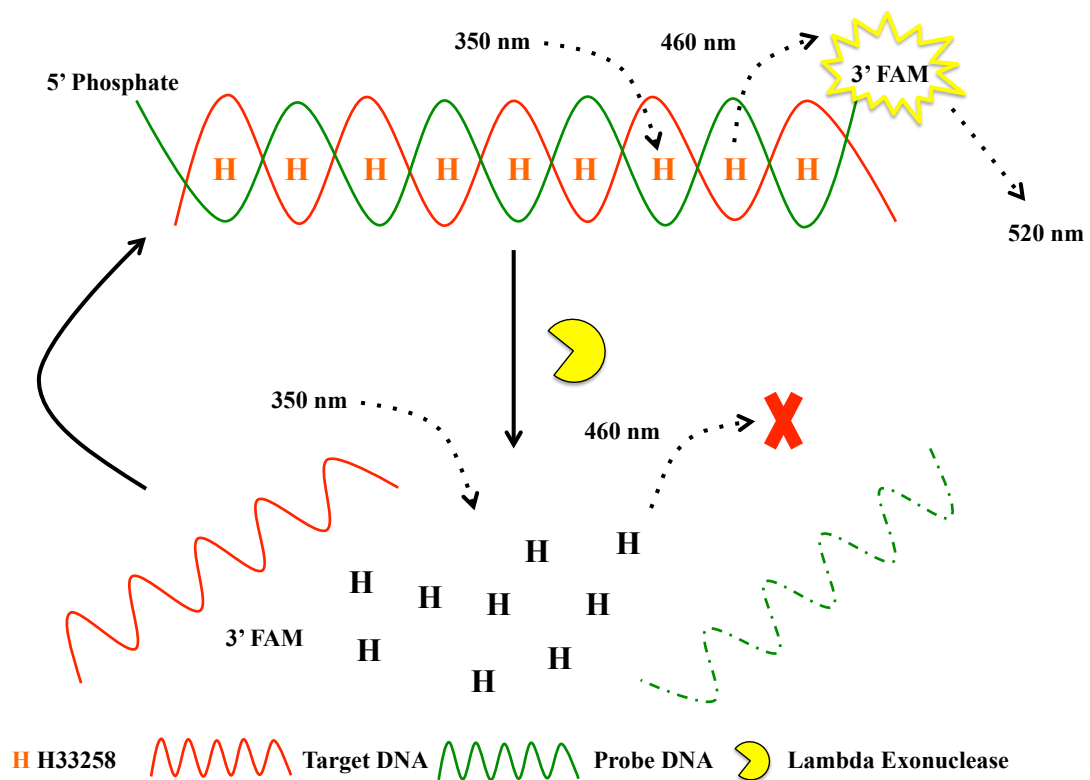


Figure 2.2 The basic mechanism of the FRET based exonuclease assay. A probe with a 3' FAM modification and 5' phosphate modification (green) is allowed to hybridise to a complementary unlabelled target sequence of DNA (red). This will increase the fluorescence emission of H33258 at 460 nm, the energy of which will be transferred to the FAM dye when the two are within the appropriate FRET distance. Upon addition of lambda exonuclease, the probe will be digested, releasing the H33258 that will decrease in fluorescence and be physically separated from its FRET partner, thus reducing the fluorescent signal. The target sequence will remain intact and can be recycled for hybridisation to another probe sequence.

If the system is excited at 350 nm and the fluorescence monitored at 520 nm, upon hybridisation of the target to the fluorescently labelled probe in the presence of H33258, there should be a marked increase in fluorescence, due to energy being transferred from the minor groove binder to the dye.

This increase in fluorescence is itself indicative of hybridisation, however, the limit of detection is confined due to the 1:1 ratio of target and probe needed to produce an observable signal. Introducing a digestive enzyme to a FRET based system has been shown previously to allow for target recycling and hence lower observable limits of detection.¹²³ Therefore, lambda exonuclease was introduced to this system to allow for target recycling in an attempt to improve upon the sensitivity.

The probe was modified at the 5' end with a phosphate moiety to ensure that lambda exonuclease would digest this particular strand of the DNA duplex. Upon digestion, the probe sequence will be reduced to mononucleotides, leaving only the single stranded target sequence. This will reduce the fluorescent output from H33258, and in turn the emission at 520 nm will drop due to the decreased activity of H33258 and also due to the movement of this minor groove binder outwith the FRET distance. Thus, the action of lambda exonuclease can be monitored via a drop in fluorescence at 520 nm. The ability of this enzyme to digest only one strand of a duplex will leave the target sequence free to hybridise with another probe, and the process will be repeated. This means that, in theory, only one strand of target DNA would be needed to allow for digestion of all the probe sequences present in the sample, and thus a method of target recycling would be realised via the action of lambda exonuclease.

2.3 Results and Discussion

The probe used in this assay required a 5' phosphate modification to ensure that this sequence would be preferentially digested, given the enzymes affinity for a phosphate group. This would leave the target sequence free to be recycled within the assay. The probe also required a 3' modification with a FAM fluorophore for use

within the FRET system. The synthetic target sequence of DNA was an unmodified 21-mer coding for the *MecA* gene of an MRSA strain.

In order for lambda exonuclease to exhibit optimum enzymatic activity, a buffer was required that contained the appropriate cofactor, in this case Mg^{2+} . Thus, all initial experiments were carried out in a buffer optimised for lambda exonuclease digestion supplied by New England Biolabs Inc. to ensure the correct fluorescent response could be obtained under these conditions.

2.3.1 Target DNA Detection using FRET

Figure 2.3 confirms the hypothesis that in the presence of a target sequence of DNA the fluorescence emission at 520 nm will increase.

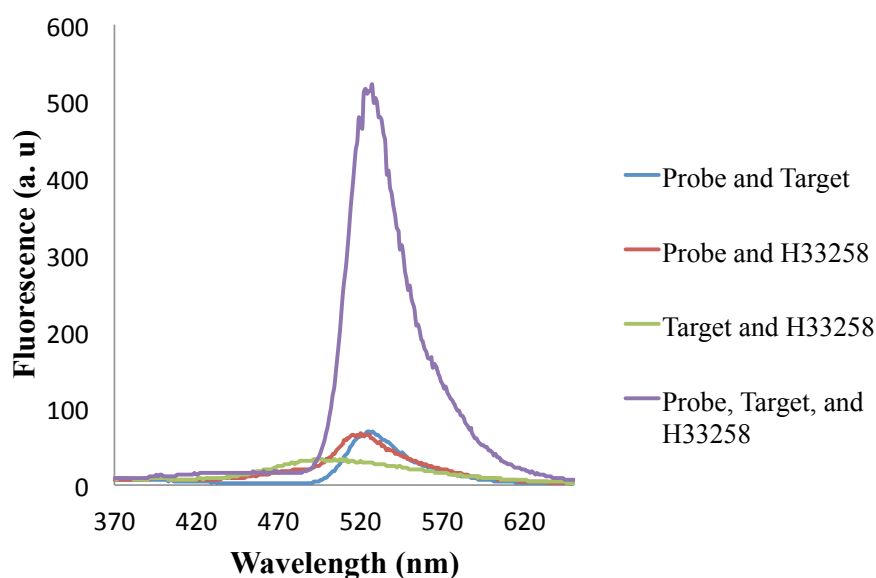


Figure 2.3 Fluorescence profiles of the FRET system and a set of controls upon excitation at 350 nm, with each component at 1 μM final concentration in 1 mL of lambda exonuclease reaction buffer (x1). The probe, target and H33258 sample represents the full assay system (purple), while controls containing probe and target (blue), probe and H33258 (red) and target and H33258 (green) were also analysed.

The probe and target were hybridised in the presence of H33258 in lambda exonuclease reaction buffer, and the fluorescence profile obtained between 370 nm and 650 nm, using an excitation wavelength of 350 nm. Without the FAM labelled probe, the emission maximum occurs in the region of the Hoechst dye at 460 nm

(green line in Figure 2.3). Without the Hoechst present, the emission maximum occurs in the FAM region since FAM can also absorb at 350 nm (blue line in Figure 2.3). When both FAM and H33258 are present, however, it becomes a FRET system. All the energy emitted by the Hoechst upon excitation is transferred to the FAM fluorophore, which is proven by the absence of an H33258 emission peak in the probe and H33258 control, as well as an increase in signal at 520 nm (red line in Figure 2.3). When the target is introduced the signal at 520 nm shows a drastic increase, due to the increased emission of H33258 in the presence of duplex DNA (purple line in Figure 2.3).

As mentioned previously, the observed increase in fluorescence seen in Figure 2.3 is itself an indication of hybridisation and therefore is a successful detection strategy for this particular target sequence. However, this method of DNA detection is by no means novel and FRET has been successfully utilised in a variety of different assay formats for the detection of DNA.³⁷ Therefore, a method of target cycling was introduced to improve upon this FRET based assay in terms of novelty and sensitivity.

2.3.2 Fluorescent DNA Melting Profiles

Upon enzymatic digestion of the probe sequence and disruption of the FRET system, the fluorescent output will decrease, meaning the activity of lambda exonuclease can be monitored via fluorescence spectroscopy. The use of a Strategene MX4000 PCR instrument allowed for precise temperature control over a set period of time, using pre-determined excitation and emission filters. This allowed for DNA hybridisation to be carried out within the instrument by heating the samples to 95 °C and cooling them to 10 °C. Additionally, the temperature control on this instrument was used to ensure that all digestions were carried out at exactly 37 °C, the optimum temperature for enzymatic activity.

Initially, it was important to reaffirm that the probe and target sequences for use within this FRET system were complementary and that they would hybridise under the desired experimental conditions. A DNA melting profile can be used for this purpose and this can be carried out using either UV-Vis or fluorescence

spectroscopy. In this case a fluorescent melt was carried out, whereby an intercalator is used that exhibits an increased fluorescent output in the presence of double stranded DNA. As the temperature is increased during a melt, the duplex separates and the fluorescent output decreases resulting in a sigmoidal curve. From this curve a melting temperature, T_m , can be obtained from the point of inflexion. This is the temperature at which half the sample exists in duplex form and half exists as single stranded DNA. The fluorescent melt was used to analyse the FAM probe and target sequence in the presence of H33258 and served the dual purpose of confirming hybridisation of the probe and target and reaffirming H33258 and FAM as a successful FRET pair (Figure 2.4).

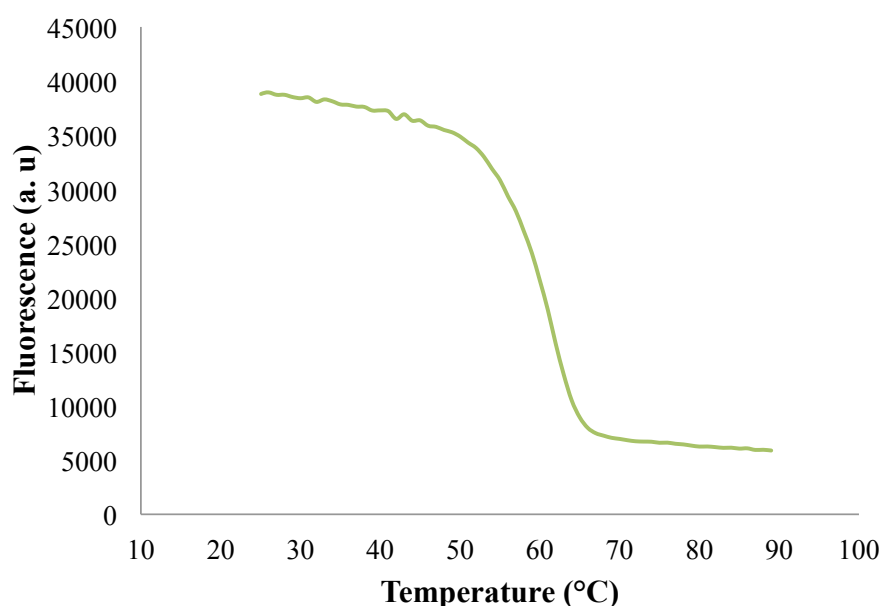


Figure 2.4 Fluorescent melting curve obtained from hybridisation of the FAM-probe and target in the presence of H33258, using 1 μ M each component in 1 mL lambda exonuclease reaction buffer (x1). Excitation and emission was monitored at 350 nm and 520 nm, respectively.

An excitation wavelength of 350 nm was applied and the fluorescent emission measured at 520 nm over a temperature range between 20 °C and 90 °C. As the temperature increases and the DNA strands denature, the H33258 is no longer in contact with double stranded DNA and hence the fluorescent output is reduced. Additionally, the minor groove binder is unable to contribute energy to the excitation of the FAM dye, due to the increase in distance between them, and hence the activity at 520 nm is seen to decrease in a sigmoidal pattern, characteristic of a DNA melting

curve. Figure 2.4 also confirms that at 37 °C, the optimum temperature for enzymatic digestion by lambda exonuclease, the probe and target is a duplex.

2.3.4 Monitoring Lambda Exonuclease Digestion using FRET

Digestion of the DNA duplex was monitored over time on the same instrumentation, again using an excitation wavelength of 350 nm and measuring the fluorescent signal at 520 nm every minute for 30 minutes, while the temperature was held at 37 °C. Firstly, the probe and target were hybridised in the presence of H33258 and this was carried out in two different buffers to try and ascertain the optimum buffer for use in lambda exonuclease digestion.

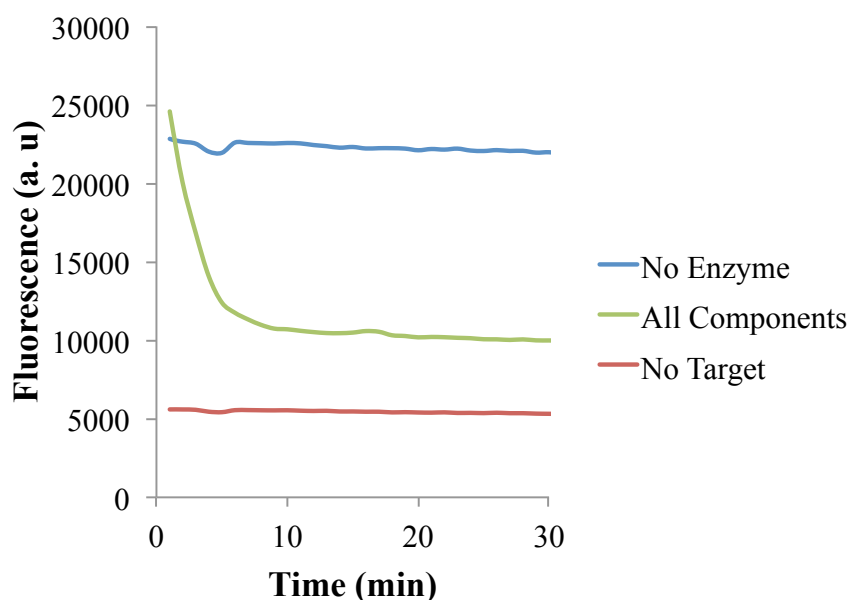


Figure 2.5 Lambda exonuclease digestion profile in the lambda exonuclease reaction buffer supplied. 0.2 μM of FAM-probe and 1 μM of target were hybridised in lambda exonuclease reaction buffer (x1) along with 1 μM of H33258 in a final reaction volume of 150 μL . 20 units of lambda exonuclease was added to the samples which were then excited at 350 nm and the fluorescence monitored at 520 nm every minute for 30 minutes. Control samples with no enzyme (blue) and no target (red) were also analysed.

Although, the buffer provided by the enzyme supplier is synthesised for this purpose, previous work on this topic has shown better enzymatic activity using a borax based buffer with an increased concentration of the desired cofactor.¹⁴⁷ Thus the two buffers investigated were lambda exonuclease reaction buffer containing 67 mM

Glycine-KOH / 2.5 mM MgCl₂, at pH 9.4 and the borax buffer containing 25 mM borax / 25 mM MgCl₂, at pH 9.4. After the hybridisation step, 20 units of lambda exonuclease were added and the digestion monitored. The enzymatic digestion results for the lambda exonuclease reaction buffer are shown in Figure 2.5. The no enzyme control represents a system where λ -exonuclease does not digest the FAM labelled probe, leaving the target and probe hybridised with a high fluorescent output. Conversely, in the no target control, the H33258 does not bind as effectively to the single stranded DNA, and a much lower fluorescent signal is observed. Background fluorescence from the FAM absorbance at 350 nm means this value is not zero. As can be seen from the fluorescent profile in Figure 2.5, the signal intensity decreases over a period of 30 minutes as the 5' phosphate labelled probe is digested leaving only the target sequence intact. The results obtained from carrying out the reaction in 25 mM borax / 25 mM MgCl₂, at pH 9.4 can be seen in Figure 2.6.

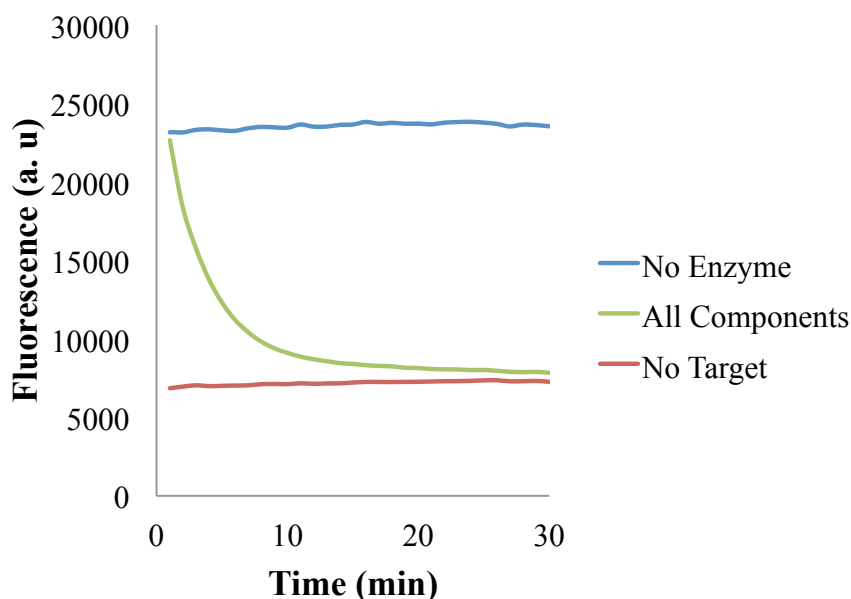


Figure 2.6 Lambda exonuclease digestion profile in a modified borax buffer. 0.2 μ M of FAM-probe and 1 μ M of target were hybridised in 25 mM borax / 25 mM MgCl₂, pH 9.4 along with 1 μ M of H33258 in a final reaction volume of 150 μ L. 20 units of λ -exonuclease was added to the samples which were then excited at 350 nm and the fluorescence monitored at 520 nm every minute for 30 minutes. Controls samples with no enzyme (blue) and no target (red) were also analysed.

Similar results were obtained when using the modified borax buffer compared to the lambda exonuclease reaction buffer. However, in the digestion profile seen in Figure 2.6, the fluorescent intensity decreases from that gained from a duplex, to single stranded DNA, suggesting a more efficient digestion compared to the profile in Figure 2.5 where the fluorescent intensity never reaches that of the single stranded DNA control. Therefore, the 25 mM borax / 25 mM MgCl₂, pH 9.4 buffer was used in all subsequent experiments.

Utilising the minor groove binder H33258, alongside an oligonucleotide labelled with a FAM dye has allowed for the successful detection of target DNA, and the activity of the digestive enzyme lambda exonuclease can be monitored using this FRET system. It is apparent that this method could be used to detect DNA in the absence of lambda exonuclease, as the higher intensity seen for the no enzyme control is indicative of hybridisation to a target sequence. However, the decrease in fluorescence upon lambda exonuclease addition indicates hybridisation of the target to a probe that is modified with a 5' phosphate group, providing an extra level of confidence that the signal seen is from hybridisation of the correct probe and target sequence. In addition, the action of lambda exonuclease, in theory, should allow for the target to be recycled, lowering the sensitivity and potentially eliminating the need for target amplification, and this was further investigated.

2.3.5 Lambda Exonuclease as a Target Cycling Strategy for DNA Detection

Since the assay provided a successful digestion curve in the presence of target DNA, the limit of detection was the next parameter to be investigated. Thus, the concentration of target was varied while other experimental parameters were kept constant and the digestion profile monitored at 520 nm using an excitation wavelength of 350 nm. As the concentration of target was lowered, however, it became more difficult to observe a digestion curve. Decreasing the concentration of target meant that there were less duplex DNA molecules in the sample to which the H33258 could bind, and thus the fluorescence emitted at 520 nm was lower in intensity, and very close to that obtained for single stranded DNA. It became apparent that since this is a negative assay, and fluorescence is reduced as the

enzymatic activity occurs, it may not be possible to prove that the target sequence is being recycled since signal amplification of a quenched assay is not possible.

Nevertheless, a concentration study was carried out to assess whether the addition of lambda exonuclease had a positive effect on the sensitivity of this assay compared to conventional FRET based DNA detection. A series of five replicates for a variety of concentrations between 1 μM and 50 nM were measured.

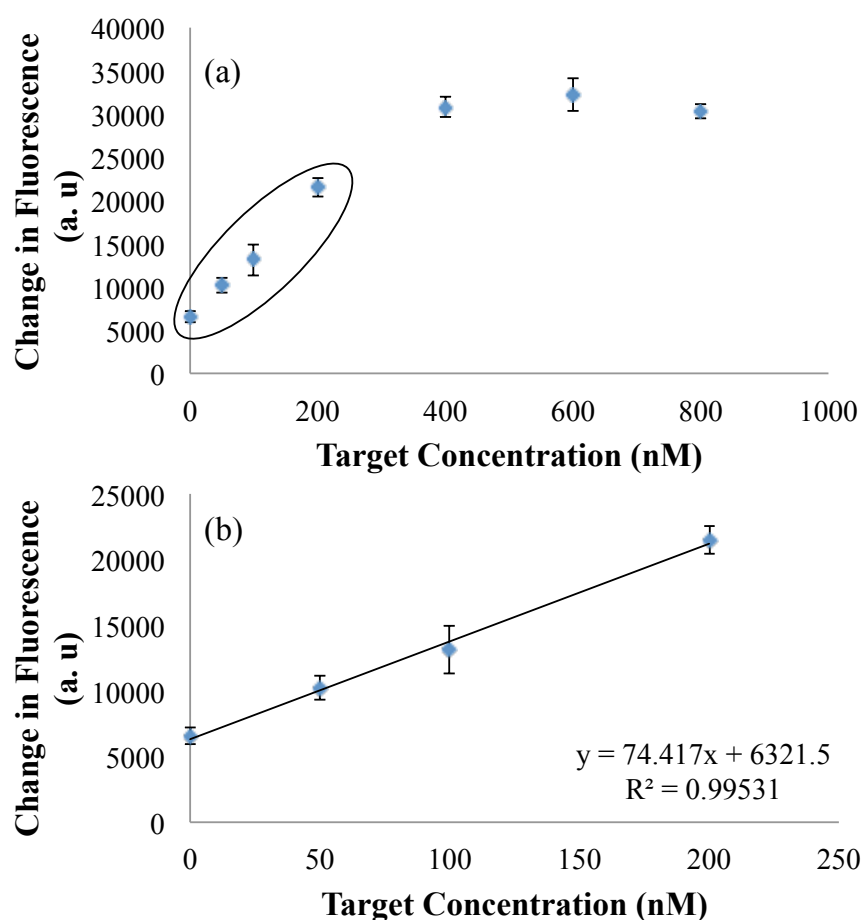


Figure 2.7 Target concentration study using 0.2 μM of probe, 1 μM of H33250 and 20 units of λ -exonuclease with varying amounts of target in 150 μL final volume of 25 mM MgCl_2 / 25 mM Borax, pH 9.4. Excitation and emission was monitored at 350 nm and 520 nm, respectively over 30 minutes and the change in fluorescence was plotted against target concentration. Error bars represent one standard deviation arising from 5 replicate samples.

Since it is a quenching assay, and the fluorescence is reduced upon hybridisation and digestion by lambda exonuclease, the change in fluorescence was calculated for each

concentration. This was done by subtracting the final fluorescent signal of the full assay from the initial fluorescent intensity, and this was plotted against concentration. The results are shown in Figure 2.7. At higher concentrations the change in fluorescence reached a plateau, due to the limited amount of FAM probe available for hybridisation (Figure 2.7 (a)). This was an unexpected result, as with a target cycling strategy all the probe sequences should be digested in the system and not limited by a 1:1 ratio of probe and target. As is seen in Figure 2.7 (b), at lower concentrations of target there is a linear relationship between the change in fluorescence and a target concentration of 50 nM was the lowest that could be observed.

The same result and limit of detection, however, was achieved when the fluorescence intensity was plotted against target concentration. Although, this was a disappointing result, it was not unexpected since this is a negative assay and thus signal amplification will not be possible.

This assay, however, is still a successful method of monitoring target hybridisation via FRET and fluorescence spectroscopy and is also an effective method of monitoring the action of lambda exonuclease. Thus, while attempts at improving the sensitivity of the DNA detection assay were abandoned, this method was used to try and prove that lambda exonuclease could provide a method of target cycling. This was achieved by carrying out digestion studies and after 30 minutes, cycling the temperature between 20 °C and 90 °C. This served the dual purpose of denaturing the enzyme and promoting further hybridisation between the remaining probe sequences and recycled target. By controlling the ratio of target to probe, in theory, after the first digestion step, the target should be recycled and free to hybridise to the remaining probe sequences. Thus, upon the addition of more active enzyme an identical profile to that obtained in the first digestion stage should be obtained.

The results obtained from these experiments, however, were not successful, and upon the addition of more enzyme and continuing to monitor the fluorescence at 520 nm, there was no change in intensity in comparison to the last point obtained from the

first digestion. This suggests that target cycling is not taking place and the ability of lambda exonuclease to provide this effect still remains to be proven.

2.4 Conclusions

It has been shown that the minor groove binder Hoechst 33258 and FAM are a successful FRET pair and can be used to detect a target DNA sequence correlating to the *MecA* gene of an MRSA strain. This FRET pair can also be used as an effective method for monitoring the enzymatic activity of lambda exonuclease on duplex DNA. This FRET assay has allowed for experimental parameters such as buffer conditions, digestion time and individual assay component concentrations to be optimised.

The DNA detection assay reported was unfortunately not amenable to signal amplification due to the fluorescent quenching aspect involved in the presence of target DNA. However, lambda exonuclease has proven to be an effective enzyme for the digestion of one strand of a DNA duplex, and thus it still has the potential to be involved within a target cycling and hence signal amplification method of DNA detection. Therefore, in conclusion, this FRET system has proven itself useful for the optimisation of experimental parameters relating to the activity of lambda exonuclease, however the method of DNA detection required modification in order to incorporate lambda exonuclease into a signal amplification strategy.

3. Amplification Free Detection of DNA by Lambda Exonuclease and SERRS

3.1 Introduction

Since early work by Mirkin and co-workers,⁷⁰ the use of DNA–nanoparticle conjugates as a simple and effective method of DNA detection has become a rapidly expanding area of research. The ability to promote aggregation via a specific hybridisation event, and exploiting the optical properties of gold nanoparticles, has led to the development of a number of sensitive colorimetric methods of DNA detection.

There are two dominant methods of promoting aggregation, crosslinking and non-crosslinking. Most of the literature, including that from Mirkin’s research team, utilises crosslinking aggregation,^{70, 85} however, there are a few examples of non-crosslinking methods.^{68, 148-150} Sato *et al*¹⁴⁸ describes the advantages of using a non-crosslinking method, however highlights the fact that, in comparison to crosslinking aggregation, a much higher concentration of target is needed. This is due to the fact that a number of oligonucleotide molecules are needed to hybridise with the probes on the nanoparticle surface to cause aggregation, and so a target amplification step such as PCR may need to be incorporated. To an extent, crosslinking aggregation is also affected by stoichiometry, since a certain number of target molecules will need to be present to provide the correct number of hybridisation events to exhibit a colorimetric response.

The process of nanoparticle aggregation has been used in a variety of different methods for the detection of DNA involving both gold and silver nanoparticles.^{59, 73, 151} The ability to detect single nucleotide polymorphisms via nanoparticle aggregation has been demonstrated⁷⁷ while detection limits have been obtained that rival the sensitivity of PCR,⁸⁰ without the need for target amplification. PCR-like sensitivity can also be realised via enzymatic signal amplification, which was discussed in Chapter 2.

The combination of DNA-nanoparticle conjugates and enzymatic activity is a relatively new avenue of research whereby the main purpose of exploiting these two factors has been to determine the enzymatic activity of a variety of different nucleases. Alivisatos and co-workers utilised gold and silver DNA-nanoparticle conjugates as a molecular ruler, to determine the length of DNA on the surface, based on the distance between nanoparticles using plasmonic analysis.⁷⁵ The group further extended this work to devise a method of monitoring the activity of certain nucleases using this molecular ruler.¹⁵² Additionally, Mirkin and co-workers devised a method of monitoring both the activity and inhibition of the enzyme DNase I.¹⁵³ Using two batches of DNA functionalised gold nanoparticles complementary to one another, aggregation was apparent in the absence of enzyme or in samples containing a DNase I inhibitor. Upon action of the enzyme the DNA duplex was disrupted, and a colour change from blue to red visualised

Although DNA-nanoparticle conjugates have been successfully used to monitor nuclease activity, literature on the use of these conjugates for DNA detection, particularly in combination with signal amplification, is sparse.

3.2 Chapter Aims

The research detailed in this chapter utilises lambda exonuclease in a slightly different manner to that discussed in Chapter 2. Similarly, the aim of introducing the enzyme is to aid sensitivity by moving away from 1:1 target and probe stoichiometries, by introducing a method of target cycling and hence signal amplification. Herein, however, we combine the properties of the enzyme along with the optical properties of metallic nanoparticles for DNA detection using both colorimetric and SERRS analysis. The basic mechanism of action can be seen in Figure 3.1.

A strand of DNA complementary to a chosen target is conjugated to a metallic nanoparticle. Upon target hybridisation, the double stranded DNA will provide an attractive site for digestion by lambda exonuclease. By incorporating a phosphate modification at the 5' end of the DNA probe, the enzyme will only digest this strand

of the double helix, leaving the target free to be recycled and hybridise with another probe.

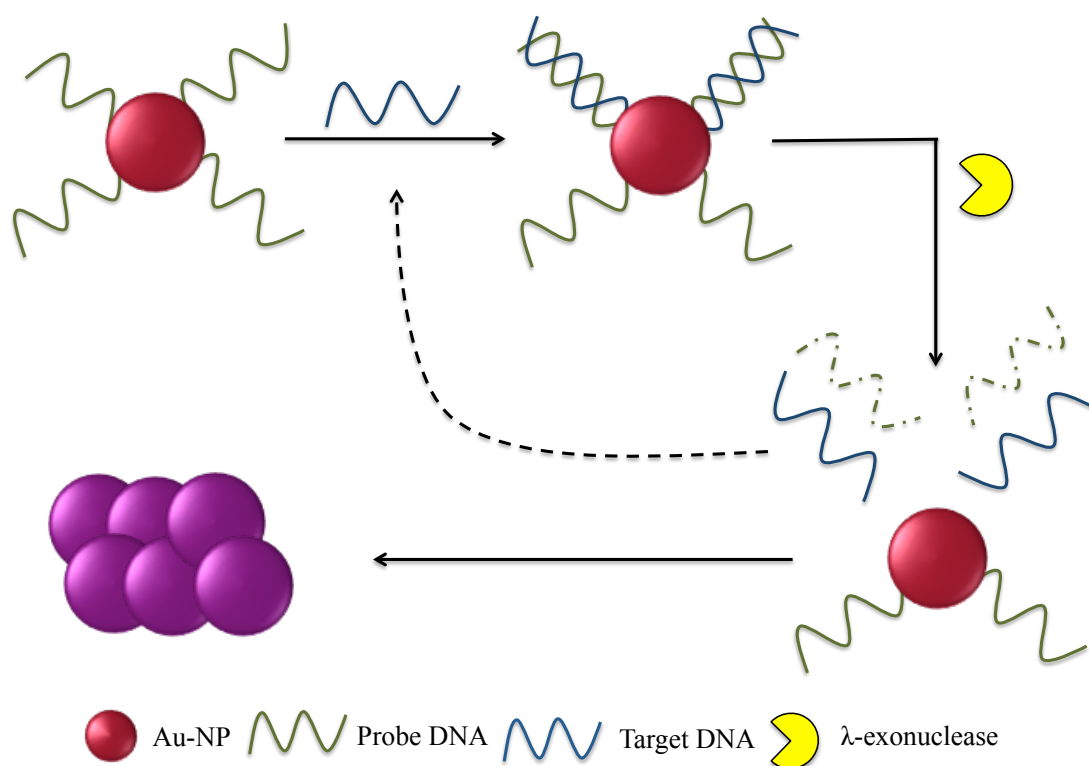


Figure 3.1 Schematic representation of the proposed DNA assay involving the digestion of a gold nanoparticle conjugated DNA probe (green) by the enzyme lambda exonuclease (yellow) in the presence of target DNA (blue).

This process will be repeated until enough DNA is removed from the surface of the nanoparticles to destabilise them under the reaction conditions, resulting in aggregation. Due to the unique properties of gold nanoparticles this process can be monitored using optical spectroscopies, and the aim is to use this aggregation to exhibit an increase in SERRS signal only when the target sequence is present.

As an alternative to this assay format, a crosslinking method of aggregation was also investigated whereby aggregation could be controlled by specific hybridisation events as opposed to destabilisation of the nanoparticles. An outline of this design can be seen in Figure 3.2. Similarly, DNA probes are conjugated to metallic nanoparticles and upon introduction of a target sequence, and subsequent digestion by lambda exonuclease, the target will be free to hybridise to another probe. The

main difference in this assay format lies in the addition of 10 adenine bases to the probe, before the region complementary to the target sequence.

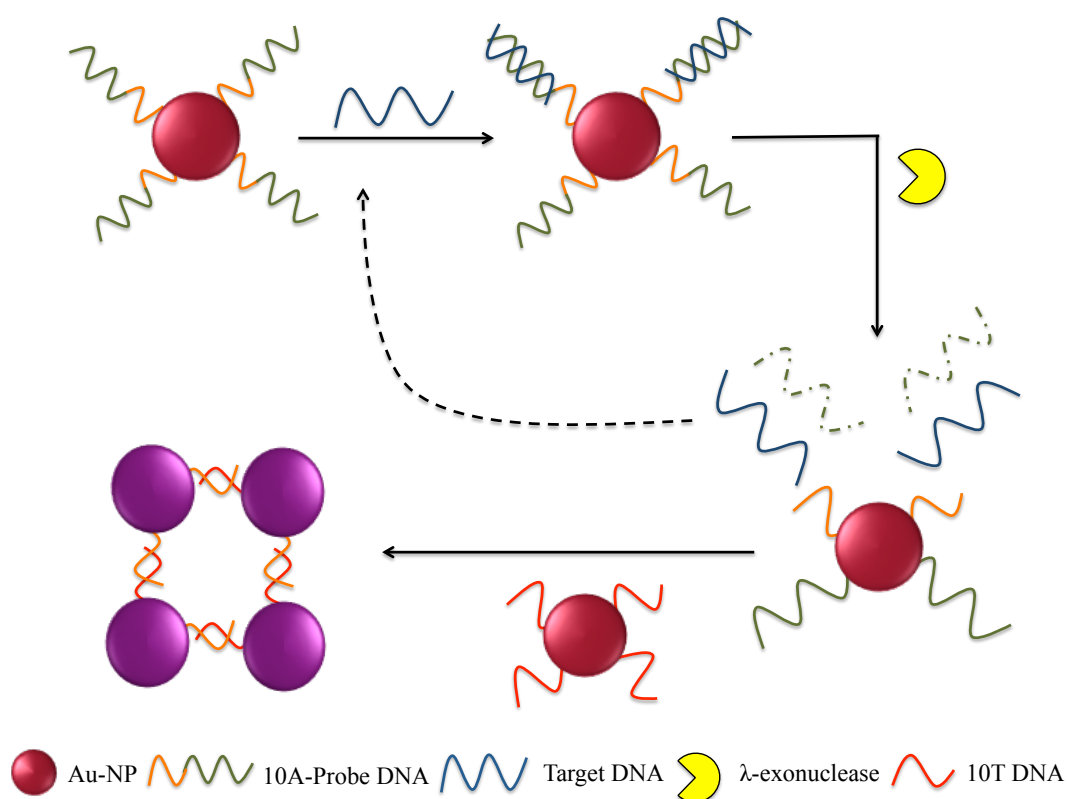


Figure 3.2 Schematic representation of the proposed crosslinking DNA assay involving the digestion of a gold nanoparticle conjugated DNA probe (green) by the enzyme lambda exonuclease (yellow) in the presence of target DNA (blue). This will leave a short 10 A sequence (orange) free to hybridise with a 10 T conjugate (red) causing aggregation of the nanoparticles.

Upon digestion of the double stranded sequence of DNA, the short sequence of adenine repeats will remain conjugated to the nanoparticle. When nanoparticles bearing only 10 thymine bases is introduced to the system, the 10A and 10T regions will hybridise, aggregating the nanoparticles. The addition of a 10A spacer to the probe sequence also provides an extra level of stability to the nanoparticle conjugates by increasing the length of the strand on the nanoparticle, and aids hybridisation by increasing the distance between the nanoparticle surface and the region of the probe sequence complementary to the target, providing a sterically more favourable environment for hybridisation.

In both assay formats, only when the target sequence of DNA is present, will the enzyme digest the probe, leading to aggregation of the nanoparticles. In the absence of target, the lambda exonuclease should have no activity due its preferential binding to double stranded DNA, and the DNA-nanoparticle conjugates should remain stable in solution. The advantage of such an assay lies in the ability of this enzyme to leave one strand of double stranded DNA intact, so that the target sequence can hybridise to another probe, and repeat the digestive cycle. In theory, only one target molecule of DNA should be needed to cause digestion of all the probes conjugated to the nanoparticles, meaning the sensitivity of such an assay could rival PCR.

There were a number of parameters that needed to be investigated in this project. Figure 3.1 and 3.2 detail the use of gold DNA-nanoparticle conjugates, and while the majority of the research described herein utilised these particular nanoparticles, silver DNA-nanoparticle conjugates are also a useful tool, particularly for SERRS analysis. Furthermore, mixed metal systems can be used that combine the stable surface chemistry of gold with the optical properties of silver and this was also investigated. SERRS active dyes were used within this assay, and although they are not detailed in the above schematics, their addition to the nanoparticle conjugates and use in the final analysis step will be discussed. The action of lambda exonuclease upon DNA conjugated to metallic nanoparticles is also an important factor that needed to be investigated, as there is no precedent in the literature.

3.3 Results and Discussion

The first step in this project, involved the synthesis of metallic nanoparticles and the conjugation of DNA to the surface.

3.3.1 DNA-Nanoparticle Conjugates

Metallic nanoparticles were prepared according to standard protocols developed by Turkevitch and Frens for the preparation of gold nanoparticles^{63, 154} and Lee and Meisel for the synthesis of silver colloid.⁸³ Initially the protocol for the preparation of 13 nm gold was followed and later on larger particles were required which were

prepared simply by altering the gold to citrate ratio, in the citrate reduction of gold chloroaurate.

The probe sequence of DNA used in this study consisted of a 21-mer region of DNA complementary to a region of the *MecA* gene of MRSA. In order for lambda exonuclease digestion to occur, this probe was modified at the 5' end with a phosphate group and was also modified at the 3' end with a thiol moiety for attachment to metallic nanoparticles via a soft acid soft base interaction. Conjugation techniques usually employ a thiol bond for this purpose, however Dougan *et al.* developed a method for the synthesis and attachment of thioctic acid (Figure 3.3) to strands of DNA,³⁸ providing a stronger bond and more stable DNA-nanoparticle conjugates.¹¹⁸ It is this attachment protocol that was used in the preparation of conjugates for the development of this exonuclease assay.

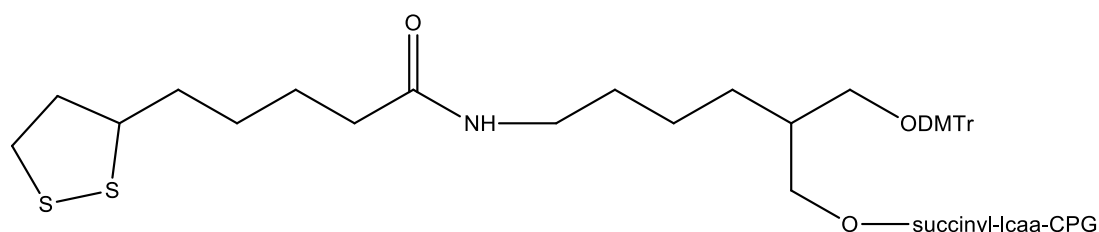


Figure 3.3 Thioctic acid linker for attachment of DNA strands to metallic nanoparticles. Upon oligonucleotide synthesis on a solid support, the trityl group will be removed and each base added in succession in the 3' to 5' direction resulting in the desired 3' thioctic acid modified DNA sequence.

The conjugation process involved the addition of DNA to the chosen suspension of nanoparticles for 24 hours before introducing phosphate buffer to 10 mM final concentration and leaving the sample for another 24 hours. The concentration of DNA used was in the region of 8.6 nmole, however, this was varied throughout experimentation depending on the stability of the sequence requiring conjugation. For example, shorter sequences of DNA, such as the 10T modified nanoparticle for the crosslinking assay, required an increased concentration of DNA to allow for stability throughout the salt ageing process. This stability results from the DNA on the surface of the nanoparticle that contains a negative phosphate backbone. This surface charge will repel the negative citrate layer on the surface of the nanoparticles,

and thus they will be electrostatically prevented from aggregating even in the presence of positive sodium ions. Additionally, the length of the DNA chain can often physically prevent the nanoparticles from aggregating, thus longer chains infer an extra level of stability, explaining why a higher concentration of shorter sequences of DNA are needed to ensure the nanoparticles are stable in solution. After the addition of phosphate buffer the sample was salt aged slowly via the addition of NaCl. This allowed for the reproducible and efficient attachment of DNA to the nanoparticle surface, by screening the repellent charges between nanoparticle surface and DNA backbone. NaCl at a concentration of 2 M was added to the sample in 0.05 M increments to a final concentration of 0.3 M. This was usually carried out over 3 days, as the slower the salt addition process the more DNA strands could be conjugated to the surface. Samples were then centrifuged at 6000 rpm for 20 minutes, the supernatant removed, and the pellets combined and stored at 4 °C. The decision was made early on to deviate from standard protocols whereby the pellet would be re-suspended in PBS buffer. This resulted from an observed increase in long term stability when the conjugate was stored in pellet form, and also due to the different buffers that would be need to be trialled in this assay for optimum digestion by lambda exonuclease.

3.3.2 *Confirming DNA Conjugation*

The ability of nanoparticles to survive the salt ageing process without aggregating is itself indicative of conjugation as the DNA will infer stability to the particles. When a sequence of un-functionalised DNA was subjected to the conjugation protocol, the gold nanoparticles very rapidly aggregated upon addition of the first salt aliquot, while those with a 3' thioctic acid modification survived even extreme salt concentrations. This can be seen visually as is depicted in Figure 3.4, where the left hand vial contains thioctic acid modified DNA and gold nanoparticles at the end of the salt ageing process

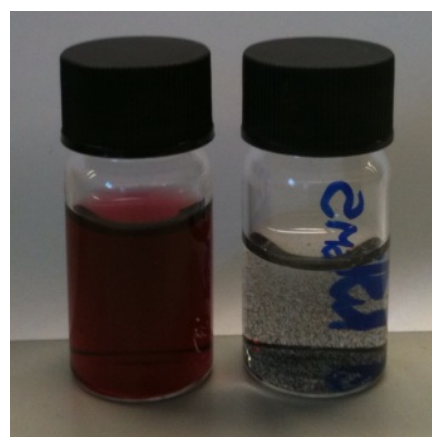


Figure 3.4 13 nm gold nanoparticles with 3' thioctic acid modified DNA (left) and unmodified DNA (right) after salt ageing, showing visual aggregation.

and the right hand vial contains DNA with no such modification and therefore the gold nanoparticles visually aggregated after the addition of 0.05 M NaCl.

This aggregation process can also be monitored using UV-Vis spectroscopy, as a confirmatory technique used to monitor aggregation. Figure 3.5 (a) shows the extinction spectra gained from unmodified silver nanoparticles and those conjugated with a 3' thioctic acid and 5' phosphate modified probe sequence of DNA for use in lambda exonuclease digestion. Similarly, Figure 3.5 (b) shows the extinction spectra of gold nanoparticles and their conjugate counterpart.

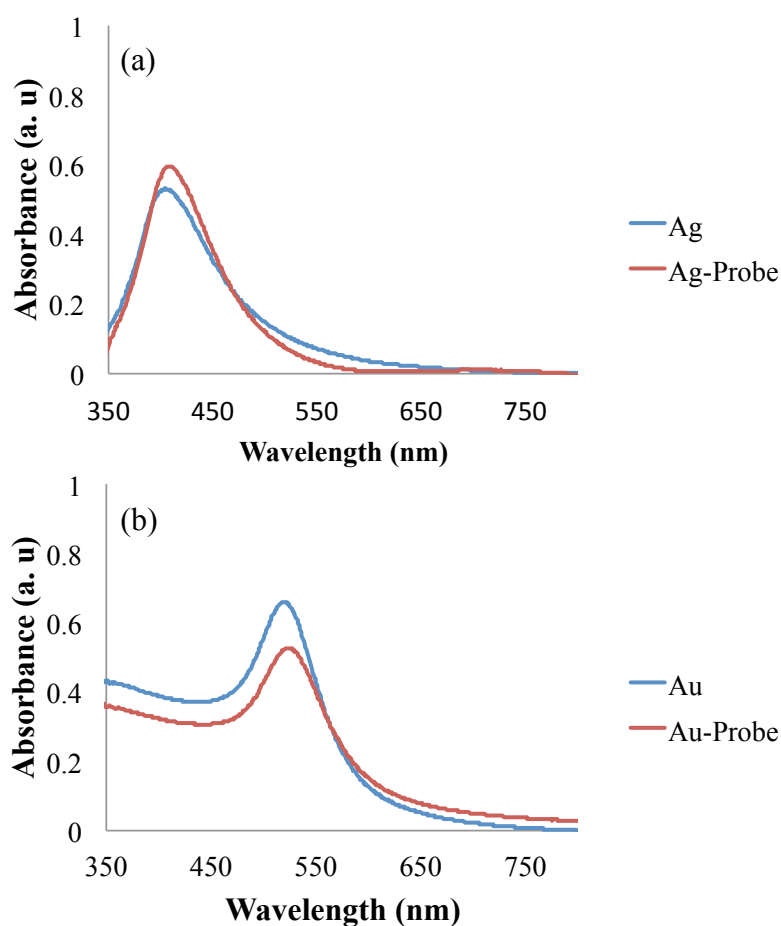


Figure 3.5 UV-Vis spectra comparing (a) 40 nm silver colloid and a DNA-silver nanoparticle conjugate and (b) 20 nm gold colloid and a DNA-gold nanoparticle conjugate

The small shift in the maximum absorbance seen when comparing unmodified and DNA modified gold and silver nanoparticles can be attributed to the change in

dielectric constant and the change in size upon addition of DNA to the surface, resulting in a red shift in the absorbance profile. The slight difference in absorbance seen in both spectra is simply due to the dilution used when comparing bare nanoparticles to the conjugate in pellet form. However, it is not significant enough to be attributed to aggregation and more importantly, there is no increase in absorbance at around 600 nm or 700 nm for the silver and gold conjugates, respectively, and hence it can be deduced that no aggregation has occurred during the conjugation process. The results obtained from UV-Vis spectroscopy provide strong evidence that the colloids are stable and the small shift in wavelength seen in Figure (a) and (b) suggests that DNA is present on the surface of the nanoparticles. However, to add an extra level of confidence, gel electrophoresis can be employed.

Gel electrophoresis is commonly used as a separation method for DNA fragments. Separation is based on the movement of these fragments through agarose or polyacrylamide gel, towards a positive electrode. Since DNA is negatively charged due to the sugar-phosphate backbone, if the positive charge on the electrode is uniform, fragments will move through the gel and can be separated according to size. Smaller DNA fragments will move faster through the gel, while the mobility of the larger fragments will be hindered. Alivisatos and co-workers have utilised gel electrophoresis as a method of determining the conformation of oligonucleotides attached to gold nanoparticles¹⁵⁵ and as a method of isolating discrete Au-DNA nanoparticle conjugates.¹⁵⁶ They also used this technique to quantitatively determine the diameters of the conjugates,⁶⁷ while altering such parameters as the number of bases and the amount of DNA per nanoparticle. Furthermore, the types of interactions between gold and DNA was investigated, and the maximum number of DNA molecules per nanoparticle was determined, all through the use of gel electrophoresis.

Where Alivisatos and co-workers used phosphine coated nanoparticles for their electrophoresis work, the conjugates used herein are citrate-capped, and should not migrate through the gel at all, as they should aggregate immediately in the buffer used if there is no DNA present on the surface to stabilise the particles. Therefore, this can be used as a method of confirming the attachment of DNA to the surface,

and for comparing the length of the DNA strand on the nanoparticle surface. This process can be seen in Figure 3.6, where bare nanoparticles have been compared with two conjugates prepared from different thioctic acid modified sequences of DNA. As expected, the bare gold nanoparticles aggregated before any migration was observed (Figure 3.6, lane 1). The same was seen for the sequence of DNA with no thioctic acid moiety (Figure 3.6, lane 2), but aggregation of this sample had already been observed during the conjugation process.

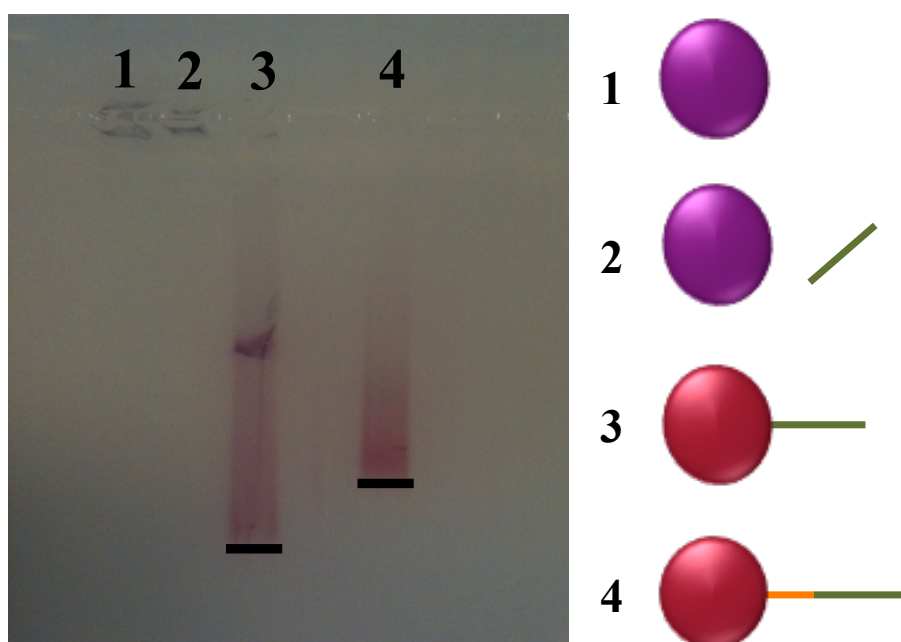


Figure 3.6 Agarose gel electrophoresis comparing bare nanoparticles and conjugates. Lane 1 and 2 show how bare nanoparticles aggregate in the electrophoresis buffer and hence remain in the well, while lanes 3 and 4 show the movement of stable conjugates containing DNA sequences of different lengths through the gel. Lane 3 contains a 21-mer probe sequence and lane 4 contains a 21-mer probe sequence and 10 adenine spacer. 15 μ L conjugate was added to 5 μ L 50:50 glycerol mixture and ran for 1.5 h in TBE buffer (x1).

The DNA conjugates were prepared from sequences modified with a 3' thioctic acid and 5' phosphate modification, the first of which contained only a probe sequence of DNA complementary to the desired target that was to be detected via the lambda exonuclease non-crosslinking assay (Figure 3.6, lane 3). The second conjugate for use in the crosslinking assay described earlier, contains an extra 10 adenine bases on the surface of the particle before the probe sequence (Figure 3.6, lane 4). These conjugates both remained stable in the Tris-Borate-EDTA (TBE) buffer and migrated

through the gel. A notable difference was seen between the conjugate with the 10A spacer, and the conjugate without. This was expected as the oligonucleotide with no spacer is shorter and so moves faster through the gel. Similar results were obtained for silver conjugates. Therefore due to the observations made throughout the conjugation process and the results of the UV-Vis spectroscopy and gel electrophoresis, it can be said with confidence that DNA-gold nanoparticle conjugates and DNA-silver nanoparticle conjugates were successfully synthesised.

3.3.3 Confirming Hybridisation on a Nanoparticle

The next step was to ensure that hybridisation would occur between the desired target sequence and the probe conjugated to the metallic nanoparticle in the buffer conditions required for enzyme digestion. Initially, the complementarity of the probe and target was proven in the absence of nanoparticles using a UV melting profile. The melting temperature, T_m , is the temperature at which half of the DNA in a sample dissociates into single strands. Therefore, below the T_m the majority of the DNA is double stranded, and above the T_m it is mostly single stranded. Since the absorbance at 260 nm of single stranded DNA is higher than that of double stranded DNA, this phenomenon can be exploited alongside UV-Vis spectroscopy to monitor hybridisation. Figure 3.7 represents a typical UV-melting curve, and demonstrates the hybridisation efficiency of the unmodified target with the probe sequence modified with a 3' thioctic acid moiety and 5' phosphate group chosen for this assay.

This DNA melting experiment was carried out in a buffer containing 25 mM borax / 25 mM $MgCl_2$ at pH 9.4, which is a modification of the lambda exonuclease reaction buffer supplied which consisted of 67 mM Glycine-KOH / 2.5 mM $MgCl_2$ at a pH of 9.4. During the FRET experiments discussed in Chapter 2, the borax buffer was proven to exhibit a more efficient digestion compared to the buffer provided by the enzyme supplier for this particular probe and target combination. As such, this buffer was used in all initial experiments concerning the digestion of DNA-conjugates by lambda exonuclease.

The sigmoidal curve seen in Figure 3.7 is characteristic of the transition between double and single stranded DNA, with the point of inflection representing the

melting temperature, T_m . Higher melting temperatures are an indication of a more stable duplex, whereas low melting temperatures may be the result of sequences which are not exactly complementary, or the result of other factors such as sequence modifications.

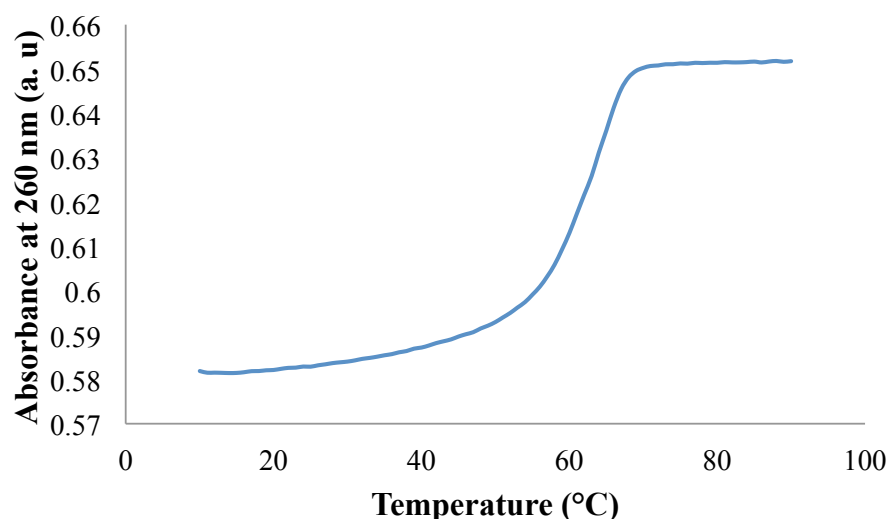


Figure 3.7 UV-Vis melting profile of the modified probe sequence with the target DNA sequence. 0.1 μM of each sequence was used in 400 μL final volume of 25 mM borax / 25 mM MgCl_2 , pH 9.4 and the temperature cycled between 10 $^\circ\text{C}$ and 90 $^\circ\text{C}$ for three ramps while monitoring the absorbance at 260 nm.

For this hybridisation there is a melting temperature of 64 $^\circ\text{C}$ indicating a stable duplex. The same melting temperature was obtained for the probe sequence with and without the 10A spacer. This result was expected as the poly-A sequence should not affect the hybridisation, although this result serves to confirm this theory.

UV-Vis spectroscopy was then used to confirm the hybridisation of probe and target when attached to a nanoparticle. This proved to be more difficult, given that gold nanoparticles, aside from their main absorbance peak at 520 nm have an additional absorbance that will mask the DNA peak at 260 nm. Additionally, since this will not be a crosslinking assay in the first instance, there will be no aggregation and hence a melting profile could not be obtained at 520 nm. This was reflected in the results obtained, however monitoring the absorbance at 520 nm over such a large temperature range did allow us to confirm that these conjugates are stable even at

extreme temperatures, and more importantly are stable at 37 °C, the optimum temperature for enzyme digestion.

Gel electrophoresis was therefore implemented as an alternative method of monitoring hybridisation, the idea being that a DNA duplex will migrate through the gel slower than a single strand (Figure 3.8). As seen before, Au-10A-Probe (Figure 3.8 lane, 1 and lane 2) did not travel as far through the gel as the Au-Probe (Figure 3.8, lane 3 and lane 4), irrespective of target addition. When target DNA was added to both Au-Probe and Au-10A-Probe, this addition did appear to hinder the movement through the gel, as can be seen in Figure 3.8 lanes 2 and 4, and this can be attributed to the presence of a duplex on the surface of the nanoparticle, confirming hybridisation of a target has taken place

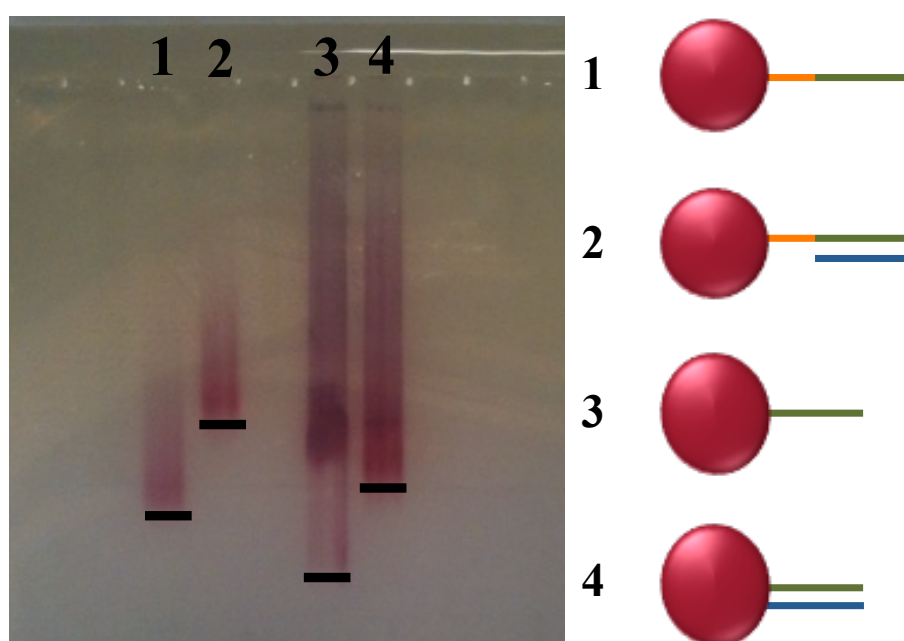


Figure 3.8 Agarose gel electrophoresis confirming hybridisation on gold nanoparticles. Lane 1 contains Au-10A-Probe, and lane 2 contains Au-10A-probe and target. Lane 3 contains Au-Probe and lane 4 is Au-probe and target. Samples were hybridised at room temperature in 25 mM borax / 25 mM MgCl₂, pH 9.4 then 15 µL sample was added to 5 µL of a 50:50 glycerol mixture and the gel ran for 1.5 h in TBE buffer (x1)

Thus, it can be concluded from both UV-Vis spectroscopy and gel electrophoresis that the target and the probe sequence of DNA for use in the lambda exonuclease

assay are complementary and that the target is able to hybridise with the probe when conjugated to a gold nanoparticle.

3.3.4 Investigating the Use of an Aggregator

Since there are two variations of the lambda exonuclease assay to be trialled, one of which is a crosslinking assay, it was important to assess the effect of introducing an ‘aggregator particle’, which consisted of 10 thymine bases conjugated to a metallic nanoparticle. This particle would be introduced after lambda exonuclease digestion of the Au-10A-Probe, when only the 10A spacer should remain on the surface. Thus, the remaining Au-10A and Au-10T should aggregate confirming target hybridisation and digestion. The only way to confirm the success of the non-crosslinking assay was to trial it in full, and the results shall be discussed later in this chapter. However, we can predict the outcome of the crosslinking assay, whereby the Au-10A and Au-10T should aggregate in solution. Therefore a control conjugate of Au-10A was prepared alongside the ‘aggregator particle’ and a number of techniques were trialled to gain an idea of the results that could potentially be obtained from this assay design.

3.3.4.1 Colourimetric Detection

Upon hybridisation of a target sequence of DNA to a nanoparticle conjugated DNA probe, and subsequent lambda exonuclease digestion, the remaining products of this assay should be an intact target which can hybridise to another probe, and a metallic nanoparticle with 10 adenine bases conjugated to the surface. Thus, upon introduction of a nanoparticle with 10 thymine bases conjugated to the surface, aggregation should occur (Figure 3.2). In order to continue with this assay, it was first important to assess that this was in fact the case and this was initially assessed visually and using UV-Vis spectroscopy. A control gold conjugate was prepared bearing a 10A sequence (Au-10A), which imitates the potential end product of digestion. This was added to the ‘aggregator particle’ (Au-10T) in the borax buffer needed for digestion, and an immediate colour change was observed which could be determined visually and spectroscopically (Figure 3.9), suggesting the Au-10A and Au-10T had hybridised as expected.

This is an ideal result as the aggregation due to the hybridisation between the Au-10A conjugate and the Au-10T conjugate is very apparent, both visually and by a considerable red shift in the extinction spectrum.

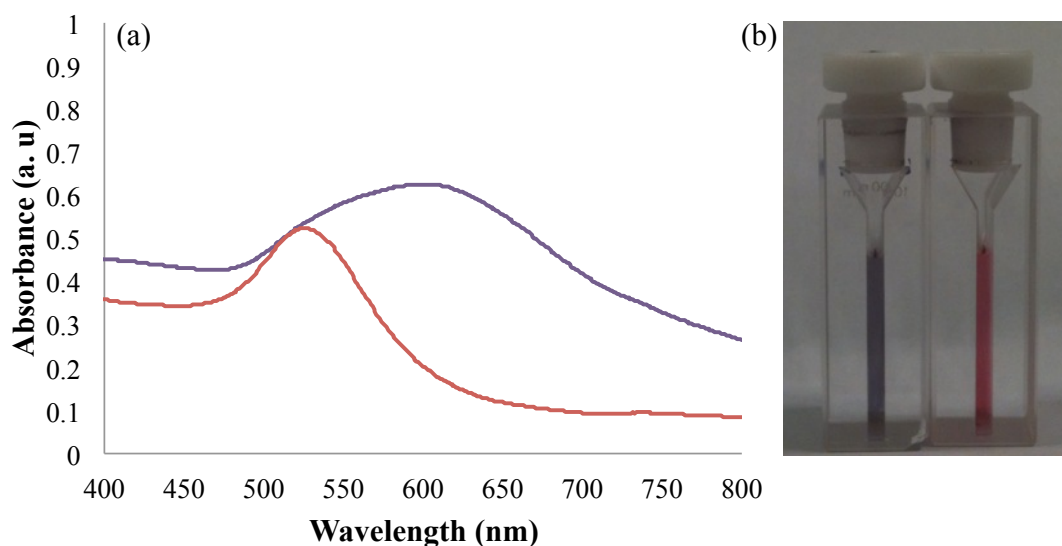


Figure 3.9 Determining aggregation (a) using extinction spectra where aggregation is apparent between Au-10A and Au-10T (purple) while Au-10A-Probe and Au-10T (red) remain stable in solution. (b) Visual detection of aggregation between Au-10A and Au-10T (left) compared to the stable solution of Au-10A-Probe and Au-10T (right). 1 nM of each conjugate was used in a final volume of 400 μ L 25 mM borax / 25 mM MgCl₂, pH 9.4.

Additionally, there is no aggregation between Au-10T and Au-10A-Probe, which represents a system where there has been no target introduced and hence no digestion. Thus, only in the presence of target and subsequent digestion should a colour change be seen.

This aggregation can be used to obtain a DNA melt for the Au-10A and Au-10T system since the absorbance at 520 nm will increase as the duplex denatures resulting in separation of the nanoparticles (Figure 3.10). This method was used to obtain a T_m of 30 °C for the gold conjugates. This demonstrates that these conjugates are not as stable as the probe and target duplex, which was expected given the shorter DNA sequences involved, and that at 37 °C, the majority of conjugates will not be hybridised.

Thus, from these experiments the hybridisation of the Au-10A final digestion product and Au-10T ‘aggregator particle’ has been confirmed, and a T_m of 30 °C has been obtained, meaning this crosslinking assay must involve a cool down step to allow for hybridisation between the Au-10A and Au-10T before any analysis can take place.

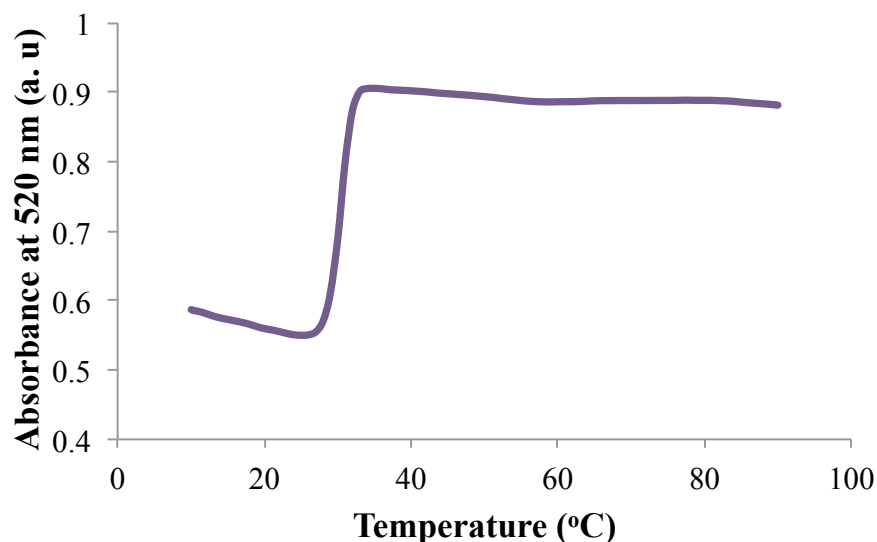


Figure 3.10 UV-Vis melting curve of Au-10A and Au-10T monitored at 520 nm. 1 nM each conjugate was analysed in a final volume of 500 μ L 25 mM borax / 25 mM $MgCl_2$, pH 9.4 over a temperature range of between 10 °C and 90 °C. 4 temperature ramps were carried out and the average given.

3.3.4.2 SERRS Analysis

It has been shown that the crosslinking assay has the potential to be monitored using plasmonics, however, the aim of this research was to ultimately develop a novel assay using surface enhanced resonance Raman scattering. Therefore, it was deemed necessary to also investigate the aggregation of the Au-10A and Au-10T conjugates using SERRS. For this purpose, a Raman active dye was needed to label the conjugates. The dye chosen must have an absorbance close to a Raman excitation wavelength to obtain resonance Raman scattering, and must have a structure with functional groups that are amenable to conjugation onto metallic nanoparticles. Thus, malachite green isothiocyanate (MG-ITC) was chosen, the structure of which can be seen in Figure 3.11. Malachite green is a non-fluorescent molecule with an absorbance maximum around 630 nm, and can thus be used in conjunction with a 633 nm laser excitation wavelength for SERRS analysis. The thiocyanate group

present on this particular form of the dye allows for attachment to metallic nanoparticles, in particular gold, via the same mechanism as thiolated DNA.

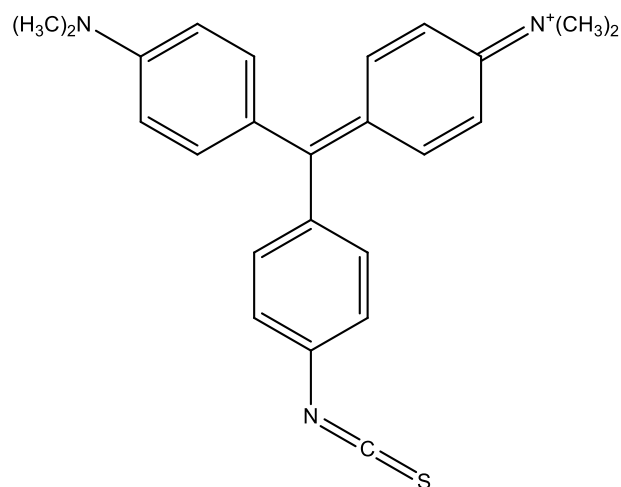


Figure 3.11 The chemical structure of malachite green isothiocyanate.

In the preparation of dye-labelled conjugates for the crosslinking assay format, the malachite green was attached only to Au-10T. The 10T sequence of DNA was initially attached via the protocol previously described, then a 1×10^{-7} M solution of the dye was added to the conjugate in a 1:1 ratio and left for 1 hour with constant stirring. The sample was then subjected to a centrifugation step to remove any excess malachite green that was not attached to the conjugate surface. This was then ready for SERRS analysis.

The Au-10A and Au-10T-(MG-ITC) conjugates were hybridised and analysed by SERRS, to determine the effect their aggregation would have on the spectra obtained. Additionally, silver conjugates were trialled as well as a mixed metal system, and the results can be seen in Figures 3.12 and 3.13. Figure 3.12 shows the results obtained from the gold conjugates and a mixed metal system. Since the dye is only present on the aggregator particle, there is very little signal obtained from the Au-10A and a large signal obtained from the Au-10T-(MG-ITC). It would be expected that hybridisation of the 10A and 10T sequences would result in aggregation and that the signal would be enhanced beyond that obtained from the 10T conjugates due to the formation of 'hotspots' between the nanoparticles. This however, is not the case and the signal obtained from the gold system only reflects

that of the Au-10T-(MG-ITC) conjugate. Even more disappointing is the drop in signal seen for the mixed metal system compared to the Ag-10T conjugate.

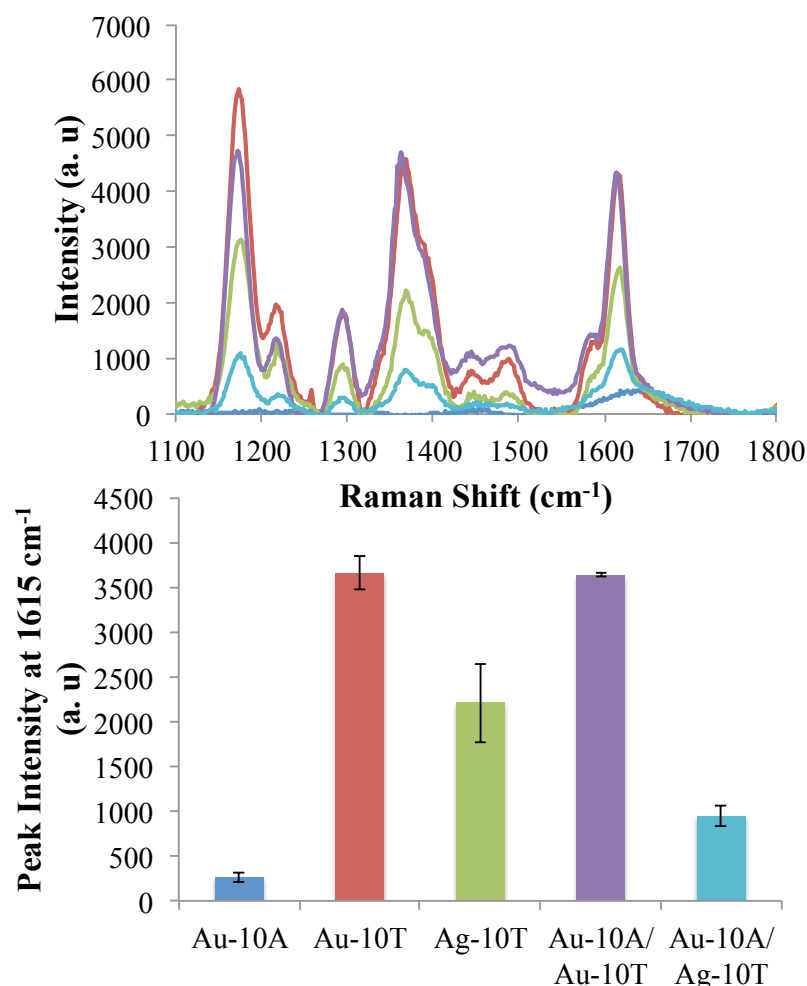


Figure 3.12 The SERRS results from Au-10A (blue), Au-10T-(MG-ITC) (red), Ag-10T-(MG-ITC) (green) and the mixed systems of Au-10A / Au-10T-(MG-ITC) (purple) and Au-10A / Ag-10T-(MG-ITC) (aqua). 3 μ L of each conjugate was hybridised in 200 μ L of lambda exonuclease reaction buffer (x1) and then analysed at a laser excitation wavelength of 633 nm at 4 mW power. 1 x 10 second accumulation was taken and each samples was scanned 5 times. The results were baseline corrected (top) using Grams software and the peak height at 1615 cm^{-1} obtained (bottom) from the uncorrected data.

The peak height at 1615 cm^{-1} was also analysed (Figure 3.12 (b)), and the results were in agreements with those from the spectra. This particular peak was chosen as it was of the greatest intensity during preliminary experiments involving malachite green isothiocyanate, and for continuity purposes was used in all subsequent experiments.

It is possible that hybridisation was not occurring, although, given the previous colourimetric results, this would be unlikely. The change in signal seen for the mixed metal system, albeit a drop in signal, perhaps alludes to the fact that there is some change happening upon hybridisation of these complementary conjugates. Therefore, it seems more likely that over-aggregation of the particles is occurring, and that they are precipitating out of solution and the nanoparticles are no longer within the interrogation beam of the laser.

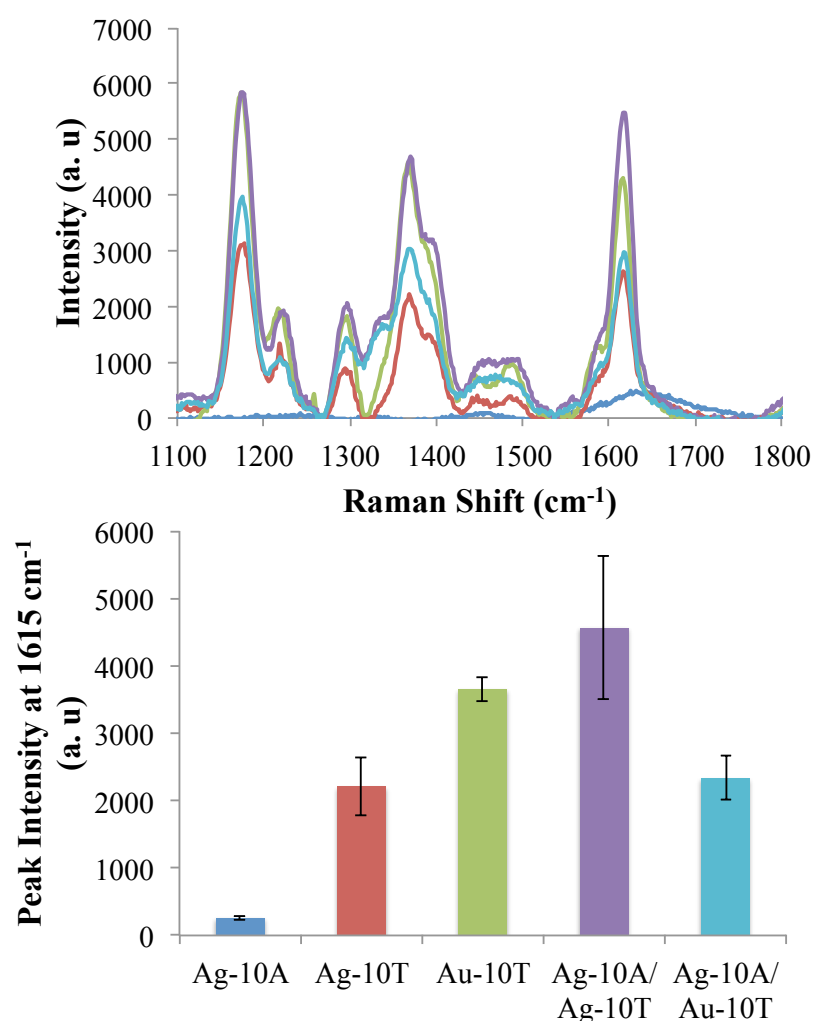


Figure 3.13 The SERRS results from Ag-10A (blue), Ag-10T-(MG-ITC) (red), Au-10T-(MG-ITC) (green) and the mixed systems of Ag-10A / Ag-10T-(MG-ITC) (purple) and Ag-10A / Au-10T-(MG-ITC) (aqua). 3 μ L of each conjugate was hybridised in 200 μ L of lambda exonuclease reaction buffer (x1) and then analysed at a laser excitation wavelength of 633 nm at 4 mW power. 1 x 10 second accumulation was taken and each samples was scanned 5 times. The results were baseline corrected (top) using Grams software and the peak height at 1615

The results obtained for the silver conjugates were slightly more promising (Figure 3.13). Unlike the gold conjugates, DNA conjugation onto silver nanoparticles proved to be much more challenging, in particular for the short 10A and 10T sequences. The pale colour of the silver conjugates compared to gold, made them less useful for analysis by gel electrophoresis, and the UV-Vis results from 10A and 10T hybridisations were not reproducible. Thus, using the control conjugate of Ag-10A alongside the labelled Ag-10T-(MG-ITC) and SERRS analysis was the best potential way of confirming hybridisation. As expected the Ag-10A has a low signal, while the Ag-10T-(MG-ITC) and Au-10T-(MG-ITC) provide an intense signal. The Ag-10A and Ag-10T-(MG-ITC) system shows an increase over the Ag-10T-(MG-ITC) signal, which is a promising result. The mixed metal system, however, mimics the result obtained in Figure 3.12, where there is a signal drop between the Au-10T-(MG-ITC) and the Ag-10A/ Au-10T-(MG-ITC) mix.

The results obtained from SERRS analysis of the control conjugates were not as expected. In particular, for the mixed metal systems, although it appears there is a change upon hybridisation, it manifests itself as a drop in signal as opposed to an increase, most likely due to a precipitation out of solution. These preliminary results indicate that, for the crosslinking assay gold conjugates would be best suited to plasmonic-based analysis, while the silver conjugates provided promising SERRS results that could hopefully be reflected in the full assay trials.

3.3.5 Full Assay Trials using Plasmonic and SERRS Analysis

Once the conjugates had been successfully synthesised and it could be said with some confidence that the desired probe and target sequence were complementary and would hybridise on the surface of a nanoparticle, both the crosslinking and non-crosslinking assay were attempted.

3.3.5.1 Plasmonic Analysis

Given the success of colorimetric detection for monitoring the aggregation between the 10A and 10T products, initial trials mainly involved the use of UV-Vis spectroscopy to monitor the change in the surface plasmon over the course of the

assay. The probe and target were hybridised in both lambda exonuclease reaction buffer and the modified borax buffer before the addition of the enzyme. The samples were incubated at 37 °C overnight while the extinction profile was obtained every 10 minutes. This was also carried out using the 10A-probe, which was hybridised to the target in the presence of the 10T conjugate before the addition of enzyme. Initial results, however were not promising and no aggregation could be seen either visually or spectroscopically for the silver or gold conjugates analysed.

An example of the results obtained is depicted in Figure 3.14, whereby the absorbance was measured between 200 nm and 800 nm at 37 °C overnight to monitor the effect of digestion on the surface plasmon band.

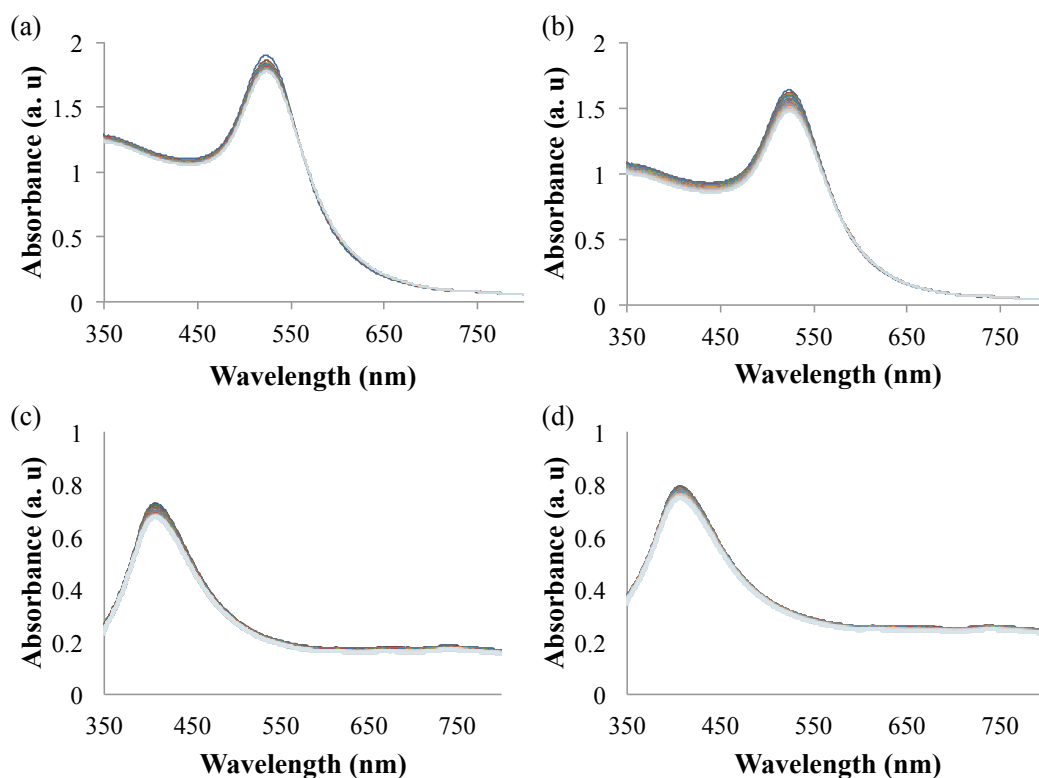


Figure 3.14 Overnight digestion studies measuring the absorbance every 10 minutes for a total of 960 minutes at 37 °C. (a) 5 nM Au-10A-Probe and 5 nM Au-10T-(MG-ITC) were hybridised with 5 µM of target in 400 µL of lambda exonuclease reaction buffer (x1). 10 µL of λ-exonuclease was added and the program started. (b) The same conditions were applied as for (a) but no target was added. (c) 5 nM of Ag-Probe was hybridised with 5 µM target in 400 µL of lambda exonuclease reaction buffer (x1) before 4 µL of enzyme was added and the program started. (d) The same conditions were applied as for (c) but no target was present.

Figure 3.14 (a) and (b) represent the gold crosslinking assay and Figure 3.14 (c) and (d) represent the silver non-crosslinking assay. There is no significant change in absorbance at 520 nm for the gold conjugates or 400 nm for the silver conjugates upon hybridisation of the target and subsequent digestion by lambda exonuclease. This result was obtained a number of times for both the crosslinking and non-crosslinking assays using both sets of conjugates and mixed metal systems. Thus, a number of optimisation experiments were carried out using UV-Vis spectroscopy as the main method of analysis. One explanation for the lack of response from the enzyme was that the sterics of the system was hindering lambda exonuclease digestion, and that the strands of DNA were too tightly packed on the surface for efficient digestion to occur. Based on the concentration of colloid used and the number of DNA molecules added during the conjugation process, there is the potential to be 172 strands of DNA on each nanoparticle. Accounting for the space available and inefficient conjugation, the actual number of strands is likely to be much less than this number. However, tight packing of the DNA was thought to be a potential problem to overcome. Additionally, the size of the enzyme in comparison to the nanoparticles could also be a potential problem, especially when using the smaller gold nanoparticles at 20 nm, and this was also investigated by carrying out digestions on 40 nm gold and silver conjugates.

As such, both assays were compared while investigating a number of variables including the use of surface spacers, different enzyme concentrations, and the order of component addition. The use of polyethylene glycol (PEG) as a surface spacer was investigated due to its larger size compared to the DNA strands. However, this was unsuccessful, and so a 10A spacer was trialled. This served the dual purpose of spacing out the probe sequence to aid hybridisation and digestion, and in the crosslinking assay provide more sites for hybridisation with the 10T conjugate. However, this was also unsuccessful, even though a number of ratios of probe to spacer were investigated. The concentration of enzyme used was decided upon according to the information provided by the supplier, New England Biolabs, from which a 5000 unit / mL stock concentration of lambda exonuclease was obtained. One unit is defined as the amount of enzyme required to produce 10 nmole of soluble deoxyribonucleotide from double-stranded DNA in 30 minutes at 37 °C. Thus it was

calculated that 1 μL , or 5 units, of DNA and an overnight digestion would be an ideal experimental setup, providing enough enzyme and a longer timescale for digestion. However, this was not the case, as no evidence of digestion was apparent via aggregation of the nanoparticles. Thus, the concentration was increased to a maximum of 10 μL or 50 units, and decreased to a minimum of 0.5 μL or 2.5 units. However, no change in the results was obtained. The order of addition of the 10T 'aggregator particle' was also investigated, as it was thought this additional conjugate could be interfering with digestion. The 10T conjugate was therefore added after the overnight digestion in a number of experiments and the samples subjected to a heating and cooling step to promote hybridisation, however, no aggregation was observed. Other variables that were investigated throughout the optimisation process included experimentation with the buffer used and the concentration of the co-factor MgCl_2 . Also the use of larger gold particles within the assay was investigated to again try and combat steric hindrance, and the 20 nm gold nanoparticles used initially were replaced by 40 nm gold nanoparticles.

A successful result was finally obtained using a 40 nm gold crosslinking assay with the MG-ITC labelled Au-10T, along with a probe sequence that incorporated a hexaethylene glycol (HEG) spacer group between the 10A region of the probe sequence and the region complementary to the target. The aim of this 10A-HEG-Probe was to try and stop digestion by lambda exonuclease before the 10A sequence. In theory, lambda exonuclease should only digest double stranded DNA, and should stop of its own accord upon reaching the poly-A region, which has no complement and should exist as a single strand on the surface of the nanoparticle after digestion. However, although lambda exonuclease has a greater enzymatic activity on double stranded DNA, single stranded digestion will still occur. It was hypothesised that upon digestion of the entire stand of DNA, lambda exonuclease could stabilise the nanoparticles once it was in close contact with the surface, explaining the adverse results seen. As a result of this, the non-crosslinking whereby the entire strand would be digested was abandoned and the HEG spacer group introduced to the 10A-probe for use within the crosslinking assay. Thus, the enzyme should be physically prevented from digesting onto the surface of the nanoparticle, leaving the 10A free to hybridise with the 10T after digestion, resulting in aggregation of the nanoparticles.

Figure 3.15 shows the successful results obtained using a decreased sample volume, lambda exonuclease reaction buffer (x1) and 4 μL of enzyme. The aggregation can be monitored both visually and spectroscopically, as a red to purple colour change is seen upon action of the enzyme, which is accompanied by a decrease in absorbance at 520 nm.

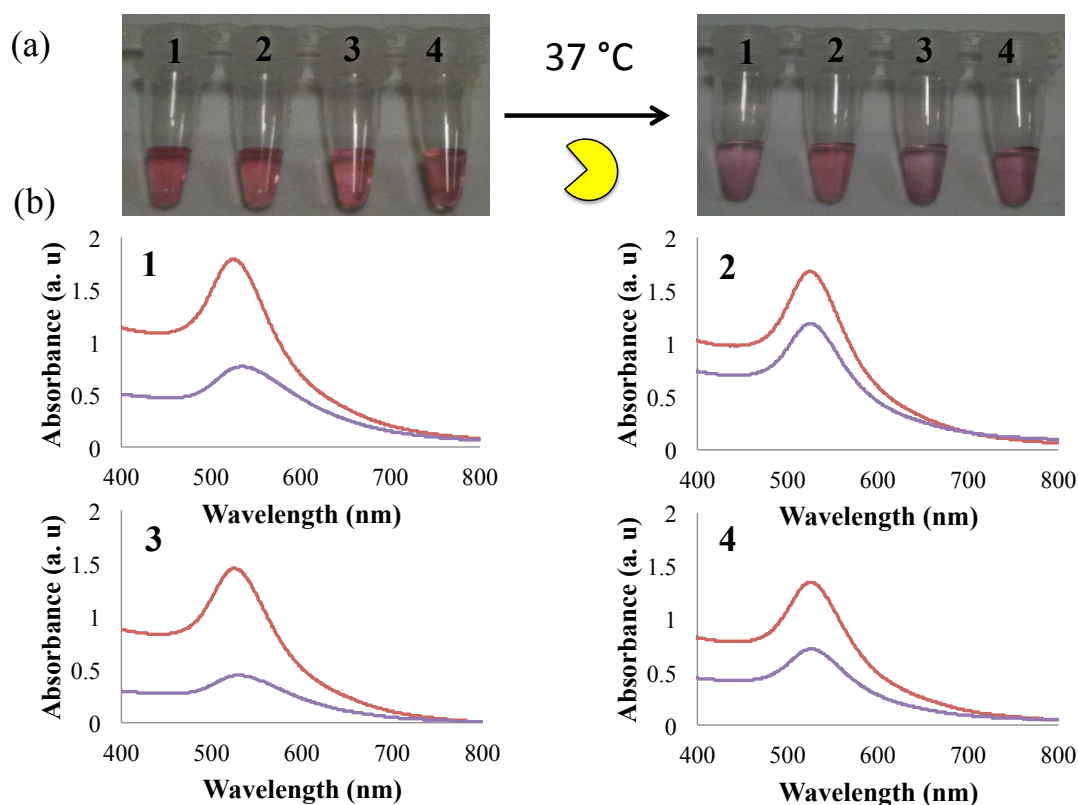


Figure 3.15 Monitoring aggregation using visual detection and UV-Vis analysis. 5 nM of Au-HEG-Probe was hybridised to 5 μM target with Au-10T labelled with MG-ITC in 100 μL of lambda exonuclease reaction buffer (x1). The samples were analysed using UV-Vis and a 100 μL glass cuvette before 4 μL of enzyme was added and the samples held at 37 °C overnight. The samples were re-analysed after digestion had occurred. The visual results (a) and the extinction spectra (b) before (red) and after (purple) digestion is shown. Sample 1 contains the full assay while 2-4 are the control samples with no enzyme, no target, and no target and no enzyme, respectively.

Although these results were deemed successful, there is an obvious flaw, in that the no target control exhibits the same response as the full assay. This experiment was deemed successful only in that a change in plasmon upon action of the enzyme is observed. However, in the no target control there is no duplex for the lambda exonuclease to digest, only a single stranded sequence of DNA, and this should not

be digested with the same efficiency as a DNA duplex, However, it seems that the single stranded digestion in this system is more prevalent than first thought, and it was deemed important to investigate this phenomenon further, the findings of which will be discussed later in this chapter.

3.3.5.2 SERRS Analysis

Since this was the first observable change in the assay, the samples that were subjected to UV-Vis analysis to provide the results in Figure 3.15 were then subjected to SERRS analysis using a 633 nm laser excitation wavelength. The samples were obtained via overnight digestion at 37 °C of the Au-10A-HEG-Probe after hybridisation with the target sequence of DNA. This was carried out in lambda exonuclease reaction buffer in the presence of Au-10T-(MG-ITC). The results of the SERRS analysis are shown in Figure 3.16.

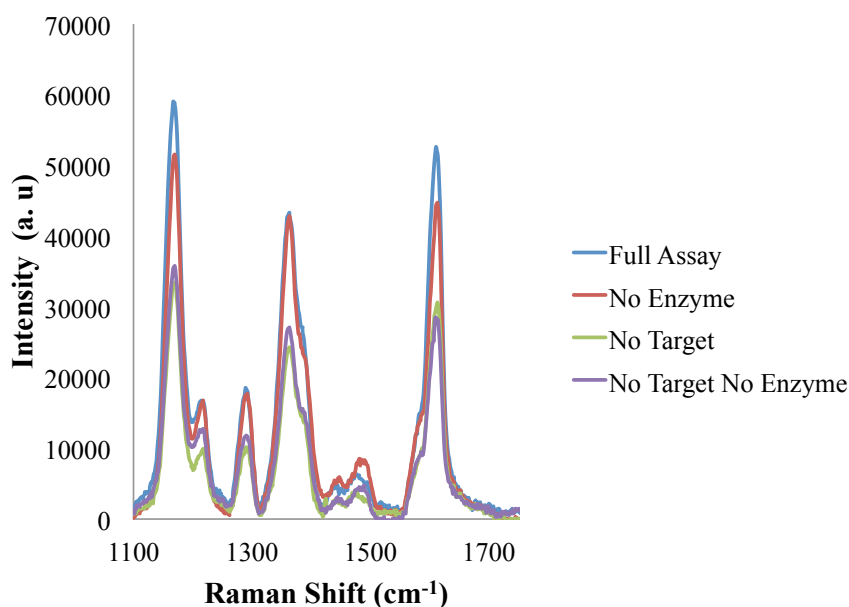


Figure 3.16 SERRS analysis of Au-10A-HEG-Probe and Au-10T-(MG-ITC) after lambda exonuclease digestion, along with a set of controls. Samples were analysed using a 633 nm laser at 4 mW power and 3 x 3 second accumulation. Samples were scanned 5 times, baseline corrected and the average taken.

There is a difference in signal when the target is present compared to when it is not which is an extremely positive result, however there is a large signal observed when the target is present but the enzyme is not, indicating that digestion and hybridisation

of the Au-10A-HEG-Probe and Au-10T-(MG-ITC) is unlikely to be causing the intense signal seen in the full assay control. This signal is too large to be considered a background signal and further work was therefore necessary to try and eliminate this problem.

Throughout these experiments, there was little or no change in plasmon observed as a result of digestion and hybridisation. SERRS was investigated a number of times, as it is a more sensitive technique than UV-Vis spectroscopy,¹⁵⁷ and it was thought that perhaps only a small number of hybridisation events were taking place that could not be detected by UV-Vis. However, most of the results obtained from SERRS were not reproducible, and the large background signals obtained from the presence of the malachite green labelled 10T particle was a significant problem. Therefore a new assay was designed to remove this background from the system.

3.3.6 Magnetic Nanoparticle Based Lambda Exonuclease Assay

An improved version of the lambda exonuclease assay was designed in order to combat the large background signals seen in the SERRS analysis. The new design can be seen in Figure 3.17.

The main difference is the implementation of magnetic iron oxide particles, which can be coated with a noble metal, giving rise to magnetic gold and silver nanoparticles. In this instance the probe sequence of DNA was conjugated to the gold or silver coated iron core particle (Au@Fe₂O₃ or Ag@Fe₂O₃), and the assay was carried out as previously described. As is shown in Figure 3.17, addition of the target sequence and digestion by lambda exonuclease should result in a magnetic nanoparticle with a 10A sequence conjugated to the surface that can hybridise to a non-magnetic 10T conjugate labelled with a SERRS active dye. The novel aspect is the addition of a magnetic separation step, which will allow for the probe conjugate and any hybridised nanoparticles to be held to one side, while the enzyme and any un-hybridised conjugates are washed away. In theory, there should only be a SERRS signal obtained in the presence of the target sequence, since, in contrast to the previous assay, the labelled conjugate will be removed from the system if hybridisation to the magnetic nanoparticle does not take place. This should serve the

dual purpose of decreasing the background signal, and concentrating the labelled particles giving rise to stronger SERRS signals.

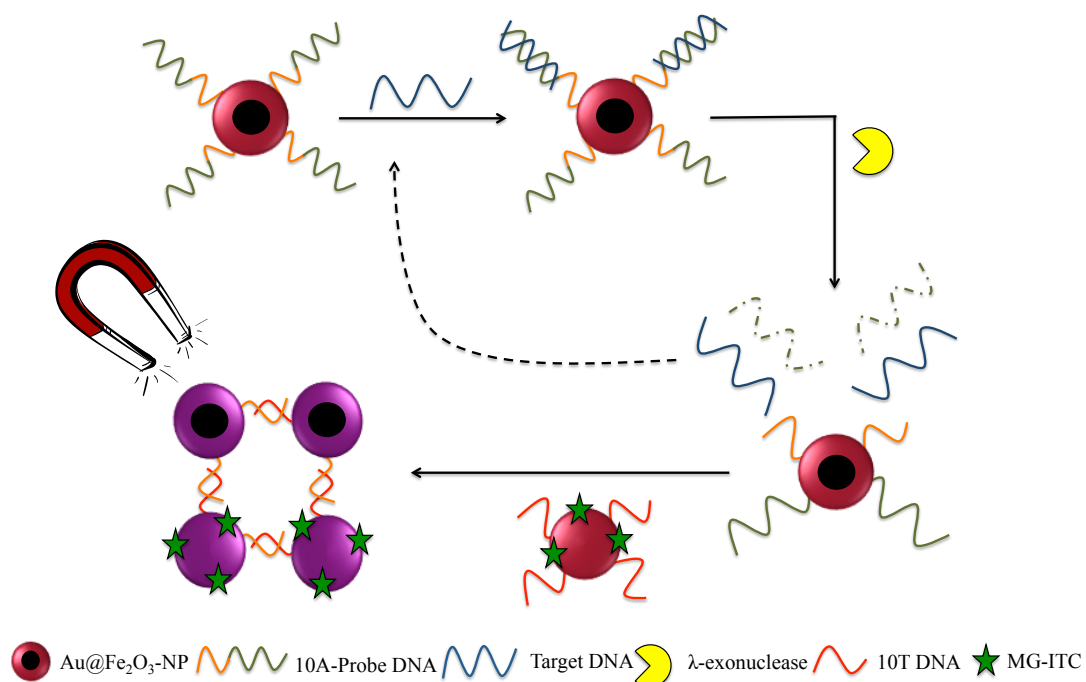


Figure 3.17 Schematic representation of the magnetic nanoparticle based assay for the detection of target DNA using λ-exonuclease and SERRS.

3.3.6.1 Characterisation of Magnetic Nanoparticles

Iron oxide nanoparticles were synthesised according to a standard protocol as detailed in experimental section 7.2.9, and coated with silver via the hydrazine hydrate reduction of silver nitrate and with gold via the glucose reduction of gold tetrachloroaurate. DNA was conjugated to the surface using the standard protocol previously described. Three conjugates were prepared on silver and gold, a 3' thiol and 5' phosphate modified sequence of DNA that incorporated a 10A sequence and HEG spacer before the probe region, a 3' thiol modified 10A sequence and a 3' thiol modified 10T sequence. For the purpose of these conjugates the 3' thioctic acid group used previously for DNA conjugations to metallic nanoparticles was replaced by a 3' thiol group. This was a more cost effective modification, and no obvious change to the stability of the nanoparticles was seen during the conjugation process.

Characterisation of these conjugates proved to be difficult given the broad UV-spectra obtained from the iron core that masked any plasmon bands from the gold or silver shell. Figure 3.18 (a) shows that the gold-shelled iron oxide particles display a slight increase in absorbance around 520 nm, however, the silver absorbance peak around 400 nm is masked by the iron oxide nanoparticles.

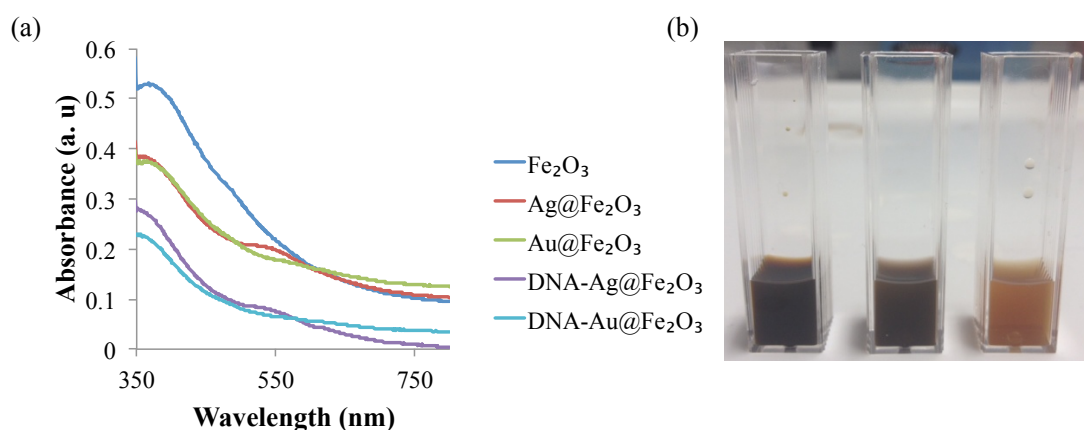


Figure 3.18 Monitoring the shelling of iron oxide nanoparticles. (a) Extinction spectra obtained from the core particles, and their shelled and conjugated counterparts. (b) From left to right, core iron oxide nanoparticles, silver coated iron oxide nanoparticles, and gold coated iron oxide nanoparticles.

Figure 3.18 (b) shows the colour change between the core particles and the gold and silver shelled particles, and therefore we can say with some confidence that the metal coating has been successful. Proving conjugation and hybridisation on a nanoparticle was problematic, since UV-Vis spectroscopy was not suitable. Dynamic light scattering (DLS) was attempted, however the particles were too small to provide consistent results. Scanning Electron Microscopy (SEM) was used to try and monitor the shelling and conjugation process, but there appeared to be no change between the different particles analysed. Thus, SERRS analysis was used to see if we could monitor hybridisation through an increase in signal.

3.3.6.2 SERRS of Magnetic Control Conjugates

The magnetic 10A control conjugated to silver and gold was analysed alongside the 10T-(MG-ITC) non-magnetic nanoparticle silver and gold conjugates. This represents the end point of the full assay whereby, after target addition and

subsequent digestion by lambda exonuclease, only 10A magnetic conjugates will remain. These can then be hybridised to malachite green labelled 10T conjugates and subjected to magnetic separation. Only in the presence of target will the malachite green signal be observed, and this result was first mimicked using control conjugates. SERRS analysis was carried out on these controls both before and after a magnetic wash step. The results for the gold conjugates before the magnetic wash step are shown in Figure 3.19.

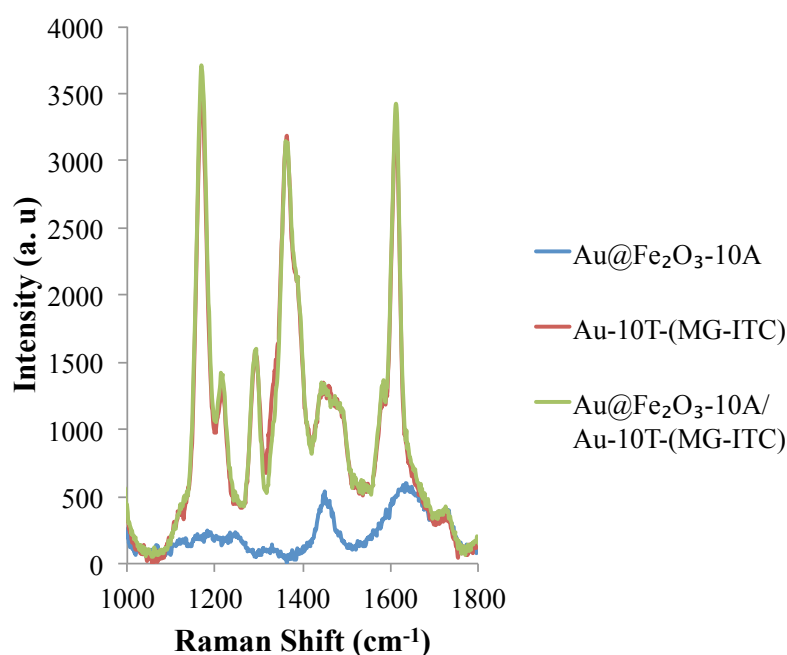


Figure 3.19 SERRS analysis of individual gold conjugates and their mixed system. 5 μL of each conjugate was hybridised in 200 μL of lambda exonuclease reaction buffer (x1) and analysed with a laser excitation wavelength of 633 nm at 4 mW power and 1 x 10 second accumulation. 5 scans of each sample were taken and an average of the baseline correction plotted.

The Au@Fe₂O₃-10A and Au-10T-(MG-ITC) conjugates were hybridised in lambda exonuclease reaction buffer. They were then immediately analysed using a laser excitation wavelength of 633 nm at 4 mW power. As expected, since there is no dye label conjugated to the surface, the Au@Fe₂O₃-10A shows very little signal. Alternatively, given the presence of the malachite green, the Au-10T-(MG-ITC) gave a large signal indicative of this Raman active dye. When both conjugates were combined however, there was no increase in signal obtained, which would indicate that hybridisation between the 10A and 10T and hence aggregation is not occurring

for these conjugates. The results obtained for the silver conjugates before the magnetic wash step can be seen in Figure 3.20.

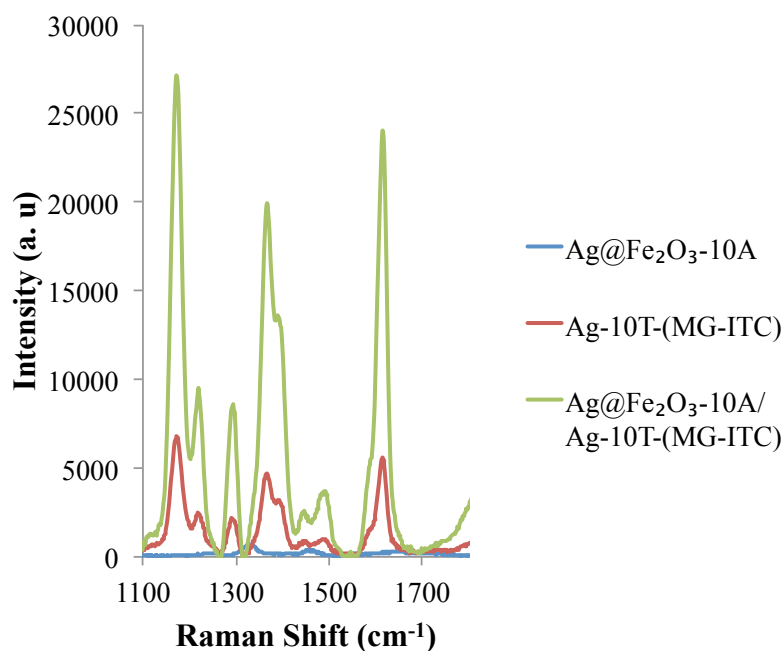


Figure 3.20 SERRS analysis of individual silver conjugates and their mixed system. 5 μL of each conjugate was hybridised in 200 μL of lambda exonuclease reaction buffer (x1) and analysed with a laser excitation wavelength of 633 nm at 2 mW power and 1 x 10 second accumulation. 5 scans of each sample were taken and an average of the baseline correction plotted.

The Ag@Fe₂O₃-10A and Ag-10T-(MG-ITC) conjugates were also hybridised in lambda exonuclease buffer and then immediately analysed using a 633 nm laser excitation wavelength, although for these samples the laser power was reduced from 4 mW to 2 mW due to the high intensity signals seen. The results obtained using the silver conjugates are much more positive than those obtained for gold, and an excellent enhancement in signal is seen when the two complementary conjugates are combined, compared to the individual malachite green labelled silver conjugate. Thus, it is likely that hybridisation is occurring, promoting aggregation between the silver nanoparticles, resulting in an increased SERRS response.

Mixed metal systems were also trialled whereby gold magnetic nanoparticles were used alongside malachite green labelled silver nanoparticles, and vice versa. The results for both of these experiments are shown in Figure 3.21 and again these results

are obtained after hybridisation in lambda exonuclease buffer and before any magnetic wash step was implemented.

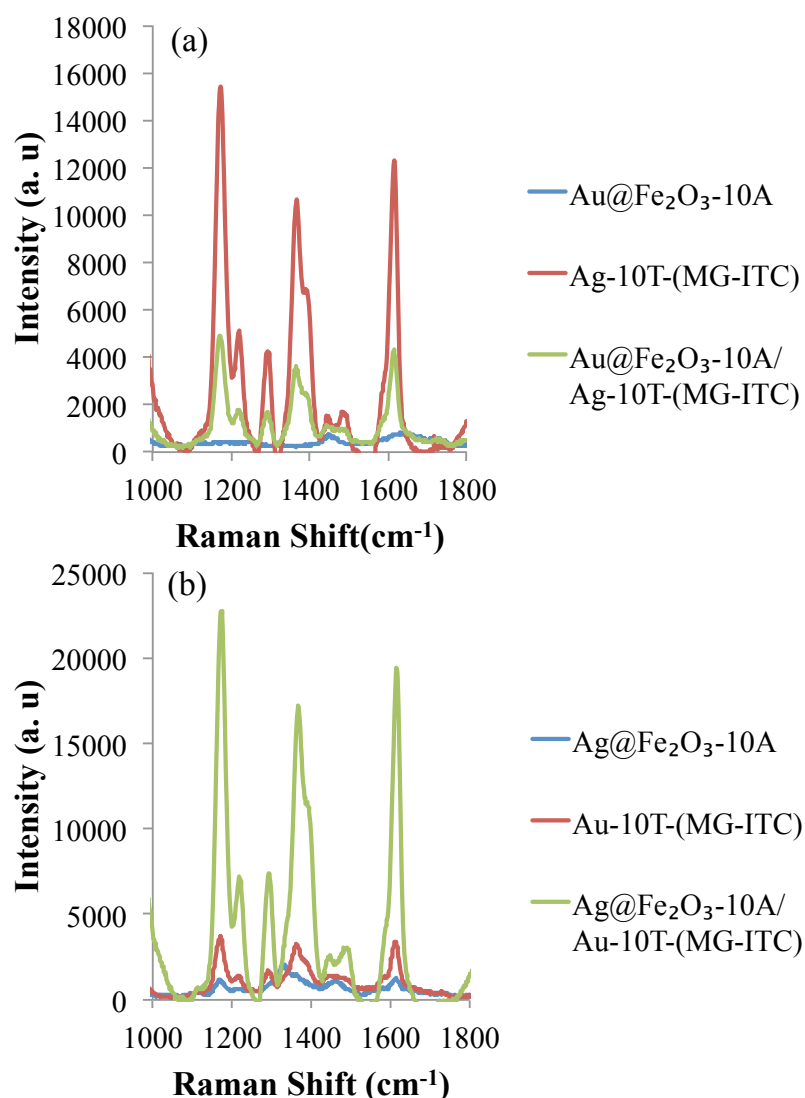


Figure 3.21 SERRS analysis of mixed metal systems and their controls. (a) Magnetic gold nanoparticles and dye labelled silver nanoparticles with their controls. (b) Magnetic silver nanoparticles and dye labelled gold nanoparticle with their controls. 5 μ L of each conjugate was hybridised in 200 μ L of lambda exonuclease reaction buffer (x1) and analysed with a laser excitation wavelength of 633 nm at 4 mW power and 1 x 10 second accumulation. 5 scans of each sample were taken and an average of the baseline correction plotted.

Figure 3.21 (a) shows the Au@Fe₂O₃-10A and Ag-10T-(MG-ITC) combination and controls when analysed using a 633 nm laser excitation wavelength at 4 mW power. The results obtained show that after hybridisation between the two conjugates the

SERRS intensity drops in comparison to the malachite green labelled silver nanoparticles on their own. If the 10A and 10T sequences were not hybridising, then the result expected would be similar to that shown in Figure 3.19, whereby there is no change in the SERRS intensity. Therefore, this drop in signal indicates that some interaction is occurring between the two conjugates and this is having a negative effect on the SERRS signal obtained. It is possible that this adverse effect could be attributed to over aggregation of the nanoparticles as has been seen previously, however, once the magnetic wash step was employed it was hoped that this problem would be overcome. Figure 3.21 (b) shows the Ag@Fe₂O₃-10A and Au-10T-(MG-ITC) combination and controls, again analysed using a 633 nm laser excitation wavelength at a power of 4 mW. The results shown here are exactly as expected and there is a large increase in SERRS intensity upon hybridisation and hence aggregation between the 10A and the 10T conjugates. Thus, the best results obtained for these control experiments before a magnetic wash step were achieved using the Ag@Fe₂O₃-10A conjugate along with either Ag-10T-(MG-ITC) or Au-10T-(MG-ITC).

Upon hybridisation of the magnetic 10A and malachite green labelled 10T sequences, there is a marked increase in SERRS signal, most likely resulting from the formation of 'hotspots' between the particles. For the purpose of this assay, and given the inconclusive results obtained from other methods of analysis, it can be said with confidence that there is DNA conjugated to the surface of the silver shelled magnetic nanoparticles and that hybridisation between the 10A and 10T sequences will occur between magnetic and non-magnetic nanoparticles resulting in an increased SERRS response. This was a very promising result, and showed a much better SERRS discrimination than for the non-magnetic exonuclease assay. These results were obtained before the magnetic separation step and so it was hoped that an even better discrimination could be obtained once the background was removed using this method. Additionally, this would give us further confidence that hybridisation has occurred, as only when the 10A and 10T sequences have hybridised, and a magnetic separation carried out to remove any un-hybridised malachite green labelled nanoparticles, will there be a signal.

The silver, gold and mixed metal samples were subjected to a magnetic wash step. The samples were placed in a magnetic separation rack, whereby the shelled iron core nanoparticles would be pulled to one side. If hybridisation had occurred between the 10A sequence on the magnetic nanoparticle and the 10T sequence on the malachite green labelled nanoparticle, then the 10T would also be pulled to one side. The samples were washed 3 times with buffer to remove any un-hybridised conjugates and the samples re-suspended in lambda exonuclease buffer for analysis by SERRS. When, the Au@Fe₂O₃-10A and Au-10T-(MG-ITC) conjugates were analysed there was no signal obtained. This was expected as Figure 3.19 showed no increase in SERRS signal upon combination of these two conjugates indicating hybridisation had not taken place. Thus, the malachite green would be washed away during the magnetic separation step and no signal indicative of this Raman active dye would be obtained. The results for the silver conjugate system are shown in Figure 3.22.

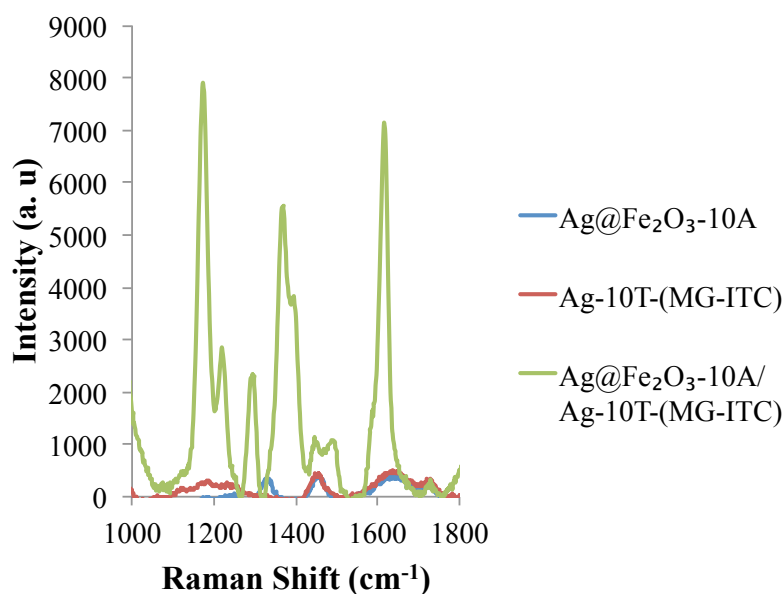


Figure 3.22 SERRS analysis of individual silver conjugates and their mixed systems. 5 μ L of each conjugate was hybridised in 200 μ L of lambda exonuclease reaction buffer (x1) and the subjected to a magnetic wash step (x3). Samples were re-suspended and analysed with a laser excitation wavelength of 633 nm at 4 mW power and 1 x 10 second accumulation. 5 scans of each sample were taken and an average plotted.

The appearance of a signal relating to malachite green is a confirmation of the process of hybridisation between conjugates. It was immediately obvious that

hybridisation between Ag@Fe₂O₃-10A and Ag-10T-(MG-ITC) had been successful and the background signal seen for Ag-10T-(MG-ITC) only had been reduced by the introduction of a magnetic separation step.

The results for the mixed metal systems were also similar to those obtained before the magnetic separation step. The Au@Fe₂O₃-10A and Ag-10T-(MG-ITC) conjugate pair, which upon combination showed a decrease in signal, resulted in no signal being obtained after the magnetic wash indicative of malachite green. This serves to confirm that no hybridisation is taking place and that the dampening in signal seen before magnetic separation is not due to over aggregation of the nanoparticles. The results obtained for the mixed metal system of Ag@Fe₂O₃-10A and Au-10T-(MG-ITC) can be seen in Figure 3.23.

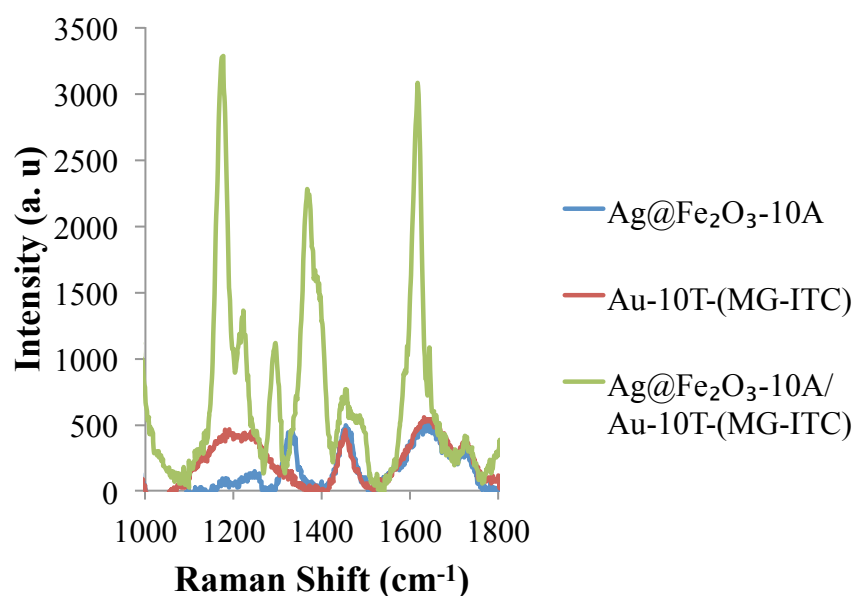


Figure 3.23 SERRS analysis of the mixed metal system after magnetic separation. 5 μ L of each conjugate was hybridised in 200 μ L of lambda exonuclease reaction buffer (x1) and then washed (x3) using magnetic separation with lambda exonuclease reaction buffer. Samples were then analysed with a laser excitation wavelength of 633 nm at 4 mW power and 1 x 10 second accumulation. 5 scans of each sample were taken and an average of the baseline correction plotted.

As was expected, there is a large signal observed for the mixed metal conjugates after the magnetic separation, indication successful hybridisation. Additionally, this magnetic separation step, has reduced any signal obtained from the malachite green

labelled conjugate providing a good discrimination between the desired signal and the background signal.

Due to their success in the SERRS analysis the Ag@Fe₂O₃-10A / Ag-10T-(MG-ITC) and Ag@Fe₂O₃-10A / Au-10T-(MG-ITC) conjugate systems were taken forward into the full assay trials.

3.3.6.3 Full Magnetic Assay Trials using SERRS Analysis

Hybridisation of the 10T ‘aggregator particle’ has been observed via an increase in SERRS signal before and after the magnetic wash step. Therefore the full assay was trialled using the conjugates proven in section 3.3.6.2 to exhibit the greatest SERRS response upon aggregation. The samples used, therefore, consisted of Ag@Fe₂O₃-10A-HEG-Probe and either Ag-10T-(MG-ITC) or Au-10T-(MG-ITC). Another parameter that was investigated in these experiments was the addition of the 10T conjugate. The order of addition was varied in two ways, where the 10T was added either before or after the digestion step. In order to achieve a closed tube system to avoid contamination, adding all the components for the assay at the same time is the best possible situation, however due to the poor results obtained for the non-magnetic assay (section 3.3.5) it was hypothesised that this 10T ‘aggregator particle’ could be interfering with the digestion process. This was investigated for the non-magnetic assay, however, the order of addition appeared to have no effect on the outcome.

Using the silver conjugate system and the mixed metal system, the full assay was carried out along with a set of controls (Figure 3.24). The magnetic probe and target were subjected to a hybridisation step before the addition of lambda exonuclease overnight at 37 °C. Two sets of each conjugate pair were prepared, where the 10T was added before digestion and after digestion. All samples were subjected to a heating and cooling step before being analysed by a laser excitation wavelength of 633 nm. Figure 3.24 details the best results obtained using the Ag@Fe₂O₃-10A-HEG-Probe and Au-10T-(MG-ITC) conjugate system where the 10T ‘aggregator particle’ was added after the digestion. The results seen were obtained before

magnetic separation and even without this step the discrimination between when the target is present and when it is absent is excellent.

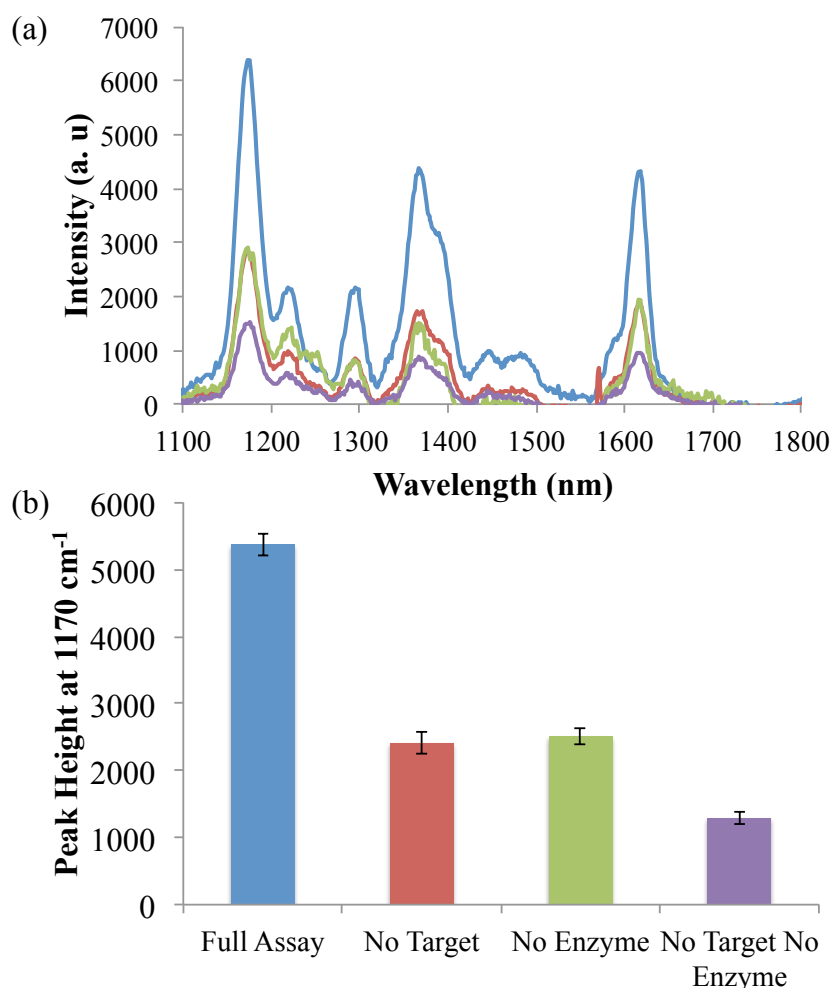


Figure 3.24 SERRS results before magnetic separation of the full assay (blue) along with the no target (red), no enzyme (green) and no target and no enzyme (purple) controls. The Ag@Fe₂O₃-10A-HEG-Probe and 1 μM target were hybridised in 200 μL of lambda exonuclease reaction buffer (x1). 2 μL λ-exonuclease was added and the samples left overnight at 37 °C to digest. The Au-10T-(MG-ITC) was added and the samples subjected to a heating and cooling step before being analysed by a 633 nm laser excitation wavelength. A 4 mW laser power was used with 1 x 10 second accumulation. Samples were scanned 5 times and the average taken to obtain (a) a baseline corrected spectra and (b) a peak height obtained by subtracting the intensity at 1120 cm⁻¹ from 1170 cm⁻¹. Error bars represent one standard deviation of 5 replicate scans

This demonstrates the first successful analysis of this lambda exonuclease assay using SERRS analysis. The Ag@Fe₂O₃-10A-HEG-Probe and Ag-10T-(MG-ITC) unfortunately showed no discrimination between samples, perhaps due to the more efficient conjugation of the 10T sequence and the MG-ITC to the gold nanoparticle.

This mixed metal system combines the advantageous surface chemistry of gold, with the ability of silver to provide strong SERRS signals, and demonstrates a good discrimination even before removal of the background signal via magnetic separation.

The samples then underwent a magnetic wash step, aiming to decrease the background signal and thus provide better discrimination, which should eventually aid in the detection of extremely low levels of target DNA. However, after this separation step there was almost no signal obtained for the mixed metal system and there was no difference due to the order of addition of the 10T. This could be the result of too few hybridisation events happening between the conjugates, and thus there are not enough dye labelled conjugates present after the wash step to exhibit a response.

Although this was a disappointing result, the use of a magnetic assay has still led to a method of detecting target DNA using lambda exonuclease and SERRS. Indeed, since the magnetic wash step was not successful, this assay is directly comparable to the non-magnetic assay discussed in section 3.2. However, the introduction of magnetic nanoparticles has allowed for the detection of target DNA, which was never achieved using the non-magnetic format. It is possible that this is the result of changing the 3' probe modification from a thioctic acid group to a thiol group. Although this was originally done to lower the cost of the assay, it is possible that conjugation using the thiol group is not as efficient, and less DNA strands on the surface of the magnetic nanoparticles have led to a more suitable site for lambda exonuclease digestion.

Due to the success in the detection of target DNA it was important to repeat this assay to assess the reproducibility of the results. As can be seen in Figure 3.25, the reproducibility of this system is disappointing, in particular the between sample variation for the full assay is quite large, and although there is discrimination between the presence and absence of target, it is not significant within one standard deviation.

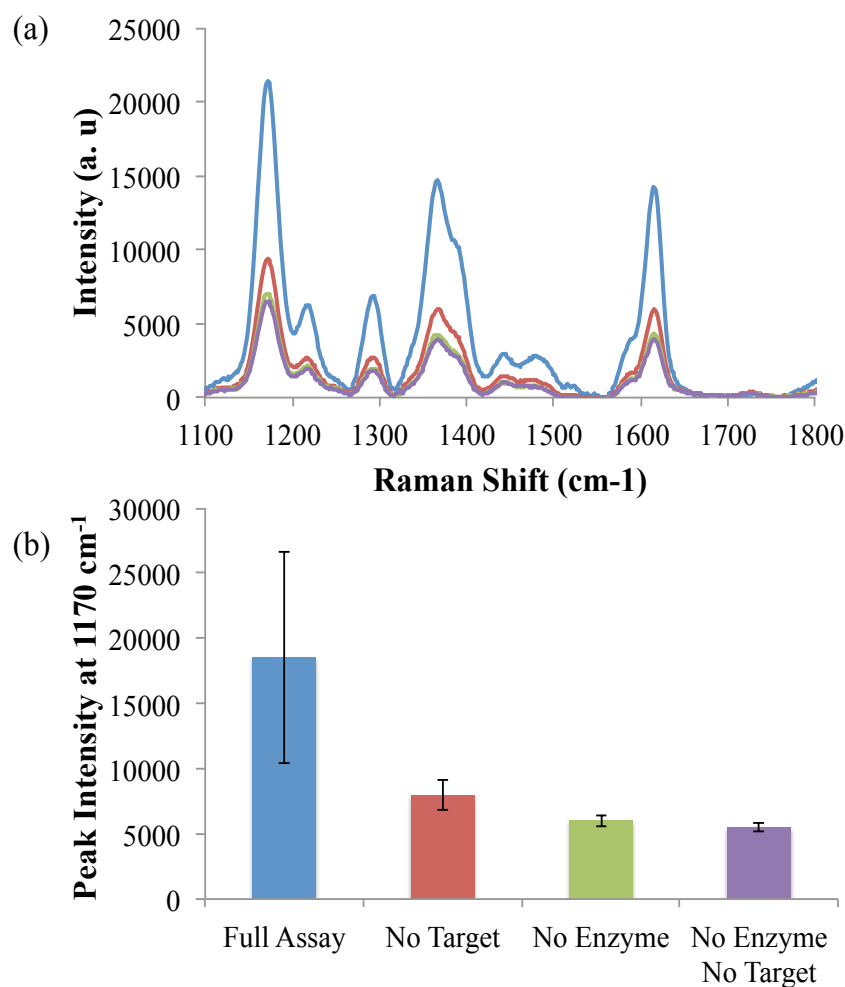


Figure 3.25 SERRS results of the full assay (blue) along with the no target (red), no enzyme (green) and no target and no enzyme (purple) controls. The Ag@Fe₂O₃-10A-HEG-Probe and 1 μ M target were hybridised in 200 μ L of lambda exonuclease reaction buffer (x1). 2 μ L lambda exonuclease was added and the samples left overnight at 37 $^{\circ}$ C to digest. The Au-10T-(MG-ITC) was added and the samples subjected to a heating and cooling step before being analysed by a 633 nm laser excitation wavelength. A 4 mW laser power was used with 1 x 10 second accumulation. 3 replicate samples were prepared and were scanned 5 times and the average taken to obtain (a) a baseline corrected spectra and (b) a peak height obtained by subtracting the intensity at 1120 cm^{-1} from 1170 cm^{-1} . Error bars represent one standard deviation of 3 replicate samples.

Having exhausted many of the parameters relating to this assay it became obvious that the ability of the enzyme to digest homogenously on the surface of the nanoparticle was perhaps problematic, and the action of lambda exonuclease was investigated further.

3.3.7 Confirming Lambda Exonuclease Digestion on a Nanoparticle

There is no literature available detailing the effect that gold or silver nanoparticles will have on the function of the digestive enzyme lambda exonuclease, and whether it is able to digest DNA conjugated to such a particle. It was therefore important to assess that the nanoparticles were not in some way inhibiting the action of the enzyme, or that steric hindrance was not interfering with the digestion process. Firstly, the digestion of the probe and the target off nanoparticles was confirmed using lambda exonuclease and Hoechst 33258.

The system used was similar to that described in Chapter 2, whereby the minor groove binder Hoechst 33258 was introduced along with the 10A-HEG-Probe and target. The samples were excited at 350 nm and the fluorescence monitored at 460 nm over time at 37 °C as the enzymatic digestion occurred. Since H33258 has a higher fluorescent output in the presence of double stranded DNA, upon action of the enzyme the fluorescence should decrease. The results are shown in Figure 3.26 (a). Upon action of the enzyme the double stranded DNA becomes single stranded and as such the fluorescent output from the H33258 decreases. Only when the target DNA and the enzyme is present does this drop in fluorescence occur. To make sure that the presence of gold nanoparticles does not inhibit enzyme activity, this experiment was repeated with the addition of Au-10T. As is seen in Figure 3.26 (b) a drop in signal is still seen when the target and enzyme is present and as such the enzyme still has digestive activity when there are gold nanoparticles present in the assay.

Finally, this experiment was carried out using the conjugates to confirm enzymatic activity in the nanoparticle based lambda exonuclease assay. Unfortunately, there was no change in signal seen using the H33258 and the gold probe conjugates. Since the gold nanoparticles will also absorb in the region of 460 nm, the emission wavelength of H33258, it was hoped that fluorescent quenching was the cause of these failed experiments as opposed to the inaction of lambda exonuclease of the gold conjugates.

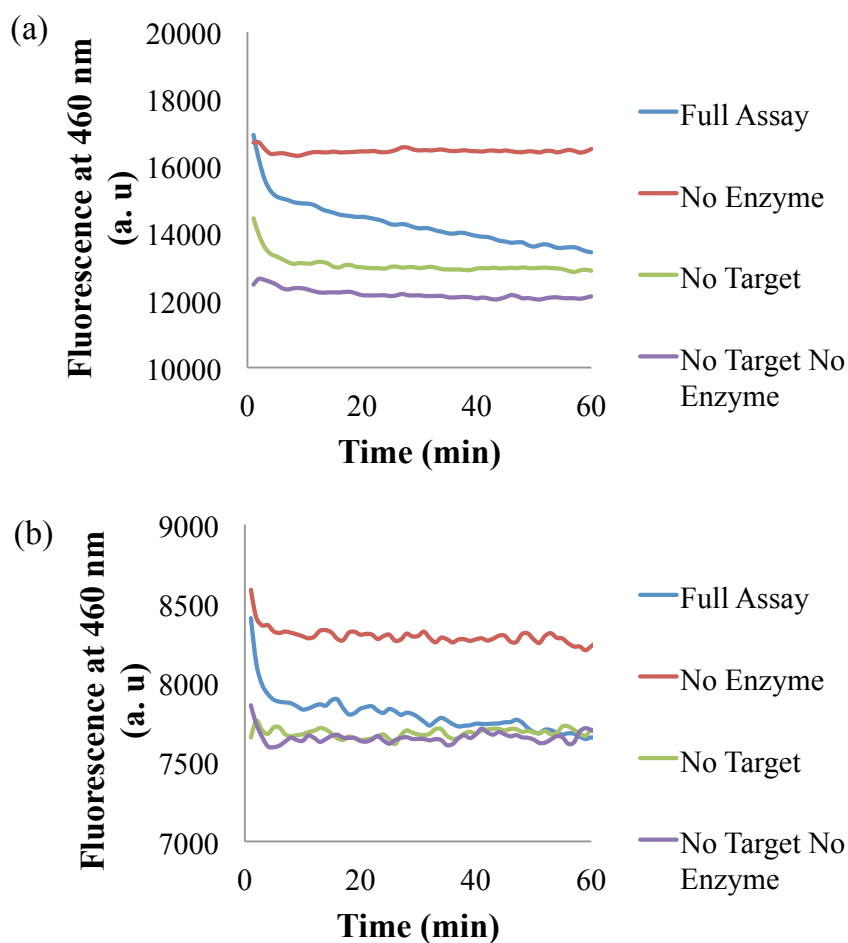


Figure 3.26 (a) Off nanoparticle digestion using 0.2 μM 10A-HEG-Probe, 0.2 μM target DNA and 0.4 μM H33258 in a 30 μL final volume of lambda exonuclease reaction buffer (x1). 1 μL λ -exonuclease was added and the fluorescence monitored at 460 nm over 60 minutes over at 37 $^{\circ}\text{C}$. (b) Digestion in the presence of nanoparticles. 5 nM 10A-HEG-Probe and 0.2 μM were hybridised in 30 μL of lambda exonuclease reaction buffer (x1) with 20 nM Au-10T. 1 μL λ -exonuclease was added and the fluorescence monitored at 460 nm over 60 minutes over at 37 $^{\circ}\text{C}$. An excitation wavelength of 350 nm was used in both experiments.

This experiment was repeated using a different instrument for fluorescent analysis. A Fluorolog instrument was used that allowed integration times to be set providing more sensitive fluorescent measurements to be obtained. The Au-10A-HEG-Probe conjugate and target sequence were hybridised in the presence of H33258 and the fluorescence was measured every 12 seconds at 465 nm over a time period of 10 minutes after the addition of lambda exonuclease. As can be seen in Figure 3.27 the decrease in fluorescence in the presence of the enzyme (Figure 3.27 (a) and (b))

suggests that digestion is in fact occurring on the surface of the nanoparticle, and that the fluorescence at 460 nm, the emission wavelength of Hoechst 33258, is decreasing as the double stranded DNA becomes single stranded. However, the digestion efficiency when there is no target present is greater than when there is target present.

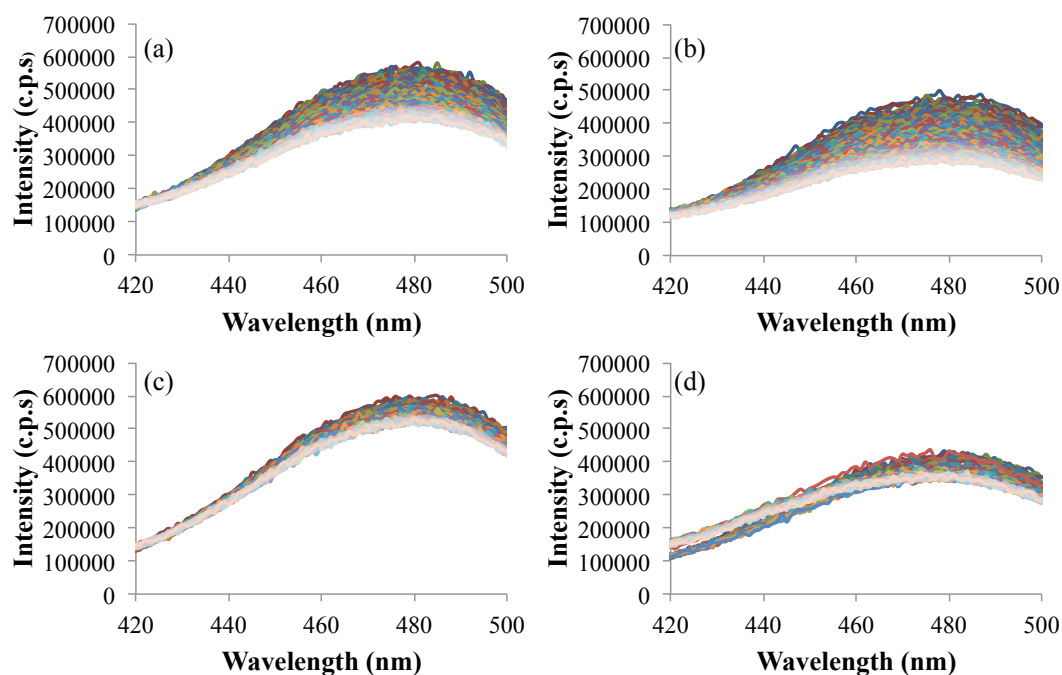


Figure 3.27 60 pM Au-10A-HEG-Probe and 1 μ M target were hybridised in the presence of 1 μ M H33258 in 100 μ L of lambda exonuclease reaction buffer (x1). 2 μ L enzyme was added and the fluorescence measured at 465 nm, using an excitation of 350 nm, every 12 seconds for a total of 10 minutes. (a) shows the results from the full assay where (b) is the no target control, (c) is the no enzyme control and (d) is the no target no enzyme control.

Thus, from these experiments it can be concluded that lambda exonuclease will digest DNA conjugated to the surface of a gold nanoparticle. However, the digestion efficiency of single stranded DNA is greater than that of double stranded DNA, and this was an unexpected result. Since the rate of single stranded digestion is inversely related to the length of the single strand of DNA, perhaps the sequence used is too short, and a longer sequence would decrease the rate of single stranded digestion in comparison to double stranded digestion. However, for the purpose of the experiments detailed herein, using the 21 base sequence, if the enzyme is able to digest single stranded DNA with the same, if not greater, efficiency as double

stranded DNA then there will never be discrimination between the presence and absence of a target sequence. Therefore, it is likely that the enzyme activity is to blame for many of the unexpected result obtained throughout this chapter.

3.4 Conclusions

A novel assay for the detection of DNA based on signal amplification via the action of the digestive enzyme lambda exonuclease has been proposed. Three different forms of this assay have been investigated, the first of which involves destabilisation of DNA-nanoparticle conjugates by digestion of the 5' phosphate probe from the surface, while the second method involves the use of a dye-labelled 'aggregator particle' for crosslinking aggregation via a specific hybridisation event. The conjugation of DNA strands to gold and silver nanoparticles was successfully confirmed visually using UV-Vis spectroscopy and gel electrophoresis. DNA melts were used to confirm hybridisation of the probe sequence to the desired target, and gel electrophoresis was again employed to great effect to monitor hybridisation on the surface of a gold nanoparticle.

The first proposed form of this assay was unfortunately unsuccessful, most likely due to the inability of the enzyme to digest enough DNA probes on the surface of the nanoparticle to cause destabilisation and aggregation. The crosslinking assay, however, provided more substantial results. Control conjugates, bearing a 10A sequence only, were hybridised to a 10T conjugate labelled with malachite green isothiocyanate, and their hybridisation was monitored visually and using UV-Vis spectroscopy. The SERRS results from the gold conjugate system yielded unexpected results, in that a decrease in signal was seen upon hybridisation. This can likely be explained via over-aggregation of the particles, which precipitated out of solution before analysis. The silver conjugate system provided the results expected of this assay and an increase in SERRS signal was observed upon aggregation of the 10A and 10T sequence. This also confirmed the success of DNA conjugation to silver nanoparticles and also that hybridisation would occur on the surface of these particles.

Initial studies into the full assay trials were unsuccessful and no change in plasmon could be seen for a number of varying experimental parameters. However, once the probe was redesigned to include a HEG spacer to stop enzymatic action before the 10A region, and optimised parameters obtained, a slight change in plasmon could be seen, upon action of the enzyme. This, however, was not reflected in the SERRS results, and large background signals obscured the discrimination between the presence and absence of target.

Thus, the third variation on this assay was designed, whereupon magnetic nanoparticles were introduced to allow a separation step in order to eliminate the background and concentrate the SERRS signal. The introduction of gold and silver coated magnetic nanoparticles led to the successful detection of 0.1 μM target DNA via the action of lambda exonuclease and SERRS analysis. Thus, the success of this assay was finally realised.

This experimental setup, however, was not used to push the boundaries of sensitivity as it was quickly found that the results were not reproducible. Given the research into the nanoparticle conjugates, it is likely that the main problem is the enzyme itself. The size of the enzyme, in particular, poses a steric problem, especially when there is tight packing of DNA to the nanoparticle surface. Overcoming this problem, it is still likely that the amount of DNA digested on the surface of the particle is not as great as when a duplex DNA is free in solution. Thus, there may only be a small amount of digestion events occurring, which would explain the small shift in plasmon. Since, SERRS is an inherently more sensitive technique, this was able to provide more sensitive results, however the lack of reproducibility cannot be ignored as it appears the enzyme cannot digest on the surface of the nanoparticle homogeneously. All of these aspects aside, upon proper functioning of the enzyme, the ability of lambda exonuclease to digest single stranded DNA is by far the greatest threat to this assay. In particular the results obtained which prove that single stranded digestion is more efficient on the surface of a nanoparticle is a truly troubling result.

In conclusion, DNA-nanoparticle conjugates have been successfully utilised alongside lambda exonuclease and SERRS analysis in an assay format amenable to signal amplification. However, the future of this assay design lies in the ability to control single stranded digestion, before it can be utilised to detect DNA at a level of sensitivity that rivals that of PCR.

4. Monitoring the Catalytic Activity of DNAzymes using Enhanced Raman Scattering

4.1 Introduction

Artificial enzymes are becoming increasingly popular in research due to their simple and cost effective synthesis in comparison to conventional protein enzymes, as well as their ability to survive harsh reaction conditions for use in a variety of diagnostic mechanisms. One such family of artificial enzymes that have become increasingly popular in the literature are catalytic sequences of DNA, known as DNAzymes.

4.1.1 Catalytic DNA

DNAzymes are functional nucleic acid sequences with specific catalytic activity. The most common of these DNAzymes is one that mimics the action of horseradish peroxidase (HRP), a glycoprotein used extensively in conventional diagnostic techniques, such as in a standard ELISA. It has an alpha helical structure, which is depicted in Figure 4.1, and binds haeme as its cofactor. The catalytic activity of an HRP-mimicking DNAzyme, is the direct result of the intercalation of the metalloporphyrin haemin into a G-quadruplex structure¹⁵⁸ (Figure 4.2), which serves as the enzymatic cofactor, thus imitating haeme binding proteins. As mentioned previously in Chapter 1, these secondary G-quadruplex structures will be formed from guanine rich DNA under the correct environmental conditions, and thus a monovalent cation is also needed for the formation of this DNAzyme.

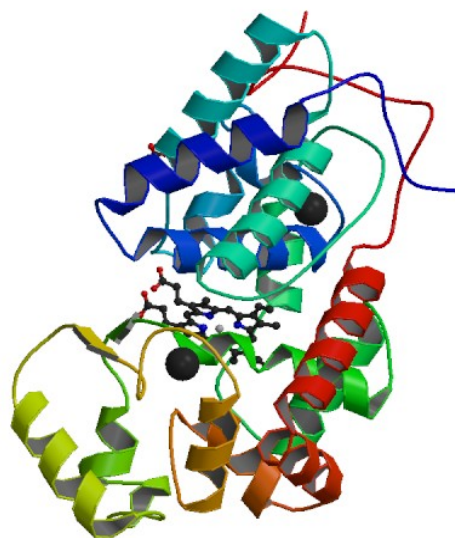


Figure 4.1 Three-dimensional view of horseradish peroxidase.

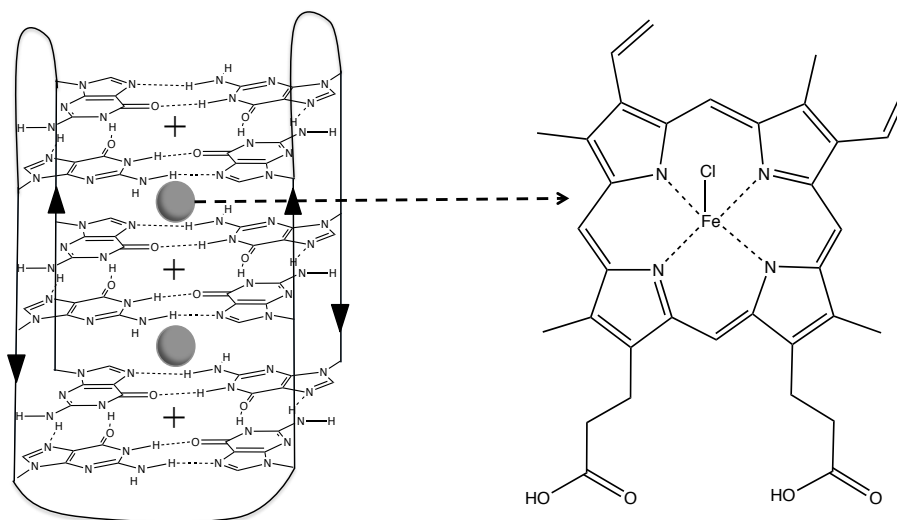


Figure 4.2 The structure of a catalytic HRP-mimicking DNAzyme. The G-quadruplex structure (left) is stabilised by monovalent cations before haemin intercalates into the complex, the structure of which is also shown (right).

Similar to G-quadruplex structures, these DNAzymes can be formed from either one, two or four strands of DNA that are rich in guanine, and can take different structural forms which can affect their catalytic activity.^{159, 160} The sequence used herein was an 18-base single strand of DNA known as PS2.M, which has previously been shown to exhibit a parallel structure in the presence of K^+ ions and an antiparallel structure with Na^+ ions.¹⁶¹ Therefore, the choice of counter ion used with DNAzymes is an important factor to investigate in order to obtain optimum catalytic activity.

Once formed, the DNAzyme complex is able to catalyse the H_2O_2 -mediated oxidation of certain peroxidase substrates, most commonly 2,2'-azino-bis(3-ethylbenzthiazoline-6-sulfonic acid) diammonium salt (ABTS)^{162, 163} and 3,3',5,5'-tetramethylbenzidine (TMB).¹⁶⁴

4.1.2 The Oxidation of ABTS

The oxidation of ABTS proceeds via a one step, one electron oxidation reaction, which is depicted in Figure 4.3. The parent molecule ($ABTS^{2-}$) is oxidised to a radical anion ($ABTS^{\bullet-}$) and this process can be monitored visually as a colourless to green colour change is observed as the reaction proceeds (Figure 4.4 (a)).

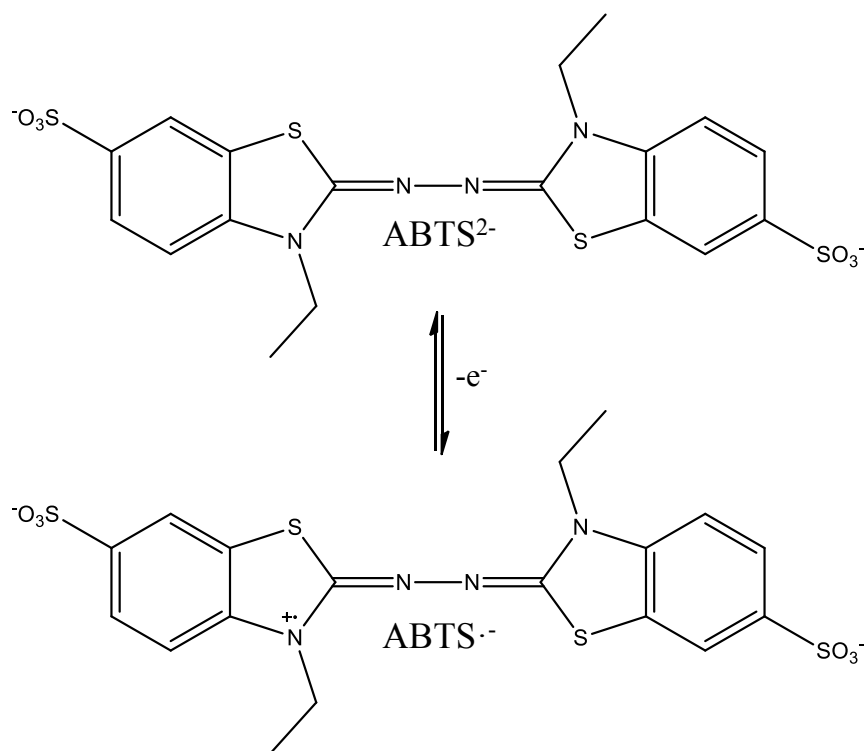


Figure 4.3 The oxidation of 2,2'-azino-bis(3-ethylbenzthiazoline-6-sulfonic acid) diammonium salt.

This oxidation can also be monitored using UV-Vis spectroscopy, since the radical anion has an absorbance at 414 nm, while the parent molecule has no absorbance, as is shown in Figure 4.4 (b).

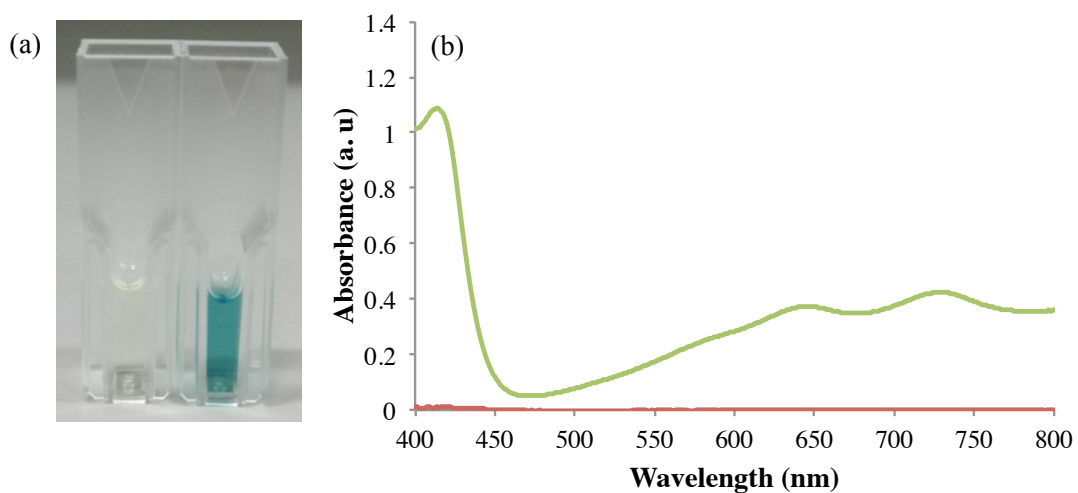


Figure 4.4 The oxidation of ABTS monitored both (a) visually and (b) using UV-Vis spectroscopy of the sample before (red) and after (green) oxidation.

An additional absorbance in the region of 700 nm, with two distinct absorbance bands, can be attributed to the formation of a radical cation from the oxidation process, which is blue in colour. This reaction is less favoured and hence it is the green colour that is predominant and provides a stronger absorbance band in the spectrum. The higher absorbance band, however, makes this substrate ideal for use in resonance Raman spectroscopy when using a laser excitation wavelength of 633 nm, and this will be discussed in detail in section 4.3.2

4.1.3 The Oxidation of TMB

Unlike ABTS, the oxidation of TMB occurs via two successive one electron oxidation steps as is shown in Figure 4.5. In the first step the parent diamine (TMB⁰) is oxidised to a radical cation (TMB^{•+}) which exists in rapid equilibrium with a charge transfer complex (CTC) of the diamine and the final diimine (TMB²⁺).¹⁶⁵

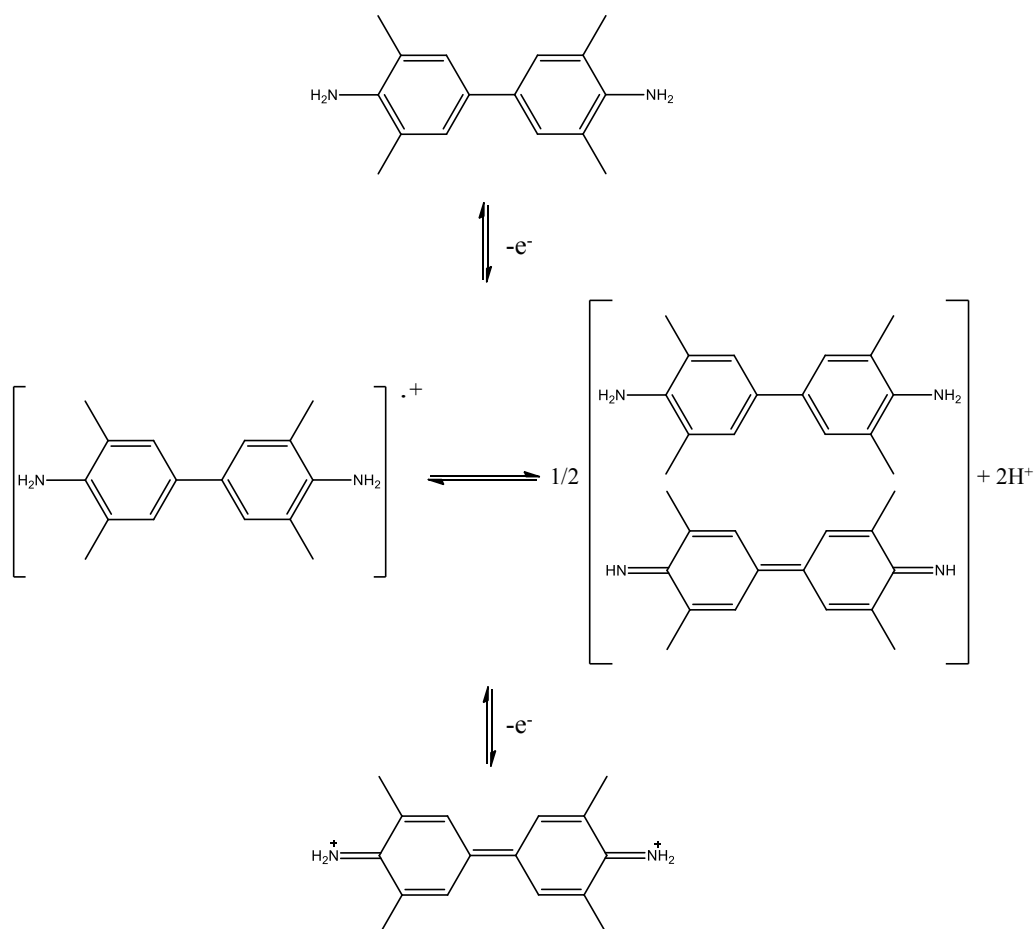


Figure 4.5 Oxidation of 3,3',5,5'-tetramethylbenzidine.

These one electron oxidation products have two distinct absorbance peaks in the extinction spectrum as can be seen in Figure 4.6. The radical cation absorbs at 370 nm while the CTC absorbs at 650 nm, and since the parent molecule has no absorbance in the visible region a colourless to blue change is observed as the one electron oxidation reaction proceeds.

Under acidic conditions, the second oxidation reaction will proceed accompanied by a colour change from blue to yellow as the final diimine is formed, and this can be monitored by the appearance of a 450 nm absorbance peak in the extinction spectrum. Since the CTC has an absorbance that is close to being in resonance with a 633 nm laser excitation wavelength, like ABTS, this reaction can also be monitored using resonance Raman scattering.

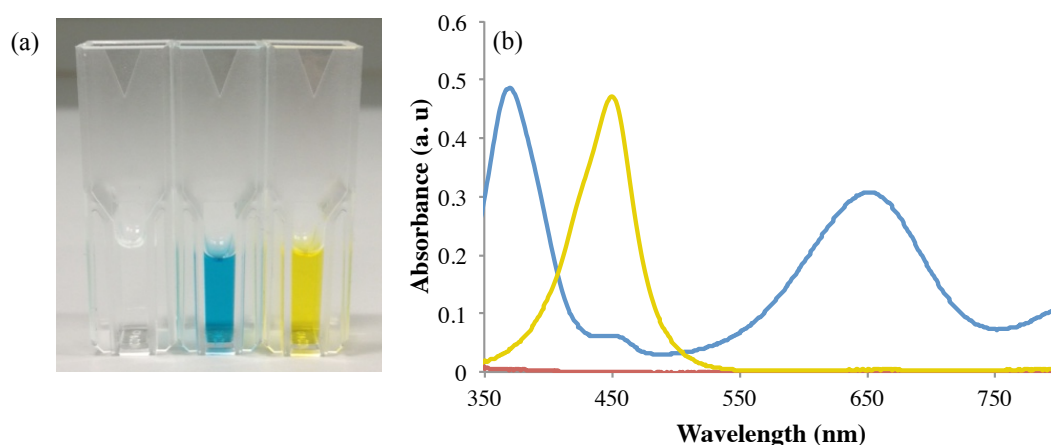


Figure 4.6 The oxidation of TMB monitored both (a) visually and (b) using UV-Vis spectroscopy of the parent diamine (red), CTC (blue), and final diimine (yellow).

4.1.4 Applications of HRP-Mimicking DNAzymes

Since the action of HRP can be mimicked using a DNAzyme, which is simple and cost effective to synthesise, these catalytic sequences of DNA have been used in a variety of applications and detection methods for a number of different analytes. ABTS in particular has been the most popular substrate for use in combination with an HRP-mimicking DNAzyme, and has been successfully used in the detection of metal ions,¹⁶⁶ proteins,¹⁶⁷ and G-quadruplex ligands.¹⁶⁸ All of these detection methods rely on the ability of the DNAzyme to catalyse the oxidation of ABTS to its

green, one electron oxidation product, a process that can be detected both visually and spectroscopically. The main application of these catalytic sequences of DNA using ABTS is for the visual and spectroscopic detection of target DNA. Willner and his research group in particular have pioneered a number of methods of DNA detection based on the oxidation of ABTS by a DNAzyme.^{162, 163, 169} One method utilises catalytic molecular beacons, whereby a region of DNAzyme is locked in a stem-loop structure.¹⁶⁹ Upon addition of a target sequence of DNA, the structure will change, much like regular molecular beacons, to favour the more stable duplex between loop and target. Upon target hybridisation, the design of the beacon will leave the DNAzyme free to complex with haemin and catalyse the oxidation of ABTS. This beacon design has since been modified and utilised by a number of other research groups for the sensitive detection of DNA using ABTS and an HRP-mimicking DNAzyme.¹⁷⁰⁻¹⁷² A major disadvantage of ABTS, however, lies in the instability of the oxidation product, which can often revert to the colourless parent molecule over time, and limits the use of this substrate in reactions that involve longer analysis timescales. As such, the use of TMB in combination with DNAzymes has seen a recent growth in the literature,¹⁷³⁻¹⁷⁵ whereby the appearance of the blue CTC is indicative of the presence of a particular analyte. TMB has also been used for the detection of target DNA,¹⁶⁴ although to a much lesser extent than ABTS.

To date, the majority of analyte detection mechanisms have utilised either visual detection or absorption spectroscopy as the main method of analysis. Recently, Willner *et al.* changed the substrate used in their catalytic beacon protocol to Amplex Red, which will undergo oxidation via a DNAzyme to give the fluorescent product Resofurin.¹⁷⁶ By changing the method of analysis to fluorescence spectroscopy, lower limits of detection for target DNA were realised.

In this work the use of a novel spectroscopy for the detection of catalytic activity by a DNAzyme in the form of resonance Raman scattering (RRS) is investigated. Since both ABTS and TMB have absorbance peaks in resonance with a laser excitation wavelength of 633 nm, these substrates were ideal for use alongside this method of analysis. Previously, work within the Centre for Molecular Nanometrology has

reported on the analysis of ABTS using SERRS for the detection of prostate specific antigen (PSA).¹⁷⁷ Additionally, Laing *et al.* reported on the first use of resonance Raman scattering for the analysis of the blue CTC oxidation product of TMB.¹⁷⁸ This was used alongside an ELISA for human tumour necrosis factor (TNF) α , and the detection limits were lowered by 50 times in comparison to traditional colourimetric detection. Both of these detection mechanisms, however, were based upon the action of HRP to catalyse the oxidation of ABTS and TMB before analysis using enhanced Raman scattering, and analysis after interaction with a DNAzyme was yet to be reported.

4.2 Chapter Aims

The initial aim of this work was to analyse the oxidation products of ABTS and TMB after interaction with a DNAzyme by resonance Raman scattering, and incorporate this method of analysis into a catalytic beacon based protocol for the sensitive detection of target DNA.

4.2.1 Assay Design

The protocol used for the detection of DNA was first developed by Willner and co-workers, who utilised catalytic beacons alongside UV-Vis spectroscopy¹⁶⁹ and fluorescence¹⁷⁶ to obtain detection limits of 0.2 μM and 1 nM, respectively, for target DNA. The outline of the detection method used is depicted in Figure 4.7.

These catalytic beacons consist of a loop region of DNA that is complementary to a desired target sequence, and a stem region that incorporates part of a guanine-rich sequence of DNA. The beacon is held together by a sequence of DNA complementary to part of this guanine-rich sequence needed for catalytic activity. In this beacon format, the DNA is unable to form a G-quadruplex and become a DNAzyme. In the presence of target DNA, just like with regular molecular beacons, the loop and target will form a sterically more favourable duplex, opening the beacon and releasing the previously locked sequence of guanine-rich DNA. This is then able to form a G-quadruplex under the correct environmental conditions, and once haemin

intercalates into the structure, will be able to catalyse the oxidation of peroxidase substrates such as ABTS and TMB.

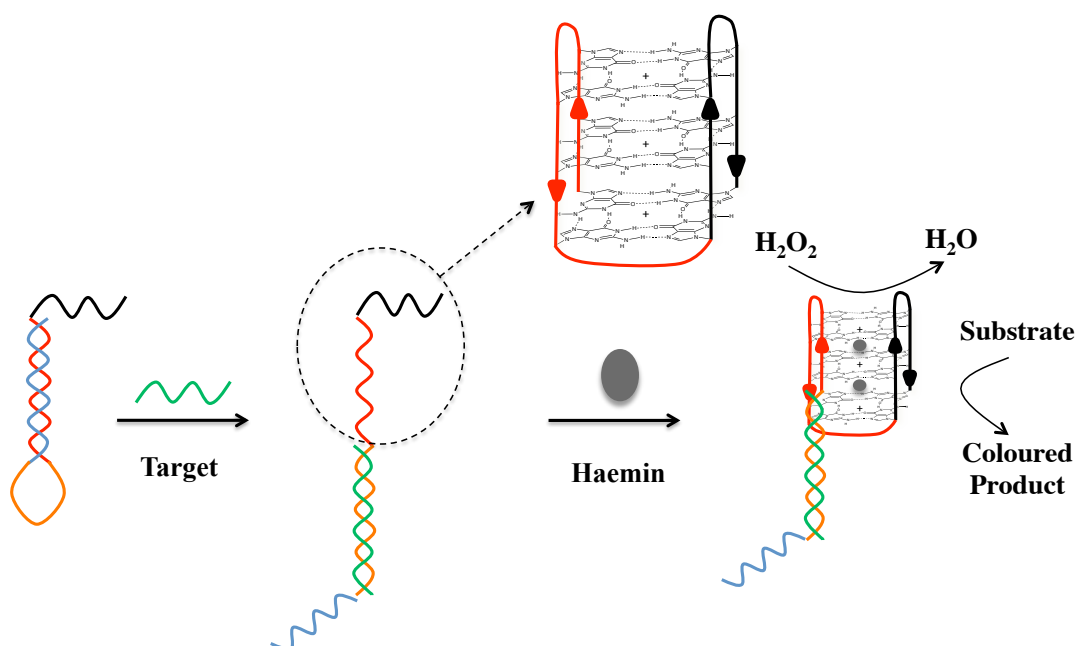


Figure 4.7 Catalytic beacons for the detection of DNA. A beacon consisting of a loop region (orange) complementary to a target sequence of DNA (green) is held together via a stem, which consists of a region of guanine-rich DNA (red) and a complementary sequence (blue). Once the target and its complement hybridise, the beacon will open, allowing the full guanine rich sequence (red and black) to form a G-quadruplex, and in the presence of haemin catalyse the oxidation of peroxidase substrates.

This protocol has been successfully utilised alongside UV-Vis and fluorescence spectroscopy, and the aim of this project was to incorporate resonance Raman scattering as a novel method of analysis into a catalytic beacon protocol for sensitive DNA detection.

4.2.2 Beacon Design

The design of the beacon was important since it had to incorporate a region of DNA complementary to the desired target, along with a section of guanine-rich DNA that could be locked in the stem region. The target used in this instance was the same 21-mer sequence coding for the *MecA* gene of an MRSA strain that was discussed in Chapter 2 and 3, while the guanine-rich sequence used was PS2.M, an 18 base long DNAzyme. The final design of the beacon is depicted in Figure 4.8.

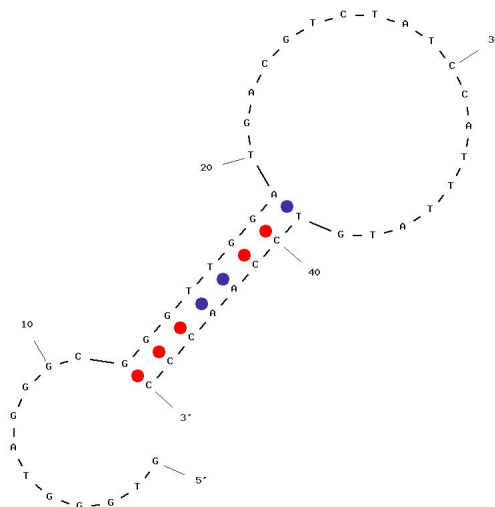


Figure 4.8 Beacon design showing the loop region complementary to the target, the stem region locked together by A-T (blue) and G-C (red) base pairing, and the guanine-rich region, part of which is contained in the stem. Modelling software from IDT Technologies, Ltd. was used to visualise the beacon design.

The DNzyme sequence used was 18 bases long, and the beacon was designed such that 7 bases were locked in the stem via A-T and G-C base pairing and hence this DNA cannot form a G-quadruplex when it exists in this structural form. This design was visualised using modelling software from IDT Technologies Ltd. and this software was also used to confirm hybridisation of the target sequence to the loop region of the beacon, based on thermodynamic stability. This beacon design was thus used alongside resonance Raman scattering for the detection of target DNA

4.3 Results and Discussion

The first step in this project was to determine the optimum parameters for DNzyme activity and investigate the suitability of resonance Raman scattering for the analysis of this activity on both ABTS and TMB.

4.3.1 Optimising DNAzyme Parameters

4.3.1.1 Cation Comparison

Since it has been reported that the G-quadruplex stabilising ion has an affect on structure and hence functionality of the DNAzyme, it was first important to assess which was the best cation to use to give optimum catalytic activity. The two substrates chosen for analysis by resonance Raman scattering were ABTS and TMB, along with two different buffers; 10 mM HEPES / 10 mM NaCl, at pH 7.1 buffer and 10 mM HEPES / 10 mM KCl, at pH 7.1 buffer. The DNAzyme sequence and haemin were allowed to complex for 30 minutes in the buffer chosen, before the addition of substrate and analysis by UV-Vis spectroscopy after 1 hour. The concentration of substrate was varied by using different volumes of a pre-mixed solution of substrate and H₂O₂ in a 1:1 ratio, which is used in a standard ELISA. Figure 4.9 (a) and (b) details the results obtained from varying the volume of ABTS in the two different buffers, while Figure 4.9 (b) and (d) details the results obtained for TMB.

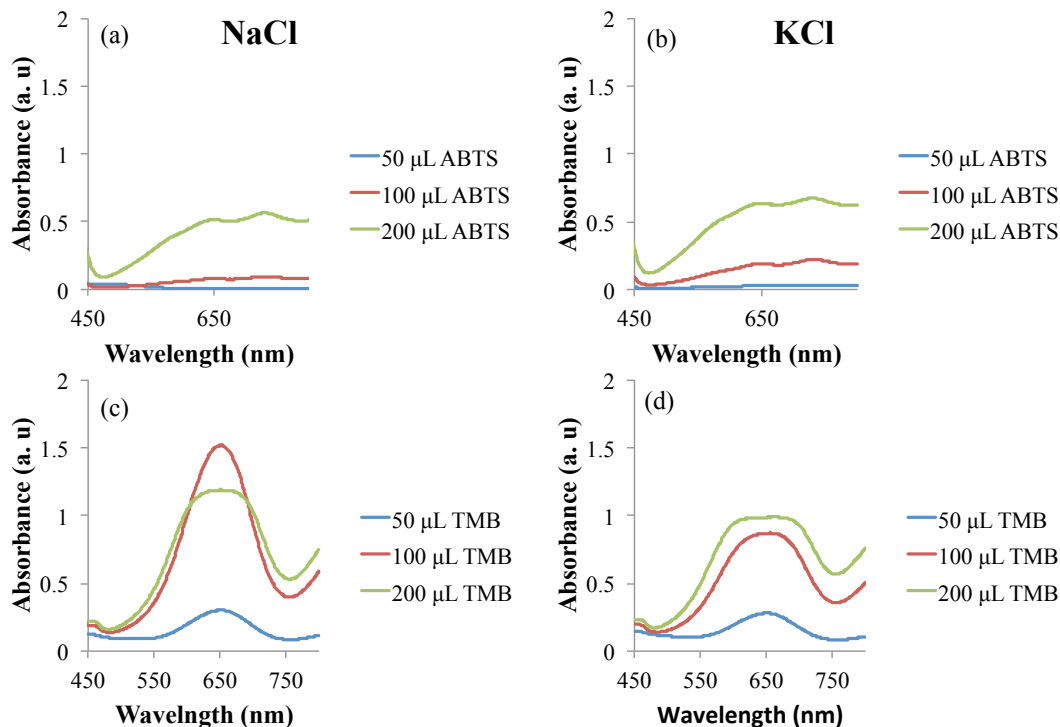


Figure 4.9 Comparison of 10 mM HEPES / 10 mM NaCl, pH 7.1 and 10 mM HEPES / 10 mM KCl, pH 7.1 buffers. 0.4 μM of DNAzyme and 0.4 μM of haemin were complexed in (a) 500 μL of NaCl buffer with ABTS/H₂O₂, (b) 500 μL of KCl buffer with ABTS/H₂O₂, (c) 500 μL of NaCl buffer with TMB/H₂O₂ and (d) 500 μL of KCl buffer with TMB/H₂O₂ for 30 minutes before analysis after 1 hour.

As expected, for ABTS as the volume of substrate was increased the absorbance increased, with the KCl buffer providing a slightly higher absorbance than the NaCl buffer. The results for TMB, however, did not follow this pattern and the highest absorbance obtained was for 100 μ L substrate in the NaCl buffer. The higher substrate volumes gave a dampened signal, perhaps due to over oxidation of the TMB to its second oxidation product, which has no absorbance in this region. Therefore 200 μ L of ABTS in 10 mM HEPES / 10 mM KCL, pH 7.1 and 100 μ L TMB in 10 mM HEPES / 10 mM NaCL, pH 7.1 were the conditions taken forward into analysis by resonance Raman scattering.

4.3.1.2 Oxidation Time

The time required for oxidation to take place was also an important factor to consider, in particular for ABTS, which has been shown to revert back to its colourless form over time, decreasing the absorbance in the region that is in resonance with the laser excitation wavelength. Additionally, TMB can proceed to the second oxidation product, which absorbs at 450 nm and, similarly, will affect the resonance Raman results. These effects were both observed visually over short periods of time (~ 15 minutes), as the ABTS turned colourless and the TMB turned green, an intermediate on the way to the final yellow oxidation product. Therefore, the amount of guanine-rich DNA used in experiments was decreased from 0.4 μ M to 0.1 μ M to try and combat this decrease in absorbance for both substrates. The absorbance for ABTS and TMB was monitored at 633 nm overnight in the presence of either Na⁺ or K⁺ ions in order to obtain an optimum analysis time and additionally confirm the correct choice of buffer for optimum peroxidase activity.

A sample containing all the components needed for DNAzyme activity was analysed for each substrate and buffer combination, which is represented by a blue line in each case in Figure 4.10. A set of controls were also analysed that consisted of substrate plus the guanine-rich DNA only (red), haemin only (green) and a nonsense sequence of DNA that is not rich in guanine and hence will not form the G-quadruplex needed for catalytic activity (purple).

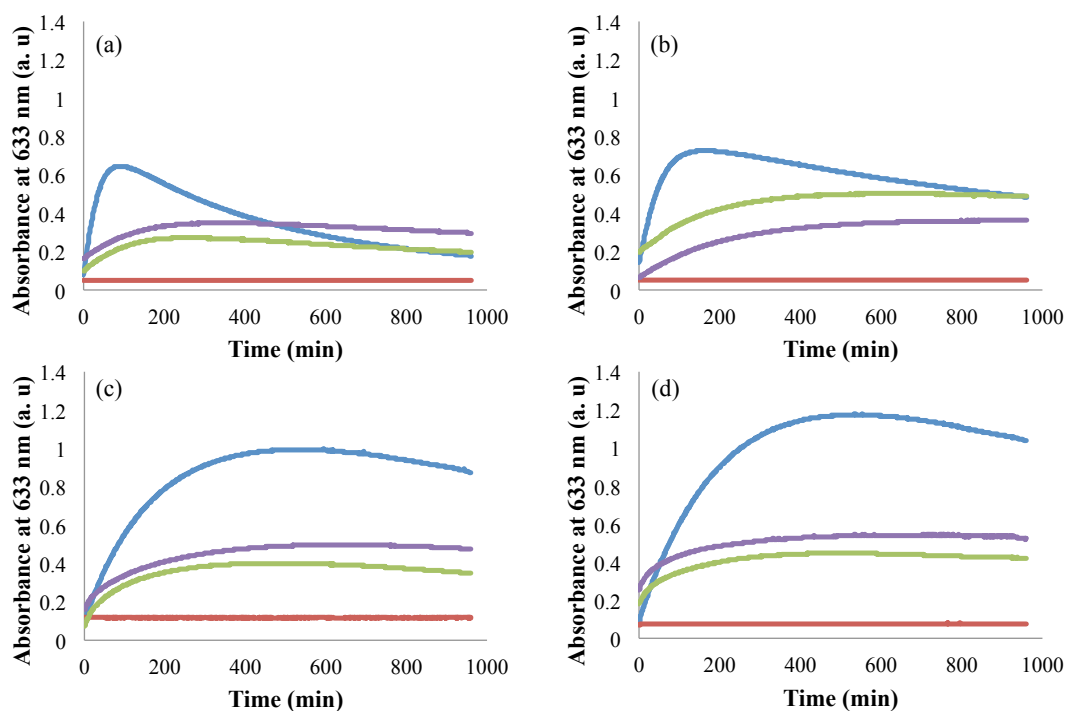


Figure 4.10 The oxidation of 200 μL of ABTS/ H_2O_2 in 500 μL final volume of (a) 10 mM HEPES / 10 mM NaCl, pH 7.1 and (b) 10 mM HEPES / 10 mM KCl, pH 7.1 and the oxidation of 100 μL TMB/ H_2O_2 in 500 μL final volume of (c) 10 mM HEPES / 10 mM NaCl, pH 7.1 and (d) 10 mM HEPES / 10 mM KCl, pH 7.1. 0.1 μM of DNAzyme and 0.1 μL of haemin were complexed in each buffer for 30 min before the addition of substrate and the absorbance at 633 nm was measured every 5 minutes for 960 minutes. A sample containing all components (blue) and controls samples were analysed that consisted of substrate plus DNA only (red), haemin only (green), and nonsense DNA (purple).

As can be seen in all spectra, when all the components needed for DNAzyme activity are present there is an increase in absorbance at 633 nm, and when there is no haemin, there is no oxidation of ABTS or TMB. Haemin itself, however, does have catalytic activity and so an increase in signal is seen for this control. Similarly, the nonsense DNA control contains haemin and so the increase in signal observed here is the result of the catalytic activity of haemin, and not from the formation of a DNAzyme. For ABTS, it is apparent that time is an important factor, as the absorbance at 633 nm will initially increase and then decrease over time for the DNAzyme system until there is no difference between this signal and the haemin background. This decrease in absorbance is slower in the presence of K^+ ions, confirming that this is the correct buffer and substrate combination. The optimum time for analysis, based on these results is 90 minutes, as this provided the biggest discrimination between signal and background. With TMB, the time taken to reach

the highest absorbance is longer, and the optimum response obtained is higher than for ABTS. The optimum analysis time is 3 hours and, unlike ABTS, this remains stable over a number of hours, retaining a good signal to background discrimination in both buffers. There is not a great difference between the ions used for TMB and based on the previous results, it was decided that TMB would continue to be analysed in an NaCl buffer. These results show that TMB provides a higher absorbance at 633 nm than ABTS, and it was thus expected that TMB would be the best substrate for analysis by resonance Raman scattering.

4.3.2 Resonance Raman Scattering of DNAzyme Activity

Once the DNAzyme parameters had been optimised, resonance Raman scattering was carried out using both ABTS and TMB to assess which substrate would give the best resonance Raman response and the greatest discrimination between the full DNAzyme system and controls.

4.3.2.1 Resonance Raman scattering of ABTS

ABTS has a primary absorbance for the radical anion at 414 nm and a secondary absorbance at 700 nm for the radical cation, the less favoured product from the reaction. Two laser excitation wavelengths were used to prove that the enhancement seen upon oxidation of ABTS is from resonance Raman scattering. The absorbance resulting from the radical cation will be in resonance with the 633 nm laser excitation wavelength, and although this is the less favoured product from the reaction, it was hoped that a strong resonance enhanced signal would be seen for ABTS after oxidation by a DNAzyme. A 514 nm excitation wavelength was also used which was off resonance with the radical anion or cation absorbance peaks. The results seen in Figure 4.11 confirms the hypothesis that the enhanced signals seen are the result of resonance Raman scattering. As can be seen in Figure 4.11 (a), there is a change in the peak intensity upon oxidation of ABTS, which can be attributed to the formation of an oxidation product in the visible region. However, this change is insignificant when compared to the analysis of the oxidation product by a 633 nm excitation wavelength, which is in resonance with the radical cation (Figure 4.11 (b)).

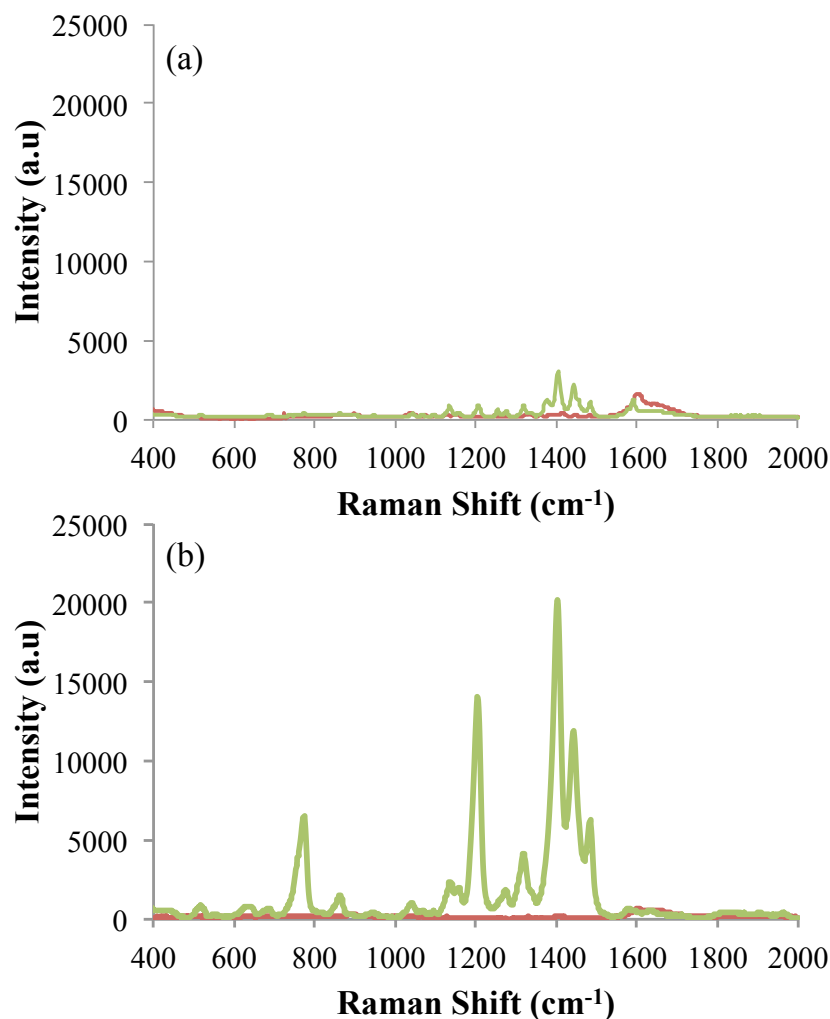


Figure 4.11 Analysis of the parent ABTS molecule (red) and the oxidation product (green) using (a) 514 nm laser excitation and (b) 633 nm laser excitation. 0.1 μM of DNAzyme and 0.1 μM of haemin were complexed for 30 minutes in 10 mM HEPES / 10 mM KCl, pH 7.1. 200 μL of ABTS/ H_2O_2 substrate was added to a final volume of 500 μL and left to react for 1.5 hours. 633 nm or 514 nm laser excitation was used at 4 mW power with 3 x 3 second accumulations. A sample volume of 60 μL was used for analysis and 5 scans of each sample were taken and baseline corrected using Grams Software.

There is no precedent in the literature for the assignment of peaks in the resonance Raman spectrum of ABTS. However, it is likely that the most intense bands at 770 cm^{-1} , 1202 cm^{-1} , and 1401 cm^{-1} are representative of C-S, sulfonic acid and aromatic ring vibrations, respectively. This data confirms that the oxidation of ABTS by a DNAzyme can be monitored using this type of Raman spectroscopy since upon formation of the radical oxidation products, which have an absorption in the visible region, the peaks correlating to ABTS are enhanced by resonance Raman scattering. A set of control samples were also analysed, similar to those used in Figure 4.10 to

confirm that the best resonance Raman enhancement was obtained for the full DNAzyme system.

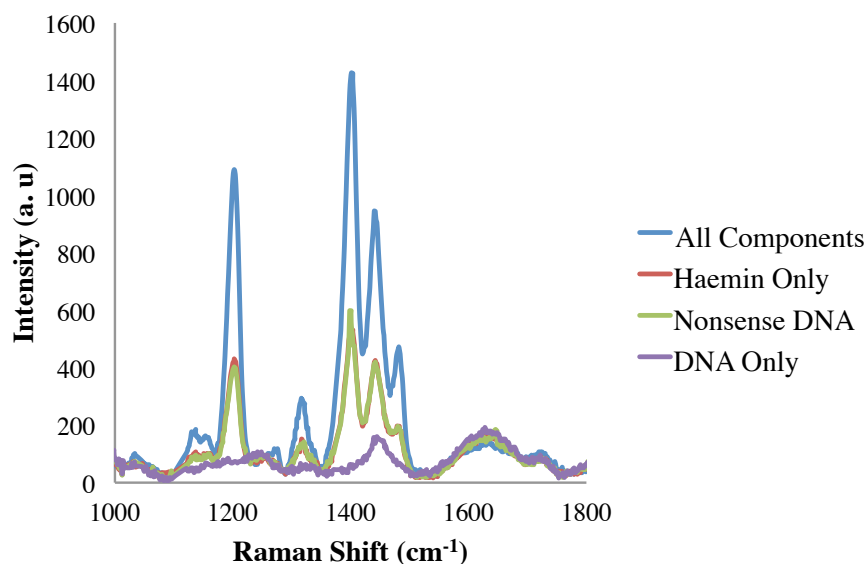


Figure 4.12 The resonance Raman scattering of ABTS after interaction with a DNAzyme (blue), and controls consisting of haemin only (red), nonsense DNA (green) and DNA only (purple). 0.1 μM of DNAzyme and 0.1 μM of haemin were allowed to complex in 10 mM HEPES / 10 mM KCl, pH 7.1, before the addition of 200 μL ABTS/H₂O₂ substrate in a final volume of 500 μL for a 1.5 hour reaction time. 5 replicate samples were prepared and scanned 5 times using 633 nm laser excitation at 4 mW power and 3 x 3 second accumulations. The spectra were baseline corrected using Grams Software.

Figure 4.12 mimics the results obtained from the UV-Vis time studies showing that when all components needed for DNAzyme activity are present, the signal is greater. Without haemin there is no catalytic activity, as there is no cofactor present to mimic the structure of HRP. Haemin itself, however, does afford a certain level of catalytic activity, and thus a background signal is present when analysing DNAzymes that utilise this particular metalloporphyrin. Similarly, for the nonsense DNA control, the signal seen is the direct result of the catalytic activity of haemin and not from the formation of a DNAzyme, since the sequence used will not be rich in guanine and hence cannot form the G-quadruplex structure required. When haemin is complexed within the G-quadruplex structure, however, the signal is enhanced, due to greater catalytic activity from the DNAzyme, and there is good discrimination for the ABTS substrate between the DNAzyme system and the background haemin signal.

The next step in the resonance Raman analysis of ABTS was to determine the lowest concentration of guanine-rich DNA that could be detected using this method. In this experiment the haemin concentration was kept constant and the concentration of guanine-rich DNA decreased, the results of which can be seen in Figure 4.13.

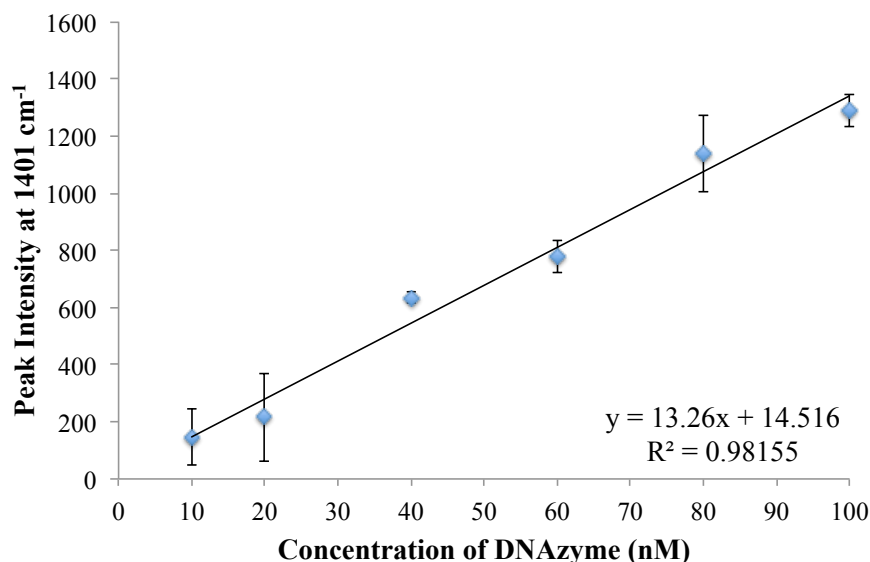


Figure 4.13 Concentration of DNAzyme versus RRS intensity. 0.1 μM of haemin was complexed with varying DNA concentrations in 10 mM HEPES / 10 mM KCl, pH 7.1 before 200 μL of ABTS/ H_2O_2 substrate was added to a final concentration of 500 μL . 5 replicate samples were prepared and 5 scans of each were taken using 633 nm laser excitation using 4 mW power and 3 x 3 second accumulations. The data points reported were obtained by subtracting the peak height at 1608 cm^{-1} for the haemin only sample from the peak height at 1608 cm^{-1} for the full DNAzyme sample. Error bars represent one standard deviation of 5 replicate samples.

The data points were obtained using the peak height at 1401 cm^{-1} , as this was the most intense band, and subtracting the background haemin sample from each concentration of guanine-rich DNA, allowing for a linear relationship between the concentration of DNAzyme and peak intensity to be realised. The lowest observable concentration observed using ABTS and resonance Raman scattering was 10 nM, and it was hoped that this limit of detection could be reflected when using RRS of DNAzymes for the detection of a target DNA sequence.

4.3.2.2 Resonance Raman Scattering of TMB

The product analysed by resonance Raman scattering due to the oxidation of TMB is the charge transfer complex resulting from the one electron oxidation reaction, which

absorbs at 650 nm. This will be the only form of TMB that is in resonance with the 633 nm excitation wavelength and thus should be the only species that will give an enhanced Raman signal. This is confirmed in Figure 4.14

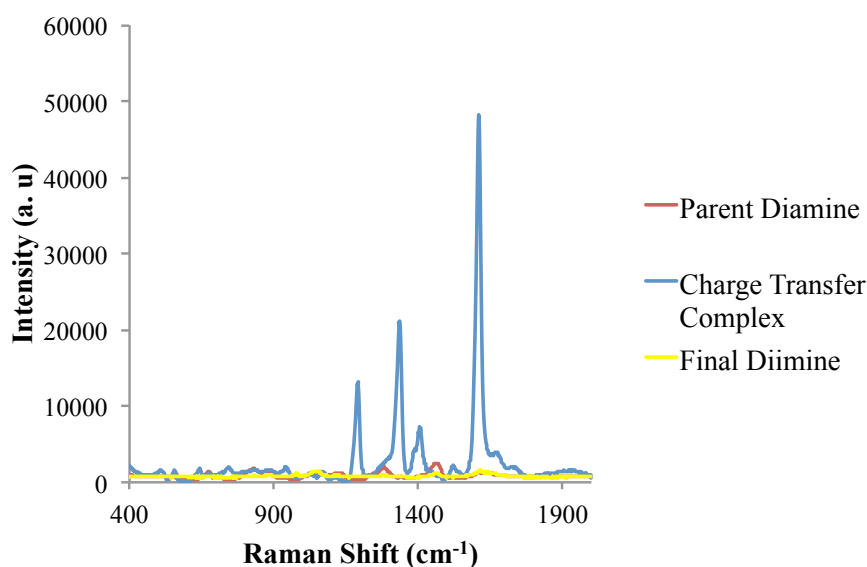


Figure 4.14 Analysis of the parent TMB molecule (red) and the first (blue) and second (yellow) oxidation products. 0.1 μM of DNAzyme and 0.1 μM of haemin were complexed for 30 minutes in 10 mM HEPES / 10 mM NaCl, pH 7.1. 100 μL of TMB/ H_2O_2 substrate was added to a final volume of 500 μL and left to react for 3 hours. 633 nm laser excitation was used at 4 mW power with 3 x 3 second accumulations. A sample volume of 60 μL was used for analysis and 5 scans of each sample were taken. The final diimine was formed by the addition of H_2SO_4 . The spectra were baseline corrected using Grams Software.

There is a large enhancement in signal seen upon action of the DNAzyme, which can be attributed to the formation of a substance that is in resonance with the chosen excitation wavelength. This is confirmation of the formation of the CTC resulting from the one electron oxidation of TMB. In their paper, Laing *et al.* demonstrated the first reported case of resonance Raman analysis of the CTC and tentatively assigned the enhanced bands to CH_3 bending modes (1191 cm^{-1}), inter-ring C-C stretching modes (1336 cm^{-1}) and a combination of ring stretching and C-H bending modes (1609 cm^{-1}),¹⁷⁸ all of which are observed in Figure 4.14 Thus, resonance Raman scattering can be successfully used to analyse this oxidation reaction. Similarly to ABTS, a set of controls were also analysed, to ensure maximum enhancement from the complete DNAzyme system.

Figure 4.15 displays a similar result to that discussed previously for ABTS. In the absence of haemin there is no catalytic activity, and hence no oxidation to form a product in resonance with the excitation source, and no enhancement in signal. Again, haemin itself can oxidise TMB to the CTC, and this is confirmed via the spectra observed for the haemin only and nonsense DNA controls.

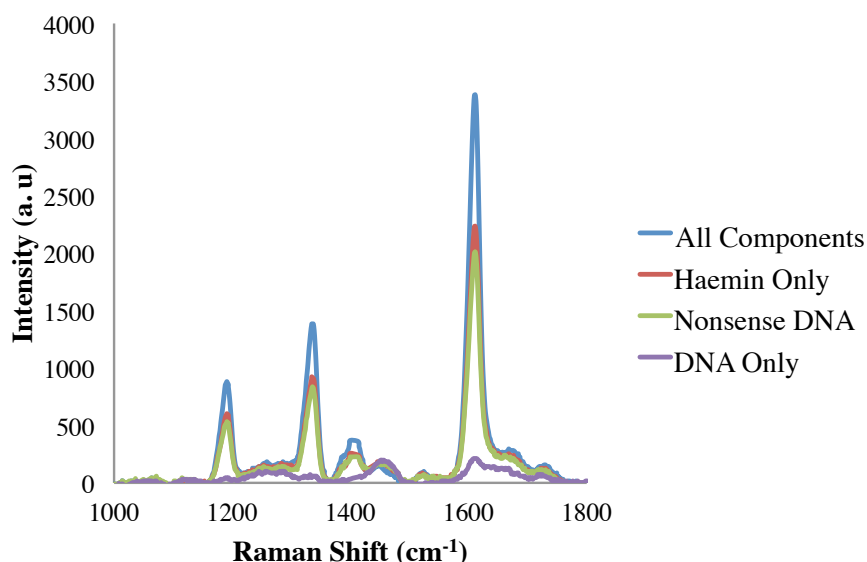


Figure 4.15 The resonance Raman scattering of TMB after interaction with a DNAzyme (blue), and controls consisting of haemin only (red), nonsense DNA (green) and DNA only (purple). 0.1 μ M of DNAzyme and 0.1 μ M of haemin were allowed to complex in 10 mM HEPES / 10 mM NaCl, pH 7.1, before the addition of 100 μ L TMB/H₂O₂ substrate to a final volume of 500 μ L for 3 hours reaction time. 5 replicate samples were prepared and scanned 5 times with a 633 nm laser excitation at 4 mW power and 3 x 3 second accumulations. The spectra were baseline corrected using Grams Software.

However, the spectrum seen in the presence of all components is more intense than the haemin background with a good discrimination and this is due to the greater catalytic activity of the haemin and G-quadruplex combination. Therefore the lowest concentration of DNAzyme that could be detected via the oxidation of TMB and analysis by resonance Raman scattering was investigated. Figure 4.16 shows the results obtained from lowering the concentration of the guanine-rich DNA while keeping all other components constant. In this case the peak height at 1608 cm⁻¹ was used in the analysis, as this is the most intense band for TMB. Unlike ABTS, the relationship between DNAzyme concentration and peak intensity follows a logarithmic trend as opposed to a linear one. This is likely the result of a combination

of the lower substrate volume and increased reaction time for the analysis of TMB compared to ABTS. Although optimisation results showed that these parameters provided the greatest discrimination between the DNAzyme signal intensity and the haemin background, this may also be the point where the substrate has been exhausted and there is no more TMB to be oxidised. Thus the signal starts to plateau as the higher concentrations of DNAzyme are used, which allows for the maximum signal to be reached faster.

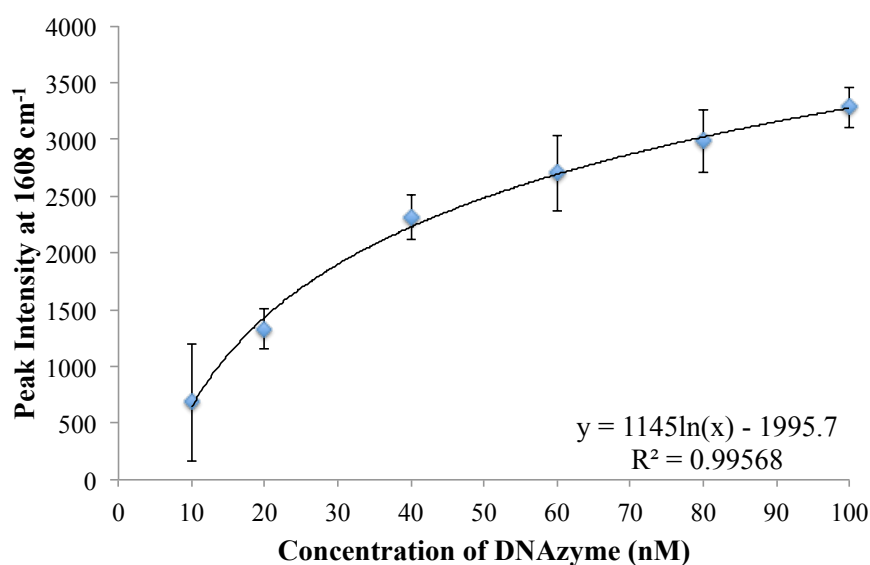


Figure 4.16 Concentration of DNAzyme versus intensity of the 1608 cm⁻¹ peak. 0.1 μM of haemin was complexed with varying DNAzyme concentrations in 10 mM HEPES / 10 mM NaCl, pH 7.1 before 100 μL of TMB/H₂O₂ substrate was added to a final concentration of 500 μL. 5 replicate samples were prepared and 5 scans of each were taken using a 633 nm laser excitation at 4 mW power and 3 x 3 second accumulations. The data points reported were obtained by subtracting the peak height at 1608 cm⁻¹ for the haemin only sample from the peak height at 1608 cm⁻¹ for the DNAzyme sample. Error bars represent one standard deviation of 5 replicates.

An observable concentration of 10 nM DNAzyme was observed when using TMB alongside resonance Raman scattering. Again, it was hoped that this detection limit could be mirrored when this method of oxidation and detection was incorporated into the catalytic beacon based assay protocol for the detection of target DNA.

4.3.3 Catalytic Beacons for DNA Detection

The assay outlined in Figure 4.7 was then used alongside the optimised parameters for DNAzyme activity in order to detect a synthetic sequence of target DNA via resonance Raman analysis.

4.3.3.1 Detection of Synthetic DNA

The beacon and target were hybridised in the appropriate buffer for the substrate used, before haemin and substrate were added and the sample left to oxidise before analysis by resonance Raman scattering. The results for ABTS are shown in Figure 4.17.

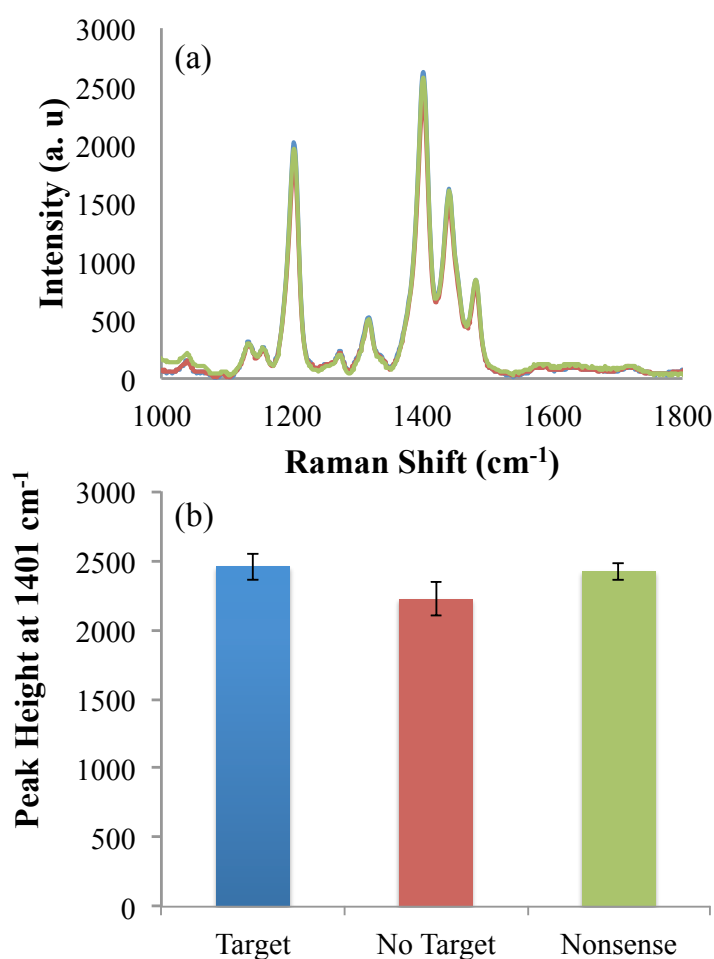


Figure 4.17 Catalytic beacons for DNA detection. 0.1 μM of beacon and 1 μM of target DNA were hybridised in 10 mM HEPES / 10 mM KCl, pH 7.1. 0.1 μM of haemin was added and complexed for 30 minutes before the addition of 200 μL of ABTS/ H_2O_2 . After 1.5 hours reaction time the samples were analysed by a 633 nm laser excitation wavelength at 4 mW using 3 x 3 second accumulations. 5 replicate samples were prepared and scanned 5 times. (a) The corrected resonance Raman spectra obtained in the presence of target (blue), without target (red) and with a nonsense sequence of DNA (green). (b) The raw data showing error bars which represent one standard deviation of 5 replicate samples.

Unfortunately, there is no discrimination between the presence and absence of target DNA. It is possible that these results can be attributed to the reverse oxidation process of ABTS and that the presence of non-resonant molecules is reducing the signal to the same intensity as the haemin background.

To try and combat this, the concentrations of beacon, haemin, and ABTS were varied. The time taken for analysis was also varied as was the buffer used, however no discrimination between signal and background was achieved. Although the successful detection of ABTS oxidation via a DNAzyme and resonance Raman scattering has been proven, this substrate was not suitable for use in the catalytic beacon assay protocol for target DNA detection.

The use of TMB as a substrate, however, yielded much more promising results. Figure 4.18 demonstrates that when the target DNA is present the beacon will open, allowing the G-quadruplex to form. Then, when haemin is added to the system, the DNAzyme will catalyse the oxidation of TMB to the CTC, which is in resonance with the 633 nm laser excitation wavelength used. As such, there is greater catalytic activity and hence an increase in signal intensity when the target is present, compared to when it is not, where the signal obtained is purely the result of the catalytic activity of haemin.

This successful result was obtained by reducing the amount of TMB / H₂O₂ substrate used, from 100 µL to 50 µL in the assay, since when higher volumes of substrate were used oxidation to the second product was apparent. This was seen via a blue to green colour change and a reduction in the intensity of the resonance Raman spectrum. This change in volume allowed for no formation of the final diimine and an excellent discrimination between target signal and the haemin background. Thus, since this method could be used to detect target DNA, a concentration study was carried out to determine the limit of detection.

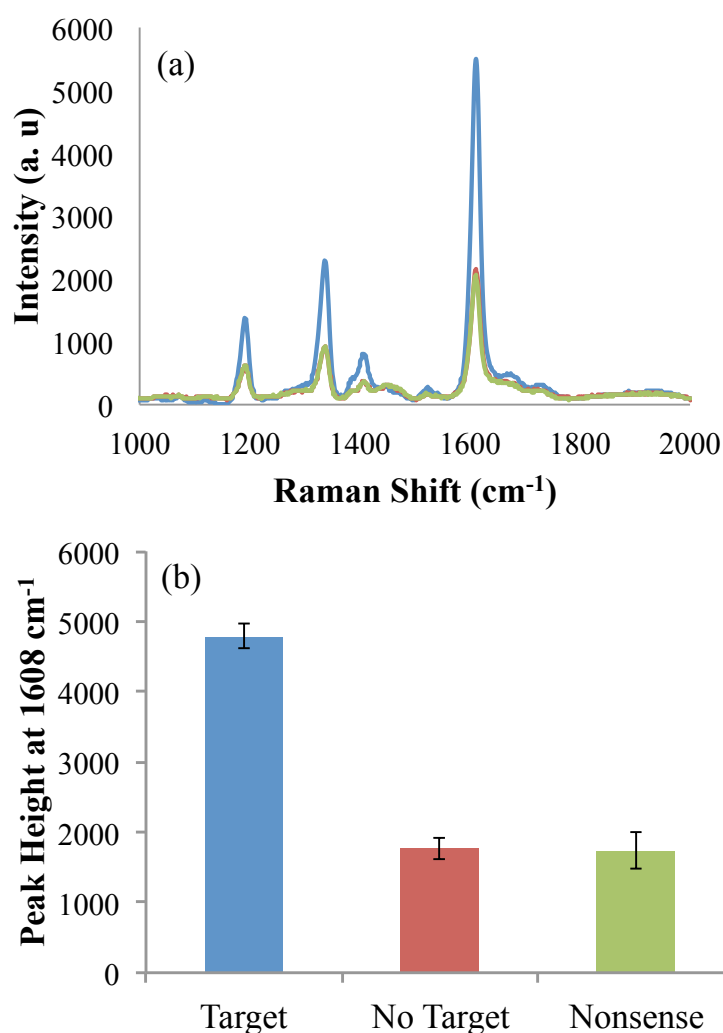


Figure 4.18 Catalytic beacons for DNA detection. 0.1 μM of beacon and 1 μM of target DNA were hybridised in 10 mM HEPES / 10 mM NaCl, pH 7.1. 0.1 μM of haemin was added and complexed for 30 minutes before the addition of 50 μL of TMB/ H_2O_2 . After 3 hours reaction time samples were analysed using power 633 nm laser excitation wavelength at 4 mW using 3 x 3 second accumulations. 5 replicate samples were prepared and scanned 5 times. (a) The corrected resonance Raman spectra obtained in the presence of target (blue), without target (red) and with a nonsense sequence of DNA (green). (b) The raw data showing error bar which represent one standard deviation of replicate samples.

To determine the detection limit for this system, the amount of beacon, haemin and TMB were kept constant, while the concentration of target DNA was varied. An example of the results obtained is shown in Figure 4.19 (a). The relationship between the concentration of target and the peak intensity follows a trend not unlike that obtained for the detection of DNAzyme (Figure 4.15). It appears that at higher concentrations of target DNA the signal plateaus, which is likely the point at which all the substrate has been used up, and this happens at a faster rate when there is

more DNAzymes free in solution due to the increased concentration of target DNA present. The response does not follow first order kinetics, however the reaction could potentially be described using Michaelis-Menten kinetics. At lower concentrations, the relationship follows a more linear trend, as can be seen in Figure 4.19 (b). From these results an observable limit of detection of 10 nM can be obtained which mimics that for the guanine rich DNA discussed previously. These results, however, are not reproducible. The data points were obtained by subtracting the background haemin signal, and in the majority of cases there was no difference, providing a variety of concentration graphs that appeared to follow no observable trend.

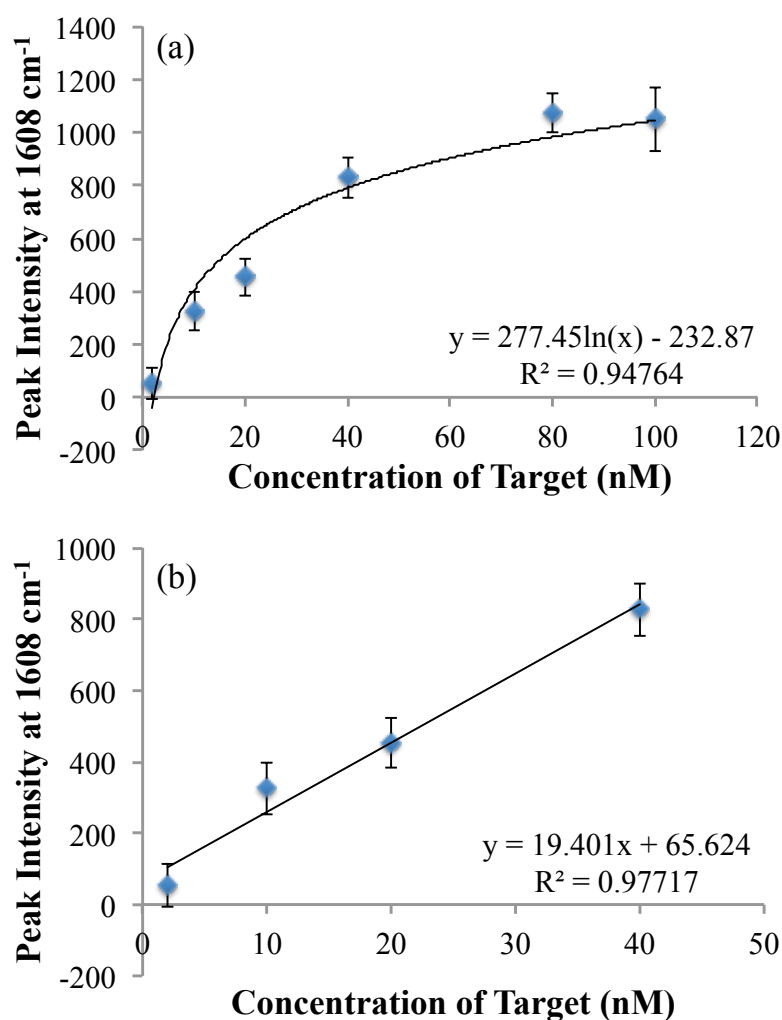


Figure 4.19 Limit of detection study for target DNA. (a) 0.1 μ M of DNAzyme was hybridised with varying amounts of target DNA in 10 mM HEPES / 10 mM NaCl, pH 7.1. 0.1 μ M of haemin was added for 30 minutes and then 50 μ L TMB/H₂O₂ added for 3 hours. 633 nm laser excitation was used at 4 mW power with 3 x 3 second accumulations and 5 scans of each sample were taken. Error bars represent one standard deviation of 5 replicate samples. (b) Linear response obtained from lower target concentrations.

A number of parameters were varied to try and obtain a linear response, such as oxidation time, component concentration and buffer salt concentrations, none of which enabled a reproducible limit of detection to be obtained. There are number of processes that must occur for the success of this assay, namely beacon opening, target hybridisation, haemin complexation, and TMB oxidation. Therefore, it is possible that this relationship will never be linear, and that we cannot use this assay for quantitative detection. However, this assay can successfully and reproducibly detect target DNA at 1 μ M concentration, and as such these catalytic beacons were used alongside PCR for the detection of target DNA.

4.3.3.2 *Detection of PCR Product*

Although these catalytic beacons could not be used to obtain a reproducible limit of detection for target DNA, it was expected that this assay could potentially be used for the detection of DNA that had been through PCR amplification. The PCR amplification was carried out according to a standard method, using a 99 base sequence of genomic DNA correlating to the *MecA* gene of an MRSA strain as the template DNA strand. It was thought that a longer sequence of DNA would be more successful in the catalytic beacon assay compared to the 21 base long exact complement used previously, as the longer sequence could potentially infer more stability to the open beacon format. This amplification process was monitored using the intercalator SYBR Green I alongside fluorescence spectroscopy as can be seen in Figure 4.20.

When the template DNA, which is the DNA requiring amplification, is added to the system, the PCR thermal cycle allows for the hybridisation of primers to the template. These primers are then elongated via an enzymatic process and mononucleotides that eventually results in the formation of a duplicate template strand. This process allows for the exponential increase of target DNA concentration that can be monitored using the intercalator SYBR Green I, whereby the fluorescence will increase in the presence of duplex DNA. Figure 4.20 confirms that the template DNA has been amplified and that there is no amplification, and hence contamination, in the no template control. The DNA obtained from this process was roughly 10 nM in concentration and the crude PCR product, without the SYBR

Green I, was taken directly from amplification into the catalytic beacon assay protocol.

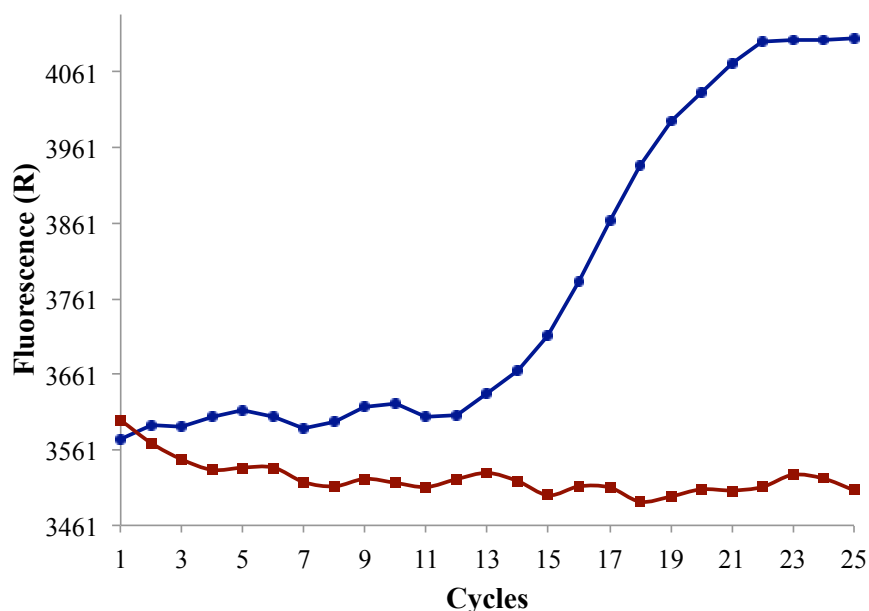


Figure 4.20 SYBR Green PCR amplification plots with template present (blue) and no template present (red). Fluorescence was measured after every thermal PCR cycle totalling 25 cycles.

The beacon assay was scaled down for the analysis of PCR product, since sample volume was restricted. 0.1 μM of the beacon and 5 μL of PCR product, from both the template and no template amplification, were hybridised in 10 mM HEPES / 10 mM NaCl, pH 7.1 before the addition of 10 nM haemin and then 40 μL TMB/ H_2O_2 in a final volume of 200 μL . The samples were then analysed using an excitation wavelength of 633 nm and the results can be seen in Figure 4.21.

Although the spectra obtained have a poor signal to noise ratio and a large background, the main peaks for the CTC can still be seen at 1608 cm^{-1} , 1330 cm^{-1} , and 1180 cm^{-1} . More importantly, these peaks increase in the presence of template in comparison to when there is no template present. This is clarified in Figure 4.21 (b) where there is a significant difference between the template and no template samples. Thus, catalytic beacons and resonance Raman scattering can be used to detect DNA that has been amplified by PCR.

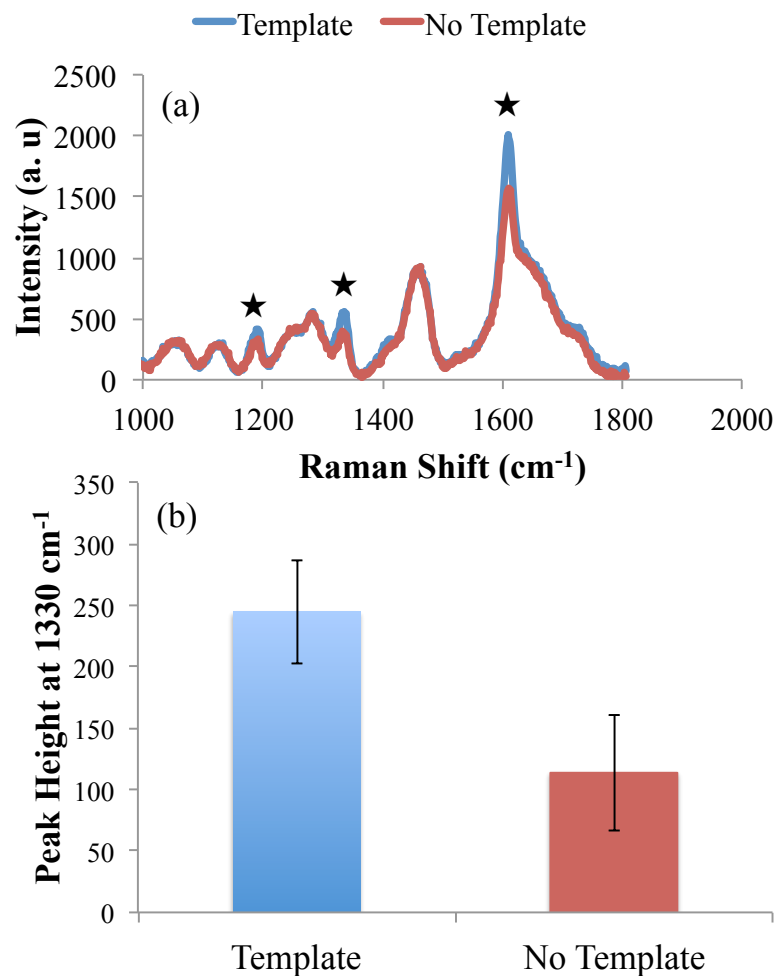


Figure 4.21 Detection of PCR product by catalytic beacons and RRS. 0.1 μM of beacon and 5 μL of PCR product, from amplification with (blue) and without (red) template DNA, were hybridised in 10 mM HEPES / 10 mM NaCl, pH 7.1. 10 nM of haemin was added and then 40 μL of TMB/ H_2O_2 in a final volume of 200 μL . Samples were analysed after 3 hours using 633 nm laser excitation at 4 mW power and 3 x 3 second accumulations. 5 replicate samples were prepared and scanned 5 times, to produce (a) the corrected spectra and (b) a comparison of the peak height at 1608 cm^{-1} . Error bars represent one standard deviation of 5 replicate samples

Catalytic beacons have been successfully utilised to detect DNA. However, the sensitivity is limited by the haemin background, and thus it was important to try and minimise this effect in order to realise a sensitive detection for target DNA using DNAzymes and resonance Raman scattering.

4.3.4 A Split Probe DNAzyme Assay for the Detection of DNA

A new assay was designed that would still incorporate DNAzyme activity and resonance Raman scattering for the detection of target DNA, but would attempt to reduce the background haemin signal that presented itself as a problem in the catalytic beacon assay protocol.

4.3.4.1 Streptavidin Coated Magnetic Beads

The basis of this new design was the addition of a magnetic wash step, which would allow for complete removal of any background signal. The basic mechanism is outlined in Figure 4.22.

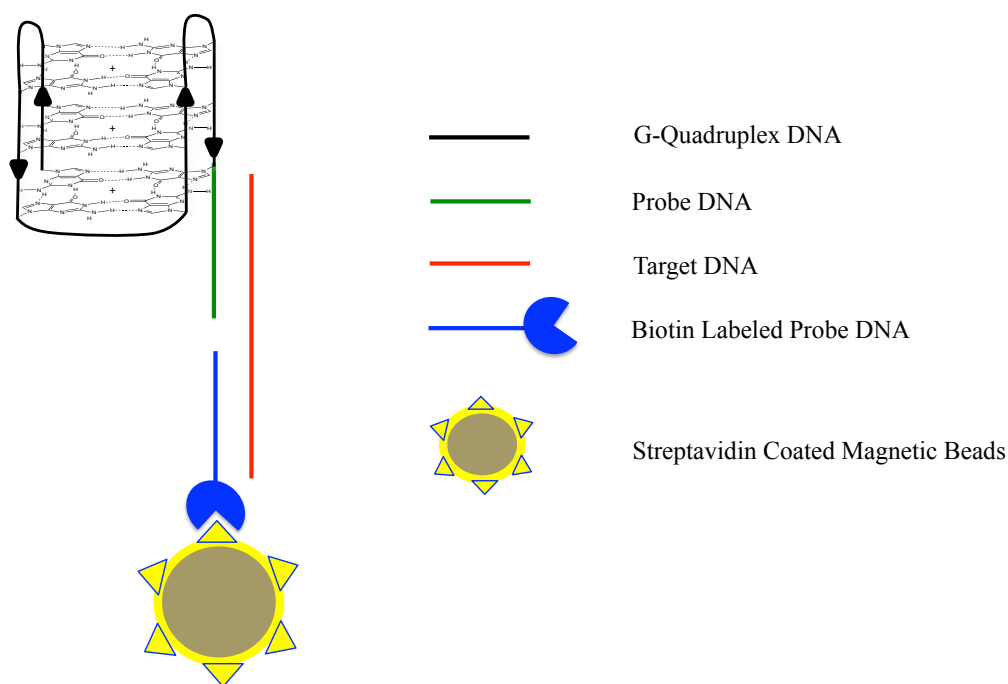


Figure 4.22 Split probe DNAzyme assay for target DNA detection. Upon addition of the target sequence (red) to the G-Quadruplex region (black and green) and biotin labelled DNA (blue), the DNAzyme will be able to survive a magnetic wash step using streptavidin coated magnetic beads. It will then be able to catalyse the oxidation of TMB. In the absence of target DNA, and no hybridisation, the DNAzyme will be washed away and no signal should be seen from the CTC.

A split probe DNA system was used, which consisted of a G-Quadruplex region of DNA and a biotin labelled DNA sequence. The G-Quadruplex was designed with a section that was complementary to a region of the desired target, and the biotin labelled DNA was also complementary to a region of this sequence. Thus, when the

target DNA is present, it hybridises together both the biotin labelled DNA and the G-Quadruplex. Upon addition of the streptavidin coated magnetic beads, there is an interaction between the biotin and the streptavidin, and upon the addition of a magnet, the whole DNAzyme system can be pulled to one side and survive a number of wash steps. In the absence of target however, only the biotin labelled DNA will be separated by the magnet, and hence no DNAzyme will be present. This means that only when the target is present will the DNAzyme be able to catalyse TMB⁰ to the CTC, allowing for an enhanced resonance Raman signal. Without the target, there will be no DNAzyme to catalyse this reaction, and hence no signal should be seen.

In theory, this design was fairly straightforward, the G-quadruplex region, target and biotin labelled DNA were hybridised in the chosen buffer before the addition of the streptavidin coated magnetic beads. This was then left to react at room temperature for 30 minutes before being washed 3 times with buffer. Haemin was then added to the system and this was again left to react for 30 minutes and the wash step repeated. The TMB / H₂O₂ substrate was added and the sample analysed after 3 hours with an excitation wavelength of 633 nm. The background signal should be minimised since, when there is no target present, only biotin labelled DNA should survive the wash step and hence no catalyst, either haemin or DNAzyme, would remain to catalyse the oxidation of TMB.

The results from initial experiments, however, were not as expected as a background signal still existed and there was no discrimination between the presence and absence of target DNA. Figure 4.23 shows the results obtained, and demonstrates that even in the absence of the biotin labelled DNA and target DNA there is still a significant signal observed. Thus, after the wash step, a catalytic agent remains, perhaps suggesting that there is some interaction between the haemin and the streptavidin coated magnetic beads. Also, there is a signal, albeit a comparatively low signal, for single stranded DNA, which should have no effect on the TMB. However, since streptavidin coated magnetic beads are present in all the samples, the beads could be causing these unexpected results.

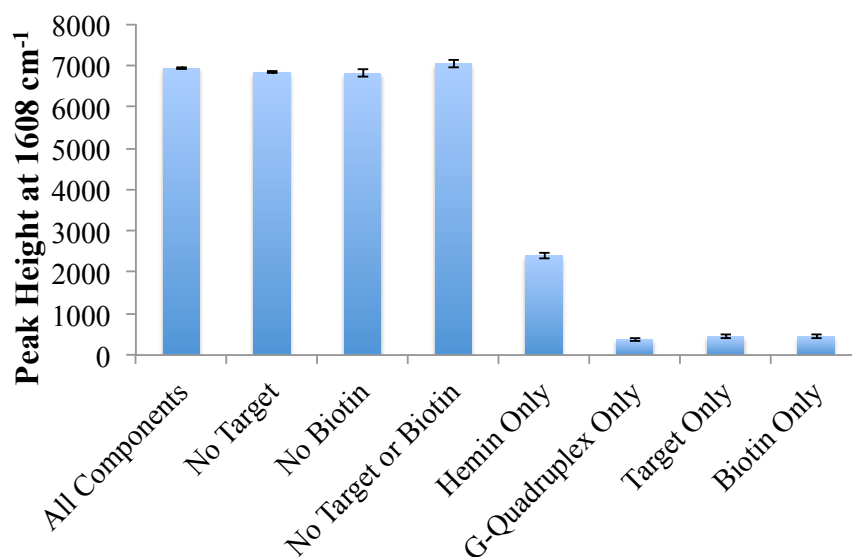


Figure 4.23 Results from the split probe magnetic separation DNAzyme assay along with a set of controls. 0.1 μM of each component were used in 500 μL of 10 mM HEPES / 10 mM NaCl, pH 7.1. After numerous wash steps 100 μL of TMB/H₂O₂ was added and analysed using 633 nm laser excitation at 4 mW power and 3 x 3 second accumulations. 5 scans were taken of each sample and error bars represent one standard deviation of 3 replicate samples.

In 2007, Yan and co-workers reported on the intrinsic peroxidase-like activity of ferromagnetic nanoparticles and noted how magnetite nanoparticles could be used to catalyse the oxidation of peroxidase substrates such as TMB.¹⁷⁹ Although the particles used in our split probe assay are coated with streptavidin, which should shield the iron core, their catalytic activity was investigated. The streptavidin coated magnetic beads and TMB / H₂O₂ were left to react for 3 hours and then analysed using resonance Raman scattering.

As can be seen in Figure 4.24, there is clear oxidation of the TMB, as can be seen by the enhanced peaks characteristic of the CTC. This oxidation is the result of the peroxidase-like activity of the iron oxide beads and as such this assay cannot be used for the quantitative detection of DNA due to the interference from these streptavidin coated magnetic beads.

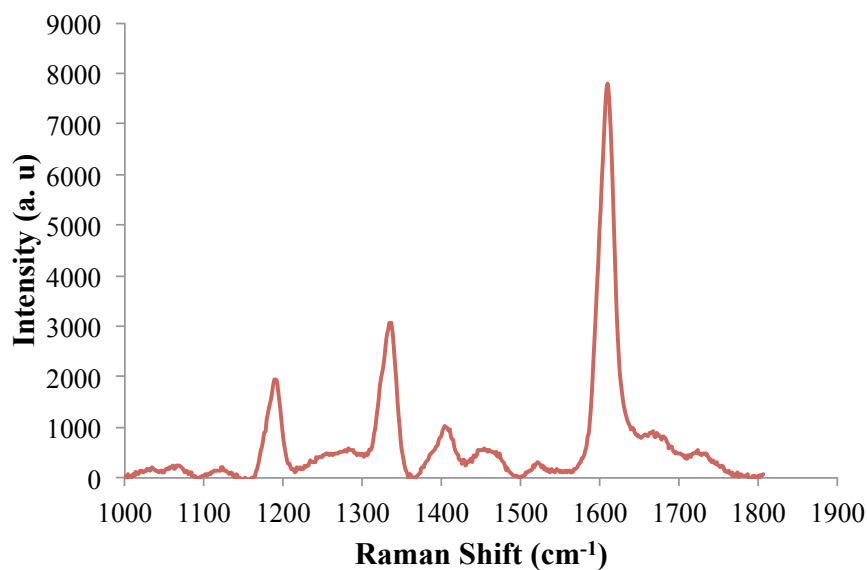


Figure 4.24 The oxidation of TMB by streptavidin coated magnetic beads. 0.1 μM of streptavidin coated magnetic beads was added to 100 μL of TMB/ H_2O_2 in 500 μL final volume and reacted for 3 hours. The sample was then analysed using 633 nm laser excitation at 4 mW power using 3 x 3 second accumulation. The data was then baseline corrected using Grams software.

4.3.4.2 Streptavidin Coated Plates

To try and combat the oxidative capabilities of streptavidin coated magnetic beads, 96-well streptavidin coated plates were used as an alternative separation method. The assay followed essentially the same format, however the biotin labelled DNA was bound to static streptavidin coated microwell plates. Thus, instead of separation via a magnet, the biotin labelled DNA and hence DNAzyme would be retained on the bottom of the well. Upon addition of TMB, oxidation should occur in the presence of target DNA, and the sample could be analysed directly within the microwell plate. This was a promising method of separation since the removal of the magnetic beads should remove any background signal. The results, however, were not as expected and can be seen in Figure 4.25.

Unfortunately, there was no discrimination in signal observed between when the target is present and when it is absent. Only when the target is present should the DNAzyme be retained on the streptavidin plates and be able to oxidise TMB to the CTC resulting in the signal observed in Figure 4.25.

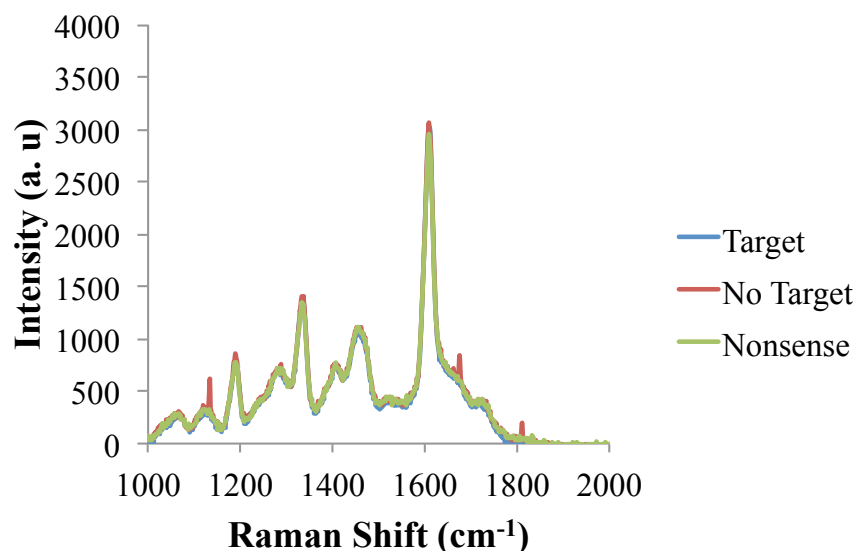


Figure 4.25 Split probe DNAzyme assay on streptavidin coated plates. 0.1 μM of target DNA, 0.1 μM of probe DNA and 10 nM of biotin labelled DNA were hybridised in 10 mM HEPES / 10 mM NaCl, pH 7.1 and then 200 μL was added to the plates. They were left to react at room temperature for 2 hours before a buffer wash step (x 3) and addition of 0.1 μM haemin. The samples were left to react in the plate for 30 minutes before another buffer wash step (x3) and the addition of 80 μL of TMB/ H_2O_2 in 200 μL buffer. The samples were analysed on plate after 3 hours with 633 nm excitation at 4 mW power and 3 x 3 second accumulations. Samples were prepared in triplicate and scanned 5 times. The results were baseline corrected and an average taken to obtain the spectra.

Thus, it was concluded that the haemin has some interaction with the streptavidin and is being retained on the plates, and so the signal seen is purely that of the haemin background that this split probe assay was designed to minimise. The presence of the target and hence DNAzyme, should of course increase the signal, however, if all the haemin is being retained while some DNAzymes are lost through inefficient hybridisation, this would explain why there is no observed difference in signal. The ratios of each components were varied to try and combat this problem, however, no successful discrimination was achieved.

Therefore, the background haemin sample could not be removed using a split probe DNAzyme detection assay combined with a separation step. Thus, surface enhanced resonance Raman scattering (SERRS) was attempted alongside DNAzyme activity to investigate what effect this would have in comparison to resonance Raman

scattering, in the hope that the discrimination between the desired signal and the background haemin signal could be minimised.

4.3.5 SERRS Analysis of DNAzyme Activity

As has been mentioned previously, SERRS has been used in combination with ABTS and HRP for the detection of PSA.¹⁸⁰ Additionally, nanoparticles have been employed alongside DNAzyme activity for the colourimetric detection of cocaine¹⁸¹ and the fluorescence detection of G-quadruplex binding ligands.¹⁸² However, as is the case with resonance Raman scattering, SERRS has never been previously used to monitor the peroxidase activity of an HRP-mimicking DNAzyme.

4.3.5.1 Metallic Nanoparticles for the Analysis of DNAzyme Activity

One of the main things to consider when adding nanoparticles to the DNAzyme system, was the charge on the surface of the nanoparticles used in comparison to the charge on the substrates. Both silver and gold nanoparticles were used in SERRS experiments that were synthesised according to standard citrate reduction protocols, resulting in a negative surface layer of citrate ions. ABTS and its oxidation product both have a negative charge, while TMB is a neutral molecule oxidised to a positive CTC. Thus, it was expected that ABTS would not be as compatible with the nanoparticles used, while a good enhancement in signal would be seen for the oxidation of TMB using a DNAzyme and analysis by SERRS.

The DNAzyme sequence and haemin were complexed for 30 minutes, before the addition of the TMB / H₂O₂ substrate. After 3 hours, either gold or silver nanoparticles were added to the sample and analysed immediately. As can be seen in the Figure 4.26 inset, there is a large increase in signal seen upon the addition of gold nanoparticles to the DNAzyme system, as expected. However, there is no discrimination between the samples that contain haemin, as they are all enhanced to the same degree. Also, in the sample that contains a sequence of DNA only, there is a slight signal seen which is very unexpected given that there is only single stranded DNA and nanoparticles in the system. Thus the CTC should not be formed and no signal should be observed. This is an interesting phenomenon and shall be discussed

further in Chapter 5, however, for the purpose of this experiment the signal seen was small enough to be ignored.

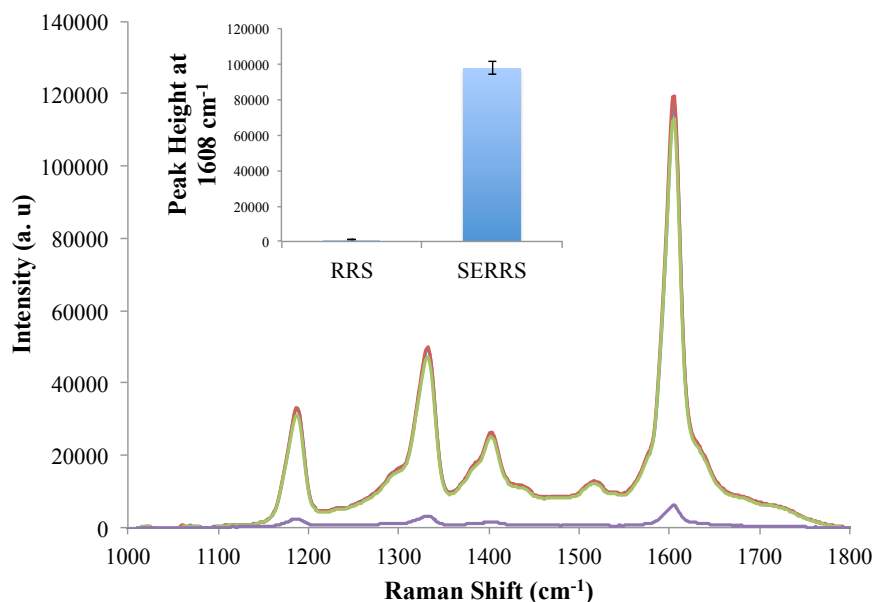


Figure 4.26 SERRS analysis of the full DNAzyme system (blue) with controls containing haemin only (red), nonsense DNA (green) and DNA only (purple). 0.1 μM of DNA and 0.1 μM of haemin were complexed in 10 mM HEPES / 10 mM NaCl, pH 7.1 for 30 minutes. 100 μL of TMB/ H_2O_2 substrate was added to 500 μL final volume of buffer and left to react for 3 hours. 200 μL of sample was added to 400 μL gold colloid and analysed using 633 nm laser excitation at 1 mW power and 3 x 3 second accumulations. Inset shows the comparison of the peak height at 1608 cm^{-1} with and without nanoparticles. Samples were scanned 5 times and error bars represent one standard deviation of 5 replicate scans.

Although a good signal was obtained, the haemin background seen in resonance Raman analysis still exists. Similar results were obtained when using silver nanoparticles, which gave an even bigger increase in signal in comparison to gold. However, once again, no discrimination could be observed between the samples that contained haemin. It was deduced that perhaps the haemin itself is interacting with the surface of the charged nanoparticles via the carboxylic acid groups on the porphyrin structure. If this co-factor interacts with metallic nanoparticles instead of the G-quadruplex structure, then no DNAzyme molecules will be formed and thus any signal observed indicative of the CTC will be the result of the oxidative capabilities of haemin alone.

Although, the discrimination between DNAzyme activity and background haemin signal was disappointing, the oxidation of TMB could be monitored using SERRS, as an enhanced signal was seen. This was not the case when using ABTS, as no oxidation could be detected via enhanced peaks representative of the radical oxidation product. This was expected due to the negative charge on both the nanoparticles used and the substrate that would likely repel each other, resulting in poor absorption of the analyte onto the surface of the nanoparticle and thus poor SERRS. To try and overcome this problem, spermine hydrochloride was used as an external charge modifying agent. This is often used alongside the SERRS analysis of DNA to serve the dual purpose of overcoming the repellent charges between the negative DNA backbone and the negative citrate layer on the surface of the nanoparticles,¹⁸³ as well as acting as an aggregating agent. In order for a good SERRS signal to be achieved, aggregation of the nanoparticles is an important factor.¹¹⁴ It is likely that the formation of the positive CTC product of TMB oxidation can itself promote aggregation of the citrate-capped nanoparticles, explaining the intense signal seen in Figure 4.26. It was therefore expected that introducing spermine after the oxidation of ABTS by a DNAzyme, would allow the oxidation product to come into close contact with the nanoparticles in order to experience a SERRS enhancement.

It is immediately obvious from Figure 4.27 that the enhancement in signal observed when using gold nanoparticles and ABTS as the substrate, is not as great as when TMB and gold are used. However, the peaks characteristic of the oxidation product of ABTS are present, therefore spermine hydrochloride has aided the SERRS analysis of ABTS oxidation by a DNAzyme. More importantly, there is a good discrimination seen between the DNAzyme signal and the background. As can be seen in the Figure 4.27 inset, there is a decrease in signal when nanoparticles are added for SERRS analysis as opposed to analysis by resonance Raman scattering, however, this is most likely the result of sample dilution via the addition of the nanoparticles.

Unfortunately, similar results were obtained when using silver nanoparticles, and therefore it was concluded that ABTS is not a suitable substrate for use in the

SERRS analysis of DNAzyme activity and only TMB was taken forward into further experiments.

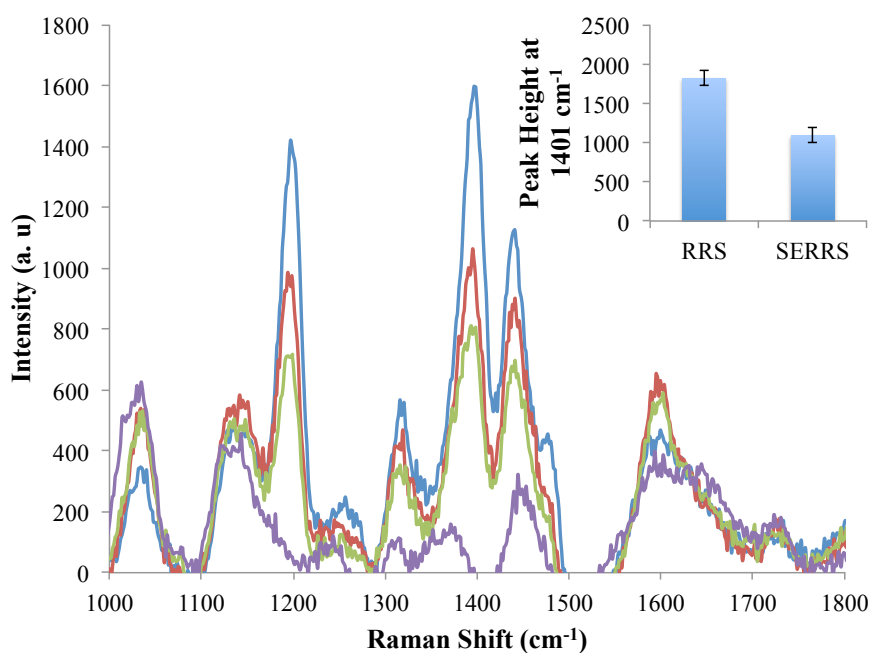


Figure 4.27 SERRS analysis of the full DNAzyme system (blue) with controls containing haemin only (red), nonsense DNA (green) and DNA only (purple). 0.1 μM of DNA and 0.1 μM of haemin were complexed in 10 mM HEPES / 10 mM KCl, pH 7.1 for 30 minutes. 200 μL of ABTS/ H_2O_2 substrate was added to 500 μL final volume of buffer and left to react for 3 hours. 200 μL of sample was added to 400 μL gold colloid and 20 μL of 0.1 M spermine hydrochloride and analysed using 633 nm laser excitation at 4 mW power using 3 x 3 second accumulations. Inset shows the comparison of peak height at 1401 cm^{-1} with and without nanoparticles. Samples were scanned 5 times and error bars represent one standard deviation of 5 replicate scans

4.3.5.2 Investigating Buffer Conditions for Improved SERRS Discrimination

Although, it was shown previously that Na^+ ions gave the best resonance Raman enhancement of the CTC, it was important to re-assess the implication of this for SERRS in an attempt to improve upon the discrimination seen between the DNAzyme system and the background haemin signal. Thus, a 10 mM HEPES / 10 mM KCl, pH 7.1 buffer was used to form the DNAzyme, before the addition of the TMB / H_2O_2 substrate and nanoparticles for analysis by SERRS. Unfortunately, when using gold nanoparticles, there was still no discrimination, and the results were similar for both Na^+ and K^+ ions. The results for silver nanoparticles, however, were

more promising and the comparison between buffer choice can be seen in Figure 4.28.

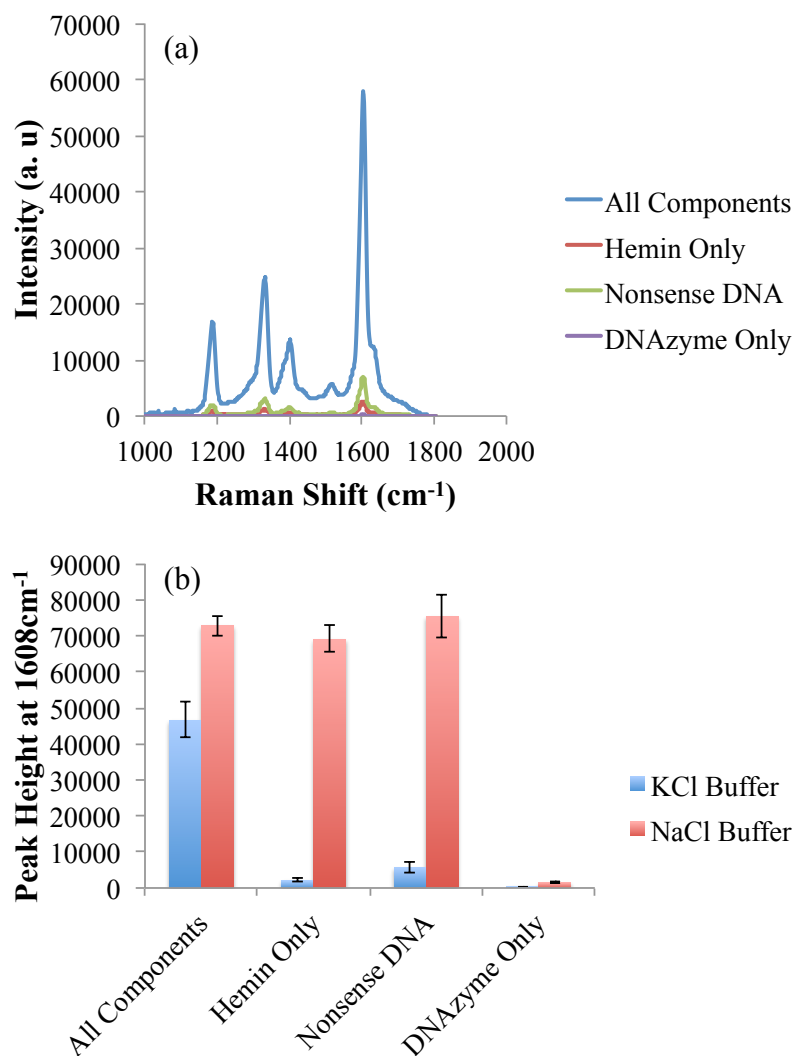


Figure 4.28 Comparison of Na⁺ and K⁺ ions for the SERRS of DNAzymes. 0.1 μM of DNA and 0.1 μM of haemin were complexed in either 10 mM HEPES / 10 mM NaCl, pH 7.1 or 10 mM HEPES / 10 mM KCl, pH 7.1 for 30 minutes before the addition of 100 μL TMB/H₂O₂ substrate to a final volume of 500 μL. This was left for 3 hours and 200 μL of sample was added to 400 μL of silver colloid. This was analysed using 633 nm laser excitation at 0.04 mW power and 3 x 3 second accumulation with 5 scans of each sample taken. (a) The results obtained using K⁺ ions were baseline corrected and an average taken to show the discrimination between the full DNAzyme system and the controls. (b) The peak height at 1608 cm⁻¹ was calculated for each sample in both buffer conditions and error bars represent one standard deviation.

As can be seen in Figure 4.28 (a) the KCl buffer provides an excellent discrimination between DNAzyme signal and background. This is confirmed in Figure 4.28 (b)

where the two buffers are compared and it is obvious that the KCl buffer provides the greatest discrimination in comparison to the NaCl buffer. Before these optimised parameters were taken forward into further experiments, it was first important to assess the reproducibility of the results obtained. Thus, the experiment was repeated and 5 replicate samples were produced for analysis.

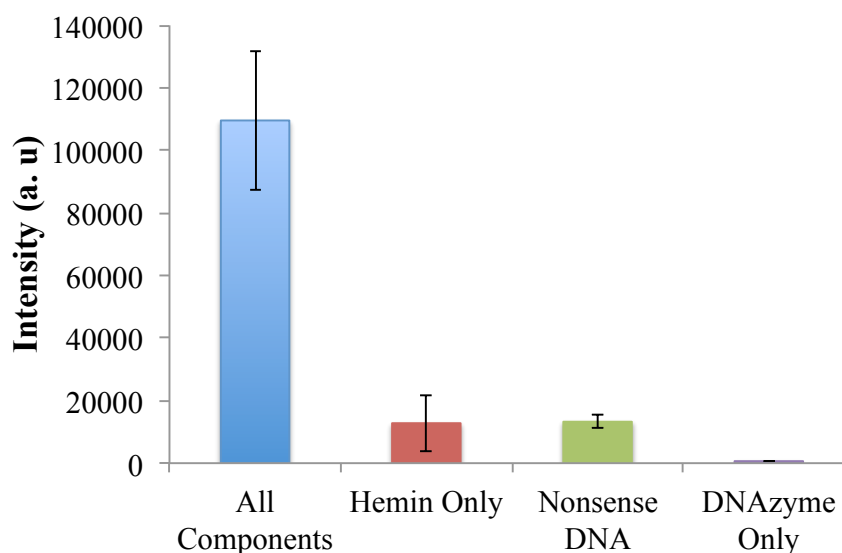


Figure 4.29 Assessing the reproducibility of the SERRS of DNAzyme activity. 0.1 μM of DNA and 0.1 μM of haemin were complexed for 30 minutes in 10 mM HEPES / 10 mM KCl, pH 7.1 for 30 minutes before the addition of 100 μL TMB/ H_2O_2 substrate to a final volume of 500 μL . 200 μL of sample was added to 400 μL of silver colloid and analysed using 633 nm laser excitation at 1 mW power and 3 x 3 second accumulations. 5 replicate samples were prepared and scanned 5 times and the average peak height at 1608 cm^{-1} was calculated. Error bars represent one standard deviation of 5 replicate samples.

As can be seen in Figure 4.29, there is a large discrimination between the signal resulting for the full DNAzyme system and the background controls. Thus, the DNAzyme in the presence of K^+ ions was used alongside the previously discussed assays in the hope that this discrimination could improve upon the detection limits obtained.

4.3.5.3 SERRS of DNAzymes for the Detection of DNA

Since the results obtained for the SERRS analysis of TMB oxidation by a DNAzyme showed great promise, the parameters used were incorporated into various detection mechanisms to try and improve upon the sensitivity obtained with resonance Raman

scattering. Firstly, the amount of guanine-rich DNA that could be detected was assessed and the results can be seen in Figure 4.30.

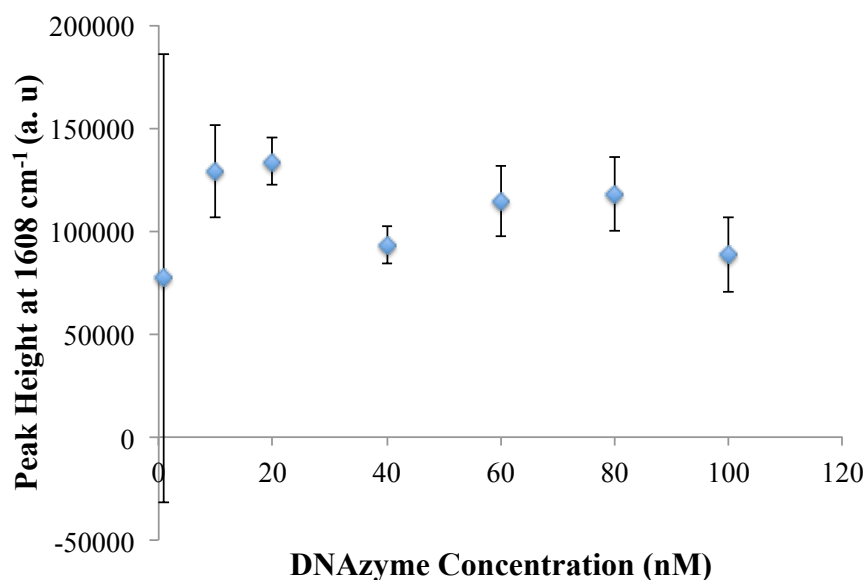


Figure 4.30 DNAzyme concentration study. 0.1 μM of haemin was complexed with varying concentrations of guanine-rich DNA in 10 mM HEPES / 10 mM KCl, pH 7.1 for 30 minutes before the addition of 100 μL of TMB/ H_2O_2 substrate to a final volume of 500 μL for 3 hours. 200 μL of sample was added to 400 μL of silver colloid and analysed using 633 nm laser excitation wavelength at 1 mW power using 3 x 3 second accumulations. 3 replicate samples were prepared and scanned 5 times each. The peak height was obtained by subtracting the intensity at 1608 cm^{-1} for the haemin only control from the full DNAzyme system. Error bars represent one standard deviation 3 replicate samples.

The results seen were not as expected, and the relationship between the concentration of guanine-rich DNA and the peak intensity at 1608 cm^{-1} did not follow a linear response. It appears that within one standard deviation, there is no change in the SERRS intensity seen as the concentration of DNAzyme is varied. The data points were achieved by subtracting the background haemin signal, and so discrimination can be seen down to 10 nM. Below this value the error bars are extremely large, and thus it can be concluded that 10 nM is the lowest observable concentration of guanine-rich DNA that can be detected, which mimics the results achieved for resonance Raman scattering.

Although this was a disappointing result, SERRS was used within the catalytic beacon assay protocol and within the split probe detection assay, to see if the results obtained previously could be improved upon by the use of nanoparticles. Unfortunately, the results were the same as for resonance Raman scattering. Within the beacon assay protocol there was no discrimination between the presence and absence of target at lower concentrations, and for the split probe assay a signal was obtained for all samples and controls. It is likely that when using these methods of detection, there is not enough DNAzyme molecules available upon the addition of target to create an enhancement comparable to that obtained when the DNAzyme is free in solution, and thus once again, the results seen are purely from the SERRS enhancement of the haemin based oxidation of TMB.

Although the SERRS of DNAzyme activity cannot be used within these particular assays for the detection of target DNA, it can be used to monitor the oxidation of TMB by a DNAzyme, and upon further work could be incorporated into the correct assay design for sensitive analyte detection.

4.4 Conclusions

Herein, we have successfully utilised resonance Raman scattering for the detection of DNAzyme activity. This is the first reported use of this technique for monitoring the oxidation of the peroxidase substrates ABTS and TMB by a DNAzyme.

Resonance Raman scattering can detect concentrations of guanine-rich DNA as low as 10 nM when using both substrates and was incorporated into a catalytic beacon assay protocol for the detection of target DNA. Unfortunately, the limits of detection were limited by the background signal seen from the haemin co-factor. However, this assay was used alongside PCR for the successful detection of target DNA and thus, although the limits of detection cannot be quantified, resonance Raman scattering can be used in conjunction with catalytic beacons for the detection of PCR amplified target DNA.

A split probe assay was designed to try and reduce the background haemin signal. However, experiments with streptavidin coated magnetic beads allowed for their catalytic properties to be realised. Thus, it can be confirmed, that these beads cannot be used as a separation technique in conjunction with peroxidase substrates, as the results will be compromised. The use of streptavidin coated plates was implemented in another attempt to reduce the background signal, without the use of oxidative ferromagnetic particles. However, the target DNA could not be detected using this method, and it is likely that there is an interaction between the haemin cofactor and the streptavidin, and that the maximum signal seen is the result of the oxidative capabilities of this cofactor alone.

SERRS was implemented within the DNAzyme system, to see how the results would compare to resonance Raman scattering. Both silver and gold nanoparticles were used and a marked increase in signal was seen when they were added to the CTC resulting from DNAzyme activity. Formation of the DNAzyme in the presence of K^+ ions and the addition of silver nanoparticles allowed for an excellent discrimination between the DNAzyme system and the background signal to be obtained. Although this success was not reflected in the detection of target DNA via the catalytic beacon or split probe assay design, this is the first reported case of SERRS as a method of analysis for DNAzyme activity.

In conclusion, enhanced Raman scattering can be used in conjunction with DNAzymes, and should be considered as an alternative spectroscopy to UV-Vis and fluorescence for specific analyte detection via their peroxidase-like activity.

5. Nanoparticles as Enzyme Mimetics

5.1 Introduction

In the previous chapter it was shown that streptavidin coated magnetic beads will oxidise certain peroxidase substrates due to the catalytic nature of the core ferromagnetic nanoparticles. During the investigation of the SERRS of DNAzyme activity it was apparent from the generation of signal from the controls containing only a sequence of DNA, that gold and silver nanoparticles could be oxidising the TMB to its one-electron oxidation product. Therefore, the use of nanoparticles as enzyme mimetics was investigated further.

The first reported case of this phenomenon was in 2007, when Yan and co-workers utilised ferromagnetic nanoparticles for the oxidation of certain peroxidase substrates.¹⁷⁹ The authors noted that this was not an unexpected result given that the Fe^{2+} and Fe^{3+} ions in solution are known to catalyse the breakdown of hydrogen peroxide, however the presence of Fe_3O_4 nanoparticles in commercially available ELISA kits demonstrates that this activity has previously been ignored. Magnetite nanoparticles were used within a novel immunoassay as capture, separation, and detection agents for clinically relevant biomarkers. It was perceived that this versatility made them ideal for use within a number of applications from biotechnology to environmental chemistry.

Similar to the rise in popularity of DNAzymes, catalytic nanoparticles are fast becoming a novel enzymatic substitution, as they are cheap and simple to synthesis and are stable over a long period of time. Since the initial publication, magnetite nanoparticles have been used alongside electrochemical sensors for the detection of hydrogen peroxide,¹⁸⁴ and in conjunction with colourimetric analysis for the detection of glucose,¹⁸⁵ organophosphorus pesticides, and nerve agents.¹⁸⁶

This catalytic activity is not restricted to magnetite nanoparticles, and there has been a recent rise in the number of publications detailing this effect using a variety of

different nanoparticles.¹⁸⁷ Examples include copper nanoclusters,¹⁸⁸ ceria nanoparticles,¹⁸⁹ and mixed metal particles such as cobalt ferrite,¹⁹⁰ which have all been used for the successful detection of hydrogen peroxide and glucose. These are common analytes which are detected using nanoparticles as enzyme mimetics, since the initial publication on ferromagnetic nanoparticles reported that their catalytic activity was pH, temperature and H₂O₂ dependant.¹⁷⁹ Thus when combined with a peroxidase substrate, commonly TMB, the oxidation reaction will only proceed in the presence of H₂O₂ which can be monitored via a colourless to blue change. Although H₂O₂ is the most common, a variety of other analytes have been detected using various nanoparticles. For example, mixed metal nanoparticles of platinum and gold have been used for the detection of acetylcholine,¹⁹¹ mercury ions,¹⁹² and within an immunosorbent assay.¹⁹³

Gold nanoparticles on their own have recently been investigated as potential enzyme mimetics. Jv *et al.* investigated the use of positively charged gold nanoparticles and their application to H₂O₂ and glucose detection.¹⁹⁴ The authors noted that these nanoparticles did exhibit peroxidase activity and that a detection limit of 500 nM could be obtained for H₂O₂. They also reported that this catalytic activity is restricted to positively charged gold nanoparticles, and that citrate capped negatively charged gold nanoparticles would not exhibit the same effect. The catalytic activity was attributed to the adsorption of H₂O₂ on the surface of the gold nanoparticles, where the oxygen bonds will be broken down to a double HO• radical. They postulated that this radical would be stabilised by the gold surface via the partial electron exchange interaction, and thus different surface charges would exhibit different catalytic behaviour. However, Wang *et al.* who subsequently published a paper comparing the peroxidase-like activity of unmodified, amino-modified and citrate-capped gold nanoparticles contested this conclusion.¹⁹⁵ They used TMB and ABTS in combination with colourimetric detection to confirm the catalytic activity of unmodified gold nanoparticles, and concluded that they have significantly higher catalytic activity towards both substrates in comparison to the surface modified gold nanoparticles. Although activity was to a lesser extent, both the amino-modified and citrate-capped nanoparticles exhibited a response, which was in contrast to the result that was previously reported. With regard to catalytic activity, it was noted that the

superficial gold atoms were a contributing factor, and that the surface charge on the nanoparticles played an important role in the catalytic activity depending on the substrate chosen, which is comparable to the results previously seen when investigating DNAzyme activity on ABTS and TMB using SERRS.

5.2 Chapter Aims

The aim of this project was to further examine the use of gold nanoparticles as an enzyme mimetic, and investigate the suitability of SERRS as a novel method of analysis. The ability of silver nanoparticles to exhibit catalytic activity was also investigated, and these nanoparticle enzyme mimetics were then used to detect H_2O_2 using SERRS. The mode of action of the nanoparticle enzyme mimetics is described visually in Figure 5.1

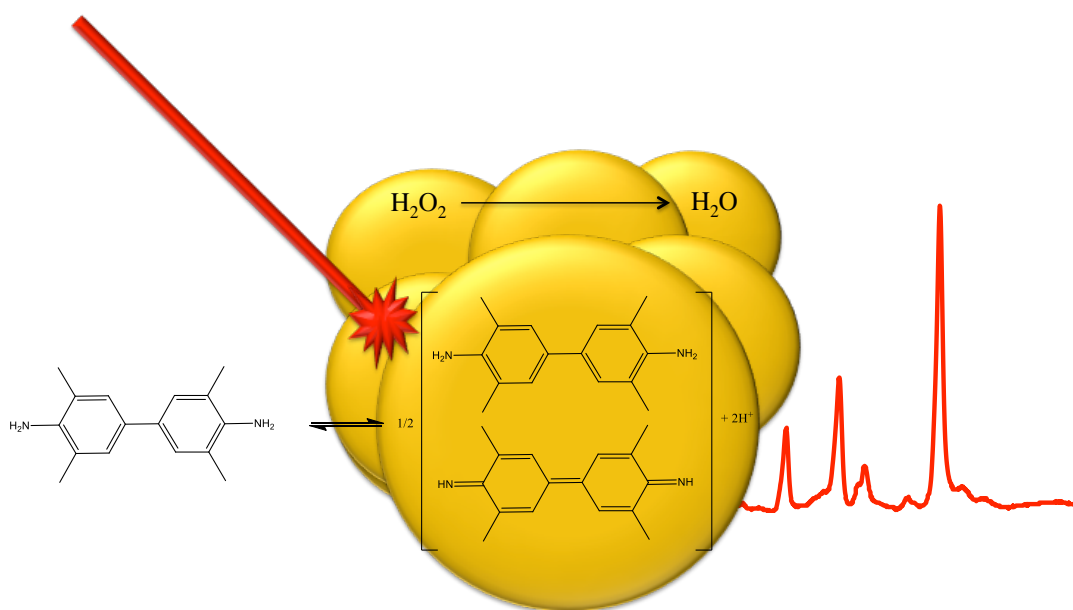


Figure 5.1 Schematic of the nanoparticle enzyme mimetic system using TMB as the peroxidase substrate.

Upon catalytic action of the nanoparticles and reduction of H_2O_2 , the chosen substrate will be oxidised to a form that is resonant with a suitable laser excitation wavelength. The nanoparticles will also provide a suitable surface for enhanced scattering and as such this system is intrinsically amenable to SERRS analysis.

5.3 Results and Discussion

5.3.1 Nanoparticle Characterisation

Metallic nanoparticles were prepared according to standard protocols developed by Turkevitch and Frens for the preparation of gold nanoparticles^{63, 154} and Lee and Meisel for the synthesis of silver colloid.⁸³ Polyethylenimine (PEI) was added to the surface of the citrate-capped silver nanoparticles to create positively charged silver nanoparticles, and positively charged gold nanoparticles were prepared via the addition of a poly(allylamine) hydrochloride (PAH) stabilising ligand to the surface. The nanoparticles were subjected to a number of characterisation methods, including UV-Vis spectroscopy, which was used to determine the concentration of the nanoparticles using their molar extinction coefficient and the Beer-Lambert law. Additionally, dynamic light scattering (DLS) was used in order to ensure their stability and determine their size. The results can be seen in Table 5.1.

Table 5.1 Characterisation data for all nanoparticles used in enzyme mimetic experimentation.

Nanoparticle	Size (nM)	Zeta Potential (mV)	pH	Concentration (nM)
Silver (-)	44.8 ± 0.3	-36.4 ± 1.6	7.96	0.28
Silver (+)	1234.3 ± 44.3	+10.6 ± 0.3	5.50	0.07
Gold (-)	41.8 ± 1.1	-35.0 ± 1.3	7.80	0.24
Gold (+)	35.7 ± 0.2	+34.3 ± 1.6	2.52	0.38

The positive silver nanoparticles have aggregated due to the PEI addition and this was reflected in the extinction spectrum obtained. However, the main purpose of these nanoparticles was to assess the effect the surface charge would have on catalytic activity, and as can be seen from the zeta potential, these particles have the desired charge.

The bulk of experiments in this chapter were carried out using the citrate-capped negative nanoparticles, and as can be seen from Table 5.1 these nanoparticles are uniform in size, have a negative and relatively high zeta potential, indicating

stability, as well as a close to neutral pH. Also, their concentrations are similar, and thus can be used without dilution for a direct comparison.

5.3.2 Citrate-Capped Gold Nanoparticles

Initial experiments were carried out using a pre-mixed TMB substrate containing a 1:1 ratio of TMB and H₂O₂, along with citrate-capped gold nanoparticles. It was first important to assess whether the concentration of nanoparticles had an effect on the catalytic activity seen, and how reaction time could affect this result.

Varying volumes of suspensions of nanoparticles were added to 200 μ L of TMB / H₂O₂ substrate solution and analysed using a 633 nm laser excitation wavelength every 10 minutes for 30 minutes. The results are shown in Figure 5.2, where it can be seen that in the absence of nanoparticles there is no oxidation of the TMB and hence no CTC present for enhanced Raman scattering.

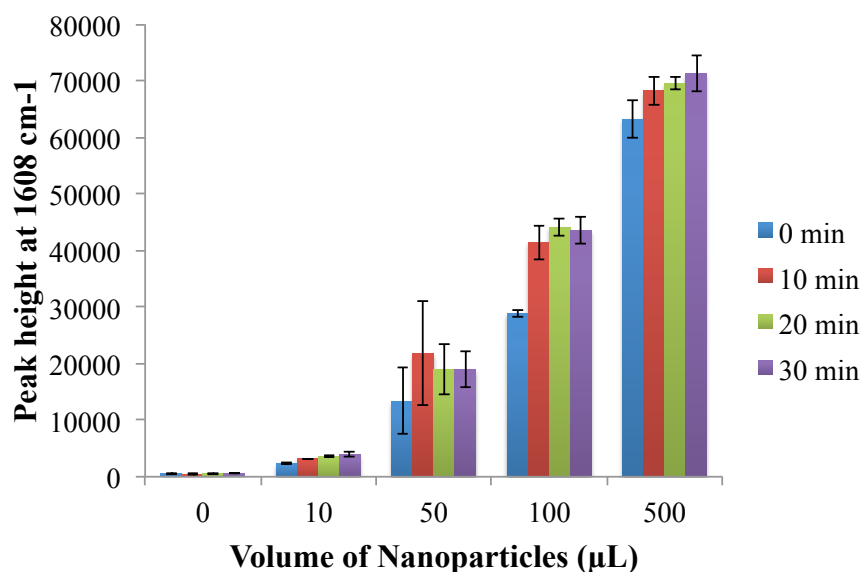


Figure 5.2 Citrate-capped gold nanoparticles and TMB reaction. 200 μ L of TMB/H₂O₂ substrate solution was added to varying amounts of gold colloid. The samples were analysed every 10 minutes for 30 minutes using a 633 nm laser excitation wavelength at 1 mW laser power and using a 1 x 10 second accumulation. 3 replicates samples were prepared for each volume of colloid and scanned 5 times. The peak height at 1608cm⁻¹ was obtained from the raw data and the average taken. Error bars represent one standard deviation.

The reaction is instantaneous, and thus there is a signal at 0 minutes due to the delay between the addition of TMB substrate and the measurement. As the volume of colloid is increased the signal obtained increases, with a good and reproducible enhancement seen using either 100 or 500 μL of gold nanoparticles. The reaction time does not appear to have a great effect on the signal seen. In particular when using 500 μL of nanoparticles, there is no great change in signal seen over the 30 minutes reaction time.

These results confirm the ability of gold nanoparticles to act as an enzyme mimetic and this is further displayed in Figure 5.3, where the spectra shown were obtained by adding 500 μL of gold nanoparticles to 200 μL of TMB / H_2O_2 substrate solution and analysing the samples immediately.

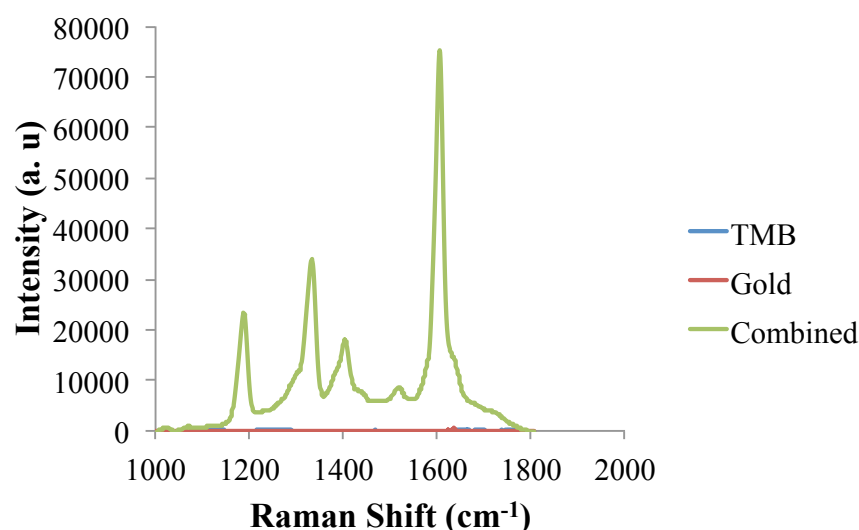


Figure 5.3 Enzyme mimetic action of citrate-capped gold nanoparticles on TMB. 500 μL of gold colloid was added to 200 μL TMB/ H_2O_2 substrate solution and analysed immediately with a 633 nm laser excitation wavelength at 1 mW using a 1 x 10 second accumulation. 3 replicates of each sample were prepared and scanned 5 times. The spectra were baseline corrected using Grams software and the average taken to produce the spectra shown.

This proves that only when the nanoparticles are present will the TMB be oxidised to its one electron oxidation product. This is seen via the enhanced signal obtained, which is characteristic of the CTC, which is in resonance with the laser excitation source used. Thus, the large enhancement seen is a result of both resonance and

surface enhanced Raman scattering, and the nanoparticles are utilised as both a catalytic agent in the reaction and the enhancing substrate for SERRS analysis. Additionally, since the large signal seen is produced with immediate analysis of the sample, gold nanoparticles behave as an extremely efficient enzyme mimetic, perhaps due to the large surface area present. This immediate analysis is advantageous, especially in comparison to the 3 hour reaction time needed for optimum oxidation of TMB by a DNAzyme.

The peaks obtained are characteristic of the CTC resulting from the one electron oxidation of TMB. However, with regards to the gold nanoparticles, apart from knowing that they can successfully catalyse the oxidation of TMB, these initial results did not give much information as to their ability to act as a suitable SERRS substrate.

Therefore, both size and zeta potential measurements were employed to monitor the aggregation of the nanoparticles as they oxidise the TMB. Figure 5.4 shows the results obtained. 500 μL of gold nanoparticles were added to 200 μL of TMB / H_2O_2 substrate and their size and zeta potential measured every 10 minutes for 30 minutes. The size significantly increases upon addition of the TMB substrate, and plateaus after 20 minutes. This size increase is an indication of aggregation and was confirmed with the zeta potential measurements. The gold colloid on its own has a zeta potential of -35 mV, which indicates stability as well as confirming a negative surface layer. Upon addition of the TMB substrate the value drops over time and eventually becomes positive. This confirms that as the oxidation proceeds the nanoparticles become less stable, which also indicates aggregation. Additionally, this change in zeta potential also demonstrates how the oxidation product of TMB is interacting with the nanoparticles. Formation of the positive CTC complex and adsorption onto the surface of the nanoparticles is likely the cause of the change in charge seen. Therefore, the nanoparticles catalyse the formation of the CTC, which adsorbs onto the surface, replacing the charge and allowing for an excellent SERRS response. These processes happen very quickly upon combination of the nanoparticles and TMB / H_2O_2 substrate, explaining the rapid increase in size and change in substrate charge.

These results were not unexpected, as the one electron oxidation product of TMB exists as a positive molecule. Thus, as the nanoparticles catalyse the oxidation reaction, the formation of the CTC promotes aggregation via the interaction between the positive charge on the substrate and the negative charge on the surface of the nanoparticles.

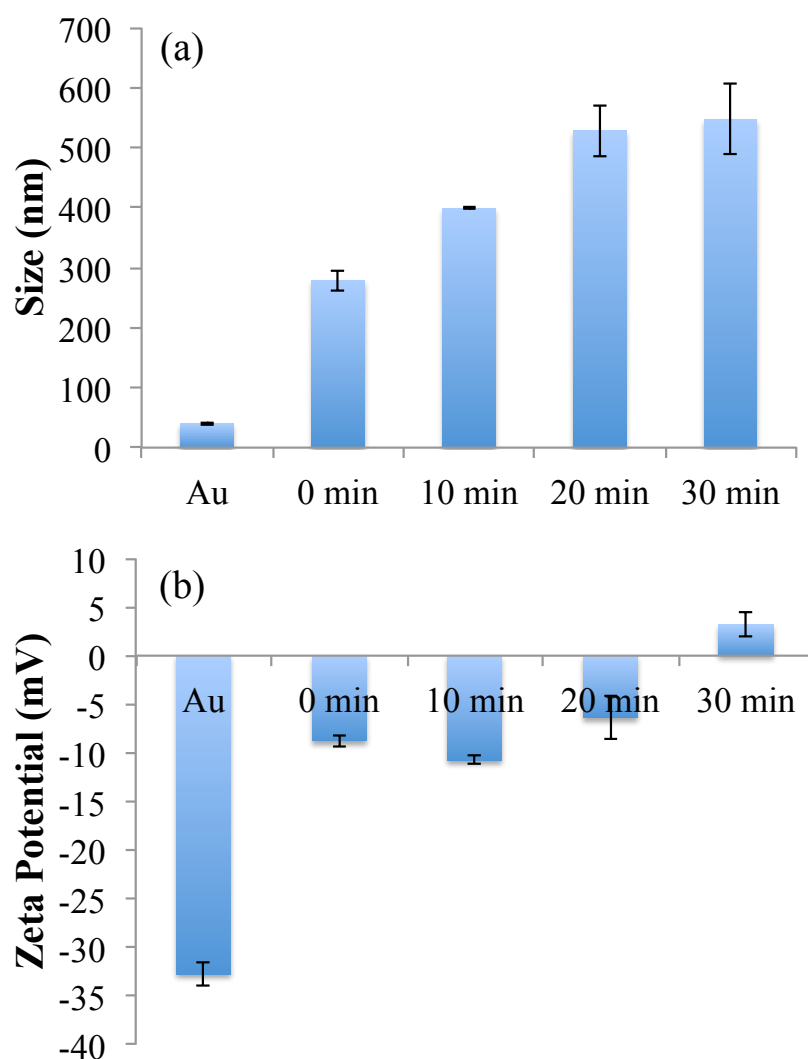


Figure 5.4 Monitoring the size and zeta potential of the gold colloid within the enzyme mimetic system. 500 μL of gold colloid was added to 200 μL of TMB/ H_2O_2 substrate to a 1 mL final volume. (a) The size of the gold nanoparticles was monitored and then again every 10 minutes for 30 minutes after the addition of TMB. (b) The zeta potential of the gold nanoparticles was measured every 10 minutes for 30 minutes after the addition of TMB. Samples were prepared and analysed in triplicate and an average obtained. Error bars represent one standard deviation of 3 replicate measurements.

These results for gold colloid and TMB confirm that gold nanoparticles are efficient enzyme mimetics and will catalyse the oxidation of TMB to its one electron oxidation product. SERRS has also been confirmed as a novel technique for the analysis of this reaction, and gold nanoparticles serve the dual purpose of catalysing the oxidation reaction and providing suitable SERRS substrates without the need for external aggregating agents. This was expected in the case of the TMB substrate using gold nanoparticles, as the charges involved on the surface of the nanoparticles and the substrate are complementary. ABTS however, is a negatively charged substrate and should repel the charges on the nanoparticle, however the ability of this substrate to be oxidised by gold nanoparticles was also investigated.

The experiments previously performed for citrate-capped gold and TMB were repeated using citrate-capped gold and ABTS. However, there was no change in the spectra observed when the volume of colloid was varied, and the reaction time had no effect on the signal. An example of the results obtained can be seen in Figure 5.5, whereby the spectra seen is not indicative of the radical product resulting from the oxidation of ABTS.

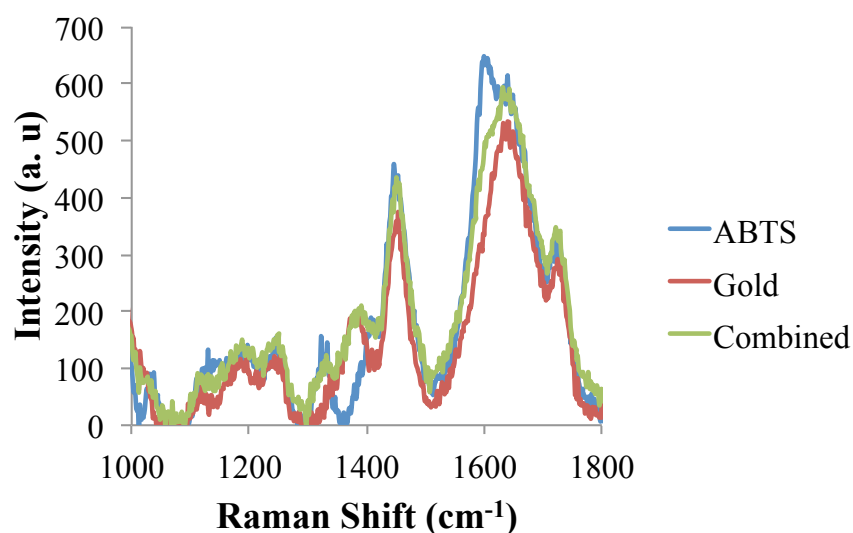


Figure 5.5 Citrate-capped gold nanoparticles and ABTS in an enzyme mimetic system. 200 μL of ABTS/ H_2O_2 substrate was added to 500 μL of citrate-capped gold colloid and analysed immediately using a 633 nm laser excitation wavelength at 4 mW laser power using 1 x 10 second accumulation. 3 replicates of each sample were prepared and scanned 5 times. The spectra were baseline corrected using Grams software and the average taken to obtain the spectra shown.

Additionally, as can be seen in Figure 5.6, there is no evidence of aggregation from the size or zeta potential measurements, as there is no change to the nanoparticles upon addition of the ABTS substrate.

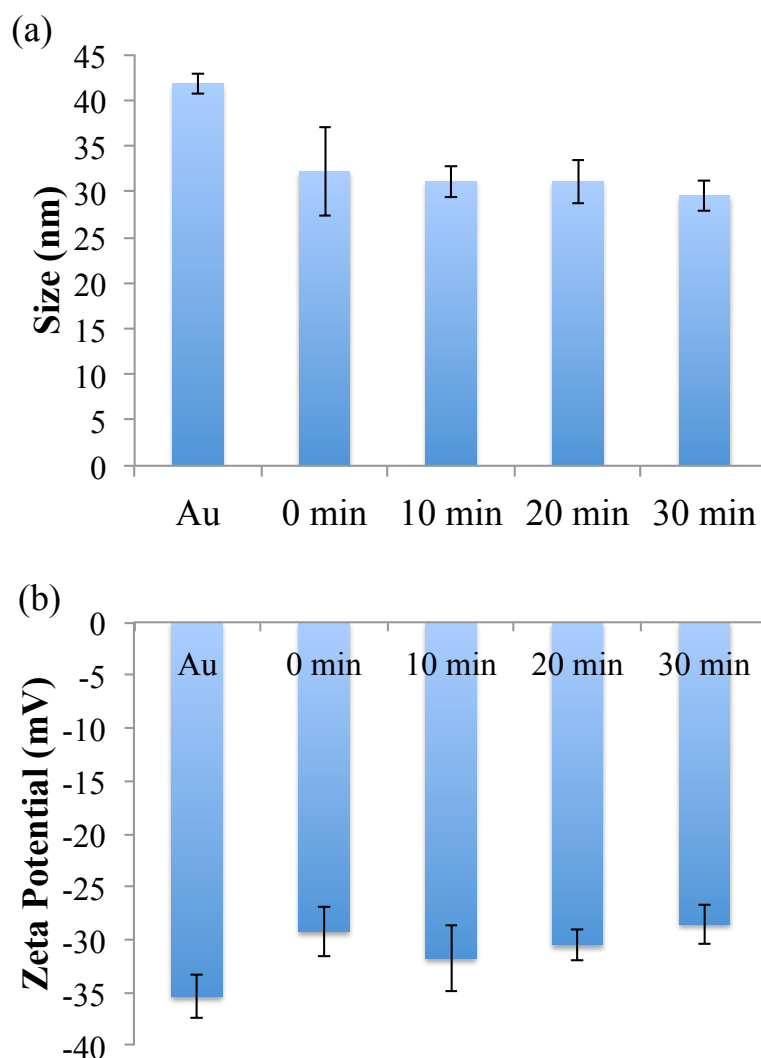


Figure 5.6 Monitoring aggregation upon the addition of citrate-capped gold nanoparticles to ABTS/H₂O₂ substrate. 500 μ L of gold colloid was added to 200 μ L ABTS substrate. (a) The size of the gold nanoparticles was measured and then again every 10 minutes for 30 minutes after the addition of ABTS substrate. (b) The zeta potential of the gold nanoparticles was measured and then again every 10 minutes for 30 minutes after the addition of ABTS substrate. Samples were prepared in triplicate and an average taken. Error bars represent one standard deviation.

These results do not necessarily confirm that the enzyme mimetic ability is limited, and the oxidation product of ABTS could be formed, however due to the repellent

charges between the ABTS radical anion and citrate-capped gold nanoparticles it is not amenable to SERRS analysis. As such gold nanoparticles are best used alongside TMB and SERRS analysis for further experimentation using enzyme mimetics.

5.3.3 Citrate-Capped Silver Nanoparticles

The peroxidase-like activity of gold nanoparticles has previously been reported,^{179, 194} although without the novel aspect of the SERRS analysis. Silver nanoparticles, however, have never been used in such a capacity and their enzyme mimetic action has not been studied. Therefore, silver nanoparticles were used alongside both TMB and ABTS in order to assess their ability to catalyse the oxidation reactions. The volume of silver colloid and the reaction time allowed before analysis were the first parameters to be investigated.

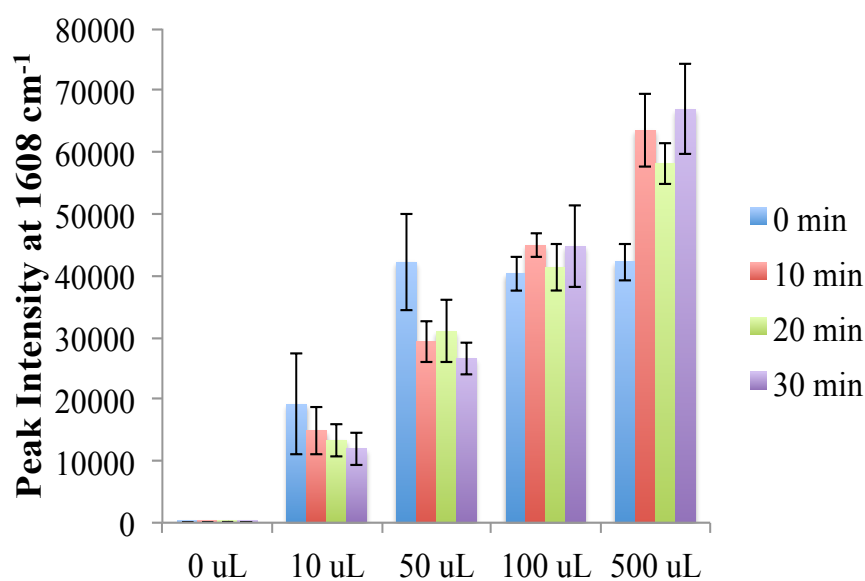


Figure 5.7 Citrate-capped silver nanoparticles and TMB reaction. 200 μL of TMB/ H_2O_2 substrate solution was added to varying amounts of silver nanoparticles. The samples were analysed every 10 minutes for 30 minutes using a 633 nm laser excitation at 1 mW laser power and using a 1 x 10 second accumulation. 3 replicates samples were prepared for each volume of nanoparticles and scanned 5 times. The peak height at 1608 cm^{-1} was obtained from the raw data and an average taken. Error bars represent one standard deviation.

200 μL of TMB / H_2O_2 substrate solution was added to varying amounts of citrate reduced silver nanoparticles and analysed every 10 minutes for 30 minutes. The

results can be seen in Figure 5.7, and the trend observed is similar to that obtained for gold nanoparticles and TMB. Firstly, in the absence of the nanoparticles there is no oxidative activity, and as the volume of nanoparticles is increased the signal obtained for the 1608 cm^{-1} CTC peak increases. However, the reaction time appeared to be more varied for the silver system, in particular for $50\text{ }\mu\text{L}$ of nanoparticles, where the signal drops over a period of 10 minutes, and for $500\text{ }\mu\text{L}$ where the signal increases after 10 minutes before stabilising for the remaining 20 minutes. Thus, $100\text{ }\mu\text{L}$ of silver nanoparticles was taken forward into further experiments as this can be analysed immediately with a good enhancement in signal and reproducible results. The spectra obtained from these parameters can be seen in Figure 5.8.

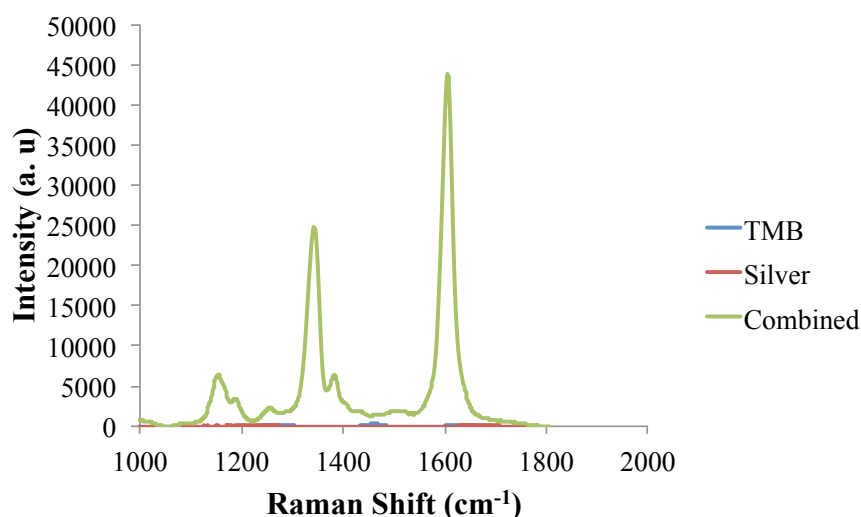


Figure 5.8 Enzyme mimetic action of citrate-capped silver nanoparticles on TMB. $100\text{ }\mu\text{L}$ of silver colloid was added to $200\text{ }\mu\text{L}$ of TMB/ H_2O_2 substrate solution and analysed immediately using a 633 nm laser excitation at 1 mW laser power using a 1×10 second accumulation. 3 replicates of each sample were prepared and scanned 5 times. Spectra were baseline corrected using Grams software and the average taken to produce the spectra seen.

This confirms that the oxidation to the CTC and thus the enhanced signal seen is purely the result of the peroxidase-like activity of silver nanoparticles, and this is the first time that silver nanoparticles have been shown to exhibit this response with a peroxidase substrate. The behaviour of the silver nanoparticles upon oxidation of the TMB was also investigated using size and zeta potential measurements.

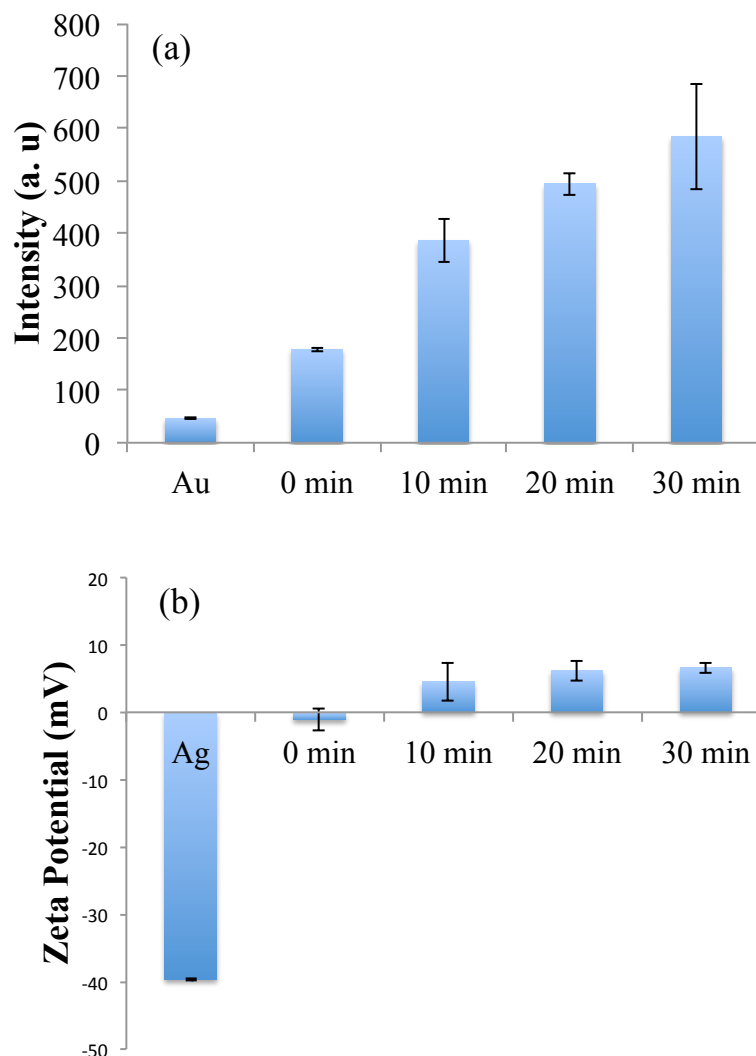


Figure 5.9 Monitoring aggregation upon the addition of citrate-capped silver nanoparticles to TMB substrate. 100 μL of silver nanoparticles was added to 200 μL of TMB/ H_2O_2 substrate. (a) The size of the silver nanoparticles was measured and then again every 10 minutes for 30 minutes after the addition of TMB substrate. (b) The zeta potential of the silver nanoparticles was measured and then again every 10 minutes for 30 minutes after the addition of TMB substrate. Samples were prepared in triplicate and an average taken. Error bars represent one standard deviation.

As can be seen in Figure 5.9, upon the addition of the TMB / H_2O_2 substrate, the size of the silver nanoparticles steadily increases indicating aggregation of the particles. Also, the zeta potential, which is -36 mV for the silver colloid, quickly becomes positive, indicating a fast formation and adsorption of the CTC onto the surface. Thus, just like for gold nanoparticles, as the oxidation reaction proceeds and the positive CTC is formed, the negatively charged silver nanoparticles will be forced to

aggregate via the newly formed oxidation product of TMB. Therefore, silver nanoparticles can also be used simultaneously for the oxidation of TMB and as an excellent SERRS substrate. This is a very positive result, as silver nanoparticles are known to be good SERRS substrates and provide better enhancements in signal when compared to gold colloid.

Silver nanoparticles were also used alongside ABTS to try and ascertain if any peroxidase-like activity could be observed. However, the results were similar to that obtained when using gold nanoparticles and can be seen in figure 5.10.

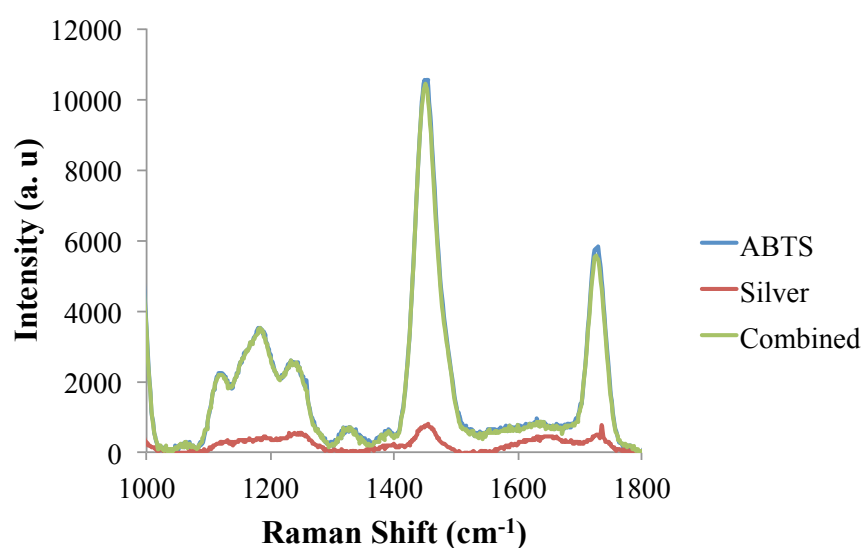


Figure 5.10 Enzyme mimetic action of citrate-capped silver nanoparticles on ABTS. 100 μL of silver colloid was added to 200 μL of ABTS/ H_2O_2 substrate solution and analysed immediately with a 633 nm laser excitation at 1 mW laser power using a 1 x 10 second accumulation. 3 replicates of each sample were prepared and scanned 5 times. Spectra were baseline corrected using Grams software and the average taken to produce the spectra shown.

The spectra seen is not indicative of the radical product arising from oxidation of ABTS, and the peaks seen are purely that of un-oxidised ABTS that has been enhanced by the presence of the silver nanoparticles. Size and zeta potential measurements were also carried out on the silver colloid after the addition of the ABTS / H_2O_2 substrate and no change in either value was observed over a 30 minute time period, similar to the results obtained for gold nanoparticles and ABTS. This confirms that no aggregation is possible when using ABTS as even if the oxidation

reaction could proceed the predominant product produced is a radical cation which would not be able to come into contact with the silver nanoparticles for surface enhanced Raman scattering to be possible, and external charge modifying agents may need to be employed. Therefore, ABTS was deemed an unsuitable substrate when using citrate-capped silver nanoparticles and SERRS in a nanoparticle enzyme mimetic system.

5.3.4 Positive Particles

Both citrate-capped gold and silver nanoparticles were able to successfully oxidise TMB to its one electron CTC that can be monitored via SERRS. However, the problem with ABTS as a substrate for nanoparticle mimetic analysis is the opposing charges between the surface of the nanoparticles and the substrate. Thus, positive particles were briefly investigated to determine whether these could be used in conjunction with ABTS to form an enzyme mimetic system.

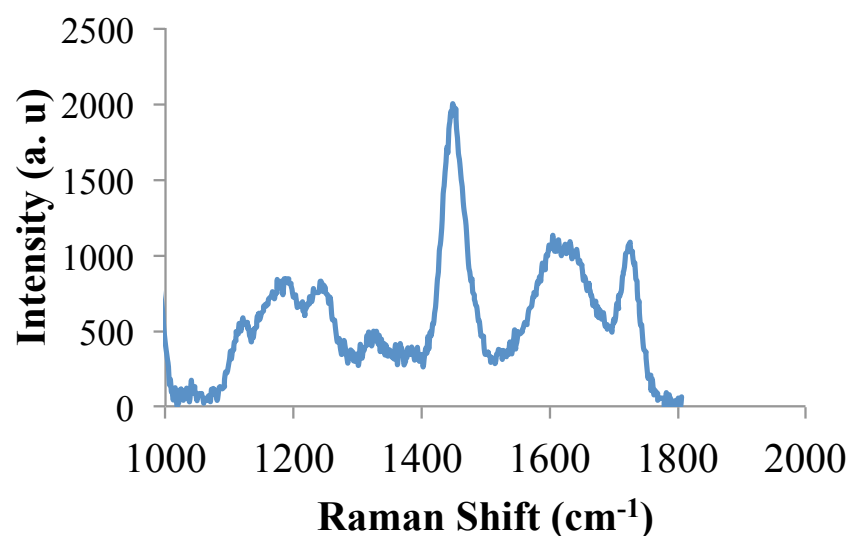


Figure 5.11 Enzyme mimetic action of PAH-stabilised gold nanoparticles on ABTS. 400 μ L of colloid was added to 200 μ L ABTS/H₂O₂ substrate solution and analysed immediately with a 633 nm laser excitation at 4 mW laser power using a 1 x 10 second accumulation. 3 replicates of each sample were prepared and scanned 5 times. Spectra were baseline corrected using Grams software and the average taken to produce the spectra seen.

Gold nanoparticles stabilised with a positive PAH ligand were synthesised and initially used to oxidise TMB. As expected, no CTC peaks were observed, due to the opposing charges between the nanoparticles and the oxidation product, meaning

SERRS enhancement did not occur. The results for ABTS can be seen in Figure 5.11. It was expected that oxidation of the ABTS could be detected by SERRS using these nanoparticles, as the radical anion produced would be able to adsorb onto the surface of these nanoparticles allowing for SERRS enhancement. Unfortunately, there is no indication that oxidation has taken place, and it was concluded that ABTS is not a suitable substrate for use within a nanoparticle enzyme mimetic system analysed by SERRS.

5.3.5 Comparing TMB Formulations

Throughout the course of the work carried out with TMB, the substrate used was a pre-mixed solution of TMB and H_2O_2 in a 1:1 ratio, optimised for oxidation to the blue CTC. The manufacturer provided no information as to any stabilising agents contained in the formulation, or the concentration of TMB. The only information that could be obtained was that the H_2O_2 present in the solution was 0.02% w/v. Up until this point, and in particular with experiments involving DNazymes, the concentration of TMB and H_2O_2 was not required. Indeed, since the substrate was optimised for oxidation to the blue CTC, it was ideal for use in experiments whereby this oxidation product was desired for resonance Raman analysis. Therefore, the volume of substrate needed for optimum analysis was all the information that was required for previous experiments. However, since these nanoparticle enzyme mimetic systems were eventually to be used as a method of H_2O_2 detection, the pre-mixed substrate could no longer be used. Thus, it was important to determine the concentration of TMB in the pre-mixed solution used in order to use a similar concentration in the nanoparticle mimetic system whereby the H_2O_2 could be varied. This concentration was determined using the un-oxidised TMB absorbance peak at 280 nm, which was used to create a calibration graph from the pure TMB. Using this graph the concentration of TMB in the pre-mixed substrate was calculated to be 3 mM, and since the manufacturer provided the concentration of H_2O_2 , a comparison between the TMB / H_2O_2 pre-mixed substrate and a manually mixed solution of TMB and H_2O_2 was carried out.

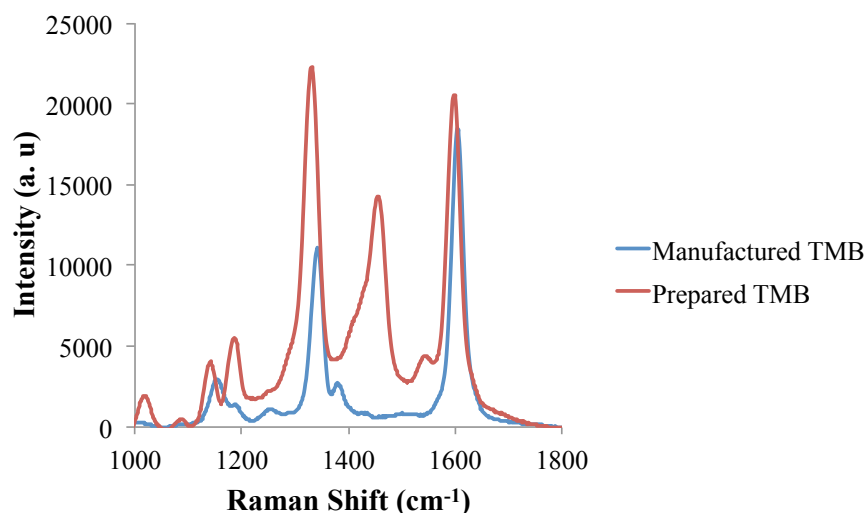


Figure 5.12 Comparison of TMB formulations after oxidation with silver nanoparticles. 200 μL of pre-mixed TMB/ H_2O_2 substrate or 100 μL of H_2O_2 (6.5 mM) and 100 μL of TMB (3 mM) were added to 100 μL of silver nanoparticles. The samples were analysed using a 633 nm laser excitation at 1 mW power and 1×10 second accumulation. 3 replicate samples were prepared and scanned 5 times. The spectra were baseline corrected using Grams software and an average taken.

The results obtained from the comparison between the pre-mixed TMB / H_2O_2 substrate solution and the individual components can be seen in Figure 5.12. The main difference seen between spectra is the appearance of an additional peak at roughly 1400 cm^{-1} for the sample obtained from the pure TMB. This peak can be attributed to the parent diamine,¹⁷⁸ and although this has no absorbance in resonance with the excitation source, it appears that the addition of the nanoparticles have allowed for enhancement of this peak through surface enhanced Raman scattering. Analysing the TMB at different laser excitation wavelengths after the addition of silver nanoparticles, and observing the presence of this peak at 1400 cm^{-1} confirmed this hypothesis. It is likely that the reason this peaks exists in the pure TMB solution and not in the pre-mixed substrate, is that the pre-mixed solution is optimised for efficient oxidation to the CTC, and thus none of the parent diamine remains within the sample to be enhanced by the presence of the nanoparticles. Apart from this anomaly and a very small change seen in the Raman shift, the peaks characteristic of the CTC are present in both samples, confirming that the silver nanoparticles will oxidise both TMB formulations. Additionally, the main peak at 1608 cm^{-1} has the same intensity for both samples analysed, and therefore this concentration of TMB

was used in further experimentation involving silver nanoparticles as enzyme mimetics.

The same experiment was carried out with citrate reduced gold nanoparticles, and the results obtained were very different as can be seen in Figure 5.13

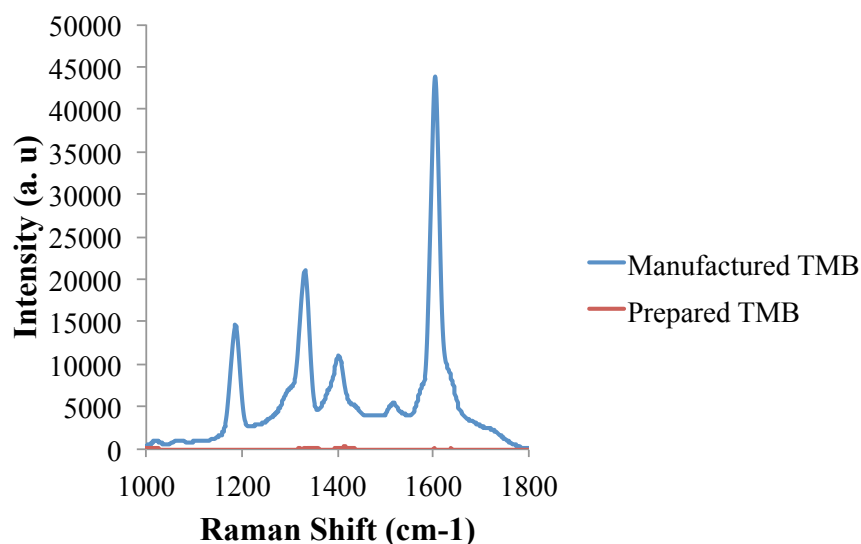


Figure 5.13 Comparison of TMB formulations after oxidation with gold nanoparticles. 200 μL of pre-mixed TMB/ H_2O_2 substrate or 100 μL of H_2O_2 (6.5 mM) and 100 μL of TMB (3 mM) was added to 500 μL of gold nanoparticles. The samples were analysed using a 633 nm laser excitation at 1 mW laser power and 1×10 second accumulation. 3 replicate samples were prepared and scanned 5 times. The spectra were baseline corrected using Grams software and an average taken.

When gold nanoparticles are used to catalyse the oxidation of TMB, the peaks indicative of the CTC are only present when the pre-mixed substrate solution is used. When TMB and H_2O_2 were manually mixed and combined with gold nanoparticles there appears to be no oxidation, and hence no SERRS signal. This is an unexpected result, and one that is difficult to explain without knowing the exact formulation of the pre-mixed TMB / H_2O_2 substrate. It can be postulated that this solution contains stabilising agents that are aiding the oxidation of the TMB by gold nanoparticles, or perhaps the concentration of H_2O_2 stated is not entirely correct, and a higher concentration of stock used alongside the manually mixed substrate would provide better results. Whatever the reason for this result, it can be concluded that citrate-capped gold nanoparticles cannot be used in conjunction with TMB for the detection

of H_2O_2 via SERRS. This result is in agreement with Jv *et al.* who reported that citrate-capped gold nanoparticles had no catalytic activity,¹⁹⁴ and in contrast to Wang *et al.* who contested this result,¹⁹⁵ demonstrating the catalytic activity of citrate capped gold nanoparticles. Thus, it is possible that these two research groups have used different formulations of TMB, which would account for the difference in catalytic activity seen.

5.3.6 Silver Nanoparticle as Enzyme Mimetics for H_2O_2 Detection

The majority of nanoparticle mimetic systems have been used for the detection of H_2O_2 since catalytic activity is dependant on this component, and there should be no oxidation of the TMB without a source of oxygen.¹⁷⁹ The detection of H_2O_2 can be of vital importance in a number of fields,¹⁸⁷ including environmental analysis and explosive detection, where a simple and rapid method of analysis is desirable. Therefore, silver nanoparticles and their peroxidase-like activity was investigated further and used for the sensitive detection of H_2O_2 .

5.3.6.1 Control Samples

Firstly, the full mimetic system and a range of controls were analysed in order to confirm that the oxidation of TMB would only occur when the silver nanoparticles and H_2O_2 were present, and that no other components were responsible for the catalytic activity. As can be seen in Figure 5.14 (a) this is exactly the case, and no catalytic activity is seen for any of the control samples analysed. The individual components on their own afforded no catalytic activity, and similarly when different mixtures were analysed that omitted one component, no peaks indicative of the CTC were present. These results also reaffirmed that in the absence of H_2O_2 there is no catalytic activity, and that the peroxidase-like nature of silver nanoparticles is H_2O_2 dependant.

The samples analysed by SERRS were then analysed using UV-Vis spectroscopy. The purpose of this was to assess whether the oxidation of TMB by silver nanoparticles could be monitored using this method of analysis. Additionally, the extinction spectrum of the silver nanoparticles was monitored to once again

determine the effect the oxidation process has on the nanoparticles, which was previously carried out using size and zeta measurements for the initial studies involving the TMB / H₂O₂ substrate solution. The results can be seen in Figure 5.14 (b).

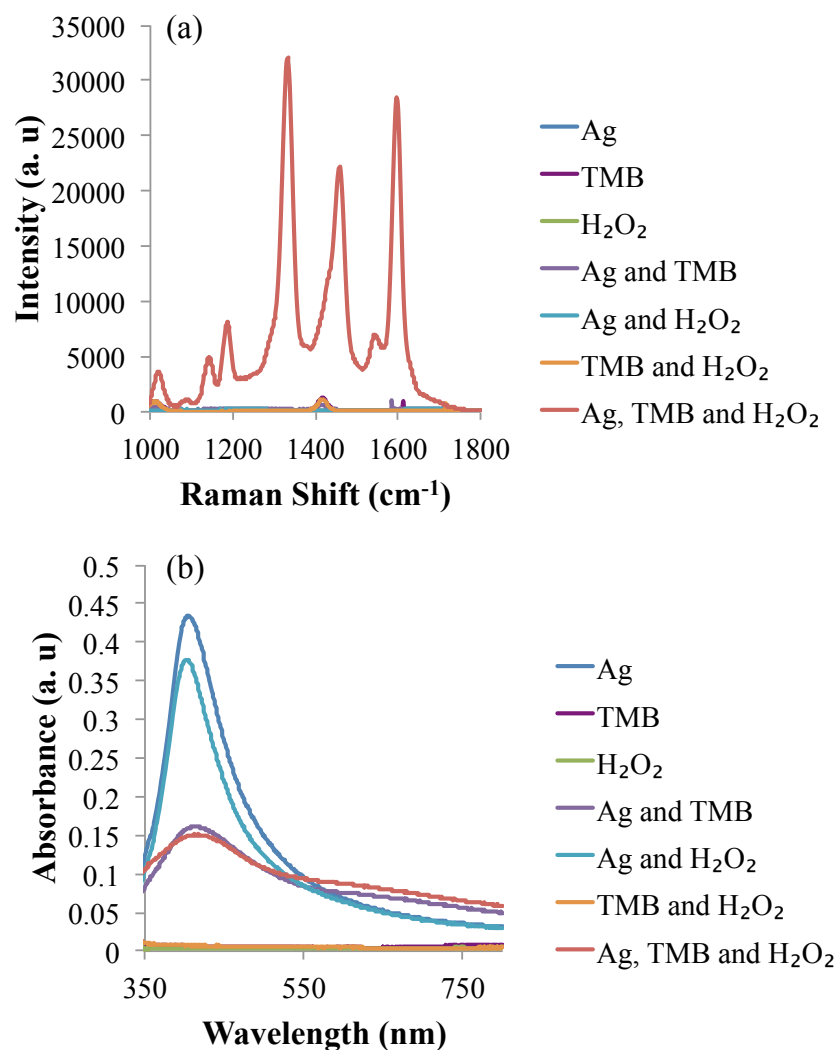


Figure 5.14 (a) SERRS spectra resulting from the Ag nanoparticle mimetic system (red) and a range of controls that investigate the presence and absence of individual components. 100 μ L of silver (0.3 nM) nanoparticles was added to 100 μ L of TMB (3 mM) and 100 μ L of H₂O₂ (6.5 mM) and analysed immediately by a laser excitation of 633 nm at 1 mW laser power using 1 x 10 second accumulation. The results shown are the average of three replicate samples and 5 scans of each sample. The spectra were baseline corrected using Grams software and an average taken. (b) Extinction profile of the nanoparticle mimetic system (red) and a range of controls. 50 μ L of each sample that was analysed by SERRS was diluted in 400 μ L for analysis by UV-Vis spectroscopy.

As expected, only when there is colloid in the sample is there a peak in the extinction spectrum at 400 nm for silver nanoparticles. The addition of H₂O₂ only to the nanoparticles has almost no effect except a slight dampening of the signal, whereas the addition of TMB alone dampens and broadens the signal, which is indicative of aggregation of the nanoparticles. This result is expected since the two amine groups on the parent molecule of TMB will have an affinity for the surface of the silver nanoparticle, and could likely cause aggregation without any oxidation to the positive CTC taking place. All the samples containing silver nanoparticles appeared visually to be stable in solution and could not be differentiated, even though the spectra obtained indicate aggregation of certain samples. Another interesting observation is the lack of an absorbance peak at 650 nm which is representative of the TMB oxidation product. This should only be apparent when TMB and H₂O₂ are combined with silver nanoparticles, and there is a slight increase in absorbance in this area for this sample. However, it is likely that this absorbance is purely the result of aggregation of the nanoparticles, as a similar result is obtained in the absence of H₂O₂. Thus, it can be concluded from these results that UV-Vis spectroscopy cannot be used to detect the oxidation of TMB by silver nanoparticles. There is no peak in the spectrum indicative of the CTC as the extinction spectrum of silver nanoparticle dominates, and the TMB and silver nanoparticles exhibit the same response as the full nanoparticle mimetic system. Therefore, SERRS is a more accurate and successful technique for analysing the peroxidase-like activity of silver nanoparticles.

5.3.6.2 Monitoring Aggregation

Throughout experiments involving the control samples for the oxidation of TMB by silver nanoparticles, it was difficult to assess the behaviour of the nanoparticles in solution. Visually, it was difficult to discriminate between any of the samples analysed, even though from the SERRS response it was obvious only one sample contained the one electron oxidation product of TMB. The results obtained from UV-Vis spectroscopy indicated aggregation of the silver nanoparticles when combined with TMB and H₂O₂ and TMB only, but gave no information regarding the mechanism of aggregation. The aggregation of the nanoparticles upon oxidation of the TMB was previously confirmed using both size and zeta potential measurements.

However, these were carried out using the TMB / H₂O₂ substrate solution, and it was important to assess whether this conclusion would hold true for the manually mixed TMB and H₂O₂. Sizing measurements were used to confirm the aggregation of the silver nanoparticles upon the oxidation of TMB and the results can be seen in Figure 5.15. The size of the silver nanoparticles was monitored every 10 minutes over a 30 minute period after the addition of TMB and H₂O₂ and this was compared to control samples that contained silver nanoparticles only, silver and TMB and silver and H₂O₂.

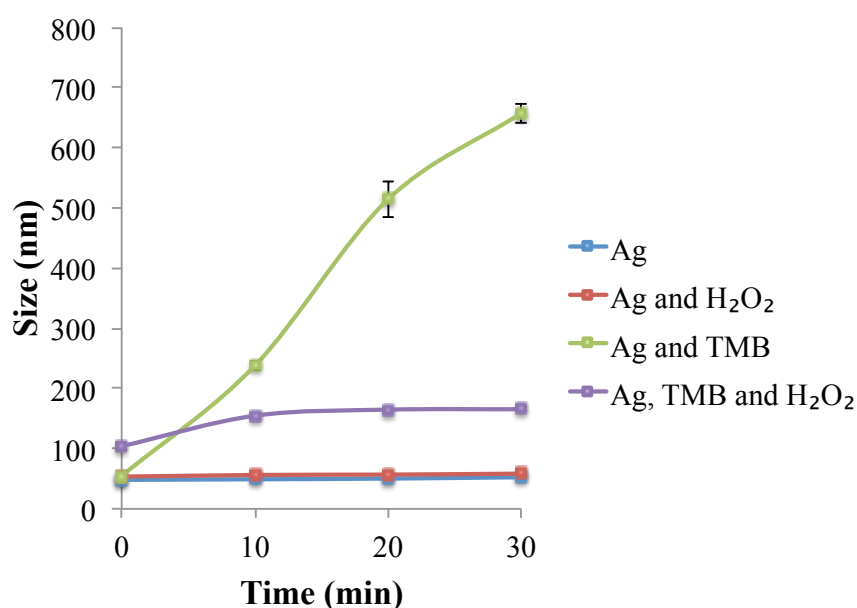


Figure 5.15 DLS results monitoring the change in size of the nanoparticles over time after the addition of 100 μ L of silver nanoparticles (0.3 nM) to 100 μ L of TMB (3 mM) and 100 μ L of H₂O₂ (6.5 mM) for the nanoparticle mimetic system (purple). Control samples of silver nanoparticles only (blue), silver and TMB (green) and silver and H₂O₂ (red) were also analysed. The results are the average of 3 replicate measurements and error bars represent one standard deviation.

As expected, there is no increase in size over time for the silver nanoparticles on their own or for the silver nanoparticles and H₂O₂, and this is consistent with the results obtained from UV-Vis analysis. When both TMB and H₂O₂ are added to the silver nanoparticles there is an immediate increase in size, indicating that aggregation has occurred. This trend gradually continues until 10 minutes, after which the nanoparticle size stabilises for the remaining period of time. The increase in size seen for the full mimetic system, however, is relatively small in comparison to the results

seen for the silver nanoparticles and TMB control. As was mentioned previously, the parent diamine molecule will serve to aggregate the silver nanoparticles in solution, which has already been confirmed via a broadening of the SPB. The large increase in size over the course of 30 minutes reaffirms this hypothesis, however, the extent to which the nanoparticle size increases for the control sample compared to when both TMB and H₂O₂ are present in the solution, suggests there is a difference in the mechanism of aggregation.

To further investigate this, zeta potential measurements were carried out to determine any change in the surface charge of the nanoparticles over time. The results can be seen in Figure 5.16, whereby it is immediately obvious that upon oxidation of the TMB the nanoparticles rapidly become positive.

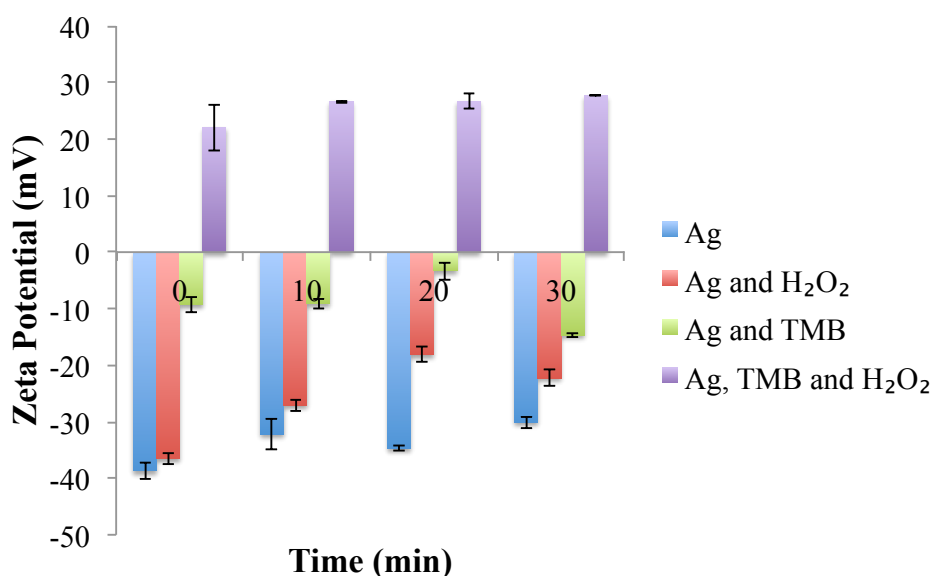


Figure 5.16 Zeta potential results monitoring the change in surface charge of the nanoparticles over time after the addition of 100 μ L of silver nanoparticles (0.3 nM) to 100 μ L of TMB (3 mM) and 100 μ L of H₂O₂ (6.5 mM) for the nanoparticle mimetic system (purple). Control samples of silver nanoparticles only (blue), silver and TMB (green) and silver and H₂O₂ (red) were also analysed. The results are the average of 3 replicate measurements and error bars represent one standard deviation.

As expected, there is very little change in the surface charge of the silver nanoparticles alone and after the addition of H₂O₂. Also, the zeta potential of the silver nanoparticles and TMB control increases, which was expected as this indicates

instability, and reaffirms the result obtained from extinction spectroscopy and DLS measurements. The change in surface charge of the sample containing silver nanoparticles, TMB and H_2O_2 , can be attributed to the formation of the CTC. This is a positively charged intermediate, therefore upon oxidation of the TMB, this reaction product appears to interact with the nanoparticles forming a positive monolayer of CTC molecules. This explains the dramatic change in zeta potential from a stable negative value (-36 mV) to a stable positive value (+28 mV) and this is indicative of the formation of stable positively charged nanoparticles. This also serves to explain the results seen using DLS (Figure 5.15), whereby upon surface functionalisation of the nanoparticles by the positive CTC, controlled aggregation occurs, resulting in a change in particle size from 50 nm to 165 nm. After 10 minutes, small clusters of positively charged silver nanoparticles are formed and remain stable over time. Contrary to this, the silver nanoparticles and TMB control sample aggregates via the interaction of the amine groups on the un-oxidised TMB, and this results in uncontrolled aggregation that continues over time. This explains the large increase in size seen, and the negative zeta potential, which indicates instability and also confirms that there is no positive monolayer formed from this particular sample.

Additionally, SEM was used to visualise the aggregation of silver nanoparticles upon oxidation of TMB to the CTC in order to further confirm this theory, and the results can be seen in Figure 5.17.

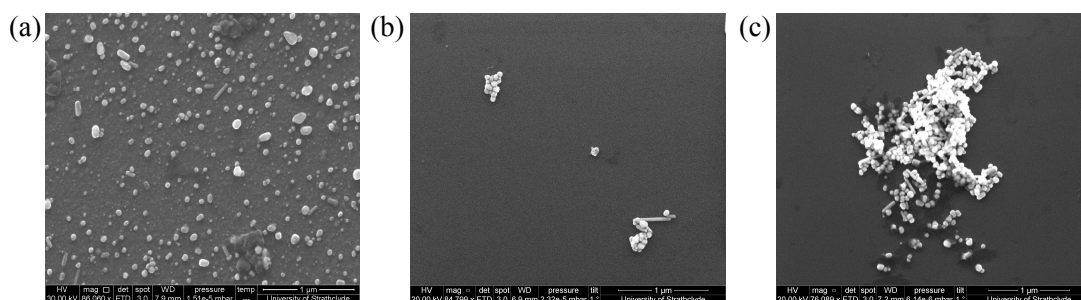


Figure 5.17 SEM images of (a) silver nanoparticles (b) silver nanoparticles after the addition of TMB and H_2O_2 and (c) silver nanoparticles after the addition of TMB only.

The silver nanoparticles remain stable and disperse in solution as can be seen in Figure 5.17 (a). Upon addition of TMB and H_2O_2 , small clusters of positively

charged particles are formed (Figure 5.17 (b)), and upon the addition of TMB only, uncontrolled aggregation occurs, resulting in the formation of large aggregates as can be seen in Figure 5.17 (c). These images serve to highlight the difference in the methods of aggregation observed between the nanoparticle mimetic system and the TMB control.

The size, zeta and SEM measurements aid in explaining the large increase in SERRS response for the sample containing all three components needed for the formation of the CTC since aggregation of the nanoparticles will result in the formation of the 'hotspots' needed for SERRS enhancement, and smaller clusters of silver nanoparticles have previously been shown to exhibit a greater SERS intensity.¹⁹⁶ Therefore, silver nanoparticles can act as both a successful enzyme mimetic and SERRS substrate within this system.

5.3.6.3 SERRS Time Studies

Since aggregated silver nanoparticles provide a good surface for SERRS enhancement, as the aggregation process proceeds it should be reflected in an increase in SERRS response. Thus, an experiment was carried out to investigate the relationship between the aggregation of the silver colloid and the SERRS response as the oxidation of TMB by silver nanoparticles proceeds. This experiment was also used to assess the optimum time for analysis that could be taken forward into the detection of H₂O₂ and the results can be seen in Figure 5.18.

The time study profile mimics that obtained from the DLS results and when all components are present, there is a rapid increase in intensity in the first stages of the reaction as the positive clusters are formed, before the signal stabilises. When there are no nanoparticles, depicted by the red markers, or no H₂O₂, depicted by the green markers, there is no increase in SERRS response. The inset in Figure 5.18, from left to right, shows the enzyme mimetic system and the controls with no H₂O₂ and no silver nanoparticles. There is a slight darkening of the yellow colour as the TMB is oxidised in the sample on the left, compared to the middle sample which contains only TMB and silver nanoparticles. This is the extent of the aggregation that can be seen visually, and there is no evidence of the blue CTC.

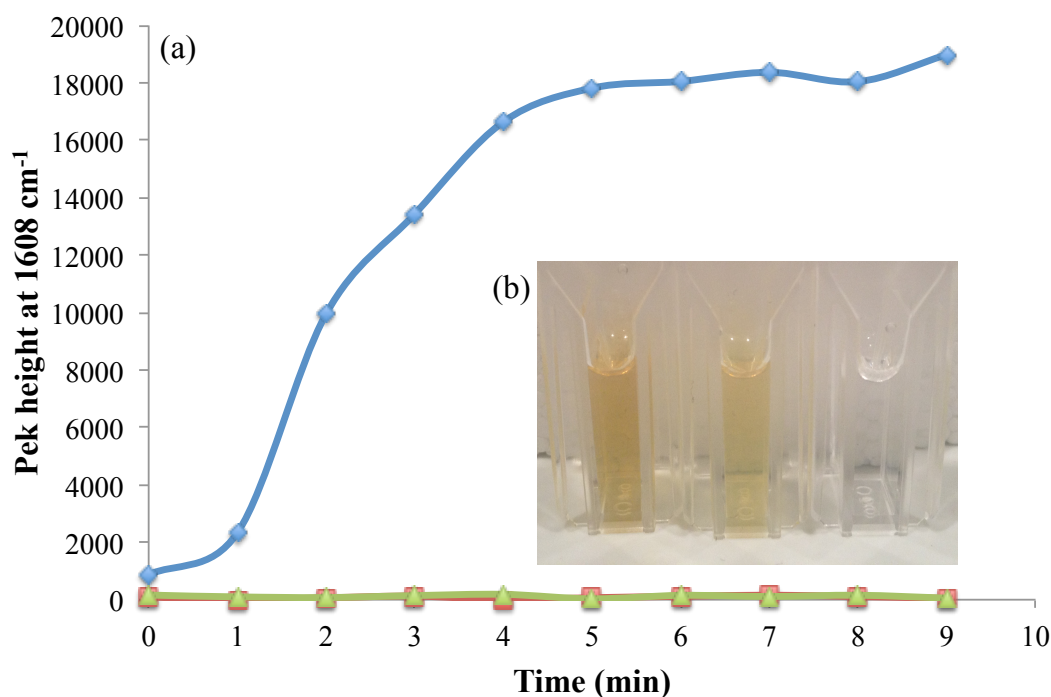


Figure 5.18 (a) The increase in SERRS response at 1608 cm^{-1} for the nanoparticle mimetic system (blue). $100\text{ }\mu\text{L}$ of silver nanoparticles (0.3 nM), $100\text{ }\mu\text{L}$ of TMB (3 mM) and $100\text{ }\mu\text{L}$ of H_2O_2 (6.5 mM) were diluted to $500\text{ }\mu\text{L}$ and the spectra taken every minute for 10 minutes using 633 nm laser excitation at 1 mW laser power using a 1×10 second accumulation. Control samples with no silver (red) and no H_2O_2 (green) were also analysed. (b) An image of the samples after analysis, from left to right is the enzyme mimetic system, no H_2O_2 and no silver nanoparticles.

In conclusion, in comparison to visual detection and the use of UV-Vis spectroscopy, SERRS is the best technique for detecting the oxidation of TMB by silver nanoparticles, and this method of analysis was used alongside these novel enzyme mimetics for the detection of H_2O_2 .

5.3.6.4 The Detection of H_2O_2

The detection of hydrogen peroxide has previously been reported using a variety of different nanoparticle mimetic systems. Magnetite nanoparticles were used alongside colourimetric analysis to obtain a detection limit of $3\text{ }\mu\text{M H}_2\text{O}_2$,¹⁸⁵ while CoFe_2O_3 magnetic particles were used in conjunction with chemiluminescence for the detection of $10\text{ nM H}_2\text{O}_2$.¹⁹⁰ Gold nanoparticles have also been used with colourimetric analysis for the detection of $0.5\text{ }\mu\text{M H}_2\text{O}_2$,¹⁹⁴ however the use of silver

nanoparticles in such detection mechanisms, in particular in combination with SERRS analysis has not been reported in the literature.

The optimisation experiments for the detection of H_2O_2 via a silver nanoparticle enzyme mimetic system were fairly straightforward, due to the few components needed. Since the H_2O_2 was to be varied, only the silver nanoparticles and TMB required optimisation. As reported previously, although increasing the concentration of colloid increased the SERRS response, there was not a significant change between 100 μL and 500 μL of colloid and since the lower amount provided a good signal with high reproducibility, this volume was used in the detection of H_2O_2 . The volume of TMB used was varied in an experiment whereby the silver colloid and H_2O_2 were kept constant. The results demonstrated that using TMB ranging between 10 μL and 100 μL of 3 mM stock solution, had very little effect on the SERRS intensity gained. As such, 100 μL of TMB was used in combination with 100 μL of silver nanoparticles for the detection of H_2O_2 . The time taken for analysis was decided based upon both the previous sizing experiments and the previous SERRS time studies, whereby after 10 minutes, there was no further change in the size, or the SERRS intensity.

Figure 5.19 shows the results gained from varying the concentration of H_2O_2 while keeping all other components constant. Figure 5.19 (a) depicts the change in spectra observed as the concentration of H_2O_2 is varied. The peaks representing the CTC decrease as the H_2O_2 is decreased but can still be observed down to a concentration of 4 μM . Figure 5.19 (b) describes the relationship between the concentration of H_2O_2 and the peak intensity at 1608 cm^{-1} representing the formation of the CTC. There is a linear response obtained which was used to calculate a limit of detection of 100 nM for this system using an international standard approach involving 3 times the standard deviation above the blank. This an improvement upon the previous detection limit of 0.5 μM obtained for gold nanoparticles.¹⁹⁴

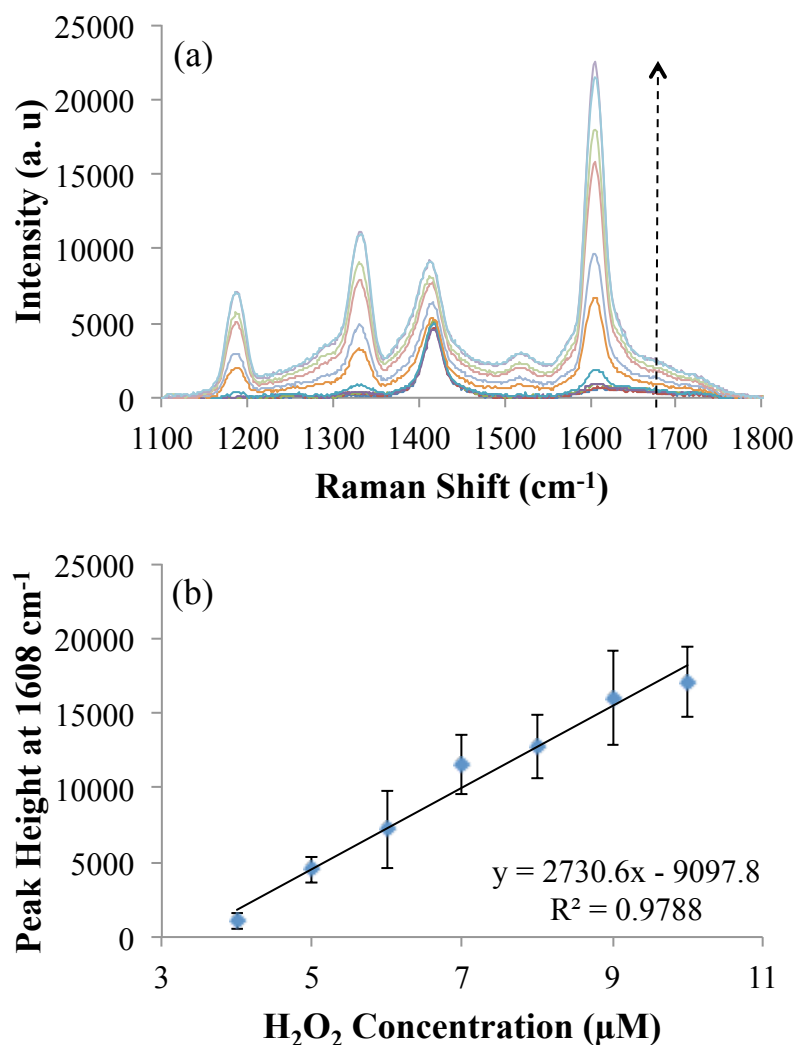


Figure 5.19 Varying concentrations of H₂O₂ were analysed with 100 μL of silver nanoparticles (0.3 nM) and 100 μL of TMB (3 mM) in a final volume of 500 μL after 10 minutes reaction time. A laser excitation of 633 nm was used at 4 mW laser power and 1 x 10 second accumulation time. (a) Spectra showing the appearance of the characteristic CTC peak as the concentration of H₂O₂ is increased. The results were baseline corrected using Grams software and the average taken to obtain the spectra shown. (b) Shows the linear relationship between concentration and peak intensity between 4 and 10 μM H₂O₂. 3 replicate samples were prepared and scanned 5 times each. The peak height was obtained from the raw data by subtracting the background signal from the control sample and the average taken to provide the plot shown. Error bars represent one standard deviation.

The limit of detection could potentially be limited by the enzyme mimetic system itself. It has been shown previously that the CTC is adsorbing onto the surface of the nanoparticles, resulting in small clusters of positively charged silver nanoparticles, and it is likely that once these clusters are formed the nanoparticles no longer exhibit catalytic activity. This would also explain the aggregation and SERRS results

reaching a plateau so quickly, and it is possible that this limit of detection could be improved by the addition of a higher concentration of nanoparticles than has been investigated herein.

It has been observed that silver nanoparticles can be used in combination with TMB and SERRS analysis for the successful detection of 100 nM H₂O₂. This is a quick, efficient and reproducible method of analysis that could potentially be extended to other analytes of interest.

5.3.6.5 Comparison Between Positive and Negative Silver Nanoparticles

The final experiment to be carried out in the investigation of silver nanoparticles as enzyme mimetics, was the comparison between particles containing an opposing surface charge.

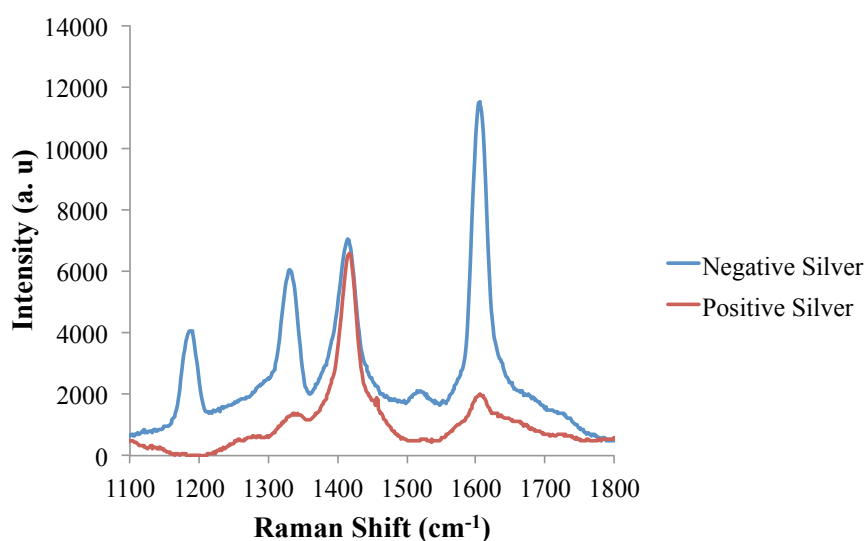


Figure 5.20 Positive and negative silver nanoparticles were compared by adding 100 μL of colloid (0.3 nM) to 100 μL of TMB (3 mM) and 300 μL of H₂O₂ (10 μM) in a final volume of 500 μL . Samples were prepared in triplicate and scanned 5 times, 10 min after addition of the colloid by an excitation wavelength of 633 nm at 4 mW using 1 x 10 second accumulation. The spectra shown were baseline corrected using Grams software.

Previous results showed that positive particles would not catalyse the oxidation of TMB / H₂O₂ substrate to the CTC. However, it was important to confirm this result using the TMB stock solution and the parameters used for the detection of H₂O₂, to

see if there was any difference in the results obtained. As can be seen in Figure 5.20, the CTC is formed in the presence of positive particles, but the SERRS signal intensity is much lower than when negatively charged silver nanoparticles are used as the catalytic element. This is most likely due to the decreased catalytic activity of the positive silver nanoparticles in comparison to the citrate capped silver nanoparticles. Additionally, these positive nanoparticles will not interact with the positive CTC in the same way as the citrate-capped nanoparticles. The repellent charges will hinder the formation of positively charged clusters that give rise to a large SERRS intensity. Thus, when using TMB as the substrate and analysis by SERRS, citrate-capped silver nanoparticles are the most successful enzyme mimetic.

5.3.7 Nanoparticle Enzyme Mimetics for use in Cellular Tracking

Although H_2O_2 is a common analyte for detection by nanoparticle enzyme mimetics, there are a variety of other potential applications. An example of such is the exploitation of the peroxidase-like activity of nanoparticles, to track their location within cells.

The use of SERS for intracellular probing is a vastly growing area of research, and as such the ability to introduce SERS substrates, namely gold nanoparticles, into a cell is of great interest. Kneipp *et al.* investigated the behavior of gold nanoparticles in living cells and their ability to serve as SERS nanoprobe in varying subcellular environments.¹⁹⁷ The authors were able to obtain a good SERS signal from the native constituents of the cell, allowing for the detection of biomolecules such as DNA and proteins. They concluded that gold nanoparticles were particularly useful for this purpose due to their small size, meaning they can be introduced to, and distributed amongst the cell with limited damage to its structural integrity. It was also noted however, that the dispersion of nanoparticles throughout the cell could not be controlled and as such a method of tracking these particles once they have entered the cell would be beneficial.

Gold and silver nanoparticles on their own both exhibit peroxidase-like activity, and experiments have shown that when combined with both TMB and H_2O_2 , an intense SERRS signal can be obtained in their presence. Thus, in theory, once nanoparticles

have entered a cell and both the substrate and H_2O_2 added, SERRS should be able to detect the locations in the cell that give a signal for the oxidation product. Since, there will be no oxidation without the nanoparticles, then for TMB, the CTC signal should only be present where the nanoparticles are located.

This is a completely novel method of nanoparticle tracking, and there has been no previous precedent for the use of nanoparticle enzyme mimetics inside cells. Silver nanoparticles were added to live Chinese hamster ovary (CHO) cells overnight before the addition of TMB and H_2O_2 for 1 hour. The results reported in Figure 5.19 are purely proof of concept and aim to highlight the potential that these nanoparticle mimetics have within the area of cellular analysis.

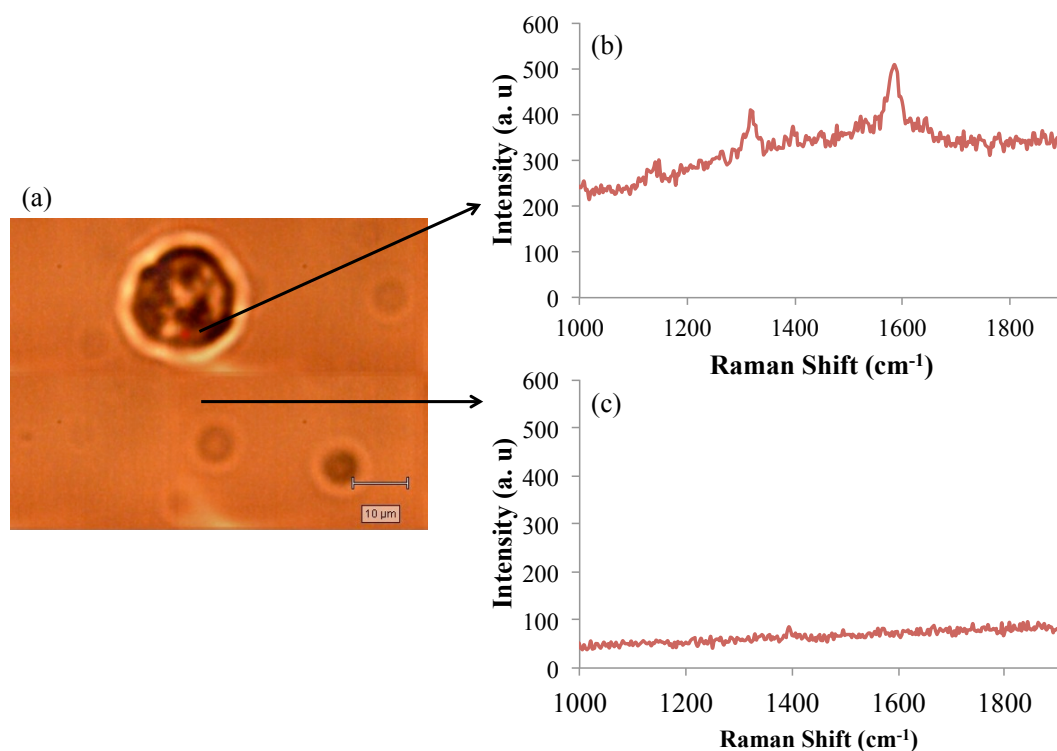


Figure 5.19 Nanoparticle tracking in live Chinese hamster ovary cells. 100 μL of silver nanoparticles (0.3 nM) were added to previously prepared cells overnight before the addition of 10 μL of TMB (3 mM) and 10 μL of H_2O_2 (6.5 mM). The cells were analysed after 1 hour using a 633 nm laser excitation wavelength at 4 mW and 1 x 10 second accumulation (a) White light of image of individual cell with a false colour (red) depicting areas of high intensity signal. (b) The signal obtained from the highlighted area within the cell. (c) The signal obtained from the cell media.

As this experiment was for proof of concept, the parameters have not been optimised. In particular, a significant amount of cell death was seen in these trials, most likely due to the high concentration of H_2O_2 used, and this parameter in particular would require stringent optimisation. Additionally, the toxicity of silver nanoparticles would need to be taken into account, and measures developed in order to combat this effect. However, for these initial proof of concept experiments (Figure 5.19), the peaks indicative of the CTC at 1608 cm^{-1} , 1330 cm^{-1} , and 1180 cm^{-1} are present within the cell, and since these peaks will only be present upon oxidation by the silver nanoparticles, it can be hypothesised that this area of high intensity signal represents the location of a cluster of nanoparticles within the cell. Additionally, almost no signal can be seen outside the cell, most likely due to the absence of silver nanoparticles. There is a small peak at 1400 cm^{-1} that has previously been attributed to the un-oxidised TMB. This further confirms that only in the presence of nanoparticles will the TMB be oxidised and that these nanoparticles are mainly present within the cell.

These nanoparticle mimetics could also potentially be used to monitor oxidative stress within a cell, which can be detected via the presence of increased levels of free radicals. Thus, if silver nanoparticles and TMB were added to cells, and a signal indicative of the CTC was present, this could be used as a method of detecting these free radical, as in the absence of H_2O_2 no signal should be formed.

It can be concluded from initial experiments with nanoparticle mimetics within cells, that the TMB substrate can be oxidised by the nanoparticles within a cellular environment and detected via SERRS. Upon further investigation of this phenomenon, this process could be optimised to devise a simple and effective method of silver and gold nanoparticle tracking within cells, and potentially develop a method for the detection of oxidative stress in cells.

5.4 Conclusions

The use of SERRS as a method of analysing the peroxidase-like activity of gold and silver nanoparticles has been reported, and this is the first time the enzyme mimetic

ability of silver nanoparticles has been shown. This is the first time this technique has been used in conjugation with nanoparticle based enzyme mimetics, and has shown to be an efficient and sensitive method of analysis for this purpose.

The oxidation of a pre-mixed TMB / H₂O₂ substrate was proven using both gold and silver nanoparticles via enhanced peaks representative of the one electron oxidation product of TMB. Unfortunately, due to opposing surface charges, the substrate ABTS could not be oxidised using these nanoparticles, and changing the charge on the surface of the gold nanoparticles had no effect on the spectrum obtained. Therefore, it was concluded that TMB was the best substrate for use in a nanoparticle enzyme mimetic system that was to be analysed by SERRS. Through size and zeta potential measurements, the nanoparticles were shown to aggregate upon oxidation of the TMB, and thus are simultaneously able to act as a catalytic agent and a SERRS substrate, requiring no external aggregating agents.

Two different TMB formulations were compared, and the pre-mixed substrate solution was analysed alongside a manually mixed TMB and H₂O₂ solution with both gold and silver nanoparticles. The silver nanoparticles were able to oxidise this manual solution providing a strong SERRS spectrum while the gold nanoparticles exhibited no catalytic activity. Therefore, it was concluded that citrate-capped silver nanoparticles alongside TMB are the best parameters for a nanoparticle enzyme mimetic system using SERRS analysis.

It has been proven that the oxidation of TMB via silver nanoparticles cannot be detected using colourimetric detection, as there is very little visual change in the appearance of the nanoparticle enzyme mimetic sample compared to a range of controls, and no peak indicative of the CTC was present in the extinction spectrum. Size and zeta measurements as well as SEM analysis was used to confirm that upon oxidation of TMB to the CTC, the silver nanoparticles formed small clusters of positively charged particles that gave rise to an excellent SERRS signal over the course of 10 minutes, proving silver nanoparticles to be a very efficient enzyme mimetic.

This is the first reported case of silver nanoparticles catalysing the oxidation of the peroxidase substrate TMB. It is also the first reported case of the analysis of the action of nanoparticle enzyme mimetics by SERRS. These artificial enzymes are amenable to SERRS analysis as they act both as reaction catalyst and SERRS substrate, allowing for a simple and efficient method of analysis. These novel enzyme mimetics have been used alongside SERRS for the detection of 100 nM H_2O_2 , a sensitive limit of detection in comparison to previously reported nanoparticle enzyme mimetic systems. They have also been used to provide positive results from initial experimentation on the applicability of silver enzyme mimetics for use in nanoparticle tracking in live cells, and could in theory be used to measure oxidative stress within a cell.

Silver nanoparticles are a simple, rapid, and cost effective alternative to conventional enzymes and along with SERRS analysis could potentially have a vast variety of applications.

6. Conclusions

This thesis can be divided into two distinct sections, the first of which investigated the use of lambda exonuclease as a target cycling strategy for PCR-less detection of DNA. The second part investigated the use of artificial enzymes in the form of both DNAzymes, for target DNA detection, and nanoparticle enzyme mimetics, for the detection of H₂O₂.

The action of lambda exonuclease upon duplex DNA was successfully monitored using a FRET system. This involved the use of the minor groove binder H33258 along with a FAM labelled probe sequence of DNA. Upon addition of a target sequence, a high fluorescent output was seen indicative of hybridisation and formation of a DNA duplex. The action of the lambda exonuclease was monitored via a decrease in fluorescence as the enzyme digested the probe strand of the duplex DNA, leaving the target free to be recycled within the assay. Although this FRET system could not be used for the sensitive detection of target DNA, it was successfully used for the optimisation of enzymatic activity. Lambda exonuclease was then incorporated into a DNA-nanoparticle conjugate based assay with both plasmonic and SERRS analysis. The design of this assay involved the hybridisation of a target sequence of DNA to a probe sequence conjugated to a metallic nanoparticle. Upon digestion by lambda exonuclease the nanoparticle would aggregate, either via destabilisation or hybridisation, which could be potentially be monitored using SERRS analysis. The action of lambda exonuclease would leave the target intact after digestion to hybridise with another probe, hence providing a method of target recycling and signal amplification.

Initially, target DNA could not be detected using any of these methods of analysis, and therefore the gold and silver nanoparticles investigated were replaced with gold and silver shelled magnetic nanoparticles. The theory behind this was to incorporate a magnetic wash step to eliminate any background signal, and these nanoparticles were able to provide a method for the detection of target DNA using lambda exonuclease and SERRS. The action of the enzyme was also investigated, and although it was proven that lambda exonuclease will digest DNA on the surface of a

nanoparticle, it was found that the enzyme had a greater activity on single stranded DNA as opposed to double stranded DNA, which is the usual substrate for this enzyme. Therefore, it was concluded that the use of lambda exonuclease in a target cycling strategy for the detection of target DNA would always be limited by this phenomenon, and a method of inhibiting this single stranded activity would need to be developed before continuing with this enzyme.

The ability of DNAzymes to exhibit peroxidase-like activity was investigated, and the use of catalytic DNA in the oxidation of the peroxidase substrates ABTS and TMB was carried out. This oxidation reaction was successfully analysed using resonance Raman scattering, a novel method of analysis for DNAzyme activity. Resonance Raman scattering was then incorporated into a catalytic beacon assay for the detection of target DNA, allowing for synthetic DNA amplified by PCR to be detected. A split probe DNAzyme assay for the detection of target DNA was also investigated, and although unsuccessful, the ability of streptavidin coated magnetic beads to oxidise peroxidase substrates was realised and it was concluded that these separation agents could not be utilised in assays where these peroxidase substrates were present as it would provide a false positive result.

SERRS was also investigated as a novel method of analysis for the action of DNAzymes, and an excellent signal and good discrimination was seen for the DNAzyme sample in comparison to the control samples when using silver nanoparticles. Although, SERRS was unsuccessful as a method of analysis within the catalytic beacon and split probe assay, the potential exists for SERRS to be an extremely sensitive technique in the detection of specific analytes using DNAzyme activity, and both RRS and SERRS should be considered as an alternative spectroscopy to fluorescence and colourimetric detection in this field.

When investigating the use of SERRS for DNAzyme activity, it was noted that a signal for the oxidation product of TMB was obtained when only nanoparticles and single stranded DNA was present. Thus it was confirmed that, similar to the magnetic beads, metallic nanoparticles can exhibit peroxidase-like activity. This phenomenon was investigated further and the use of both gold and silver

nanoparticles as enzyme mimetics was carried out. The catalytic activity of gold nanoparticles has previously been reported in the literature, however, this was the first investigation into the use of silver nanoparticles as an enzyme mimetic. Also, most methods of detection reported utilise colourimetric analysis and this was the first reported case of using SERRS for the detection of nanoparticle mimetic action. The nanoparticles were able to act as both catalytic agent, and substrate for SERRS analysis allowing excellent signals to be obtained for the peroxidase substrate TMB after oxidation using either gold or silver nanoparticles. Different formulations of TMB were investigated and it was concluded that silver nanoparticles provided the best level of catalytic activity and SERRS signal and were used for the detection of H₂O₂. A limit of detection of 100 nM was achieved which is lower than that previously reported for gold nanoparticles using colourimetric detection. The use of this phenomenon to visualise nanoparticles in live cells was also briefly investigated, and the promising results obtained allow the vast potential of the nanoparticle enzyme mimetics to be realised.

Nanoparticles enzyme mimetics are simple, cost effective and rapid to synthesis, in comparison to natural enzymes. They provide efficient catalytic activity and are amenable to SERRS analysis. Thus, nanoparticle enzyme mimetics should be considered in future applications as an alternative to conventional protein enzymes in a number of assay for a variety of applications.

7. Experimental

7.1 Monitoring the Action of Lambda Exonuclease for the Detection of DNA using FRET

7.1.1 Materials

Lambda exonuclease and lambda exonuclease reaction buffer (x10) were obtained from New England Biolabs, UK. Hoechst 33258 was obtained from Sigma Aldrich, UK, as was borax solution. All other buffer components were purchased from VWR International, UK.

7.1.1.2 Oligonucleotide Sequences

The probe used in these experiments was a 21-mer with a 5' phosphate modification and 3' FAM C7 modification and was ordered from AtdBio Ltd, UK. The target sequence was synthesised in house at the start of the project and was subsequently ordered from Eurofins MWG Operon, Germany.

Table 7.1 Oligonucleotide sequences used for monitoring the action of lambda exonuclease for the detection of DNA using FRET.

Name	Sequence (5'-3')	5' Modification	3' Modification
Probe	ATGACGTCTATCCATTTATGT	Phosphate	FAM
Target	ACATAAATGGATAGACGTCAT	None	None

7.1.2 Instrumentation

All UV-Vis measurements were carried out using a Cary 300 Bio UV-Vis Spectrophotometer with a Peltier temperature controller. Oligonucleotides were synthesised on a MerMade 6 oligonucleotide synthesiser. HPLC was carried out on a Dionex P680 HPLC pump with photodiode array detector, using a Phenomenex Clarity 3 μ m Oligo-RP column for reversed phase analysis. Fluorescence measurements were carried out on a Cary Eclipse fluorescence spectrometer, and

also on a Strategene Mx4000 Multiplex Quantitative PCR System for precise temperature control. This instrument was later updated to a Strategene Mx3005P system.

7.1.3 Preliminary Fluorescence Measurements

Preliminary fluorescence measurements were carried out on a Cary Eclipse fluorescence spectrophotometer, using 1 cm plastic cuvettes, with a 1 mL sample volume. 1 μ M of FAM-Probe and target DNA was used along with a 1 mg/ml solution of H33258 (2.4 mM). All components were made up to a final volume of 1 mL with lambda exonuclease reaction buffer (x1) and analysed immediately. The emission spectrum of these samples were determined, exciting at 350 nm on the Cary Eclipse and measuring the fluorescent emission from 370 nm to 600 nm.

7.1.4 Fluorescent DNA Melts

1 μ M of FAM-Probe and target DNA along with 1 μ M of H33258 were made up to 150 μ L with lambda exonuclease reaction buffer (x1) in PCR tube strips with optical caps. Using a Strategene Mx4000 PCR instrument, the temperature was cycled between 25 $^{\circ}$ C and 95 $^{\circ}$ C, increasing or decreasing the temperature by 1 $^{\circ}$ C per minute. An excitation wavelength of 350 nm was used and the fluorescent signal at 520 nm was measured every minute. Three heating and cooling cycles were carried out and the average taken to obtain a melting profile.

7.1.5 Monitoring Lambda Exonuclease Digestion using FRET

0.2 μ M of FAM-Probe and 1 μ M of target DNA were hybridised in 150 μ L final volume of 25 mM Borax / 25 mM MgCl₂, pH 9.4 buffer along with a final concentration of 1 μ M of H33258 in PCR tubes with optical caps. This was carried out using the temperature program on the Strategene Mx4000 to heat the samples to 95 $^{\circ}$ C and then cool to 25 $^{\circ}$ C before the digestion step. After hybridisation 20 units of lambda exonuclease enzyme was added to the samples. Excitation and emission was pre-set using optical filters of 350 nm and 516 nm, respectively. Three fluorescence measurements were taken at 516 nm every minute after the addition of

the enzyme, over a period of 30 minutes while the temperature was held at 37°C. Control samples with no lambda exonuclease and no target DNA were also analysed.

7.1.6 Lambda Exonuclease for DNA Detection

Samples were made up to 150 µl with a final concentration of 1 µM of H33258 and 1 µM of FAM-Probe, with varying amounts of target DNA in 25 mM Borax / 25 mM MgCl₂, pH 9.4. Samples were hybridised using the Mx4000 using the temperature cycling method previously described. 20 units of λ-exonuclease enzyme was added to the samples and the temperature held at 37 °C. An excitation wavelength of 350 nm was used and the fluorescent emission at 516 nm measured every minute after the addition of lambda exonuclease. The change in fluorescent intensity over the 30 minute period was plotted against target concentration. 5 replicate samples were prepared and the average taken to obtain the results and error bars seen.

7.2 Amplification Free Detection of DNA by Lambda Exonuclease and SERRS

7.2.1 Materials

Lambda exonuclease and lambda exonuclease reaction buffer (x10) were obtained from New England Biolabs, UK. The majority of buffer materials were obtained from VWR International, UK. Hoechst 33258 was obtained from Sigma Aldrich, UK, as was the borax solution. All materials needed for the synthesis of nanoparticles used within this chapter, including sodium citrate, sodium tetrachloroaurate and silver nitrate were obtained from Sigma Aldrich, UK. Agarose for use within gel electrophoresis experimentation was obtained from Bioline Reagents Ltd., UK and TBE (x10) was obtained from Sigma Aldrich, UK. Malachite green isothiocyanate dye was obtained from Invitrogen Life Technologies, UK.

7.2.1.1 Oligonucleotide Sequences

The probe used in these experiments was a 21-mer with a 5' phosphate modification and either a 3' thioctic acid modification or 3' thiol modification and was ordered

from AtdBio Ltd, UK. The target sequence used was ordered from Eurofins MWG Operon, Germany. Polynucleotides of 10 A and 10 T with a 3' thioctic acid or 3' thiol modification were also ordered from AtdBio Ltd, UK

Table 7.2 Oligonucleotide sequences used for the detection of DNA using lambda exonuclease and SERRS

Name	Sequence (5'-3')	5' Modification	3' Modification	Mid-Sequence Modification (*)
TA-Probe	ATGACGTCTA TCCATTTATGT	Phosphate	Thioctic Acid	None
TA-10A-Probe	ATGACGTCTA TCCATTTATGT AAAAAAAAAA	Phosphate	Thioctic Acid	None
TA-10A-HEG-Probe	ATGACGTCTA TCCATTTATGT (*)AAAAAAAA AA	Phosphate	Thioctic Acid	HEG
TH-10A-HEG-Probe	ATGACGTCTA TCCATTTATGT (*)AAAAAAAA AA	Phosphate	Thiol	HEG
TA-10T	TTTTTTTTTT	None	Thioctic Acid	None
TA-10A	AAAAAAAAAA	None	Thioctic Acid	None
TH-10T	TTTTTTTTTT	None	Thiol	None
TH-10A	AAAAAAAAAA	None	Thiol	None
Target	ACATAAATGG ATAGACGTCA T	None	None	None

7.2.2 Instrumentation

All UV-Vis measurements were carried out using a Cary 300 Bio UV-Vis Spectrophotometer with a Peltier temperature controller. Samples were analysed in 1 cm glass cuvettes and scanned from 200 nm to 800 nm. Raman spectra were collected using a Renishaw inVia microscope system with a HeNe laser (633 nm). Samples were analysed in 1.5 mL semi-micro disposable plastic cuvettes using a 20 x long working distance objective. WiRE 2.0 software (Renishaw PLC) was used to run the analysis and spectra were baseline corrected using varying functions and a Level and Zero levelling mode in Grams software. Fluorescent measurements were carried out using a Strategene Mx3005P PCR instrument or with a Horiba Scientific FluoroLog spectrofluorometer with a Xenon lamp in combination with a Peltier cooling unit.

7.2.3 Preparation of Gold and Silver Nanoparticles

All glassware was soaked in aqua regia (HCl, HNO₃ 3:1 v/v) for 1-2 hours before it was used in the preparation of gold and silver colloid. The glassware was then rinsed with triply distilled water gained from an in-house filtration system, before being neutralised with sodium carbonate, and poured down the sink with excess water.

For the preparation of 13 nm gold nanoparticles, a 1 litre 3-necked round bottom flask and glass link stirrer was cleaned with aqua regia. 500 ml of triply distilled water was added to the flask with 50 mg of sodium tetrachloroaurate. The solution was stirred using the glass link stirrer above a Bunsen burner until boiling. At this point, 75 mg of sodium citrate was added, and then boiled for 15 minutes, before being allowed to cool. For the preparation of larger gold nanoparticles, in the region of 40 nm, the ratio of gold to citrate was varied. Concentrated gold colloid was prepared via centrifugation for 1 hour 50 minutes at 6000 rpm. The supernatant was removed and the remaining nanoparticles in each of the sample tubes combined.

For the synthesis of silver nanoparticles, 500 ml of distilled water was heated to 45 °C in a 3 necked round bottom flask (1L). 90 mg of silver nitrate (dissolved in 10 ml d.H₂O) was added and heating continued until boiling. 10 ml of a 1% aqueous solution of sodium citrate was added and the temperature maintained for 90 minutes

before being allowed to cool to room temperature. Constant stirring was maintained throughout using a glass linked stirrer.

7.2.4 Preparation of DNA Nanoparticle Conjugates

Thioctic acid or thiol modified oligonucleotides (8.6 nmol) were added to either gold nanoparticles (3 mL, 17 nM) or silver nanoparticles (3 mL, 0.3 nM) in a glass vial, and left overnight. Phosphate buffer ($\text{NaH}_2\text{PO}_4/\text{Na}_2\text{HPO}_4$, 60 mM, pH 7) was added to 10 mM final concentration. NaCl (2 M) was then added in aliquots, increasing the salt concentration in 0.05 M increments to a final concentration of 0.3 M. This salt ageing process was carried out over three consecutive days.

The conjugates were added to 1 ml eppendorf tubes and centrifuged at 6000 rpm for 20 minutes (x3). The supernatant was discarded and the resulting highly coloured pellets were combined and stored at 4 °C.

SERRS active conjugates were prepared by adding malachite green isothiocyanate (1 mL, 1×10^{-6} M) to the conjugate solution (1 mL) in a 1:1 ratio for 1 hour with constant stirring. The samples were then centrifuged at 6000 rpm for 20 minutes and washed with distilled water (x3) before the pellets combined and stored at 4 °C.

7.2.5 Gel Electrophoresis of DNA Nanoparticles Conjugates

Gel electrophoresis was carried out on an Agarose gel that was prepared by dissolving 100 mg of Agarose in 100 mL of TBE buffer (0.5x) using a microwave, and then allowing the gel to cool and set for 30 minutes. 15 μL of nanoparticle conjugates (10 nM) was diluted with glycerol (4x), and injected into 20 μL wells. The gel was run in 0.5x TBE buffer for 90 minutes and the band visualised using the strong colour of the conjugates.

7.2.6 DNA Melting Experiments

These experiments were carried out on a Cary 300 Bio UV-Visible spectrophotometer fitted with a Cary temperature control unit. A quartz cell with a 1 cm path length with a fitted cap was used for the samples. 0.1 μM of probe and

target DNA were diluted to a final volume of 400 μ L with lambda exonuclease reaction buffer (x1). The temperature was cycled between 10 $^{\circ}$ C and 90 $^{\circ}$ C at a rate of 1 $^{\circ}$ C per minute, and the absorbance measured at 260 nm every minute. The program was used to automatically calculate the average T_m for the eight cycles run.

7.2.7 UV-Vis Detection of Lambda Exonuclease Digestion

A Cary 300 Bio UV-Visible spectrophotometer was used for the measurement of extinction spectra, scanning between 200 nm and 800 nm. Varying concentrations of conjugates were hybridised prior to analysis by cycling the temperature between 10 $^{\circ}$ C and 90 $^{\circ}$ C on a heating block. Control samples were then analysed immediately. For the full assay format, varying amounts of lambda exonuclease were added to the conjugates and kept at 37 $^{\circ}$ C overnight for optimum digestion in either lambda exonuclease reaction buffer or 25 mM borax / 25 mM $MgCl_2$, pH 9.4 depending on the experiment. Exact conditions are given within the figure captions in the results and discussion chapter. This digestion was either carried out on a heating block before the samples were transferred to a 1 cm quartz micro-cuvette for analysis by UV-Vis spectroscopy or using a scanning kinetics programme on the spectrometer that allowed for precise temperature control while measuring the absorbance every 5 minutes for a total of 960 minutes.

7.2.8 SERRS of DNA Nanoparticle Conjugates

SERRS active DNA nanoparticle conjugates were prepared according to the protocol outlined in section 7.2.5 using malachite green isothiocyanate dye. Varying concentrations of conjugate were used in experiments along with two different buffers and varying amounts of enzyme. Exact conditions for individual experiments are given in the figure captions in the results and discussion section. The standard protocol for analysis by SERRS first involved hybridisation of the conjugates to the target DNA in the chosen buffer, and this was carried out by cycling the temperature between 10 $^{\circ}$ C and 90 $^{\circ}$ C (x3) on a heating block. The enzyme was added and digestion left to occur at 37 $^{\circ}$ C overnight on a heating block. Samples were then transferred to a 1 cm plastic micro-cuvette or a clear-96 well plate for analysis by SERRS. A 633 nm laser excitation wavelength was used at 4 mW laser power using 3 x 3 second accumulations. Samples were always scanned 5 times to ensure

between scan reproducibility and were analysed using WiRE software and processed using Grams software, which was also used to baseline correct the spectra.

7.2.9 Synthesis of Gold and Silver Shelled Magnetic Nanoparticles

A stock solution of iron oxide nanoparticles were synthesised by preparing a 25 mL solution of 0.4 M Fe²⁺ (iron (II) chloride tetrahydrate, 1.98g), 0.8 M Fe³⁺ (iron (III) chloride hexahydrate, 5.335g) and 0.4 M HCl (821µL). This solution was added dropwise to 250 mL of a 1.5 M NaOH (15.058g) solution in a 3 necked round bottom flask (previously cleaned with aqua regia) at 50 °C on a heating mantle with constant stirring. After 20 minutes this solution was allowed to cool before being washed with 300 mL of distilled water (x2) and then 100 mL of 0.1 M HNO₃ (x1). The precipitate formed was dissolved in 125 mL of 0.1 M HNO₃. Half of this solution was then heated to 90 °C with constant stirring for 40 minutes before cooling to room temperature. The solution was centrifuged at 8000 rpm for 20 minutes and washed with distilled water (x3). This final product was re-suspended in 250 mL of water.

For the preparation of silver-shelled magnetic nanoparticles, 2 mL of the stock solution, 8 mL of distilled water and 250 µL of 1% sodium citrate were added to a glass vial for 15 minutes. Then, 200 µL of 1% aqueous AgNO₃ was added for 5 minutes followed by 25 µL of 0.2 M hydrazine hydrate. A further 2 aliquots of the hydrazine hydrate and AgNO₃ were added in the same way, with 10 minute intervals between each addition. These reactions were carried out under constant sonication. Finally, 200 µL of 1% sodium citrate was added and the vial was sonicated for a further 20 minutes. The nanoparticles were centrifuged at 600 rpm for 20 minutes and washed with distilled water (x2) before being subjected to a magnetic wash step to obtain the final silver coated magnetic nanoparticles.

For the preparation of gold-shelled magnetic nanoparticles, 1 mL of stock magnetic nanoparticles were added to 1 mL of 0.005 M sodium tetrachloroaurate solution with 0.5 g of glucose in a glass vial and placed in a sonicator for 30 minutes. Samples were then agitated in a water bath held at 60 °C for 2 hours before being cleaned using 2 centrifugation steps (6000 rpm, 20 minutes) and a magnetic separation step.

7.2.10 DNA Magnetic Nanoparticle Conjugates

Oligonucleotide sequences were conjugated to the surface of these gold and silver-shelled magnetic nanoparticles using the method previously described in section 7.2.4, and made SERRS active using the protocol also described in section 7.2.4.

7.2.11 SERRS of DNA Magnetic Nanoparticle Conjugates

The protocol for SERRS analysis of the gold and silver-shelled magnetic nanoparticles for use within the lambda exonuclease assay is similar to that previously described for the non-magnetic nanoparticles, with the main difference being the introduction of a magnetic wash step. The conjugates were hybridised with the target sequence of DNA in lambda exonuclease reaction buffer (x1) to a final volume of 500 μ L on a heating block by cycling the temperature between 10 °C and 90 °C. Control samples were analysed immediately, with SERRS analysis before and after a magnetic wash step. In the full assay the enzyme was added and the digestion left to occur overnight at 37 °C. Samples were transferred from eppendorfs into plastic micro-cuvettes for SERRS analysis using a 633 nm laser excitation wavelength at 4 mW power along with 3 x 3 second accumulations. Samples were also analysed both before and after the magnetic wash step (x3), whereby a magnet was used to pull the conjugates to one side of an eppendorf while buffer wash used to wash away any un-hybridised DNA. After this wash step, the samples were re-suspended in 500 μ L of buffer and again analysed using SERRS. Samples were always scanned 5 times using WiRE software and analysed using Grams software which was used to baseline correct the spectra obtained.

7.2.12 Confirming Digestion on a Nanoparticle

Two methods were used to confirm digestion on the surface of a nanoparticle. The first utilised a Strategene Mx3005P PCR instrument. A final concentration of 5 nM of TA-10A-HEG Probe gold conjugate was hybridised with a final concentration of 0.2 μ M of target DNA in the presence of 1 μ M of H33258 (final concentration) in 30 μ L of lambda exonuclease reaction buffer (x1) before the addition of 20 units (4 μ L) of lambda exonuclease enzyme. An excitation wavelength of 350 nm was used and the fluorescent emission measured at 516 nm every minute for 60 minutes after the addition of the enzyme, while keeping the temperature constant at 37 °C.

The second method utilised a Horiba Scientific FlouroLog spectrofluorometer. A final concentration of 60 pM of TA-10A-HEG-Probe gold conjugate was hybridised with 1 μ M target DNA in the presence of 1 μ M of H33258 (final concentrations) in 30 μ L lambda exonuclease reaction buffer (x1). 20 units (4 μ L) of enzyme was added to the samples contained in a glass cuvette and a Peltier cooling unit used to keep the samples at 37 °C. An excitation wavelength of 350 nm was used and an fluorescent profile between 380 nm and 500 nm obtained every 12 second for a total of 10 minutes after the addition of the enzyme.

7.3 Resonance Raman and Surface Enhanced Resonance Raman Scattering of DNAzyme Activity for Oligonucleotide Detection

7.3.1 Materials

Haemin was purchased from Sigma Aldrich, UK as was buffer components 4-(2-Hydroxyethyl)piperazine-1-ethanesulfonic acid (HEPES), sodium chloride and potassium chloride, as well as all materials required in the synthesis of metallic nanoparticles. SureBlue™ TMB microwell peroxidase substrate (1-component) was purchased from KPL, inc., USA. ABTS one component HRP microwell substrate was purchased from SureModics IVD, USA. Streptavidin coated magnetic beads were purchased from New England Biolabs, UK and streptavidin coated clear 96-well plates were obtained from Thermo Scientific, UK.

7.3.1.1 Oligonucleotide Sequences

All DNA oligonucleotides were purchased from Eurofins MWG Operon, Germany, and are shown in Table 7.2.

Table 7.3 Oligonucleotide sequences for use in experimentation on RRS and SERRS of DNAzyme activity for DNA detection. Italics represent the PS2.M sequence within the beacon and split probe DNAzyme sequence

Name	Sequence (5'-3')	3' Modification	5' Modification
PS2.M	GTGGGTAGGGCGGGTT GG	None	None
Beacon	<i>GTGGGTAGGGCGGGTTG</i> GATGACGTCTATCCATT TATGTCCAACCC	None	None
Target	ACATAAATGGATAGAC GTCAT	None	None
Split Probe Biotin-DNA	TCAGCTGCATAT	Biotin	None
Split Probe Target	ATGTGCAGCTGACACG TGGCAATG	None	None
Split Probe DNAzyme	<i>GTGGGTAGGGCGGGTTG</i> GAAAAACACCACTCAT CA	None	None

7.3.2 Instrumentation

UV-Vis absorption spectra were carried out using a Cary 300 Bio UV-vis spectrometer. Samples were analysed in 1 cm quartz cuvettes and scanned from 200 nm to 800 nm. Raman spectra were collected using a Renishaw inVia microscope system with a HeNe laser (633 nm). Samples were analysed in 1.5 mL semi-micro disposable plastic cuvettes using a 20 x long working distance objective. WiRE 2.0 software (Renishaw PLC) was used to run the analysis and spectra were baseline corrected using varying functions and a 'level and zero' levelling mode in Grams software.

7.3.3 Formation of DNAzymes

A 5 mM haemin stock solution in DMSO was prepared and stored at 2 °C. For initial experiments, 200 µL of 1 µM PS2. M sequence was incubated with 40 µL of 5 µM haemin at 25 °C for 30 min in either 10 mM HEPES / 10 mM NaCl, pH 7.1 or 10

mM HEPES / 10mM KCl, pH 7.1. ABTS or TMB substrate was added to 500 μ L final volume and UV-Vis and RRS measurements were taken after approximately 3 hours. Subsequently, the DNAzyme and haemin concentration were reduced to 0.1 μ M to prevent over oxidation of the substrates, and the oxidation time was changed to 1 hour for ABTS and 3.5 hours for TMB based on the results from UV-Vis time studies. These time studies were carried out by reacting a final concentration of 0.1 μ M of guanine-rich DNA with 0.1 μ M of haemin (final concentration) in 500 μ L of both buffers for 30 minutes. Either 200 μ L of ABTS or 100 μ L of TMB substrate was then added and the absorbance at 633 nm measured every 5 minutes for a total of 960 minutes. The substrate volume was fixed at 100 μ L for TMB and 200 μ L for ABTS, as a result of initial experiments in which the substrate volume and buffer were varied and analysed between 200 nm and 800 nm.

7.3.4 Resonance Raman Scattering of DNAzymes

The oxidation of ABTS by a DNAzyme was carried out by reacting 0.1 μ M guanine-rich DNA and 0.1 μ M haemin (final concentrations) in 500 μ L of 10 mM HEPES / 10 mM KCl, pH 7.1 for 30 minutes. 200 μ L of ABTS substrate was added and left to oxidise for 1 hour before analysis using a 633 nm laser excitation at 4 mW power and 3 x 3 second accumulations and was carried out on the ABTS substrate before and after reaction with a DNAzyme. This experiment was also carried out using a 514 nm laser excitation source at 4 mW power and 3 x 3 second accumulations. A sample volume of 60 μ L was used and analysed in a 96-well plate, with each sample scanned 5 times. The spectra were obtained using WiRE software and baseline corrected using Grams. An average of the 5 scans were used to display the results obtained.

The oxidation of TMB by a DNAzyme was carried out by reacting 0.1 μ M guanine-rich DNA and 0.1 μ M haemin (final concentrations) in 500 μ L of 10 mM HEPES / 10 mM NaCl, pH 7.1 for 30 minutes. 100 μ L of ABTS substrate was added and left to oxidise for 3.5 hours before analysis using a 633 nm laser excitation at 4 mW power and 3 x 3 second accumulations and was carried out on the TMB substrate before and after reaction with a DNAzyme. The final oxidation product of TMB was

also obtained and analysed by adding an aliquot of H₂SO₄ to the sample. A sample volume of 60 µL was used and analysed in a 96-well plate, with each sample scanned 5 times. The spectra were obtained using WiRE software and baseline corrected using Grams. An average of the 5 scans were used to display the results obtained.

The same protocol was used for both TMB and ABTS to obtain a set of controls by omitting certain components needed for DNAzyme activity, and replacing the missing components with buffer to ensure consistent concentrations.

7.3.5 DNAzyme Concentration Study

Optimum conditions were used to determine the lowest concentration of guanine-rich DNA that could be detected using both TMB and ABTS substrate. The protocol outlined in section 7.3.5 for the analysis of DNAzyme activity by RRS was carried out with the concentration of guanine-rich DNA varied. 5 replicate samples were prepared and scanned 5 times using a 633 nm laser excitation wavelength at 4 mW laser power and 3 x 3 second accumulations. The raw data was obtained using Grams software and the peak height at 1401 cm⁻¹ for ABTS and 1608 cm⁻¹ obtained by subtracting the background haemin sample for each concentration of guanine-rich DNA. The intensity was plotted against concentration to obtain a linear relationship for ABTS and a logarithmic relationship for TMB.

7.3.6 Catalytic Beacon Assay Protocol

50 µL of 1 µM beacon and 5 µL of 100 µM target DNA were hybridised in 10 mM HEPES / 10 mM NaCl, pH 7.1 (TMB) or 10 mM HEPES / 10 mM KCl, pH 7.1 (ABTS) at 90 °C for 10 minutes and 10 °C for 10 minutes. 10 µL of 5 µM haemin was added and allowed to complex for 30 minutes at room temperature. 100 µL of TMB solution or 200 µL of ABTS solution was added to a final volume of 500 µL and RRS measurements were taken approximately 1 hour (ABTS) or 3.5 hours (TMB) later using both centred (1400 cm⁻¹) and extended scans (200-2000 cm⁻¹). A 633 nm laser excitation wavelength was used at 4 mW power and using 3 x 3 second accumulations. 5 replicate samples were prepared and scanned 5 times and the average of the results from the baseline correction shown.

The lowest observable concentration of target DNA was determined using the protocol outlined for TMB, where the peak intensity at 1608 cm^{-1} was obtained from the raw data by subtracting the background haemin signal from each concentration of target DNA and plotting the results against concentration. Again, 5 replicate samples were prepared and analysed 5 times to obtain an average value and the standard deviation calculated.

7.3.7 Catalytic Beacons for the Detection of PCR Product

A 99-base synthetic DNA sequence with a region complementary to the catalytic beacon was amplified via a PCR cycle, according to a standard protocol carried out by Mhairi Harper and using reagents from a manufactured PCR kit. The success of this amplification was monitored using the double stranded DNA intercalator SYBR-Green and fluorescent measurements taken at the end of each PCR cycle over the course of 25 cycles. A control sample with no template DNA was also prepared. The two samples, representing the presence and absence of target DNA were incorporated into the catalytic beacon protocol outlined previously for the TMB substrate. 3 replicate samples were analysed 5 times using a 633 nm laser excitation wavelength at 4 mW with 3 x 3 second accumulations. Both the raw data and the baseline corrected spectra were obtained using grams software and an average taken to obtain the results.

7.3.8 Split Probe DNAzyme Assay Protocol

A final concentration of $0.1\ \mu\text{M}$ of the split probe biotin-DNA, the split probe DNAzyme and the target DNA were hybridised in $500\ \mu\text{L}$ of $10\ \text{mM}$ HEPES / $10\ \text{mM}$ NaCl, pH 7.1. Streptavidin coated magnetic beads were used in a 1:1 ratio with the concentration of biotin labelled DNA, and were washed 3 times with buffer. The beads were re-suspended in $10\ \text{mM}$ HEPES / $10\ \text{mM}$ NaCl, pH 7.1 and added to the hybridised DNA sample. The sample was left at room temperature for 20 minutes with shaking before carrying out a magnetic wash step (x3) with the chosen buffer and re-suspending the sample to $500\ \mu\text{L}$. A final concentration of $0.1\ \mu\text{M}$ of haemin was added and the sample left to react for 30 minutes with constant shaking. Another magnetic wash step (x3) was carried out before the addition of $100\ \mu\text{L}$ of

TMB. After 3 hours the samples were transferred to a plastic micro-cuvette for analysis using a 633 nm laser excitation wavelength at 4 mW laser power and 3 x 3 second accumulations. A set of controls were also carried out in this experiment omitting certain components needed for catalytic activity to be observed, and replacing these components with buffer to ensure consistent concentrations.

This assay was repeated using streptavidin coated 96-well plates as opposed to streptavidin coated magnetic beads. Final concentrations of 0.1 μM of the split probe DNAzyme, 0.1 μM of target DNA and 10 nM of the split probe biotin-DNA were hybridised in 200 μL of either 10 mM HEPES / 10 mM NaCl, pH 7.1 or 10 mM HEPES / 10 mM KCl, pH 7.1 in an eppendorf. Prior to use, the streptavidin coated plates were washed (x3) with the chosen buffer. The hybridised DNA sample was then added to the streptavidin coated well, and the plate left to shake for 2 hours at room temperature. The sample wells were then washed (x3) with the chosen buffer and a final concentration of 0.1 μM of haemin in 200 μL of the buffer added to the wells. The plate was left at room temperature to shake for a further 30 minutes before another wash step (x3) was carried out. 80 μL of TMB in 200 μL final volume of buffer was added to the wells and left to react for 3 hours. The samples were analysed in the plates using a 633 nm laser excitation at 4 mW laser power and using 3 x 3 second accumulations. A set of controls was also carried out in this experiment omitting certain components needed for catalytic activity to be observed.

7.3.9 *SERRS of DNAzyme Activity*

Citrate reduced gold and silver nanoparticle suspensions were prepared according to the standard protocol outlined in section 7.2.3. The initial basic protocol involved the addition of final concentrations of 0.1 μM of guanine rich DNA to 0.1 μM haemin in 500 μL 10 mM HEPES / 10 mM NaCl, pH 7.1 for 30 minutes. 100 μL of TMB was added and after 3 hours, 200 μL of the sample was added to either 400 μL of gold or silver nanoparticles. The samples were analysed immediately after the addition of the nanoparticles in plastic micro-cuvettes using a 633 nm laser excitation wavelength at 1 mW laser power and 3 x 3 second accumulations. The analysis of ABTS was carried out using a similar experimental set up, although with 200 μL of

ABTS substrate and a 1-hour oxidation time before analysis. Also, after the addition of either gold or silver nanoparticles, 20 μL of 0.1 M spermine hydrochloride was added before analysis at 633 nm using a laser power of 1 mW.

Buffer conditions were compared by reacting final concentrations of 0.1 μM of guanine rich DNA and 0.1 μM of haemin in either 10 mM HEPES / 10 mM NaCl, pH 7.1 or 10 mM HEPES / 10 mM KCl, pH 7.1. 100 μL of TMB was added and after 3 hours, 200 μL of the prepared sample was added to 400 μL of silver nanoparticles and analysed at 633 nm with a laser power of 0.04 mW and 3 x 3 second accumulations. To assess the reproducibility of the successful buffer, 5 samples were prepared and scanned 5 times. The average spectra was taken from the raw data and the baseline corrected spectra using Grams software.

The observed limit of detection of guanine rich DNA was obtained by complexing a final concentration of 0.1 μM of haemin with varying concentrations of DNA in 500 μL final volume of 10 mM HEPES / 10 mM KCl, pH 7.1 for 30 minutes. 100 μL of TMB was added for 3 hours before 200 μL of the sample was added to 400 μL of silver colloid. 5 replicate samples were prepared for each concentration of DNA and scanned 5 times at 633 nm using a laser power of 1 mW and 3 x 3 second accumulations. The raw data was obtained using Grams software and the peak height at 1608 cm^{-1} obtained for each concentration of DNA.

SERRS detection was incorporated into the catalytic beacon assay by following the protocol for the detection of target DNA outlined in section 7.3.5, with a KCl buffer used and with 400 μL of silver nanoparticles added before analysis using a 633 nm laser excitation wavelength at 1 mW laser power. Similarly, the protocol for the split probe assay using streptavidin coated plates outlined in section 7.3.7 was followed for the detection of target DNA. 400 μL was added to the sample obtained from the well plate and analysed immediately at 633 nm at 1 mW laser power.

7.4 Nanoparticles as Enzyme Mimetics

7.4.1 Materials

3,3',5,5'-tetramethylbenzidine (TMB), sodium citrate tribasic dehydrate, silver nitrate, sodium tetrachloroaurate, poly(allylamine), dimethyl sulfoxide (DMSO) and poly(ethyleneimine) (PEI) were all purchased from Sigma Aldrich, UK. Hydrogen peroxide (30% w/v) was purchased from Fisher Scientific, UK.

7.4.2 Instrumentation

UV-Vis absorption spectra were carried out using a Cary 300 Bio UV-vis spectrometer. 500 μ L sample volumes were analysed in 1 cm glass cuvettes and scanned from 200 nm to 800 nm. Size and zeta measurements were carried out using a Malvern Zetasizer Nano Series. 1 mL samples volumes were analysed in 2-sided 1 cm plastic cuvettes for size measurements and a Malvern dip cell kit for zeta measurements. Raman spectra were collected using a Renishaw inVia microscope system with a HeNe laser (633 nm). Samples were analysed in 1 cm semi-micro disposable plastic cuvettes using a 20 x long working distance objective. WiRE 2.0 software (Renishaw PLC) was used to run the analysis and spectra were baseline corrected using a linear function and a 'level and zero' levelling mode in Grams software. Cell studies were carried out using a Renishaw In Via inverted microscope system using an excitation wavelength of 633 nm with the laser set to line focus using a 600 gr/mm grating.

7.4.3 Nanoparticle Synthesis

Citrate-capped gold and silver nanoparticles were prepared according to a standard protocol outlined in section 7.2.3.

Positive silver nanoparticles were obtained by adding a 1 % solution of polyethylenimine (PEI) to citrate-capped silver nanoparticles and shaking for approximately 5 minutes, before confirming the change in charge using zeta measurements. Positive gold nanoparticles were synthesised by adding 76.6 mg of chloroauric acid to 380 mL of distilled water, along with 36.4 mg of poly(allylamine)

Hydrochloride (PAH) which was dissolved and sonicated in 20 mL of distilled water. The mixture was then heated to 98°C for 10-15 minutes until the colour changed to a deep red.

7.4.4 Nanoparticle Characterisation

UV-Vis spectroscopy was used to obtain the maximum absorbance and concentration of colloid. 50 µL of the as synthesised silver nanoparticles were diluted in 500 µL distilled water and scanned from 200 to 800 nm. Size and zeta measurements were obtained by analysing 1 mL of nanoparticles on a Malvern Zetasize in a 1 cm plastic cuvette and dip cell, respectively.

7.4.5 Initial Experimentation

Initial SERRS studies were carried out by adding 200 µL of either TMB or ABTS substrate to varying amounts of gold or silver nanoparticles and the spectra obtained at 10-minute intervals over a period of 30 minutes. A laser excitation wavelength of 633 nm at 1 mW laser power and a 1 x 10 second accumulation was used to analyse the samples and the raw data used to obtain an average of the 5 scans taken to observe the trend in peak intensity at 1608 cm⁻¹ with varying time and nanoparticles volume.

200 µL of either TMB or ABTS substrate solution was added to either gold (500 µL) or silver (100 µL) nanoparticles in a total volume of 1 mL. Both size and zeta measurements were taken of the nanoparticles and then again at 10 minute intervals after the addition of substrate for a total of 30 minutes. This experiment was repeated 3 times for each combination of substrate and colloid and the average taken to produce the results.

The catalytic ability of positive nanoparticles was investigated by adding 200 µL of either TMB or ABTS substrate to 500 µL of PAH stabilised gold nanoparticles. The samples were analysed immediately using a 633 nm laser excitation wavelength at 4 mW laser power and a 1 x 10 second accumulation.

TMB formulations were prepared by adding 200 μL of the TMB / H_2O_2 substrate solution to either 100 μL of silver nanoparticles or 500 μL of gold nanoparticles and analysing the samples. This was compared to the spectrum obtained from the addition of 100 μL of TMB (3 mM) and 100 μL of H_2O_2 (6.5 mM) to either 100 μL of silver nanoparticles or 500 μL of gold nanoparticles. All samples were analysed using a 633 nm laser excitation source at 1 mW power with 1 x 10 second accumulations. The spectra were baseline corrected using Grams software to obtain a comparison between formulations.

7.4.6 Preparation of TMB and H_2O_2 Stock Solutions

2.4 mg of TMB was dissolved in 5 mL DMSO to create a 3 mM stock solution that was freshly prepared before each experiment. A 0.02 % stock solution of H_2O_2 was prepared by dissolving 3 μL of 30 % H_2O_2 in 5 ml distilled water. This was further diluted to a 10 μM stock solution and again was freshly prepared on the day of analysis.

7.4.7 Silver Control Experiments

100 μL of silver nanoparticles (0.3 nM) was added to 100 μL of TMB (3 mM) and 100 μL of H_2O_2 (6.5 mM) giving a total volume of 300 μL . Samples were analysed immediately using 633 nm laser excitation and a 10 second accumulation time. Samples were prepared in triplicate and 5 scans of each were taken. The samples were then analysed by UV-vis spectroscopy by diluting 50 μL in 500 μL and scanning between 200 nm and 800 nm.

7.4.8 Size and Zetasize Experiments

100 μL of silver nanoparticles (0.3 nM) were added to 100 μL of TMB (3 mM) and 100 μL of H_2O_2 (6.5 mM) and diluted a final volume of 1 mL with distilled water. 3 size and zeta measurements were taken every 10 minutes over the course of 30 minutes, and an average value taken. Control experiments were also analysed according to this method, replacing missing components with distilled water.

7.4.9 SEM Analysis

Silicon wafers (Agar Scientific) were cleaned with methanol and oxygen plasma (Diener electronic femto oxygen plasma cleaner). Two samples were prepared and the silicon chips were suspended in the solution overnight. The samples consisted of 100 μL of silver nanoparticles (0.3 nM) in distilled water, 100 μL of silver nanoparticles (0.3 mM), 100 μL of TMB (3 mM) and 100 μL of H_2O_2 (6.5 mM) or 100 μL of silver nanoparticles (0.3 nM) and 100 μL of TMB (3 mM). Samples were analysed using a Sirion 200 Shottky field emission electron microscope operating at an accelerating voltage of 30 kV and a magnification of 500 nm.

7.4.10 SERRS Time Study

100 μL of silver nanoparticles (0.3 nM), 100 μL of TMB (3 mM), and 100 μL of H_2O_2 (6.5 mM) were diluted to 500 μL using distilled water and analysed using 633 nm laser excitation and a 10 second accumulation every minute for 10 minutes. Controls samples with no silver nanoparticles and no H_2O_2 were also analysed in the same manner.

7.4.11 H_2O_2 Concentration Study

100 μL of silver nanoparticles (0.3 nM) and 100 μL of TMB (6.5 mM) were kept constant throughout experimentats, while the H_2O_2 concentration was varied between 0 and 10 μM , in a final sample volume of 500 μL . Samples were prepared in triplicate and analysed after 10 minutes reaction time using a 633 nm laser excitation wavelength and 1 x 10 second accumulation. 5 scans of each sample were taken and the average obtained. The peak height at 1608 cm^{-1} for the control sample (0 μM H_2O_2) was subtracted from the peak height at 1608 cm^{-1} for each concentration of H_2O_2 and plotted against concentration to obtain a linear plot between 4 and 10 μM .

7.4.12 Comparing Positive and Silver Nanoparticles

100 μL of TMB (3 mM) and 300 μL of H_2O_2 (6.5 mM) were prepared and 100 μL of either positive (0.07 nM) or negative (0.3 nM) silver nanoparticles were added to the sample. After 10 minutes the samples, which were prepared in triplicate, were analysed using a 633 nm laser excitation and a 10 second accumulation. The spectra

were baseline corrected using GRAMS and the average value obtained.

7.4.13 Nanoparticle Tracking in Cells

Live Chinese Hamster Ovary (CHO) cells were obtained from Dr Narayana Sirimuthu within the Centre for Molecular Nanometrology. 100 μL of silver colloid (0.3 nM) was added to the cell solution overnight, and then 10 μL of TMB (3 mM) and 10 μL of H_2O_2 (6.5 mM) added the following morning and the samples analysed after 1 hour. The cells were visualised and scanned using a line focussed laser at 633 nm with 1 mW laser power and 1 x 10 second accumulation time. WiRE software was used to obtain a false colour image of the cell, indicating areas of high intensity, which were used to obtain the spectra for TMB within the cells.

8. References

1. Watson, J. D.; Crick, F. H., *Nature* **1953**, *171* (4356), 737-8.
2. Watson, J. D.; Crick, F. H., *Nature* **1953**, *171* (4361), 964-7.
3. Dawson, M. H.; Sia, R. H. P., *J. Exp. Med.* **1931**, *54*.
4. Avery, O. T.; MacLeod, C. M.; McCarty, M., *J. Exp. Med.* **1944**, *79* (2), 137-159.
5. Pauling, L.; Corey, R. B., *Proc. Natl. Acad. Sci. U. S. A.* **1953**, *39* (2), 84-97.
6. Franklin, R. E.; Gosling, R. G., *Nature* **1953**, *171* (4356), 740-1.
7. Franklin, R. E.; Gosling, R. G., *Nature* **1953**, *172* (4369), 156-7.
8. Wilkins, M. H. F.; Strokes, A. R.; Wilson, H. R., *Nature* **1953**, *421* (6921), 398-400; discussion 396.
9. Zamenhof, S.; Brawerman, G.; Chargaff, E., *Biochimica et Biophysica Acta* **1952**, *9* (4), 402-5.
10. Meselson, M.; Stahl, F. W., *Proc. Natl. Acad. Sci. U. S. A.* **1958**, *44* (7), 671-82.
11. Crick, F., *Nature* **1970**, *227* (5258), 561-&.
12. Campbell, N. A.; Reece, J. B., *Biology*. Sixth ed.; Benjamin Cummings: San Fransisco, 2002.
13. Bang, I., *Biochem. Z.* **1910**, *26*, 293-311.
14. Gellert, M.; Lipsett, M. N.; Davies, D. R., *Proc. Natl. Acad. Sci. U. S. A.* **1962**, *48* (12), 2013-&.
15. Huppert, J. L., *Chem. Soc. Rev.* **2008**, *37* (7).
16. Burge, S.; Parkinson, G. N.; Hazel, P.; Todd, A. K.; Neidle, S., *Nucleic Acids Res.* **2006**, *34* (19), 5402-5415.
17. Smargiasso, N.; Rosu, F.; Hsia, W.; Colson, P.; Baker, E. S.; Bowers, M. T.; De Pauw, E.; Gabelica, V., *J. Am. Chem. Soc.* **2008**, *130* (31), 10208-10216.
18. Laughlan, G.; Murchie, A. I. H.; Norman, D. G.; Moore, M. H.; Moody, P. C. E.; Lilley, D. M. J.; Luisi, B., *Science* **1994**, *265* (5171), 520-524.
19. Viglasky, V.; Bauer, L.; Tluckova, K., *Biochem.* **2010**, *49* (10), 2110-2120.
20. Pedroso, I. A.; Duarte, L. F.; Yanez, G.; Burkewitz, K.; Fletcher, T. M., *Biopolymers* **2007**, *87* (1), 74-84.

21. Yu, H. Q.; Miyoshi, D.; Sugimoto, N., *J. Am. Chem. Soc.* **2006**, *128* (48), 15461-15468.
22. Parkinson, G. N.; Lee, M. P. H.; Neidle, S., *Nature* **2002**, *417* (6891), 876-880.
23. Kim, M. Y.; Vankayalapati, H.; Kazuo, S.; Wierzba, K.; Hurley, L. H., *J. Am. Chem. Soc.* **2002**, *124* (10), 2098-2099.
24. Kim, M. Y.; Gleason-Guzman, M.; Izbicka, E.; Nishioka, D.; Hurley, L. H., *Cancer Res.* **2003**, *63* (12), 3247-3256.
25. Lipps, H. J.; Rhodes, D., *Trends Cell Biol.* **2009**, *19* (8), 414-422.
26. Biffi, G.; Tannahill, D.; McCafferty, J.; Balasubramanian, S., *Nat Chem* **2013**, *advance online publication*.
27. Tyagi, S.; Kramer, F. R., *Nat. Biotechnol.* **1996**, *14* (3), 303-308.
28. Michelson, A. M.; Todd, A. R., *Journal of the Chemical Society (Resumed)* **1955**, 2632-2638.
29. Smith, M.; Rammler, D. H.; Goldberg, I. H.; Khorana, H. G., *J. Am. Chem. Soc.* **1961**, *84*, 430-440.
30. Schaller, H.; Weimann, G.; Lerch, B.; Khorana, H. G., *J. Am. Chem. Soc.* **1963**, *85*, 3821-3827.
31. Letsinger, R. L.; Lunsford, W. B., *J. Am. Chem. Soc.* **1976**, *98*, 3655-3661.
32. Letsinger, R. L.; Finnan, J. L.; Heavner, G. A.; Lunsford, W. B., *J. Am. Chem. Soc.* **1975**, *97*, 3278-3279.
33. Caruthers, M. H., *Science* **1985**, *230* (4723), 281-285.
34. Caruthers, M. H., *Accounts Chem. Res.* **1991**, *24* (9), 278-284.
35. <http://www.linktech.co.uk/> (accessed June 2010).
36. Tolun, G.; Myers, R. S., *Nucleic Acids Res.* **2003**, *31* (18), 6.
37. Didenko, V. V., *Biotechniques* **2001**, *31* (5), 1106-+.
38. Dougan, J. A.; Karlsson, C.; Smith, W. E.; Graham, D., *Nucleic Acids Res.* **2007**, *35* (11), 3668.
39. Letsinger, R. L.; Elghanian, R.; Viswanadham, G.; Mirkin, C. A., *Bioconjugate Chem.* **2000**, *11* (2), 289-291.
40. Dougan, J. Synthesis of new ligands for biomolecular nanoparticle functionalisation. University of Strathclyde, Glasgow, 2009.

41. Xiao, M.; Phong, A.; Ha, C.; Chan, T.-F.; Cai, D.; Leung, L.; Wan, E.; Kistler, A. L.; DeRisi, J. L.; Selvin, P. R.; Kwok, P.-Y., *Nucleic Acids Res.* **2007**, *35* (3).
42. Protozanova, E.; Zhang, M.; White, E. J.; Mollova, E. T.; Broeck, D. T.; Fridrikh, S. V.; Cameron, D. B.; Gilmanshin, R., *Anal Biochem* **2010**, *402* (1), 83-90.
43. Förster, T., *Ann. Physik* **1948**, *437*.
44. Lakowicz, J. R., *Principles of Fluorescence Spectroscopy*. 3rd Edition ed.; Springer: 2006.
45. <http://nobelprize.org>. (accessed January 2010).
46. Saiki, R. K.; Scharf, S.; Faloona, F.; Mullis, K. B.; Horn, G. T.; Erlich, H. A.; Arnheim, N., *Science* **1985**, *230* (4732), 1350-1354.
47. Saiki, R. K.; Gelfand, D. H.; Stoffel, S.; Scharf, S. J.; Higuchi, R.; Horn, G. T.; Mullis, K. B.; Erlich, H. A., *Science* **1988**, *239* (4839), 487-491.
48. Holland, P. M.; Abramson, R. D.; Watson, R.; Gelfand, D. H., *Proc. Natl. Acad. Sci. U. S. A.* **1991**, *88* (16), 7276-7280.
49. Gibson, U. E. M.; Heid, C. A.; Williams, P. M., *Genome Res.* **1996**, *6* (10), 995-1001.
50. Heid, C. A.; Stevens, J.; Livak, K. J.; Williams, P. M., *Genome Res.* **1996**, *6* (10), 986-994.
51. Lang, R.; Pfeffer, K.; Wagner, H.; Heeg, K., *J. Immunol. Methods* **1997**, *203* (2), 181-192.
52. Whitcombe, D.; Theaker, J.; Guy, S. P.; Brown, T.; Little, S., *Nat. Biotechnol.* **1999**, *17* (8), 804-807.
53. Higuchi, R.; Dollinger, G.; Walsh, P. S.; Griffith, R., *Bio-Technology* **1992**, *10* (4), 413-417.
54. Zipper, H.; Brunner, H.; Bernhagen, J.; Vitzthum, F., *Nucleic Acids Res.* **2004**, *32* (12), 10.
55. Giglio, S.; Monis, P. T.; Saint, C. P., *Nucleic Acids Res.* **2003**, *31* (22), 5.
56. Fernandez, F.; Gutierrez, J.; Sorlozano, A.; Romero, J. M.; Soto, M. J.; Ruiz-Cabello, F., *Microbiol. Res.* **2006**, *161* (2), 158-163.
57. Thelwell, N.; Millington, S.; Solinas, A.; Booth, J.; Brown, T., *Nucleic Acids Res.* **2000**, *28* (19), 3752-3761.

58. <http://www.nature.com/nnano/focus/plenty-of-room/index.html> (accessed 2013).
59. Rosi, N. L.; Mirkin, C. A., *Chem. Rev.* **2005**, *105* (4), 1547-1562.
60. Daniel, M. C.; Astruc, D., *Chem. Rev.* **2004**, *104* (1), 293-346.
61. Farady, M., *Philosophical Transactions of the Royal Society* **1857**, *147*, 145-181.
62. J, T., *Discuss Farady Society* **1951**, *11*.
63. Frens, G., *Nature-Physical Science* **1973**, *241* (105), 20-22.
64. Giljohann, D. A.; Seferos, D. S.; Daniel, W. L.; Massich, M. D.; Patel, P. C.; Mirkin, C. A., *Angew. Chem.-Int. Edit.* **2010**, *49* (19), 3280-3294.
65. Moores, A.; Goettmann, F., *New J. Chem.* **2006**, *30* (8), 1121-1132.
66. Mie, G., *Annalen der Physik* **1908**, *330* (3), 377-445.
67. Pellegrino, T.; Sperling, R. A.; Alivisatos, A. P.; Parak, W. J., *J. Biomed. Biotechnol.* **2007**, *9*.
68. Zhao, W.; Brook, M. A.; Li, Y. F., *ChemBioChem* **2008**, *9* (15), 2363-2371.
69. Giersig, M.; Mulvaney, P., *Langmuir* **1993**, *9* (12), 3408-3413.
70. Mirkin, C. A.; Letsinger, R. L.; Mucic, R. C.; Storhoff, J. J., *Nature* **1996**, *382* (6592), 607.
71. Alivisatos, A. P.; Johnsson, K. P.; Peng, X.; Wilson, T. E.; Loweth, C. J.; Bruchez, M. P.; Schultz, P. G., *Nature* **1996**, *382* (6592), 609.
72. Niemeyer, C. M., *Angew. Chem.-Int. Edit.* **2001**, *40* (22), 4128-4158.
73. Cutler, J. I.; Auyeung, E.; Mirkin, C. A., *J. Am. Chem. Soc.* **2012**, *134* (3), 1376-1391.
74. Loweth, C. J.; Caldwell, W. B.; Peng, X. G.; Alivisatos, A. P.; Schultz, P. G., *Angew. Chem.-Int. Edit.* **1999**, *38* (12), 1808-1812.
75. Sonnichsen, C.; Reinhard, B. M.; Liphardt, J.; Alivisatos, A. P., *Nat Biotech* **2005**, *23* (6), 741-745.
76. Letsinger, R. L.; Mirkin, C. A.; Park, S. J.; Viswanadham, G.; Zhang, L., *Nucleic Acids Res Suppl* **2001**, (1), 1-2.
77. Storhoff, J. J.; Elghanian, R.; Mucic, R. C.; Mirkin, C. A.; Letsinger, R. L., *J. Am. Chem. Soc.* **1998**, *120* (9), 1959-1964.
78. Elghanian, R.; Storhoff, J. J.; Mucic, R. C.; Letsinger, R. L.; Mirkin, C. A., *Science* **1997**, *277* (5329), 1078-1081.

79. Taton, T. A.; Mirkin, C. A.; Letsinger, R. L., *Science* **2000**, 289 (5485), 1757-1760.
80. Nam, J.-M.; Stoeva, S. I.; Mirkin, C. A., *J. Am. Chem. Soc.* **2004**, 126 (19), 5932-5933.
81. Prigodich, A. E.; Randeria, P. S.; Briley, W. E.; Kim, N. J.; Daniel, W. L.; Giljohann, D. A.; Mirkin, C. A., *Anal. Chem.* **2012**, 84 (4), 2062-2066.
82. Zhang, K.; Hao, L.; Hurst, S. J.; Mirkin, C. A., *J. Am. Chem. Soc.* **2012**, 134 (40), 16488-16491.
83. Lee, P. C.; Meisel, D., *J. Phys. Chem.* **1982**, 86 (17), 3391-3395.
84. Thompson, D. G.; Enright, A.; Faulds, K.; Smith, W. E.; Graham, D., *Anal. Chem.* **2008**, 80 (8), 2805.
85. Graham, D.; Thompson, D. G.; Smith, W. E.; Faulds, K., *Nat. Nanotechnol.* **2008**, 3 (9), 548.
86. Smekal, A., *Naturwissenschaften* **1923**, 11 (43), 873-875.
87. Raman, C. V.; Krishnan, K. S., *Nature* **1928**, 121, 501-502.
88. Smith, E.; Dent, G., *Modern Raman Spectroscopy: A Practical Approach*. John Wiley & Sons, Ltd: Chichester, UK, 2005.
89. Fleischmann, M.; Hendra, P. J.; McQuillan, A. J., *Chem. Phys. Lett.* **1974**, 26 (2), 163.
90. Jeanmaire, D. L.; Van Duyne, R. P., *Journal of Electroanalytical Chemistry and Interfacial Electrochemistry* **1977**, 84 (1), 1-20.
91. Albrecht, M. G.; Creighton, J. A., *J. Am. Chem. Soc.* **1977**, 99 (15), 5215.
92. Van Duyne, R. P.; Hulteen, J. C.; Treichel, D. A., *J. Chem. Phys.* **1993**, 99 (3), 2101.
93. Gibson, K. F.; Correia-Ledo, D.; Couture, M.; Graham, D.; Masson, J.-F., *Chem. Commun.* **2011**, 47 (12), 3404.
94. Perney, N. M. B.; Garca de Abajo, F. J.; Baumberg, J. J.; Tang, A.; Netti, M. C.; Charlton, M. D. B.; Zoorob, M. E., *Physical Review B* **2007**, 76 (3), 035426.
95. Stacy, A. M.; Vanduyne, R. P., *Chem. Phys. Lett.* **1983**, 102 (4), 365.
96. Nie, S.; Emory, S. R., *Science* **1997**, 275 (5303), 1102.
97. Dieringer, J. A.; Lettan, R. B.; Scheidt, K. A.; Van Duyne, R. P., *J. Am. Chem. Soc.* **2007**, 129 (51), 16249.

98. Harper, M. M.; McKeating, K. S.; Faulds, K., *Phys. Chem. Chem. Phys.* **2013**.
99. Faulds, K.; Barbagallo, R. P.; Keer, J. T.; Smith, W. E.; Graham, D., *Analyst* **2004**, *129* (7), 567-568.
100. Papadopoulou, E.; Bell, S. E. J., *Chem. Commun.* **2011**, *47* (39), 10966.
101. Stokes, R. J.; Macaskill, A.; Lundahl, P. J.; Smith, W. E.; Faulds, K.; Graham, D., *Small* **2007**, *3*, 1593.
102. Faulds, K.; McKenzie, F.; Smith, W. E.; Graham, D., *Angew. Chem.-Int. Edit.* **2007**, *46* (11), 1829-1831.
103. Isola, N. R.; Stokes, D. L.; Vo-Dinh, T., *Anal. Chem.* **1998**, *70* (7), 1352.
104. Graham, D.; Mallinder, B. J.; Whitcombe, D.; Smith, W. E., *ChemPhysChem* **2001**, *2* (12), 746-748.
105. Graham, D.; Mallinder, B. J.; Whitcombe, D.; Watson, N. D.; Smith, W. E., *Anal. Chem.* **2002**, *74* (5), 1069-1074.
106. Monaghan, P. B.; McCarney, K. M.; Ricketts, A.; Littleford, R. E.; Docherty, F.; Smith, W. E.; Graham, D.; Cooper, J. M., *Anal. Chem.* **2007**, *79* (7), 2844.
107. Harper, M. M.; Robertson, B.; Ricketts, A.; Faulds, K., *Chem. Commun.* **2012**, *48* (75), 9412.
108. Wabuyele, M. B.; Vo-Dinh, T., *Anal. Chem.* **2005**, *77* (23), 7810.
109. Wang, H.-N.; Vo-Dinh, T., *Nanotechnology* **2009**, *20* (6), 065101.
110. MacAskill, A.; Crawford, D.; Graham, D.; Faulds, K., *Anal. Chem.* **2009**, *81* (19), 8134-8140.
111. van Lierop, D.; Faulds, K.; Graham, D., *Anal. Chem.* **2011**, *83* (15), 5817-5821.
112. Cunningham, D.; Littleford, R. E.; Smith, W. E.; Lundahl, P. J.; Khan, I.; McComb, D. W.; Graham, D.; Laforest, N., *Faraday Discuss.* **2006**, *132*, 135-145.
113. Khan, I.; Cunningham, D.; Littleford, R. E.; Graham, D.; Smith, W. E.; McComb, D. W., *Anal. Chem.* **2006**, *78* (1), 224-230.
114. Faulds, K.; Littleford, R. E.; Graham, D.; Dent, G.; Smith, W. E., *Anal. Chem.* **2004**, *76* (3), 592.
115. McKeating, K. S.; Dougan, J. A.; Faulds, K., *Biochem. Soc. Trans.* **2012**, *40* (4), 597-602.

116. Cao, Y. W. C.; Jin, R. C.; Mirkin, C. A., *Science* **2002**, 297 (5586), 1536.
117. Qian, X. M.; Zhou, X.; Nie, S. M., *J. Am. Chem. Soc.* **2008**, 130 (45), 14934.
118. Barrett, L.; Dougan, J. A.; Faulds, K.; Graham, D., *Nanoscale* **2011**, 3 (8), 3221.
119. McKenzie, F.; Faulds, K.; Graham, D., *Nanoscale* **2010**, 2 (1), 78.
120. Blackburn, G. M.; Gait, M. J.; Loakes, D.; Williams, D. M., *Nucleic Acids in Chemistry and Biology*. 3rd Edition ed.; RSC Publishing: 2006.
121. Little, J. W., *J Biol Chem* **1967**, 242 (4), 679-86.
122. Li, J. J.; Chu, Y.; Lee, B. Y.-H.; Xie, X. S., *Nucleic Acids Res.* **2008**, 36 (6), Article No.: e36.
123. Zuo, X.; Xia, F.; Xiao, Y.; Plaxco, K. W., *J. Am. Chem. Soc.* **2010**, 132 (6), 1816.
124. Zhang, M.; Guan, Y. M.; Ye, B. C., *Chem. Commun.* **2011**, 47 (12), 3478-80.
125. Cui, L. A.; Ke, G. L.; Zhang, W. Y.; Yang, C. Y. J., *Biosensors & Bioelectronics* **2011**, 26 (5), 2796-2800.
126. Bi, S.; Li, L.; Cui, Y., *Chem. Commun.* **2012**, 48 (7), 1018-1020.
127. Xu, Q. F.; Cao, A. P.; Zhang, L. F.; Zhang, C. Y., *Anal. Chem.* **2012**, 84 (24), 10845-10851.
128. Xu, W.; Xue, X. J.; Li, T. H.; Zeng, H. Q.; Liu, X. G., *Angew. Chem.-Int. Edit.* **2009**, 48 (37), 6849.
129. Dougan, J. A.; MacRae, D.; Graham, D.; Faulds, K., *Chem. Commun.* **2011**, 47 (16), 4649-4651.
130. Little, J. W.; Lehman, I. R.; Kaiser, A. D., *J Biol Chem.* **1967**, 242 (4), 672-8.
131. Carter, D. M.; Radding, C. M., *J Biol Chem.* **1971**, 246 (8), 2502-&.
132. Sriprakash, K. S.; Lundh, N.; Moonhuh, M.; Radding, C. M., *J Biol Chem.* **1975**, 250 (14), 5438-5445.
133. Kovall, R.; Matthews, B. W., *Science* **1997**, 277, 1824-1827.
134. Thomas, K. R.; Olivera, B. M., *J Biol Chem.* **1978**, 253 (2), 424-429.
135. Subramanian, K.; Rutvisuttinunt, W.; Scott, W.; Myers, R. S., *Nucleic Acids Res.* **2003**, 31 (6), 1585-1596.
136. Zhang, J. J.; McCabe, K. A.; Bell, C. E., *Proc. Natl. Acad. Sci. U. S. A.* **2011**, 108 (29), 11872-11877.

137. Singer, V. L.; Jones, L. J.; Yue, S. T.; Haugland, R. P., *Analytical Biochemistry* **1997**, *249* (2), 228-238.
138. Ahn, S. J.; Costa, J.; Emanuel, J. R., *Nucleic Acids Res.* **1996**, *24* (13), 2623-2625.
139. Choi, S. J.; Szoka, F. C., *Analytical Biochemistry* **2000**, *281* (1), 95-97.
140. Teng, M.; Usman, N.; Frederick, C. A.; Wang, A. H. J., *Nucleic Acids Res.* **1988**, *16* (6), 2671-2690.
141. Muller, W.; Gautier, F., *Eur. J. Biochem.* **1975**, *54* (2), 385-394.
142. Latt, S. A.; Stetten, G., *J. Histochem. Cytochem.* **1976**, *24* (1), 24-33.
143. Guan, Y.; Zhou, W.; Yao, X. H.; Zhao, M. P.; Li, Y. Z., *Anal. Chim. Acta* **2006**, *570* (1), 21-28.
144. Ahmed, M. U.; Idegami, K.; Chikae, M.; Kerman, K.; Chaumpluk, P.; Yamamura, S.; Tamiya, E., *Analyst* **2007**, *132* (5), 431-438.
145. Takahashi, M.; Okada, J.; Ito, K.; Hashimoto, M.; Hashimoto, K.; Yoshida, Y.; Furuichi, Y.; Ohta, Y.; Mishiro, S.; Gemma, N., *Analyst* **2005**, *130* (5), 687-693.
146. Laube, U.; Kiderlen, A. F., *Parasitol. Res.* **1998**, *84* (7), 559-564.
147. Jeorett, A. Amplification Free Direct Genomic Sequence Analysis by Optical Spectroscopy. University of Strathclyde Glasgow, 2010.
148. Sato, K.; Hosokawa, K.; Maeda, M., *Anal. Sci.* **2007**, *23* (1), 17-20.
149. Sato, K.; Hosokawa, K.; Maeda, M., *J. Am. Chem. Soc.* **2003**, *125* (27), 8102-8103.
150. Sato, K.; Hosokawa, K.; Maeda, M., *Nucleic Acids Res.* **2005**, *33* (1), 5.
151. Letsinger, R. L.; Mirkin, C. A.; Park, S. J.; Viswanadham, G.; Zhang, L., *Nucleic Acids Research Supplement* **2001**, (1), 1-2.
152. Liu, G. L.; Yin, Y.; Kunchakarra, S.; Mukherjee, B.; Gerion, D.; Jett, S. D.; Bear, D. G.; Gray, J. W.; Alivisatos, A. P.; Lee, L. P.; Chen, F. F., *Nat Nano* **2006**, *1* (1), 47-52.
153. Xu, X. Y.; Han, M. S.; Mirkin, C. A., *Angew. Chem.-Int. Edit.* **2007**, *46* (19), 3468-3470.
154. Turkevich, J.; P.C, S.; Hillier, J., *Discuss Faraday Soc.* **1951**, *11*, 55-75.
155. Parak, W. J.; Pellegrino, T.; Micheel, C. M.; Gerion, D.; Williams, S. C.; Alivisatos, A. P., *Nano Lett.* **2003**, *3* (1), 33-36.

156. Zanchet, D.; Micheel, C. M.; Parak, W. J.; Gerion, D.; Alivisatos, A. P., *Nano Lett.* **2001**, *1* (1), 32-35.
157. Craig, D.; Graham, D.; Faulds, K.; Simpson, J., *Chem. Commun.* **2012**.
158. Travascio, P.; Witting, P. K.; Mauk, A. G.; Sen, D., *J. Am. Chem. Soc.* **2001**, *123* (7), 1337-1348.
159. Kong, D. M.; Yang, W.; Wu, J.; Li, C. X.; Shen, H. X., *Analyst* **2010**, *135* (2), 321-326.
160. Kong, D. M.; Cai, L. L.; Guo, J. H.; Wu, J.; Shen, H. X., *Biopolymers* **2009**, *91* (5), 331-339.
161. Majhi, P. R.; Shafer, R. H., *Biopolymers* **2006**, *82* (6), 558-569.
162. Cheglakov, Z.; Weizmann, Y.; Beissenhirtz, M. K.; Willner, I., *Chem. Commun.* **2006**, (30), 3205-3207.
163. Weizmann, Y.; Beissenhirtz, M. K.; Cheglakov, Z.; Nowarski, R.; Kotler, M.; Willner, I., *Angew. Chem.-Int. Edit.* **2006**, *45* (44), 7384-7388.
164. Li, B. L.; Du, Y.; Li, T.; Dong, S. J., *Anal. Chim. Acta* **2009**, *651* (2), 234-240.
165. Josephy, P. D.; Eling, T.; Mason, R. P., *J. Biol. Chem.* **1982**, *257* (7), 3669-3675.
166. Zhu, X.; Gao, X. Y.; Liu, Q. D.; Lin, Z. Y.; Qiu, B.; Chen, G. N., *Chem. Commun.* **2011**, *47* (26), 7437-7439.
167. Li, D.; Shlyahovsky, B.; Elbaz, J.; Willner, I., *J. Am. Chem. Soc.* **2007**, *129* (18), 5804-5805.
168. Kong, D. M.; Wu, J.; Ma, Y. E.; Shen, H. X., *Analyst* **2008**, *133* (9), 1158-1160.
169. Xiao, Y.; Pavlov, V.; Niazov, T.; Dishon, A.; Kotler, M.; Willner, I., *J. Am. Chem. Soc.* **2004**, *126* (24), 7430-7431.
170. Fu, R.; Jeon, K.; Jung, C.; Park, H. G., *Chem. Commun.* **2011**, *47* (35), 9876-9878.
171. Song, Y.; Zhang, W.; An, Y.; Cui, L.; Yu, C.; Zhu, Z.; Yang, C. J., *Chem. Commun.* **2012**, *48* (4), 576-578.
172. Zheng, A.-X.; Li, J.; Wang, J.-R.; Song, X.-R.; Chen, G.-N.; Yang, H.-H., *Chem. Commun.* **2012**, *48* (25), 3112-3114.

173. Zhang, J.; Gao, Q. L.; Chen, P. P.; Chen, J. H.; Chen, G. N.; Fu, F. F., *Biosensors & Bioelectronics* **2011**, *26* (10), 4053-4057.
174. Yang, X.; Li, T.; Li, B. L.; Wang, E. K., *Analyst* **2010**, *135* (1), 71-75.
175. Li, T.; Li, B. L.; Wang, E. K.; Dong, S. J., *Chem. Commun.* **2009**, (24), 3551-3553.
176. Golub, E.; Freeman, R.; Niazov, A.; Willner, I., *Analyst* **2011**, *136* (21), 4397-4401.
177. Stevenson, R.; Ingram, A.; Leung, H.; McMillan, D. C.; Graham, D., *Analyst* **2009**, *134* (5), 842.
178. Laing, S.; Hernandez-Santana, A.; Sassmannshausen, J.; Asquith, D. L.; McInnes, I. B.; Faulds, K.; Graham, D., *Anal. Chem.* **2011**, *83* (1), 297-302.
179. Gao, L.; Zhuang, J.; Nie, L.; Zhang, J.; Zhang, Y.; Gu, N.; Wang, T.; Feng, J.; Yang, D.; Perrett, S.; Yan, X., *Nat Nano* **2007**, *2* (9), 577-583.
180. Stevenson, R.; Ingram, A.; Leung, H.; McMillan, D. C.; Graham, D., *Analyst* **2009**, *134* (5), 842-844.
181. Du, Y.; Li, B. L.; Guo, S. J.; Zhou, Z. X.; Zhou, M.; Wang, E. K.; Dong, S. J., *Analyst* **2011**, *136* (3), 493-497.
182. Qiao, Y.; Deng, J.; Jin, Y.; Chen, G.; Wang, L., *Analyst* **2012**, *137* (7), 1663-1668.
183. Graham, D.; Faulds, K., *Chem. Soc. Rev.* **2008**, *37* (5), 1042-1051.
184. Zhang, Z.; Zhu, H.; Wang, X.; Yang, X., *Microchim Acta* **2011**, *174* (1-2), 183-189.
185. Wei, H.; Wang, E., *Anal. Chem.* **2008**, *80* (6), 2250-2254.
186. Liang, M.; Fan, K.; Pan, Y.; Jiang, H.; Wang, F.; Yang, D.; Lu, D.; Feng, J.; Zhao, J.; Yang, L.; Yan, X., *Anal. Chem.* **2012**, *85* (1), 308-312.
187. Xie, J.; Zhang, X.; Wang, H.; Zheng, H.; Huang, Y., *TrAC Trends in Anal. Chem.* **2012**, *39* (0), 114-129.
188. Hu, L.; Yuan, Y.; Zhang, L.; Zhao, J.; Majeed, S.; Xu, G., *Anal. Chim. Acta* **2013**, *762* (0), 83-86.
189. Jiao, X.; Song, H.; Zhao, H.; Bai, W.; Zhang, L.; Lv, Y., *Analytical Methods* **2012**, *4* (10), 3261-3267.
190. Shi, W.; Zhang, X.; He, S.; Huang, Y., *Chem. Commun.* **2011**, *47* (38), 10785-10787.

191. Wang, C.-I.; Chen, W.-T.; Chang, H.-T., *Anal. Chem.* **2012**, *84* (22), 9706-9712.
192. Tseng, C.-W.; Chang, H.-Y.; Chang, J.-Y.; Huang, C.-C., *Nanoscale* **2012**, *4* (21), 6823-6830.
193. He, W.; Liu, Y.; Yuan, J.; Yin, J.-J.; Wu, X.; Hu, X.; Zhang, K.; Liu, J.; Chen, C.; Ji, Y.; Guo, Y., *Biomaterials* **2011**, *32* (4), 1139-1147.
194. Jv, Y.; Li, B.; Cao, R., *Chem. Commun.* **2010**, *46* (42), 8017-8019.
195. Wang, S.; Chen, W.; Liu, A.-L.; Hong, L.; Deng, H.-H.; Lin, X.-H., *ChemPhysChem* **2012**, *13* (5), 1199-1204.
196. Larmour, I. A.; Faulds, K.; Graham, D., *J. Phys. Chem. C* **2010**, *114* (31), 13249-13254.
197. Kneipp, J.; Kneipp, H.; McLaughlin, M.; Brown, D.; Kneipp, K., *Nano Lett.* **2006**, *6* (10), 2225.

Appendix : Publications

1. *Nanoparticle Assembly for Sensitive DNA Detection using SERRS*
K. S. McKeating, J. A. Dougan, K. Faulds. *Biochem. Soc. Trans.*, 2012, **40**, 591-602
2. *Recent Developments and Future Directions in SERS for Bioanalysis*
M. Harper, K. S. McKeating, K. Faulds. *Phys. Chem. Chem. Phys.*, 2013, **15**, 5312-5328
3. *Resonance Raman Scattering of Catalytic Beacons for DNA Detection*
K. S. McKeating, D. Graham, K. Faulds. *Chem. Commun.*, 2013, **49**, 3206-3208
4. *Investigating the use of Silver Nanoparticles as an Enzyme Mimetic using Surface Enhanced Raman Scattering*
K. S. McKeating, S. Sloan-Dennisoun, D. Graham and K. Faulds (under review)